Phenomenological aspects of the n and n' mesons

Emilio ROYO

UNIVERSITAT AUTÒNOMA DE BARCELONA

DOCTORAL THESIS

Phenomenological aspects of the η and η' mesons

Author:
Emilio ROYO

PhD Advisor:
Dr. Rafel ESCRIBANO

A thesis submitted in fulfilment of the requirements
for the degree of Doctor of Philosophy

in the

Institut de Física d'Altes Energies
Department de Física

May 17, 2023

"*Nature is simple if you know how to look at her.*"

Murray Gell-Mann

Abstract

The phenomenology of the neutral and long-lived η and η' mesons constitutes an ideal flavour-conserving laboratory for investigating the dynamics of quantum chromodynamics in the non-perturbative regime, as well as its relevant symmetry-breaking mechanisms. In addition to this, the decays of these states have been identified, and have gained plenty of attention in recent years, as unmatched probes in the context of high-precision measurements to observe potential departures from the Standard Model predictions and, therefore, as a potential window for discovering new physics beyond the Standard Model. As a result of this, many broad experimental programmes in high-intensity-frontier centres have been designed for this purpose, holding promise for a new and exciting era of η and η' physics at the precision frontier.

It is within this context that we explore several phenomenological aspects of the η and η' mesons in this thesis. We begin by studying the mixing in the π^0-η-η' system from radiative $V \to P\gamma$ and $P \to V\gamma$ decays using a phenomenological model that incorporates explicit breaking of the isospin symmetry. We then move on to analyse the Standard Model scalar and vector meson exchange contributions to the doubly radiative decays $\eta^{(\prime)} \to \pi^0\gamma\gamma$ and $\eta' \to \eta\gamma\gamma$, presenting for the first time theoretical predictions for the latter. Next, we investigate the sensitivity of these decays to signatures of a hypothetical leptophobic B boson that couples to the baryon number. We provide improved constraints on the B-boson mass m_B and coupling to Standard Model particles α_B, and perform fits to the available diphoton invariant mass distribution data. The results from this analysis may be of relevance for the B-boson search programmes at existing and forthcoming light-meson facilities, such as KLOE(-II) and Jefferson Lab Eta Factory experiments. We then follow with a detailed analysis of the Standard Model predictions for the C-conserving semileptonic decays $\eta^{(\prime)} \to \pi^0 l^+ l^-$ and $\eta' \to \eta l^+ l^-$ ($l = e$ or μ), which may be used to identify potential discrepancies with high-precision measurements at future η and η' factories. Theoretical predictions for the four $\eta' \to \pi^0 l^+ l^-$ and $\eta' \to \eta l^+ l^-$ branching ratios and dilepton invariant mass distributions are presented in this thesis for the first time. Finally, we study potential CP-violating signatures in $\eta^{(\prime)} \to \pi^0 \mu^+ \mu^-$ and $\eta' \to \eta \mu^+ \mu^-$ decays using the Standard Model effective field theory as the general framework to capture new physics, and we assess the prospect of observing them at the future REDTOP experiment.

Acknowledgements

This PhD thesis is the result of just over four years of hard work as a 'part-time member' of the IFAE and the Física Teòrica group at the Universitat Autònoma de Barcelona.

I am specially grateful to my PhD advisor, Rafel Escribano, who has been extremely flexible accommodating my difficult schedule, as well as patient and understanding over the years. Thank you for all the late night discussions and for helping me learn a bit about this fascinating subject.

I'd also like to thank Sergi Gonzàlez Solís for a great collaboration and without whom one chapter of this thesis would not have been possible. Likewise, I want to thank Pablo Sánchez Puertas who has been instrumental for the completion of another chapter.

I owe a big 'thank you' to all my family —parents, sister, wife (and little Berta)— for their unconditional support. Nothing would have been possible without them.

Finally, I would like to dedicate this work to my wife, Aida, for all the hours I haven't spent with her and for enduring without a single complaint my day-to-day struggles.

Contents

List of Abbreviations

BR	Branching Ratio
BSM	Beyond the Standard Model
C	Charge Conjugation
CM	Centre of Mass
χPT	Chiral Perturbation Theory
EFT	Effective Field Theory
EOM	Equation of Motion
HLS	Hidden Local Symmetry
IR	Infrared
Large-N_C χPT	Large Number of Colours Chiral Perturbation Theory
LEC	Low Energy Constant
LO	Leading Order
LσM	Linear Sigma Model
nEDM	Neutron Electric Dipole Moment
NLO	Next to Leading Order
NWA	Narrow Width Approximation
P	Parity Inversion
pQCD	Perturbative Quantum Chromodynamics
OZI	Okubo Zweig Iizuka
QCD	Quantum Chromodynamics
QED	Quantum Electrodynamics
QFT	Quantum Field Theory
RχT	Resonance Chiral Theory
RGE	Renormalisation Group Equation
SM	Standard Model
T	Time Reversal
UV	Ultraviolet
VEV	Vacuum Expectation Value
VMD	Vector Meson Dominance

To my wife, Aida,
for her love, support and patience.

Chapter 1

Introduction

The Standard Model of particle physics (SM) is our current best scientific theory to describe the most fundamental building blocks of Nature, encapsulating our understanding of elementary particles and their interactions. Specifically, it is a mathematically consistent $SU(3)_C \times SU(2)_L \times U(1)_Y$ gauge theory of the strong, electromagnetic and weak interactions [1, 2].

The SM consists of two gauge field theories: i) quantum chromodynamics (QCD), which is the non-abelian $SU(3)_C$ component of the $SU(3)_C \times SU(2)_L \times U(1)_Y$ SM gauge group, it is non-chiral and it describes the strong interactions of coloured quarks and gluons, and ii) the (standard model of) electroweak interactions, which is based on the $SU(2)_L \times U(1)_Y$ gauge group, it is chiral and its gauge symmetry group is spontaneously broken down to $U(1)_Q$ after electroweak symmetry breaking, generating the mass of the weak bosons through the Higgs mechanism [1–6], as well as the mass of all quarks and charged leptons from Yukawa terms in the SM Lagrangian.

As it is well known, asymptotic freedom is a property of some non-abelian gauge theories, such as QCD [7, 8], that results in an energy-dependent behaviour of the coupling constant —otherwise known as the running of the coupling— such that it becomes weaker at short distances or high momentum, enabling the use of perturbative techniques to perform calculations in this energy regime. This, indeed, is the case for QCD where at high energies one can construct a perturbative expansion in powers of the renormalised coupling $\alpha_s(\mu_R^2)$ to obtain theoretical predictions for physical observables.[1] Contrary to this, perturbation theory fails to be applied in the low-energy regime of QCD, as the expansion in powers of α_s no longer converges [3, 4]. In the non-perturbative regime of QCD, other techniques such as effective field theories, dispersive techniques or lattice QCD are required to make progress.

Most aspects of the SM have been successfully tested in detail at colliders, accelerators and non-accelerator experiments, and it has precisely predicted a wide variety of physical phenomena [2, 9]. In addition, it has provided a successful framework for many observations in cosmology and astrophysics [2]. Among its major triumphs are the agreement with experiment of the anomalous magnetic dipole moment of the electron to within 1 part in a trillion [10], the successful prediction of the existence of the Higgs boson, the gluon, the top and charm quarks, and the W and Z bosons (as well as their masses) [11]. Despite its huge successes, the SM leaves some phenomena unexplained and, thus, there are reasons to believe that the SM is not the *final* theory [12]. For example, it fails to incorporate Einstein's theory of General Relativity, it does not provide a viable dark matter particle candidate with the required properties as deduced from astrophysical and cosmological observations,[2] and it does not fully explain the observed matter-antimatter asymmetry present in the universe. Moreover, the SM neutrinos are massless whilst the observed neutrino oscillations in flight require them to have a small mass and whether they are Dirac or Majorana particles is still

[1] Of course, μ_R is an unphysical renormalisation scale and, thus, all physical observables must be independent of it.

[2] It must be noted that modified gravity models can account for galaxy rotation measurements and, thus, may provide an explanation for dark matter. A review of these ideas is outside the scope of the present work though.

unclear. In addition, the so-called hierarchy problem presents an important challenge to the SM as one would *naturally* expect that the mass of the Higgs boson, which has been experimentally established to be at the electroweak energy scale —i.e. $m_H = 125.25 \pm 0.17$ GeV $\sim \Lambda_{\rm EW} (\sim 100$ GeV)—, should receive huge quantum contributions bringing it up to the next energy scale for new physics —such as, e.g., the Planck scale, $\Lambda_{\rm Planck} \sim 10^{19}$ GeV— unless there is an exquisitely precise cancellation between the quadratic radiative corrections and the Higgs bare mass [2]. Supersymmetry and warped extra dimensions have long been postulated as potential solutions to the hierarchy problem but the lack of any experimental evidence after years of extraordinary efforts at high energy colliders have led these theories to loose traction.

It is likely that the SM is just a low-energy approximation to some currently unknown ultraviolet (UV) completion theory, where the SM Lagrangian represents the leading order term of the more fundamental theory in the effective field theory (EFT) perturbative expansion. Should this be the case, then it would be remarkable that the leading term of such an EFT expansion is a perturbatively renormalisable quantum field theory (QFT) in the conventional sense, which means that, technically, the SM is a mathematically consistent and fully predictive theory all the way up to the Planck scale, where the effects of quantum gravity ought to become important. In this sense, it is not beyond the realm of possibility that there may be no intermediate particle physics between the electroweak energy scale and the Planck mass [13].

Given the current economic, social and political state of affairs —as well as the public perception—, the option of building new particle accelerators in the future with even higher energies that may help shed light into the above issues remains uncertain, which calls for different strategies to find new physics beyond the Standard Model (BSM). An interesting alternative to direct searches is precision measurements that may be sensitive to new physics. These measurements, which are carried out at low-energy high-intensity experimental facilities, are compared with theoretical predictions from the SM and any potential deviations that may appear would then be attributed to the effect of BSM physics. Of course, to fully exploit this experimental programme, adequate and precise theoretical predictions are crucial.

In this context, the phenomenology of the neutral and long-lived η and η' mesons provides a unique flavour-conserving laboratory to test low-energy QCD and search for new BSM physics [14], which is down to the special nature of these mesons. In particular [14, 15],

- the η meson is a pseudo-Goldstone boson of the spontaneously broken chiral symmetry of QCD,
- the η' meson is largely influenced by the axial $U(1)_A$ anomaly of QCD,
- the η and η' mesons are eigenstates of the charge conjugation (C), parity (P), the product CP, and G-parity operators,
- all their additive quantum numbers are zero, which amounts to all their decays being flavour-conserving, and
- all their strong and electromagnetic decays are forbidden at lowest order due to symmetries (e.g. C, P, angular momentum, G-parity, etc.), which means that the SM contribution to their decays is highly suppressed.

Accordingly, the η and η' decays provide extraordinary opportunities to test the chiral dynamics of QCD at low energies, extract fundamental parameters of the SM such as the light quark masses, study potential small violations of the discrete fundamental symmetries and, possibly, provide a window to the dark sector (i.e. BSM physics) [14, 15].

In this thesis, we investigate several phenomenological aspects of the η and η' mesons with the aim of contributing to improve the state of knowledge through the calculation of some novel or improved SM theoretical predictions, so that comparison with future measurements in high-intensity low-energy experiments allows to confirm, or otherwise, any potential departure from the SM and, therefore, new physics BSM.

In the first five chapters, we provide a brief introduction to the theoretical framework that is employed in subsequent chapters. In particular, Chapter 2 presents a basic introduction to QCD, including a discussion of the symmetries of the QCD Lagrangian, as well as the quark model and the axial $U(1)_A$ anomaly of QCD. Chapter 3 covers the topic of effective field theories (EFTs) and presents some useful EFTs to characterise QCD in the low- and medium-energy regimes, such as chiral perturbation theory (χPT), large number of colours (large-N_C) χPT, resonance chiral theory (RχT), vector meson dominance (VMD) and the $U(3) \times U(3)$ linear sigma model (LσM). In addition, we provide a concise account of the Standard Model effective field theory (SMEFT). Chapter 4 is dedicated to the analysis of the η-η' mixing within the framework of large-N_C χPT, which enables the inclusion of the η' as the ninth pseudo-Goldstone boson of the spontaneously broken $U(3)_L \times U(3)_R \to U(3)_V$ chiral symmetry of QCD. In Chapter 5, we explore the complex plane in elementary particle physics, and we discuss topics such as the S-matrix, resonances and dispersion relations. We conclude Part I of this thesis with Chapter 6, which introduces the topic of CP violation in the SM, including a discussion of discrete symmetries and CP violation in the quark sector.

In the following five chapters, we present the contribution to knowledge of this thesis. Specifically, we present in Chapter 7 an enhanced phenomenological model that includes violations of the isospin symmetry to quantify the admixtures of the η and η' with the π^0 in the context of radiative transitions between vector (V) and pseudoscalar (P) mesons. We then proceed to perform statistical fits to the most recent $VP\gamma$ experimental data, which shows that the current experimental uncertainties allow for isospin-symmetry violations with a confidence level of approximately 2.5σ. In Chapter 8, we perform a detailed analysis of the doubly radiative decays $\eta^{(\prime)} \to \pi^0\gamma\gamma$ and $\eta' \to \eta\gamma\gamma$ within the VMD and LσM frameworks. We provide theoretical predictions for the diphoton invariant mass distributions and associated integrated branching ratios, and we compare them with the available experimental data. In Chapter 9, we study the sensitivity of the $\eta^{(\prime)} \to \pi^0\gamma\gamma$ and $\eta' \to \eta\gamma\gamma$ decays to signatures of a leptophobic B boson in the MeV–GeV mass range using the VMD and LσM frameworks to characterise the exchange of vector and scalar resonances within the SM. Using experimental data for these processes, we improve the current constraints on the B-boson mass m_B and coupling to SM particles α_B. In Chapter 10, we present an in-depth analysis of the C-conserving semileptonic decays $\eta^{(\prime)} \to \pi^0 l^+ l^-$ and $\eta' \to \eta l^+ l^-$, with $l = e$ or μ, within the framework of the VMD model and provide predictions for the decay widths and dilepton energy spectra. In Chapter 11, we investigate the prospect of observing new-physics signatures through CP violation in $\eta^{(\prime)} \to \pi^0 \mu^+ \mu^-$ and $\eta' \to \eta \mu^+ \mu^-$ decays at the REDTOP experiment using the SMEFT as the theoretical framework to parameterise BSM CP-violating effects. We find that the experiment's projected statistics are not competitive, using the above semileptonic decays, with respect to the limits already stablished by the neutron electric dipole moment (nEDM) experiments.

We conclude this thesis with a summary of the work carried out and an overview of our findings in Chapter 12, together with some final conclusions.

Part I

THEORETICAL FRAMEWORK

Chapter 2

Quantum chromodynamics

In this chapter, the essential concepts of quantum chromodynamics (QCD) are introduced. The QCD Lagrangian is presented, alongside its fundamental properties, and a discussion of its exact and approximate symmetries is given. Moreover, a brief presentation of the quark model and the axial $U(1)_A$ anomaly of QCD is provided.

2.1 Introduction

Quantum chromodynamics is the modern theory of the strong interactions. Its fundamental degrees of freedom are non-chiral spin-1/2 fermion fields, known as quarks, and spin-1 gauge boson fields, called gluons, with their dynamical behaviour being controlled by the non-abelian gauge theory of $SU(3)$ coloured charges.

The choice of gauge group comes down to the empirical fact that the quarks are colour triplets but all the hadrons, which are complex bound systems of quarks and gluons, are colour singlets (i.e. colour neutral) [16]. Accordingly, quarks are said to be in the fundamental representation of the $SU(3)$ colour group, whilst gluons transform under the adjoint representation of the $SU(3)$ colour group [1]. Neither quarks nor gluons are observed as free particles in Nature.

The QCD Lagrangian is given by [2]

$$\mathcal{L}_{\text{QCD}} = -\frac{1}{4}G^i_{\mu\nu}G^{i\mu\nu} + \sum_f \bar{q}^A_f i\not{D}^B_A q_{fB} - \sum_f m_f \bar{q}^A_f q_{fA} + \theta_{\text{QCD}}\frac{g_s^2}{32\pi^2}G^{i\mu\nu}\widetilde{G}^{i\mu\nu}\,, \quad (2.1)$$

where μ and ν are Lorentz indices, A and B are gauged colour indices running from 1 to $N_C = 3$ (i.e. quarks come in three colours), $f = u, d, s, c, b, t$ is the ungauged flavour index, and the gluon field strength tensor can be written as

$$G^i_{\mu\nu} = \partial_\mu G^i_\nu - \partial_\nu G^i_\mu - g_s f_{ijk} G^j_\mu G^k_\nu\,, \quad (2.2)$$

with $G^i = G^{i\dagger}$ being the eight Hermitian gluon fields and i, j, k running from 1 to $N_C^2 - 1 = 8$. Furthermore, g_s in Eqs. (2.1) and (2.2), often expressed as $\alpha_s = g_s^2/4\pi$, is the QCD coupling constant, $\widetilde{G}^i_{\mu\nu}$ is the dual of the gluon field tensor, i.e. $\widetilde{G}^i_{\mu\nu} \equiv \frac{1}{2}\epsilon_{\mu\nu\sigma\rho}G^{i\sigma\rho}$, and the gauge covariant derivative is given by

$$D^{\mu B}_A \equiv (D^\mu)_{AB} = \partial^\mu \delta^B_A - i g_s G^{\mu B}_A\,, \quad (2.3)$$

where

$$G^B_A = (G^A_B)^\dagger = \sum_{i=1}^{8} G^i T^i_{AB} \quad (2.4)$$

represents the gluon field in tensor or matrix notation. Moreover, the $T^i_{AB} \equiv \lambda^i_{AB}/2$ are the eight 3×3 generators of the $SU(3)$ group, which encode the fact that a gluon's interaction

with a quark rotates the quark's colour in $SU(3)$ space [1], with λ_i being the eight linearly independent, Hermitian and traceless Gell-Mann matrices, i.e.

$$\lambda_1 = \begin{pmatrix} 0 & 1 & 0 \\ 1 & 0 & 0 \\ 0 & 0 & 0 \end{pmatrix}, \quad \lambda_2 = \begin{pmatrix} 0 & -i & 0 \\ i & 0 & 0 \\ 0 & 0 & 0 \end{pmatrix}, \quad \lambda_3 = \begin{pmatrix} 1 & 0 & 0 \\ 0 & -1 & 0 \\ 0 & 0 & 0 \end{pmatrix},$$

$$\lambda_4 = \begin{pmatrix} 0 & 0 & 1 \\ 0 & 0 & 0 \\ 1 & 0 & 0 \end{pmatrix}, \quad \lambda_5 = \begin{pmatrix} 0 & 0 & -i \\ 0 & 0 & 0 \\ i & 0 & 0 \end{pmatrix}, \quad \lambda_6 = \begin{pmatrix} 0 & 0 & 0 \\ 0 & 0 & 1 \\ 0 & 1 & 0 \end{pmatrix}, \tag{2.5}$$

$$\lambda_7 = \begin{pmatrix} 0 & 0 & 0 \\ 0 & 0 & -i \\ 0 & i & 0 \end{pmatrix}, \quad \lambda_8 = \frac{1}{\sqrt{3}} \begin{pmatrix} 1 & 0 & 0 \\ 0 & 1 & 0 \\ 0 & 0 & -2 \end{pmatrix},$$

which satisfy the Lie algebra

$$[T^i, T^j] = i f_{ijk} T^k, \tag{2.6}$$

where f_{ijk} are the structure constants of the $SU(3)$ group.

The Feynman rules associated to the QCD Lagrangian are a quark-antiquark-gluon ($q\bar{q}g$) vertex proportional to g_s, a 3-gluon vertex proportional to g_s and a 4-gluon vertex proportional to g_s^2 [1]. The triple and quartic gluon self-interaction terms, which ultimately are responsible for the asymptotic freedom property of QCD [3, 4], originate from the third term in Eq. (2.2). In order to be able to use perturbation theory with the Lagrangian from Eq. (2.1), a gauge fixing term is required so that the propagator for the gluon field can be properly defined [3, 9]. The choice

$$\mathcal{L}_{\text{gauge-fixing}} = -\frac{1}{2\lambda} (\partial^\mu G^i_\mu)^2 \tag{2.7}$$

fixes the class of covariant gauges with gauge parameter λ. In addition, given that QCD is a non-abelian theory, the gauge fixing term must be supplemented by a ghost term. This is usually expressed as

$$\mathcal{L}_{\text{ghost}} = \partial_\mu \eta^{i\dagger} (D^\mu_{ij} \eta^j), \tag{2.8}$$

where η^i is a complex scalar field which obeys Fermi statistics and D^μ_{ij} is the covariant derivative in the adjoint representation of $SU(3)$ [3, 9]. This class of Lagrangian terms are known as Faddeev-Popov ghosts.

The strong interactions are invariant under the discrete symmetries *charge conjugation* (C), *parity inversion* (P), *time reversal* (T), and the CP and CPT products. The first three terms in Eq. (2.1) respect these symmetries. The last term, which is associated to the more complicated structure of the QCD vacuum, observes gauge invariance and does not spoil the renormalisability of QCD but it can lead to large violations of CP unless the phase parameter θ_{QCD} is very small [2]. Experimentally, limits on ultracold neutrons and atomic mercury constrain this parameter to $\theta_{\text{QCD}} \lesssim 10^{-10}$ [1]. The question as to why the θ_{QCD} phase is so small in Nature is referred to as the strong CP problem and, whilst several potential solutions have been proposed over the decades such as the Peccei-Quinn mechanism [17, 18], the puzzle remains unresolved.

Apart from the phase parameter θ_{QCD} and the *current* quark masses m_f, which are generated by the spontaneous breaking of the electroweak symmetry,[1] the only free parameter in QCD is the strong coupling constant $g_s(\mu_R^2)$. Its value in turn depends on the

[1] Note that, when one considers QCD alone, the m_f parameters can be thought of as bare masses.

renormalisation scale μ_R, which is taken to be the typical momentum scale of the process. This dependence is known as the *running* of the renormalised strong gauge coupling whereby $\alpha_s(\mu_R^2) = g_s^2(\mu_R^2)/4\pi$ decreases for large μ_R (short distance) and the theory becomes asymptotically free with quasi-free quarks and gluons [2, 5], enabling a perturbative analysis of QCD (pQCD) in this regime. For small μ_R (large distance), $\alpha_s(\mu_R^2)$ becomes large and perturbation theory can no longer be employed. The strong coupling and gluon self-interactions (presumably) lead to the *confinement* of quarks, gluons and any coloured states, so that only colour-singlet hadrons (i.e. mesons and baryons) can emerge [2]. In experiments, though, both regimes may be important to account for different aspects of a process. Fortunately, for many processes the short- and long-distance effects can be factorised, with the short-distance effects being calculable using pQCD and the long-distance effects can be accounted for by means of parton distribution function, which in turn are obtained directly from experiment [2, 9]. Notwithstanding this, for some other low-energy processes alternative approaches such as QCD lattice or effective field theories, e.g. chiral perturbation theory (χPT), are required to make progress [19].

The strong coupling constant, $\alpha_s(\mu_R^2)$, satisfies the following renormalisation group equation (RGE)

$$\mu_R^2 \frac{d\alpha_s}{d\mu_R^2} = \beta(\alpha_s) = -(b_0\alpha_s^2 + b_1\alpha_s^3 + b_2\alpha_s^4 + \cdots)\,, \tag{2.9}$$

where[2] $b_0 = (11C_A - 4n_f T_R)/(12\pi) = (33 - 2n_f)/(12\pi)$ is referred to as the 1-loop β-function coefficient, with n_f being the number of quark flavours, the 2-loop coefficient is $b_1 = [17C_A^2 - n_f T_R(10C_A + 6C_F)]/(24\pi^2) = (153 - 19n_f)/(24\pi^2)$, and the 3-loop coefficient is $b_2 = (2857 - \frac{5033}{9}n_f + \frac{325}{27}n_f^2)/(128\pi^3)$ [1]. The coefficient b_2 is renormalisation-scheme dependent and here the modified minimal subtraction scheme ($\overline{\text{MS}}$) has been adopted. One must note that the minus sign on the right-hand side of Eq. (2.9) is the origin of asymptotic freedom. It is important to note that the β-function coefficients, b_i, are given for the coupling of an effective theory in which n_f out of all the quark flavours are considered light, i.e. $m_f \ll \mu_R$, whilst the heavier quark flavours decouple from the theory [1]. Assuming a constant number of flavours and neglecting all the β-function coefficients but b_0, one can easily find the analytic solution

$$\alpha_s(\mu_R^2) = \left[b_0 \ln\left(\frac{\mu_R^2}{\Lambda^2}\right)\right]^{-1}, \tag{2.10}$$

where Λ is a constant of integration corresponding to the scale at which the perturbative expansion of the coupling no longer converges.

As already mentioned, free quarks have never been observed and this experimental fact is understood as a result of the confining property of the strong interactions at long distances. Accordingly, the up (u), down (d), strange (s), charm (c) and bottom (b) quarks all hadronise, whilst the top (t) quark decays before it has time to hadronise [1]. The fact that free quarks are not found in Nature raises difficulties when defining their masses. Two prescriptions are usually employed: i) the pole mass, m_q, which corresponds to the position of the pole of the quark propagator and has got a clearer physical interpretation but suffers from non-perturbative ambiguities, and ii) the $\overline{\text{MS}}$ mass, $\overline{m}_q(\mu_R^2)$, which depends on the renormalisation scale μ_R and is, therefore, not physical. Light quark masses are often quoted in

[2] Some useful colour algebra relations are in order at this point [1]: $T^i_{AB}T^i_{BC} = C_F\delta_{AC}$, where $C_F \equiv (N_C^2 - 1)/(2N_C) = 4/3$ is the colour factor associated with gluon emission from a quark; $f_{ijk}f_{ljk} = C_A\delta_{il}$, where $C_A \equiv N_C = 3$ is the colour factor associated with gluon emission from a gluon; and $T^i_{AB}T^j_{AB} = T_R\delta_{ij}$, where $T_R = 1/2$ is the colour factor for a gluon to split into a $q\bar{q}$ pair.

the $\overline{\text{MS}}$ scheme at the $\mu_R \sim 2$ GeV scale, whilst the masses of the heavier quarks are quoted using either prescription. The pole and $\overline{\text{MS}}$ masses are related by [1]

$$m_q = \overline{m}_q(\overline{m}_q^2)\left[1 + \frac{4\alpha_s(\overline{m}_q^2)}{3\pi} + \mathcal{O}(\alpha_s^2)\right], \tag{2.11}$$

whilst the scale-dependence of $\overline{\text{MS}}$ masses is given at lowest order by [1]

$$\mu_R^2 \frac{d\overline{m}_q(\mu_R^2)}{d\mu_R^2} = \left[-\frac{\alpha_s(\mu_R^2)}{\pi} + \mathcal{O}(\alpha_s^2)\right]\overline{m}_q(\mu_R^2)\,. \tag{2.12}$$

To conclude this section, it is worth highlighting that hadrons not involving the c or b quarks receive relatively little contribution from the current quark masses and, thus, their masses are dominated by the dynamical or constituent quark mass $m_{\text{dyn}} \sim M_{p,n}/3 \sim \Lambda_{\text{QCD}}$, which is associated to the spontaneous breaking of the $SU(3)_L \times SU(3)_R$ chiral symmetry of QCD. The exception to this is the pseudoscalar octet, which are pseudo-Goldstone bosons with masses generated by the explicit chiral breaking from the current quark masses [2].

2.2 Symmetries of the QCD Lagrangian

2.2.1 Local gauge invariance

The QCD Lagrangian in Eq. (2.1) has the property that it is invariant under the colour $SU(3)$ group of local gauge transformations of the quark fields [3, 4]

$$q(x) \to Uq(x) \equiv e^{i\theta_j(x)T^j}q(x)\,, \tag{2.13}$$

where θ_i are the group parameters, T^i are the generators of the $SU(3)$ group of transformations, with Lie algebra defined by the commutation relations from Eq. (2.6), and a summation over the repeated index j is implicit.

Imposing local gauge invariance on the free Dirac Lagrangian of coloured quark fields requires the introduction of eight gauge boson fields G_μ^i, the gluons, which transform as

$$G_\mu^i \to G_\mu^i + \frac{1}{g}\partial_\mu\theta^i - f_{ijk}\theta^j G_\mu^k \tag{2.14}$$

and a covariant derivative of the form [cf. Eq. (2.3)]

$$\partial^\mu \to D_\mu \equiv \partial_\mu - ig_s T_j G_\mu^j\,, \tag{2.15}$$

which ultimately leads to the Lagrangian shown in Eq. (2.1), after adding the gauge-invariant free Lagrangian term for the gluon fields, i.e. $-\frac{1}{4}G_{\mu\nu}^i G_i^{\mu\nu}$.

Local gauge invariance requires the gauge fields to be massless, since a Proca-like mass term in the Lagrangian violates local gauge symmetry [3, 4, 6, 20]. Consequently, one must resort to a subtle procedure involving the introduction of a complex scalar doublet field (the Higgs field), the spontaneous breaking of the electroweak gauge symmetry $SU(2)_L \times U(1)_Y \to U(1)_Q$ and the so-called Higgs mechanism, in order to generate the masses for the $W^\pm$ and Z weak gauge bosons. Similarly, the quark (and charged lepton) masses cannot be introduced through the standard Dirac Lagrangian mass term, $-mq\bar{q}$, as it spoils the $SU(2)_L$ symmetry of the electroweak interactions and, therefore, the renomalisability of the gauge theory [2, 6, 20]. In order to address this, the masses of the quarks have to be generated by means of additional Yukawa terms in the SM Lagrangian, coupling the fermions to

the Higgs doublet, which, after spontaneous breaking of the electroweak symmetry, acquires a non-zero vacuum expectation value, ultimately leading to the generation of the fermion masses [3, 4, 20].

Before concluding this subsection, it is worth highlighting that the introduction of the gauge fixing term of Eq. (2.7) into the general QCD Lagrangian explicitly spoils its gauge invariance [4, 9]. However, this is innocuous in this particular case, as the S-matrix elements and, therefore, the physical observables, remain independent of the gauge fixing choice λ [9].

2.2.2 Exact symmetries

According to Weinberg [6, 21], quantum field theory appears to be an inevitable consequence of Lorentz invariance, quantum mechanics and cluster decomposition, without additional assumptions about locality or causality. Consequently, QCD includes the full symmetry group of special relativity, i.e. rotations in space and boosts, which in turn expresses the proposition that the laws of physics are the same for all inertial observers. Even though some approaches to quantum gravity appear to require small violations of Lorentz invariance at energies approaching the Planck scale, currently, there is no experimental evidence for low-energy Lorentz-violating signatures that may suggest that Lorentz invariance is not an exact symmetry of Nature. In addition, the local gauge symmetry of colour $SU(3)$ discussed in the previous subsection is believed to be an exact symmetry of the QCD Lagrangian, which in turn is required to ensure unitarity[3] for massless spin-1 fields.[4] As it turns out, non-abelian gauge theories with spontaneous symmetry breaking, such as the SM, happen to be renormalisable in the conventional sense [22].

The first two terms of the QCD Lagrangian in Eq. (2.1) are invariant under the discrete symmetries P, C and T, which are satisfied individually and in combination (e.g. CPT invariance). These discrete symmetries are in agreement with the observed properties of the strong interactions [1, 9]. However, the additional gauge invariant term of mass dimension four that can be added to the QCD Lagrangian, i.e. the third term in Eq. (2.1), which is associated to the complicated structure of the QCD vacuum [23–25], complicates the analysis of the above discrete symmetries at the quantum level. An interaction term like this violates both P and T but conserves C, so it violates CP. However, the strong interactions are invariant under CP, which means that the phase θ_{QCD} must be very small to account for the experimental evidence. It should be noted that setting $\theta_{\text{QCD}} = 0$ would not solve the problem, as it could still be regenerated by CP-violating effects from the electroweak interactions that are known to exist in Nature [9].

2.2.3 Approximate symmetries

In this subsection, we follow the presentation of Ref. [9] as it introduces the different approximate symmetries in a natural and logical manner.

Let us begin by considering just the u and d quark fields from the quark sector of the QCD Lagrangian from Eq. (2.1)

$$\mathcal{L}_{\text{q}} = \sum_{f=u,d} \bar{q}_f (i \not{D} - m_f) q_f \,. \tag{2.16}$$

[3] Unitarity implies that, in the Schrödinger picture, the norm of a state $|\Psi, t\rangle$ is constant for all t, which in a quantum theory is equivalent to the statement of conservation of probability.

[4] For the optical theorem to hold in general, which is a direct consequence of unitarity, the numerator of a propagator must be equal to the sum over physical spin states [4]. This for massless spin-1 fields is achieved so long as gauge invariance and the Ward identity hold.

A global phase redefinition of the quark fields leaves the Lagrangian invariant, giving rise to the conservation of baryon number in the strong interactions.

Next, we consider approximate symmetries that couple different quark flavours. To this end, one can rewrite Eq. (2.16) as

$$\mathcal{L}_{\rm q} = \bar{q}(i\not{D} - M)q\,, \tag{2.17}$$

where matrix notation for the quark fields has been introduced,[5]

$$q = \begin{pmatrix} u \\ d \end{pmatrix}, \tag{2.18}$$

and the mass matrix M is given by

$$M = \begin{pmatrix} m_u & 0 \\ 0 & m_d \end{pmatrix}. \tag{2.19}$$

Since $m_d - m_u$ is much smaller than the hadronic mass scale ($\Lambda_{\rm QCD} \sim 250$ MeV), one can assume that the masses of the up and down quarks are approximately degenerate, $m_u \approx m_d$. A direct consequence of this is that the mass matrix can now be factorised and the symmetry of the Lagrangian is significantly enhanced, becoming invariant under a $SU(2)$ transformation acting on the quark fields

$$q \to U(\phi_\alpha)q = e^{i\frac{\vec{\phi}\cdot\vec{\sigma}}{2}}q\,, \tag{2.20}$$

where the σ^i, with $i = 1, 2, 3$, are the Pauli matrices taken to be

$$\sigma^1 = \begin{pmatrix} 0 & 1 \\ 1 & 0 \end{pmatrix}, \quad \sigma^2 = \begin{pmatrix} 0 & -i \\ i & 0 \end{pmatrix}, \quad \sigma^3 = \begin{pmatrix} 1 & 0 \\ 0 & -1 \end{pmatrix}. \tag{2.21}$$

The above $U(2)_V$ symmetry can be decomposed into the product $SU(2)_V \times U(1)_V$, where $SU(2)_V$ corresponds to the isotopic spin symmetry (isospin), which becomes exact in the $m_u = m_d$ limit, and $U(1)_V$ to the quark number conservation. According to Noether's theorem, the conserved currents associated to isospin can be written as

$$J_i^\mu = \bar{q}\gamma^\mu\sigma_i q\,. \tag{2.22}$$

The flavour $SU(2)_V$ symmetry can be increased by assuming that the strange quark also degenerates in mass, i.e. $m_u \approx m_d \approx m_s$. This gives rise to the approximate flavour $SU(3)_V$ symmetry, which ultimately enables the classification of the hadrons in various irreducible representations [26]: an octet of $1/2^+$ baryons p, n, Λ^0, $\Sigma^{\pm,0}$, $\Xi^{-,0}$; an octet of 0^- mesons $K^{+,0}$, $\pi^{\pm,0}$, η, $\overline{K}^{-,0}$; an octet of 1^- mesons $K^{*+,0}$, $\rho^{\pm,0}$, ω, $\overline{K^*}^{-,0}$; and a decuplet of $3/2^+$ baryons $\Delta^{++,+,0,-}$, $\Sigma^{*+,0,-}$, $\Xi^{*0,-}$, Ω^-.

Given that the masses of the three light quarks (i.e. u, d and s) are significantly smaller than the masses of the heavy quarks (i.e. c, b and t), one may assume that $m_{u,d,s} = 0$, which largely enhances the symmetry of the QCD Lagrangian. Introducing the left- and right-handed projection operators

$$\gamma_L = \frac{1}{2}(1-\gamma^5), \quad \gamma_R = \frac{1}{2}(1+\gamma^5), \tag{2.23}$$

[5] A word of caution is in order here, as in this thesis q sometimes refers to a generic quark field whilst in other cases it refers to a vector of quark fields, and the distinction should be clear from the context.

which satisfy $\gamma_L^2 = \gamma_L, \gamma_R^2 = \gamma_R$ and $\gamma_L \gamma_R = 0$, allows one to decompose the quark fields into left- and right-handed components

$$\begin{aligned} q_L &= \gamma_L q = \frac{1-\gamma^5}{2} q\,, \\ q_R &= \gamma_R q = \frac{1+\gamma^5}{2} q\,, \end{aligned} \tag{2.24}$$

which in the quark massless limit correspond to the negative and positive helicities, respectively. The Lagrangian from Eq. (2.17) can, therefore, be written in this limit as

$$\mathcal{L}_q = \bar{q}_L i \not{D} q_L + \bar{q}_R i \not{D} q_R\,. \tag{2.25}$$

One can easily see from Eq. (2.25) that the Lagrangian for massless quarks contains no coupling between the left- and right-handed fermion fields. This in turn means that this Lagrangian is invariant under two independent rotations of the left- and right-handed fields, yielding a global $U(3)_L \times U(3)_R$ symmetry

$$\begin{aligned} q_L \to q'_L &= e^{i\frac{\beta_a \lambda^a}{2}} q_L\,, \\ q_R \to q'_R &= e^{i\frac{\beta'_a \lambda^a}{2}} q_R\,, \end{aligned} \tag{2.26}$$

where the λ^a are the Gell-Mann matrices from Eq. (2.5), with a running from 1 to 8. This symmetry is known as the chiral symmetry of QCD, which is exact only in the quark massless limit.

In the absence of quark masses, the QCD Lagrangian contains no dimensional parameters. Accordingly, in this limit the Lagrangian is invariant under the scale transformations

$$q(x) \to \lambda^{3/2} q(\lambda x)\,, \quad G^i_\mu(x) \to \lambda G^i_\mu(\lambda x)\,, \tag{2.27}$$

with q and G^i being the quark and gluon fields, and QCD becomes scale invariant as a classical theory. Quantum corrections, though, result in the trace of the symmetric QCD energy-momentum tensor to take a non-zero value, known as the trace anomaly of QCD, which breaks the scale invariance of the quantum theory by introducing the renormalisation scale when defining the coupling constant [3–5]. The trace anomaly is, therefore, proportional to the β-function and is ultimately responsible for the origin of the hadron masses. An exception to this are the pseudoscalar mesons, which in the chiral limit are Nambu-Goldstone modes of a spontaneously broken global flavour-$SU(3)_A$ symmetry.

2.2.4 The chiral symmetry of QCD

As explained in previous subsection, in the chiral limit, i.e. $m_{u,d,s} \to 0$, the QCD Lagrangian is invariant under global $U(3)_L \times U(3)_R$ chiral transformations at the classical level. The flavour $U(3)_L \times U(3)_R$ group of symmetries can in turn be decomposed into $SU(3)_L \times SU(3)_R \times U(1)_L \times U(1)_R$ and the Noether currents associated to these (continuous) symmetries are [3]

$$\begin{aligned} J^\mu_L &= \bar{q}_L \gamma^\mu q_L\,, \quad J^\mu_R = \bar{q}_R \gamma^\mu q_R\,, \\ J^{\mu a}_L &= \bar{q}_L \gamma^\mu T^a q_L\,, \quad J^{\mu a}_R = \bar{q}_R \gamma^\mu T^a q_R\,, \end{aligned} \tag{2.28}$$

where, once again, the $T^a = \lambda^a/2$ are the generators of the $SU(3)$ group of symmetry transformations. The sum of left- and right-handed currents gives rise to the vector currents [2, 3]

$$J^\mu_V = J^\mu_R + J^\mu_L = \bar{q}\gamma^\mu q\,, \quad J^{\mu a}_V = J^{\mu a}_R + J^{\mu a}_L = \bar{q}\gamma^\mu T^a q\,, \tag{2.29}$$

whilst the difference results in the corresponding axial-vector currents

$$J^{\mu}_{A} = J^{\mu}_{R} - J^{\mu}_{L} = \bar{q}\gamma^{\mu}\gamma^{5}q\,, \quad J^{\mu a}_{A} = J^{\mu a}_{R} - J^{\mu a}_{L} = \bar{q}\gamma^{\mu}\gamma^{5}T^{a}q\,. \tag{2.30}$$

The above currents are conserved at the classical level but quantum effects known as anomalies spoil the conservation law for the singlet axial-vector current. As it turns out, the more complex nature of the QCD vacuum makes the $U(1)_A$ not a true symmetry of QCD, despite being an apparent symmetry of the QCD Lagrangian in the chiral limit [25].

The charges associated to the Noether currents in Eq. (2.28) are

$$Q_{L(R)} = \int d^{3}x\; J^{\mu}_{L(R)}(x)\,, \quad Q^{a}_{L(R)} = \int d^{3}x\; J^{\mu a}_{L(R)}(x)\,, \tag{2.31}$$

which enable one to write the vector and axial-vector charges as

$$\begin{aligned} Q_V &= Q_R + Q_L\,, \quad Q_A = Q_R - Q_L\,, \\ Q^{a}_{V} &= Q^{a}_{R} + Q^{a}_{L}\,, \quad Q^{a}_{A} = Q^{a}_{R} - Q^{a}_{L}\,, \end{aligned} \tag{2.32}$$

with the following behaviour under parity inversion [27]

$$\begin{aligned} Q_V &\xrightarrow{\mathrm{P}} Q_V\,, \quad Q_A \xrightarrow{\mathrm{P}} -Q_A\,, \\ Q^{a}_{V} &\xrightarrow{\mathrm{P}} Q^{a}_{V}\,, \quad Q^{a}_{A} \xrightarrow{\mathrm{P}} -Q^{a}_{A}\,. \end{aligned} \tag{2.33}$$

Spontaneous breaking of a symmetry occurs when the symmetry group of the solutions to a theory is dynamically determined to be less than the symmetry of the original Lagrangian [9]. This in turn happens when the ground state of the theory is not invariant under the full group of symmetry transformations. In the particular case that we are discussing, the QCD vacuum, $|0\rangle$, is invariant under the action of the vector charges but it is not under the action of the axial-vector charges

$$Q^{a}_{V}\,|0\rangle = 0\,, \quad Q^{a}_{A}\,|0\rangle \neq 0\,. \tag{2.34}$$

Accordingly, the octet of vector currents, $J^{\mu a}_{V}$, reflects the approximate flavour-$SU(3)_V$ symmetry, which is experimentally observed in the hadronic spectrum. As well as this, the conservation laws associated to the octet of axial-vector currents, $J^{\mu a}_{A}$, are not observed in the particle spectrum, suggesting that the global chiral $SU(3)_L \times SU(3)_R$ symmetry of the QCD Lagrangian is spontaneously broken down to $SU(3)_V$ and the $J^{PC} = 0^{-}$ pseudoscalar mesons appear in the physical spectrum as an octet of (pseudo-)Goldstone bosons [26, 28]. However, since the light-quark masses are non-zero, the chiral symmetry is also explicitly broken, giving rise to Goldstone particles that are not exactly massless [19, 28].

The fact that $Q^{a}_{A}\,|0\rangle \neq 0$, cf. Eq. (2.34), implies non-vanishing matrix elements of the axial-vector currents [27]. This in turn means that the octet of pseudoscalar mesons can be created by the axial-vector currents [3, 4]

$$\langle 0|\, J^{\mu a}_{A}(x)\,|\phi^{b}(p)\rangle = ip^{\mu} f_{\phi}\delta^{ab} e^{-ip\cdot x}\,, \tag{2.35}$$

where $\phi^{b} = \pi, K, \eta$ are Nambu-Goldstone modes and f_ϕ is the corresponding pseudoscalar decay constant. The divergence of the above matrix elements is given by

$$\langle 0|\, \partial_{\mu} J^{\mu a}_{A}(0)\,|\phi^{b}(p)\rangle = p^{2} f_{\phi}\delta^{ab}\,, \tag{2.36}$$

which explicitly shows that in the chiral limit the octet of axial-vector currents is conserved,

i.e. $p^2 = M_\phi^2 = 0$. For non-vanishing light-quark masses, the axial-vector currents are partially conserved only [3].

The mechanism responsible for the breaking of the chiral symmetry of QCD is directly connected to the ground state of QCD having a non-zero expectation value for the quark bilinears $\langle q\bar{q}\rangle$ [4]. This can be understood by noting that, if the quarks were massless, the energy cost of generating quark-antiquark pairs would be very small [3]. Since $m_{u,d} \approx 0$, the QCD vacuum is expected to contain a condensate of quark-antiquark pairs characterised by a non-zero vacuum expectation value

$$\langle 0|\, q\bar{q}\,|0\rangle = \langle 0|\, u\bar{u} + d\bar{d}\,|0\rangle \neq 0\,. \tag{2.37}$$

The fermion pairs that constitute this condensate must necessarily have zero total linear and angular momenta, as required by their associated conservation laws. This leads to the pairing of quarks and antiquarks with opposite helicities

$$\langle 0|\, q\bar{q}\,|0\rangle \equiv \langle 0|\, q_R\bar{q}_L + q_L\bar{q}_R\,|0\rangle\,. \tag{2.38}$$

This mixture of helicities causes the quarks to acquire effective masses as they move through the vacuum, ultimately spoiling the chiral symmetry of the strong interactions [3].

The chiral $U(3)_L \times U(3)_R$ decomposition into $SU(3)_L \times SU(3)_R \times U(1)_V \times U(1)_A$ presents two additional global symmetries: the $U(1)_V$ and $U(1)_A$ unitary symmetries. The former corresponds to the conservation of baryon number and, as already mentioned, the latter gives rise to neither a conserved current, $\partial_\mu J_A^\mu \neq 0$, nor a Goldstone boson in the physical spectrum. The non-conservation of the singlet axial-vector current results in the mass of the singlet pseudoscalar meson η' not vanishing in the chiral limit. The $U(1)_A$ anomaly of QCD and its solution will be studied in more detail in Sec. 2.4.

2.3 The quark model

Out of the degrees of freedom of QCD, gluons carry no intrinsic quantum numbers beyond colour charge, which is believed to be permanently confined in Nature. Consequently, most of the quantum numbers of strongly interacting particles —the hadrons— are given by the quantum numbers of the constituent quarks and antiquarks [1]. For this reason, the quark model, which describes the properties of hadrons emphasising the role of the minimum quark-content part of their wavefunction, generally works well providing a number of good predictions.

Back in the early 1960s, the $SU(3)$ symmetry group, which is an approximate global symmetry of the strong interactions and extends the $SU(2)$ isospin subgroup, was proposed by Gell-Mann and Y. Ne'eman [29, 30] to account for the fact that the low-lying mesons and baryons can be organised in octets. This classification in terms of baryons and mesons becomes much simpler when reexpressed in terms of the three lightest quarks, i.e. u, d and s. These transform under isospin as a doublet (u, d) and a singlet (s), whilst under $SU(3)$ as a fundamental triplet (and the antiquarks as $\overline{3}$) [2]

$$q = \begin{pmatrix} u \\ d \\ s \end{pmatrix} \to e^{i\frac{\vec{\beta}\cdot\vec{\lambda}}{2}} q\,, \quad \bar{q} = \begin{pmatrix} \bar{u} & \bar{d} & \bar{s} \end{pmatrix} \to \bar{q} e^{-i\frac{\vec{\beta}\cdot\vec{\lambda}}{2}}\,. \tag{2.39}$$

The $SU(3)$ symmetry group can be expressed in terms of its defining representation, the 3×3 unitary matrices with determinant one, where its $N = 8$ generators are given by $T^i = \lambda^i/2$, with the λ^i being the Gell-Mann matrices from Eq. (2.5). Given that the $SU(3)$ group has got rank 2, two generators, i.e. T^3 and T^8, can be simultaneously diagonalised

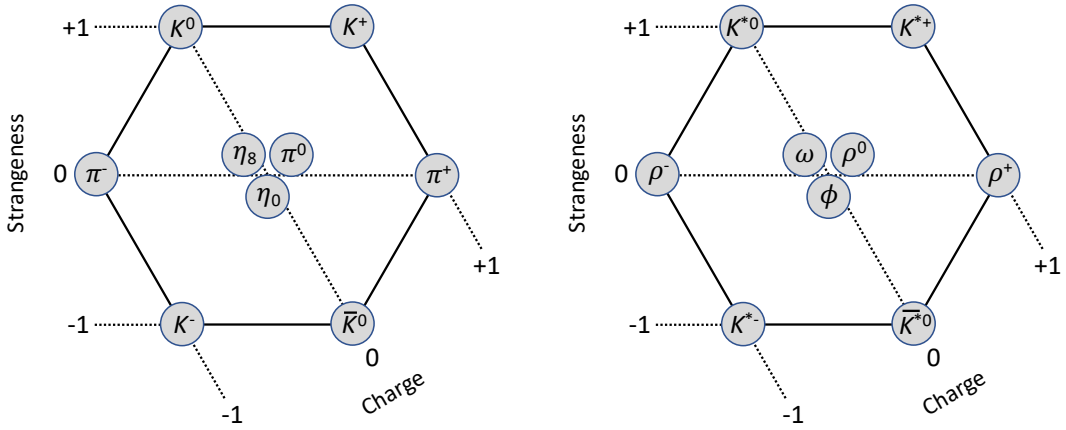

FIGURE 2.1: Nonet of pseudoscalar $J^{PC} = 0^{-+}$ and vector $J^{PC} = 1^{--}$ mesons consisting of up, down and strange quarks.

with the Hamiltonian [2]. These give rise to the quantum numbers

$$Q = I_3 + \frac{\mathcal{Y}}{2}, \quad I_3 = T^3, \quad \mathcal{Y} = \frac{2}{\sqrt{3}}\, T^8, \tag{2.40}$$

where Q is electric charge, I_3 is the third component of isospin and $\mathcal{Y} = B + S$ is the strong hypercharge, with B and S standing for baryon number and strangeness, respectively. The low-dimensional representations of $SU(3)$ are the 1, 3, $\overline{3}$, 6, $\overline{6}$, 8, 10, $\overline{10}$ and 27, with the 1, 8 (adjoint) and 27 being real, whilst the others complex. The observed light hadrons can be assigned to the 1, 8, 10 and $\overline{10}$ representations [2].

The approximate degeneracy of masses for the three light quarks gives rise to the flavour-$SU(3)$ symmetry, which is only roughly realised in Nature, but it still provides reasonable predictions to the $\sim 25\%$ level [2]. Much better predictions can be obtained from flavour $SU(2)$ —or isospin—, which is also an approximate global symmetry of the strong interactions, with violations of order $\sim 1\%$ down to the $u-d$ quark mass difference and electromagnetic effects (i.e. the u and d quarks have different charges).

In the quark model, the observed baryons are interpreted as three-quark states, i.e. qqq, with totally antisymmetric wavefunctions. In fact, the need to have an antisymmetric wavefunction for the Δ^{++} baryon constituted a crucial experimental hint for the introduction of colour charge as a new degree of freedom of the strong interactions.[6] The mesons in turn are bound quark-antiquark pair states, i.e. $q\bar{q}$, and have vanishing baryon number $B = 0$. A quark and antiquark can combine to form an octet and singlet, i.e. $3 \times \overline{3} = 8 + 1$. This is,[7]

$$\begin{aligned} q \times \bar{q} &= \begin{pmatrix} u\bar{u} & u\bar{d} & u\bar{s} \\ d\bar{u} & d\bar{d} & d\bar{s} \\ s\bar{u} & s\bar{d} & s\bar{s} \end{pmatrix} = M + \frac{\eta'}{\sqrt{3}}\, I \\ &= \begin{pmatrix} \frac{2u\bar{u}-d\bar{d}-s\bar{s}}{3} & u\bar{d} & u\bar{s} \\ d\bar{u} & \frac{2d\bar{d}-u\bar{u}-s\bar{s}}{3} & d\bar{s} \\ s\bar{u} & s\bar{d} & \frac{2s\bar{s}-u\bar{u}-d\bar{d}}{3} \end{pmatrix} + \frac{1}{3}\begin{pmatrix} u\bar{u} & d\bar{d} & s\bar{s} \end{pmatrix}\begin{pmatrix} 1 & 0 & 0 \\ 0 & 1 & 0 \\ 0 & 0 & 1 \end{pmatrix}, \end{aligned} \tag{2.41}$$

[6] The wavefunction of a baryon can be written as $|qqq\rangle_A = |\text{colour}\rangle_A \times |\text{space, spin, flavour}\rangle_S$, where the subscripts S and A stand for symmetric and antisymmetric under the exchange of any two equal-mass quarks [1].

[7] Note that in Eq. (2.41) and Table 2.1 we employ the common identifications of the physical η and η' states with the mathematical pseudoscalar octet and singlet states, respectively. For a detailed account of the η-η' mixing, see Chapter 4.

TABLE 2.1: Quark content, charge and mass of the lightest mesons.

J^P	Meson	Quark content	Charge	Mass [MeV]
0^-	$\pi^\pm$	$u\bar{d}$, $d\bar{u}$	$1, -1$	139.57039
	π^0	$(u\bar{u}-d\bar{d})/\sqrt{2}$	0	134.9768
	$K^\pm$	$u\bar{s}$, $s\bar{u}$	$1, -1$	493.677
	K^0, $\overline{K}^0$	$d\bar{s}$, $s\bar{d}$	0	497.611
	η	$(u\bar{u}+d\bar{d}-2s\bar{s})/\sqrt{6}$	0	547.862
	η'	$(u\bar{u}+d\bar{d}+s\bar{s})/\sqrt{3}$	0	957.78
0^+	$f_0(500)$ aka σ	$(u\bar{u}+d\bar{d}+s\bar{s})/\sqrt{3}$	0	~ 500
	$K_0^*(700)$ aka κ	$u\bar{s}$, $d\bar{s}$, $s\bar{d}$, $s\bar{u}$	$1, 0, -1$	~ 845
	$a_0(980)$	$u\bar{d}$, $(u\bar{u}-d\bar{d})/\sqrt{2}$, $d\bar{u}$	$1, 0, -1$	~ 980
	$f_0(980)$	$(u\bar{u}+d\bar{d}-2s\bar{s})/\sqrt{6}$	0	~ 990
1^-	ρ	$u\bar{d}$, $(u\bar{u}-d\bar{d})/\sqrt{2}$, $d\bar{u}$	$1, 0, -1$	775.26
	ω	$(u\bar{u}+d\bar{d})/\sqrt{2}$	0	782.66
	K^*	$u\bar{s}$, $d\bar{s}$, $s\bar{d}$, $s\bar{u}$	$1, 0, -1$	895.5
	ϕ	$s\bar{s}$	0	1019.461

where M is the pseudoscalar octet expressed in terms of quarks and $\eta' = (u\bar{u}+d\bar{d}+s\bar{s})/\sqrt{3}$ is the pseudoscalar singlet state [2]. Fig. 2.1 shows a graphical representation of the pseudoscalar meson nonet.

Quarks are strongly interacting spin-1/2 fermion fields and by convention have positive parity, whereas their associated antiparticles have negative parity. As well as this, quarks have additive baryon number $B = 1/3$ and antiquarks $B = -1/3$. By convention, the flavour quantum number of a quark has the same sign as its charge Q [1]. For an orbital angular momentum ℓ of the $q\bar{q}$ state, the parity P of the meson is found to be $P = (-1)^{\ell+1}$.[8] The meson's total angular momentum J is given by the well-known relation $|\ell - s| \leq J \leq |\ell + s|$, where $s = 0$ for anti-parallel quark spins and $s = 1$ for parallel quark spins. The charge conjugation C of the $q\bar{q}$ state, which is only defined for mesons made of quarks and their own antiquarks, is given by $C = (-1)^{\ell+s}$ and the generalised G-parity by $G = (-1)^{I+\ell+s}$, where I corresponds to the multiplet isospin [1].

The mesons are classified by their J, P and C quantum numbers in J^{PC} multiplets. The $\ell = 0$ states are the pseudoscalars (0^{-+}) and the vectors (1^{--}), whilst the $\ell = 1$ are the scalars (0^{++}), the axial vectors (1^{++}) and (1^{+-}), and the tensors (2^{++}). A summary of the lightest mesons showing their quark content, charges and masses is given in Table 2.1. It should be noted that mesons with natural spin-parity[9] and $CP = -1$ (i.e. 0^{+-}, 1^{-+}, 2^{+-}, etc.) are forbidden in the $q\bar{q}$ model, and so is the $J^{PC} = 0^{--}$ state. It is important to highlight that isoscalar states with the same J^{PC} mix, as we shall investigate in Chapter 7. The existence of other exotic meson states, such as tetraquarks and other non-$q\bar{q}$ states, is also predicted by the quark model but shall not be covered in this short review and the interested reader is referred to Chapter 15 of Ref. [1].

[8] Note that parity conservation for a multi-particle system, e.g. the $A \to B + C$ decay, implies $P(A) = P(B) \cdot P(C) \cdot (-1)^\ell$.

[9] Natural spin-parity states have $P = (-1)^J$.

2.4 The axial $U(1)_A$ anomaly of QCD

An anomaly occurs when a symmetry of the classical action is not a true symmetry of the full quantum theory.[10] Continuous symmetries imply conserved Noether currents but if a symmetry is anomalous then the associated Noether current is not conserved, receiving contributions that arise from quantum corrections [5]. If the non-conserved current couples to a massless spin-1 gauge boson, then the Ward identity is violated, unphysical longitudinal polarisations can be produced and unitarity is spoiled [4]. Accordingly, gauge symmetries must be anomaly free in a consistent quantum theory.[11] This is not the case for global anomalies as they do not lead to inconsistencies.

As explained in detail in some Sec. 2.2.4, the QCD Lagrangian for n_f quark flavours has got a large global symmetry, $U(n_f)_V \times U(n_f)_A$, in the limit of vanishing quark masses, $m_f \to 0$. Given that $m_{u,d,s} \ll \Lambda_{\rm QCD}$, the limit in which the mass of the three light quarks is sent to zero should be a sensible approximation and, thus, one would anticipate the strong interactions to be approximately $U(3)_V \times U(3)_A$ invariant [25]. Experimentally, one finds that the vector symmetry corresponding to flavour $SU(3)$ times baryon number, $U(3)_V = SU(3)_V \times U(1)_B$, is a good approximate symmetry of Nature. On the other hand, quark condensates $\langle u\bar{u}\rangle = \langle d\bar{d}\rangle \neq 0$ are dynamically generated, which spontaneously break the axial $U(3)_A$ symmetry down, and, thus, one expects to find experimental traces of nine Nambu-Goldstone bosons but only eight light pseudoscalar states are found in the hadronic spectrum, with no signs of the ninth light state, as $M^2_{\eta'} \gg M^2_{\pi^0}$.[12] This was coined the $U(1)_A$ problem by Weinberg [32]. The resolution to this problem is given by the axial anomaly of QCD,[13] which in turn can be understood through the direct analysis of the Adler-Bell-Jackiw [33, 34] fermion triangle diagram or, alternatively, by means of the path integral formalism [35]. In the former, if one or three of the fermion triangle vertices involve the coupling to an axial-vector current, the corresponding diagrams diverge linearly[14] resulting in an anomalous divergence of the currents in perturbation theory [2], whilst in the latter the fermion measure is not invariant under the anomalous symmetry transformation [35], with the anomaly arising from non-trivial Jacobian factors in the path integral measure.[15] Denoting $\langle J^\alpha_A J^\mu_V J^\nu_V\rangle$ as the matrix element for the 3-point function, one finds that $\partial_\mu\langle J^\alpha_A J^\mu_V J^\nu_V\rangle = 0$ and $\partial_\nu\langle J^\alpha_A J^\mu_V J^\nu_V\rangle = 0$, so that the Ward identity is satisfied for the vector currents, whereas $\partial_\alpha\langle J^\alpha_A J^\mu_V J^\nu_V\rangle \neq 0$, resulting in the axial current not being conserved in the quantum theory [4].

The axial anomaly has got two applications of particular importance in the SM. One is connected to the non-conservation of the flavour-$SU(3)$ singlet axial current discussed

[10] Note that we have a symmetry in classical physics if the symmetry transformation $\varphi \to \varphi + \delta\varphi$ leaves the action $S(\varphi)$ invariant. For the same symmetry to hold in the quantised version of the theory, the transformation must leave the path integral $\int [d\varphi]\, e^{iS(\varphi)}$ invariant. Of course, the integration measure $[d\varphi]$ is not necessarily invariant under the symmetry transformation, which may lead to anomalies.

[11] This is, of course, the case for the SM where the anomalies associated to the chiral $SU(2)_L \times U(1)_Y$ symmetry group cancel between quarks and leptons within a generation [4, 31]. There are no anomalies for pure QED or QCD since they are non-chiral [2].

[12] From the symmetry group theory factors, one finds that the mass of the diagonalised η' should satisfy $M_{\eta'} < \sqrt{3} M_{\pi^0}$ [32], which is not the case in Nature.

[13] The axial anomaly is also known as the $U(1)_A$ anomaly or chiral anomaly.

[14] The subtraction of linearly divergent integrals, that would vanish if one could shift the integration variable, are in fact finite with the result proportional to the shift [4].

[15] In particular, the effect on the path integral measure of fermion fields is

$$\int [d\bar{\psi}]\,[d\psi] \to \int [d\bar{\psi}]\,[d\psi] \exp\left(i\theta \int \frac{g_s^2}{32\pi^2} \epsilon^{\mu\nu\alpha\beta} G^a_{\mu\nu} G^a_{\alpha\beta} \right). \tag{2.42}$$

above. Explicit calculation of the anomalous triangle diagram results in [25]

$$\partial_\mu J^\mu_A = \frac{3g_s^2}{32\pi^2} G^a_{\alpha\beta}\widetilde{G}^{a\alpha\beta}\,, \qquad \left(\widetilde{G}^{a\alpha\beta} \equiv \frac{1}{2}\epsilon^{\alpha\beta\rho\sigma}G^a_{\rho\sigma}\right). \tag{2.43}$$

This effect is responsible for keeping the ninth pseudoscalar meson, the singlet η' state, from being a pseudo-Goldstone boson [5]. The other application is the decay $\pi^0 \to \gamma\gamma$ which, historically, led to the discovery of the $U(1)_A$ anomaly. In this instance, one is interested in the isovector axial current, $J^{(3)}_{A\mu}$, which transforms as the third component of a flavour-$SU(3)$ octet

$$J^{(3)}_{A\mu} = \bar{u}\gamma_\mu\gamma^5 u - \bar{d}\gamma_\mu\gamma^5 d\,. \tag{2.44}$$

Direct calculation shows that the divergence of this current is anomalous and does not vanish in the chiral limit [5]

$$\partial^\mu J^{(3)}_{A\mu} = 2i\left(m_u\bar{u}\gamma^5 u - m_d\bar{d}\gamma^5 d\right) + \frac{e^2 N_C}{24\pi^2}F_{\mu\nu}\widetilde{F}^{\mu\nu}\,, \tag{2.45}$$

where $F_{\mu\nu}$ is the electromagnetic field strength, $\widetilde{F}^{\mu\nu} \equiv \frac{1}{2}\epsilon^{\mu\nu\rho\sigma}F_{\rho\sigma}$ is its dual and N_C is the number of QCD colours. We can see that the divergence of the axial current in Eq. (2.45) is not zero, even in the quark-massless limit, and it is an operator capable of producing two photons [36].

There is a deep connection between the axial anomaly and the vacuum of QCD. Under the $U(1)_A$ transformation $q_f \to e^{i\alpha\gamma^5/2}q_f$, the chiral anomaly affects the action by [25]

$$\delta S = \alpha\int d^4x\,\partial_\mu J^\mu_A = \alpha\frac{g_s^2 n_f}{32\pi^2}\int d^4x\, G^{\mu\nu}_a\widetilde{G}_{a\mu\nu}\,. \tag{2.46}$$

However, one should note that the pseudoscalar density $G^{\mu\nu}_a\widetilde{G}_{a\mu\nu}$ may be written as a total derivative, i.e. $G^{\mu\nu}_a\widetilde{G}_{a\mu\nu} = \partial_\mu K^\mu$, with [37]

$$K^\mu = \epsilon^{\mu\nu\alpha\beta}\left(G^a_\nu G^a_{\alpha\beta} - \frac{g_s}{3}f^{abc}G^a_\nu G^b_\alpha G^c_\beta\right), \tag{2.47}$$

where G^a_μ and $G^a_{\mu\nu}$ are the gluon gauge fields and the associated field strength tensors, respectively. Accordingly, δS is a pure surface integral and, if one employs the naive boundary condition $G^a_\mu = 0$ at spatial infinity, then $\int d^4x\,\partial_\mu K^\mu = 0$ and the $U(1)_A$ appears to be a symmetry of QCD again. The resolution to this was given by 't Hooft in Refs. [23, 24] where he showed that the correct boundary conditions at spatial infinity are either $G^a_\mu = 0$ or a (topologically non-trivial) gauge transformation of 0. Employing these boundary conditions, then $\int d^4x\,\partial_\mu K^\mu \neq 0$ and the $U(1)_A$ turns out not to be a symmetry of QCD.

In the $G^a_0 = 0$ gauge, one has spatial gauge fields G^a_i only. Now, under a 'large' gauge transformation[16] $\Lambda(\mathbf{x})$, defined such that

$$G^a_i T^a \equiv G_i \to \Lambda(\mathbf{x})G_i\Lambda(\mathbf{x}) + \frac{i}{g_s}[\Delta_i\Lambda(\mathbf{x})]\Lambda^{-1}(\mathbf{x})\,, \tag{2.48}$$

where the T^a are the $SU(3)$ symmetry group generators, the vacuum configurations of QCD either vanish or have the form $ig_s^{-1}[\Delta_i\Lambda(\mathbf{x})]\Lambda^{-1}(\mathbf{x})$ (see Refs. [5, 25] for details). In this

[16] Gauge transformations that are homotopic (i.e. continuously deformable) to the identity are called 'small' gauge transformations, whilst homotopically non-trivial gauge transformations that cannot be deformed to the identity are called 'large' gauge transformations [38].

gauge, one can classify the vacuum configurations by how $\Lambda(\mathbf{x})$ goes to unity as $\mathbf{r} \to \infty$

$$\Lambda_n(\mathbf{x}) \to e^{i2\pi n} \text{ as } \mathbf{r} \to \infty, \text{ with } n = 0, \pm 1, \pm 2, \ldots, \tag{2.49}$$

where the integer n is known as the winding number. In order to have a gauge-invariant vacuum state, one needs to consider the contribution from all configurations with non-zero winding number, such as the coherent superposition

$$|\theta_{\rm QCD}\rangle = \sum_n e^{-in\theta_{\rm QCD}} |n\rangle , \tag{2.50}$$

where here $\theta_{\rm QCD}$ is an arbitrary parameter. The presence of a non-zero $\theta_{\rm QCD}$ vacuum induces an extra phase in a generic matrix elements of the form [5]

$${}_{\rm out}\langle\theta_{\rm QCD}| X |\theta_{\rm QCD}\rangle_{\rm in} = \sum_{n,m} e^{i(m-n)\theta_{\rm QCD}} {}_{\rm out}\langle m| X |n\rangle_{\rm in} , \tag{2.51}$$

where X is some quantum operator. This phase can be accounted for in the path integral formalism by adding a new term to the QCD action

$${}_{\rm out}\langle\theta_{\rm QCD}| X |\theta_{\rm QCD}\rangle_{\rm in} = \int [dG_\mu][d\psi][d\bar{\psi}] X e^{iS_{\rm QCD} + i\theta_{\rm QCD} \frac{g_s^2}{32\pi^2} \int d^4x G^a_{\mu\nu} \widetilde{G}^{a\mu\nu}} , \tag{2.52}$$

where the exponential of the winding-number difference, i.e. $e^{i(m-n)\theta_{\rm QCD}}$ in Eq. (2.51), is equivalent to the new exponential factor containing $G^a_{\mu\nu}\widetilde{G}^{a\mu\nu}$ in Eq. (2.52). Hence, the resolution of the $U(1)_A$ problem consists of effectively adding an extra term to the QCD Lagrangian [i.e. the last term in Eq. (2.1)], which in turn is associated to the complicated nature of the QCD vacuum. As discussed before, this term violates parity and time reversal invariance, and induces a neutron electric dipole moment that allows setting experimental upper bounds to this parameter, $\theta_{\rm QCD} \lesssim 10^{-10}$. The question as to why $\theta_{\rm QCD}$ is so small is known as the strong CP problem [25].

The problem is exacerbated when one considers QCD in conjunction with the weak interactions. As it is well known, CP violation in the SM arises from the Yukawa couplings between the Higgs doublet and the fermions (see Chapter 6 for details). After spontaneous electroweak symmetry breaking, the Higgs field picks up a vacuum expectation value and these couplings give rise to mass matrices for the quarks that are neither diagonal nor CP invariant [5]. One then has to perform chiral rotations on the left- and right-handed quarks to shift all CP violation into the Cabibbo-Kobayashi-Maskawa (CKM) matrix. For three generations of fermions, the CKM matrix can be taken real up to a single phase, which is known as the weak CP phase [4]. However, given that different left- and right-handed rotations are required, one eventually encounters an axial $U(1)$ rotation and, since the path-integral fermionic measure is not invariant under $U(1)_A$ rotations, the term

$$\mathcal{L}_{\theta_F} = \theta_F \frac{g_s^2}{32\pi^2} \epsilon^{\mu\nu\alpha\beta} G^a_{\mu\nu} G^a_{\alpha\beta} \tag{2.53}$$

is generated in the QCD Lagrangian [cf. Eq. (2.42)].[17] In particular, by denoting M' as the mass matrix[18] in the original quark basis and M as the diagonalised mass matrix [5]

$$M = S_L^\dagger M' S_R , \quad \psi_L = S_L^\dagger \psi'_L , \quad \psi_R = S_R^\dagger \psi'_R , \tag{2.54}$$

[17] Note that one also generates similar terms for the weak and electromagnetic fields in this process. However, these phases can be removed with additional rotations of just the right-handed fields [4].

[18] Note that, here, the u and d mass matrices have been combined into a single mass matrix.

where $\psi'_{R,L}$ and $\psi_{R,L}$ are the weak and mass eigenstates, respectively, then one is allowed to write $\theta_F = \arg(\det M')$ and $\bar{\theta} \equiv \theta_{\rm QCD} + \arg(\det M')$. Note that an arbitrary change of path integration variables cannot have any physical effects, so observable quantities cannot depend on $\theta_{\rm QCD}$ or θ_F but only on the basis independent combination $\bar{\theta}$, which in the full theory corresponds to the coefficient of the $G\widetilde{G}$ term [4, 26].

One possible solution to the strong CP problem is that one of the quark masses vanishes. This is because in this case one has got the ability to remove θ_F by performing an additional axial phase transformation on the massless quark. However, from the analysis of quark-mass ratios, there is strong evidence that all the quarks have non-zero masses [26]. A different way to naturally explain why $\bar{\theta}$ is so small is the mechanism proposed by Peccei and Quinn [18] whereby $\bar{\theta}$ becomes a dynamical variable which relaxes to a minimum of an effective potential, at which P and CP are conserved, requiring the existence of a light spinless particle, the axion. This model was ruled out by experiment soon after its proposal but other models following the same general idea have been proposed over the years (see Refs. [1, 25]). At the time of writing this thesis, no experimental evidence for axions or axion-like particles has been found.

Chapter 3

Effective field theories

In this chapter, we review the fundamental concepts of effective field theories (EFTs) and introduce several important EFTs for hadronic physics, such as chiral perturbation theory (χPT), large-N_C χPT (which is the EFT of QCD in the chiral and large number of colours limit), resonance chiral theory (RχT), vector meson dominance (VMD) and the $U(3) \times U(3)$ linear sigma model (LσM).[1] At the end of the chapter, we also present the Standard Model effective field theory (SMEFT), for which the SM is the leading order term approximation in the EFT expansion of a more fundamental theory.

3.1 Introduction to effective field theories

In the 1960s and 1970s, it was widely regarded that any sensible physical theory would need to take the form of a renormalisable quantum field theory [6]. Indeed, the requirement of renormalisability played a crucial role in the development of the SM.[2] However, as it turns out, the cancellation of ultraviolet (UV) divergences does not depend on renormalisability;[3] instead, so long as every one of the infinite number of interactions allowed by the symmetries of the theory is included, then there are always counterterms available to cancel all UV divergences and the so-called non-renormalisable theories turn out to be just as renormalisable as renormalisable theories [6].[4] In fact, all the realistic theories that are used today to describe physics at accessible energies are actually effective field theories (EFTs) and it is accepted that they require an infinite number of non-renormalisable interactions, even though at sufficiently low energies one expects that all the non-renormalisable interactions are highly suppressed [6].

[1] It should be highlighted that, strictly speaking, VMD and the LσM are not EFTs but phenomenological models. In any case, they are reviewed in this chapter.

[2] As a reminder, the interaction terms of a Lagrangian with coupling constants that have positive or zero mass dimension are renormalisable, whilst interaction terms whose couplings have negative dimensionality are non-renormalisable. Note that renormalisable theories require only a finite number of counterterms to absorb the UV divergences, whilst non-renormalisable theories require an infinite number of counterterms to absorb them.

[3] The renormalisability condition can be expressed as [6]

$$\Delta_i \equiv 4 - \delta_i - \sum_f n_{if}(s_f + 1) \geq 0\,, \tag{3.1}$$

where Δ_i is the mass dimensionality of the coupling constant of an interaction term of type i, δ_i is the number of derivatives associated to the interaction of type i, n_{if} is the number of fields of type f in interactions of type i, and s_f is (with some qualifications) the spin of fields of type f.

[4] It is important to note that quantum field theory in itself has no content beyond analyticity, unitarity, cluster decomposition and symmetry. Accordingly, when one calculates matrix elements from Feynman diagrams using the most general Lagrangian that involves the relevant degrees of freedom and satisfies the assumed symmetries of the theory, then one is simply constructing the most general possible S-matrix that is consistent with analyticity, perturbative unitarity, cluster decomposition and the assumed symmetry principles [26, 39]. Accordingly, there is nothing especial about renormalisability apart from the fact that there is a clear advantage in having a finite number of counterterms and renormalisation conditions.

The basic idea underlying the construction of an EFT is that a simpler theory can be constructed when one deals with a quantum field theory (QFT) containing two or more different energy scales, e.g. m and M with $m \ll M$. This is achieved by performing a systematic expansion in the ratio of these scales. An effective Lagrangian is, therefore, derived by 'integrating out' the heavy degrees of freedom associated to the high energy scale[5] from the generating functional of Green's functions, which allows one to obtain a non-local action functional that can be expanded in an infinite tower of local operators $O_i^{(\mathcal{D})}$ [19]

$$\mathcal{L}_{\rm EFT} = \sum_{\mathcal{D}\geq 0,i} \frac{c_i^{(\mathcal{D})}}{M^{\mathcal{D}-d}} O_i^{(\mathcal{D})}\,, \tag{3.2}$$

where $\mathcal{D}$ is the mass dimension of the operator $O_i^{(\mathcal{D})}$ and d is the number of space-time dimensions. For fixed $\mathcal{D}$, the set $\{O_i^{(\mathcal{D})}\}$ forms a basis of local composite operators constructed out of the fields of the low-energy theory. These operators are only constrained by the symmetries of the low-energy theory, such as Lorentz invariance, gauge invariance and global symmetries, such as C, P, T, flavour symmetries, etc. The dimensionless coefficients $c_i^{(\mathcal{D})}$ are the so-called Wilson coefficients.

There is a deep connection between renormalisation theory and EFTs. In conventional renormalisation theory, UV divergences are regularised by imposing a UV cut-off Λ, rendering the loop integrals regular, to then take the limit $\Lambda \to \infty$ (which implicitly assumes that the theory holds for arbitrarily large momentum scales) and absorb the UV divergencies into the redefinition or renormalisation of some quantities of the theory in such a way that physical observables are independent of the renormalisation conditions [3, 4, 6]. On the other hand, in Wilson's approach [40, 41], one imposes a 'floating' finite UV cut-off Λ and assumes that the theory holds for $E \ll \Lambda$; one must then ensure that the bare constants of the theory depend on Λ in such a way that all physical observables are independent of the precise value of the cut-off [6], which amounts to the statement of observable quantities being Λ-independent.[6] There is an interesting parallelism between the Wilsonian approach and the procedure of constructing effective Lagrangians, where one essentially splits up the contributions from virtual particles in long- and short-distance modes. That is,[7]

$$\int_0^\infty \frac{d\omega}{\omega} = \int_0^\Lambda \frac{d\omega}{\omega} + \int_\Lambda^\infty \frac{d\omega}{\omega}\,, \tag{3.3}$$

where the first term is sensitive to infrared (IR) physics and is absorbed into the matrix elements $\langle O_i^{(\mathcal{D})}\rangle$, whilst the second term is sensitive to UV physics and is absorbed into the Wilson coefficients $c_i^{(\mathcal{D})}$ [19] [see Eq. (3.2)].[8] One can now change the arbitrary parameter $\Lambda \to \Lambda'$, such that

$$\int_0^\infty \frac{d\omega}{\omega} = \int_0^{\Lambda'} \frac{d\omega}{\omega} + \int_{\Lambda'}^\infty \frac{d\omega}{\omega}\,, \tag{3.4}$$

[5] Note that this view is today considered as old-fashioned. An alternative approach is to think of EFTs in terms of the physical problem one is trying to solve, rather than as the limit of some other theory [19]. The EFT is, consequently, constructed out of the relevant dynamical degrees of freedom of the problem at hand. This is quite obvious in χPT, for example, where the theory is written in terms of mesons or baryon fields and in no sense the short-distance quarks and gluons are integrated out explicitly.

[6] Note that the renormalisation group equations (RGE) have essentially the same form in the two schemes of renormalisation, although the Wilsonian RG can be implemented through the path integral where one can literally integrate out all the short-distance degrees of freedom with energies $E > \Lambda$ [4].

[7] Note that in the EFT context, Λ and M correspond to two different energy scales, the former representing the arbitrary scale at which one splits the long- and short-distance modes and the latter corresponding to the characteristic energy scale of the UV physics.

[8] Note that a key feature in formulating EFTs is locality, which results in a separation of scales, i.e. factorisation of the field theory amplitudes into short-distance Lagrangian coefficients and long-distance matrix elements [19].

but the physics must remain unchanged

$$\mathcal{L}_{\rm EFT} = \sum_{\mathcal{D}\geq 0,i} \frac{c_i^{(\mathcal{D})}(\Lambda)}{M^{\mathcal{D}-d}} O_i^{(\mathcal{D})}(\Lambda) = \sum_{\mathcal{D}\geq 0,i} \frac{c_i^{(\mathcal{D})}(\Lambda')}{M^{\mathcal{D}-d}} O_i^{(\mathcal{D})}(\Lambda')\,, \tag{3.5}$$

which means that, given that the operators $O_i^{(\mathcal{D})}$ are the same on both sides of the equality, the couplings of the theory [i.e. the Wilson coefficients $c_i^{(\mathcal{D})}$] must depend on Λ. Thus, we are led to the following general form of the effective Lagrangian

$$\mathcal{L}_{\rm EFT} = \sum_{\mathcal{D}\geq 0,i} \frac{c_i^{(\mathcal{D})}(\mu)}{M^{\mathcal{D}-d}} O_i^{(\mathcal{D})}(\mu)\,, \tag{3.6}$$

whose matrix elements are independent of the energy scale μ. The $O_i^{(\mathcal{D})}(\mu)$ in Eq. (3.6) are renormalised composite operators defined in dimensional regularisation and the $\overline{\rm MS}$ scheme, whilst the $c_i^{(\mathcal{D})}(\mu)$ are the corresponding renormalised Wilson coefficients, which contain all the information about the short-distance physics that has been integrated out,[9] and can be thought of the running couplings of the effective theory. From the requirement that the effective action $S_{\rm eff}$ must be μ-independent, one can write in matrix notation [19]

$$\frac{d\vec{c}(\mu)}{d\ln\mu} = \boldsymbol{\gamma}^T(\mu)\vec{c}(\mu)\,, \tag{3.7}$$

with $\boldsymbol{\gamma}$ being the anomalous-dimension matrix of the composite operators.

In $d = 4$ space-time dimensions, Eq. (3.6) can be written as

$$\mathcal{L}_{\rm EFT} = \mathcal{L}_{\mathcal{D}\leq 4} + \frac{\mathcal{L}_5}{M} + \frac{\mathcal{L}_6}{M^2} + \ldots\,, \tag{3.8}$$

where all the operators of mass dimension $\mathcal{D} \leq 4$ are contained in $\mathcal{L}_{\mathcal{D}\leq 4}$. It can be seen from this expression that $\mathcal{L}_{\rm EFT}$ has to be treated as an expansion in powers of $1/M$. In fact, if one attempts to sum terms to all orders, then the EFT power counting rules are violated and the EFT breaks down. Let us show how to systematically organise calculations by considering a scattering amplitude $\mathcal{A}$ normalised to have mass dimension zero. At some typical momentum scale p, a single insertion of a dimension $\mathcal{D}$ operator gives a contribution to the amplitude of order

$$\mathcal{A} \sim \left(\frac{p}{M}\right)^{\mathcal{D}-4}\,, \tag{3.9}$$

where the mass dimension $1/M^{\mathcal{D}-4}$ comes from the coefficient associated to the operator $O^{(\mathcal{D})}$ [see Eq. (3.6)] and the powers of p in the numerator are generated by kinematic factors, such as external momenta, to make the amplitude dimensionless. A set of insertions from higher-dimension operators renders

$$\mathcal{A} \sim \left(\frac{p}{M}\right)^{n}\,, \tag{3.10}$$

with

$$n = \sum_i (\mathcal{D}_i - 4)\,, \tag{3.11}$$

where one sums over the i inserted operators. This is known as the EFT power counting formula, which also holds for graphs containing loops [19]. Accordingly, corrections of

[9] Note that the difference in UV structure of the full theory and the EFT is addressed by means of the matching procedure.

order p/M are given by diagrams with a single insertion of $\mathcal{L}_5$, $(p/M)^2$ corrections are given by graphs with a single insertion of $\mathcal{L}_6$ or two insertions of $\mathcal{L}_5$, and so on.

One can now explicitly see how the requirement of including all possible higher-dimension operators consistent with the symmetries of the theory in an EFT allows the renormalisation of loop divergences: $\mathcal{L}_6$ operators are needed to renormalise loop diagrams containing two insertions of $\mathcal{L}_5$, $\mathcal{L}_8$ operators are needed to renormalise loop graphs with two insertions of $\mathcal{L}_6$, etc. It is important to note that, when using multiple insertions of operators with $\mathcal{D}-4>0$, the above procedure generates operators of arbitrarily high dimension. This is not the case, though, for multiple insertions of operators from $\mathcal{L}_{\mathcal{D}\leq 4}$, i.e. the renormalisable Lagrangian. This is down to the fact that in this instance $\mathcal{D}-4\leq 0$, which in turn means that we generate operators with $\mathcal{D}\leq 4$ only[10] that are already included in $\mathcal{L}_{\mathcal{D}\leq 4}$ [19]. This is the difference between renormalisable theories and EFTs.

3.2 Chiral perturbation theory

Chiral perturbation theory (χPT) is the effective field theory of QCD at energies much lower than typical hadronic masses. It is, thus, a systematic and model-independent approximation of QCD based on the symmetries of the underlying theory and general principles of quantum field theory. In this section, we follow the presentation from Ref. [19], Chapter 3, and also Ref. [28].

Given the energy gap separating the eight pseudoscalar mesons from the rest of the hadronic particle spectra, one may assume that these states are approximately massless modes in a Nambu-Goldstone effective field theory. As it turns out, their Nambu-Goldstone nature implies strong constraints on their interactions, which can be analysed on the basis of an effective Lagrangian expanded in powers of momenta over some characteristic scale, with the pattern of symmetry breaking

$$G\equiv SU(n_f)_R\times SU(n_f)_L\;\rightarrow\; H\equiv SU(n_f)_V\,, \tag{3.12}$$

giving rise to n_f^2-1 Nambu-Goldstone fields $\phi_a(x)$.[11] With the choice of coset representative $\xi(\vec{\phi})\equiv[\xi_L(\vec{\phi}),\xi_R(\vec{\phi})]\in G$, the field coordinates in the coset space G/H can be changed with the chiral transformation $g\equiv(g_L,g_R)\in G$

$$\xi_L(\vec{\phi})\xrightarrow{\text{G}} g_L\xi_L(\vec{\phi})h^\dagger(\vec{\phi},g)\,,\quad \xi_R(\vec{\phi})\xrightarrow{\text{G}} g_R\xi_R(\vec{\phi})h^\dagger(\vec{\phi},g)\,, \tag{3.15}$$

[10] The counterterms for negative-dimension operators are not needed since they do not generate divergences.

[11] Remember that in the $O(N)$ sigma model, where $\Phi(x)^T\equiv(\phi_1,\phi_2,...,\phi_N)$ is an N-dimensional vector of real scalar fields, the Lagrangian has got a global $O(N)$ symmetry, under which $\Phi(x)$ transforms as an $O(N)$ vector, and a degenerate ground-state manifold satisfying $|\Phi|^2=\sum_i\phi_i^2=v^2$, which can be rotated to any particular direction using the $O(N)$ symmetry. The vacuum manifold consists of the $N-1$ dimensional sphere S^{N-1} and the particular vacuum choice Φ_0 remains invariant under the $O(N-1)$ subgroup. The pattern of $O(N)\rightarrow O(N-1)$ spontaneous symmetry breaking makes the vacuum not invariant under the action of the $N(N-1)/2-(N-1)(N-2)/2=N-1$ broken generators T^a, giving rise to $N-1$ Nambu-Goldstone bosons, which in turn parameterise the rotations of the particular vacuum choice Φ_0 over the vacuum manifold S^{N-1}. Performing a polar decomposition, one can express the N-component field $\Phi(x)$ as

$$\Phi(x)=\left[1+\frac{S(x)}{v}\right]U(x)\Phi_0\,, \tag{3.13}$$

where $S(x)$ is a Hermitian scalar field, which corresponds to the massive radial excitation, and the $N-1$ Nambu-Goldstone fields $\phi_a(x)$ are encoded in the unitary matrix

$$U(x)=\exp\left\{iT^a\frac{\phi_a(x)}{v}\right\}. \tag{3.14}$$

where the compensating transformation $h \in H$, required to get back to the chosen coset representative, is the same in the two chiral sectors since they are related by a parity transformation that leaves H invariant [19]. One can combine the two chiral relations in Eq. (3.15) into

$$U(\vec{\phi}) \equiv \xi_R(\vec{\phi})\xi_L^\dagger(\vec{\phi}) \xrightarrow{\text{G}} g_R U(\vec{\phi}) g_L^\dagger \,, \tag{3.16}$$

and using the canonical choice of coset representative $\xi_R(\vec{\phi}) = \xi_L^\dagger(\vec{\phi}) \equiv u(\vec{\phi})$, which involves only the broken axial generators, the $n_f \times n_f$ unitary matrix $U(\vec{\phi})$ takes the form

$$U(\vec{\phi}) = u(\vec{\phi})^2 = \exp\left\{ i\sqrt{2}\,\frac{\Phi}{F} \right\}, \quad \Phi(x) \equiv \sqrt{2}\,\widehat{T}^a \phi_a(x) \,, \tag{3.17}$$

with F being a characteristic energy scale needed to make the exponent massless. For $n_f = 3$, one has

$$\Phi \equiv \frac{\vec{\lambda}}{\sqrt{2}}\vec{\phi} = \sum_{a=1}^{8} \frac{\lambda_a}{\sqrt{2}}\phi_a = \begin{pmatrix} \frac{1}{\sqrt{2}}\pi^0 + \frac{1}{\sqrt{6}}\eta_8 & \pi^+ & K^+ \\ \pi^- & -\frac{1}{\sqrt{2}}\pi^0 + \frac{1}{\sqrt{6}}\eta_8 & K^0 \\ K^- & \overline{K}^0 & -\frac{2}{\sqrt{6}}\eta_8 \end{pmatrix}. \tag{3.18}$$

The matrix $U(\vec{\phi})_{ij}$ can be thought of parameterising the zero-energy excitations over the quark vacuum condensate $\langle 0|\, \bar{q}_L^j q_R^i \,|0\rangle \propto \delta_{ij}$, where i, j are flavour indices, which in turn triggers the dynamical breaking of the chiral symmetry.

In order to obtain a model-independent description of the Nambu-Goldstone dynamics at low energies, one must write the most general Lagrangian in terms of the matrix field $U(\vec{\phi})$ consistent with the chiral symmetry of Eq. (3.12), i.e. invariant under the transformation in Eq. (3.16). The Lagrangian can be organised as an expansion in powers of momenta or, equivalently, increasing number of derivatives. Since QCD respects parity inversion, the number of derivatives should be even

$$\mathcal{L}_{\text{eff}}(U) = \sum_{n=1} \mathcal{L}_{2n} \,. \tag{3.19}$$

Owing to the unitarity of the U matrix, one requires at least two derivatives in order to generate non-trivial interactions. Accordingly, to lowest order, $\mathcal{O}(p^2)$, one finds

$$\mathcal{L}_2 = \frac{F^2}{4} \text{Tr}\Big[\partial_\mu U^\dagger \partial^\mu U \Big] \,. \tag{3.20}$$

As a result of the non-linear functional form of $U(\vec{\phi})$, the $\mathcal{L}_2$ Lagrangian gives rise to the kinetic terms and a tower of interactions involving an increasing number of pseudoscalars, which can be explicitly seen by expanding U in powers of Φ. At next-to-leading order (NLO), the $\mathcal{O}(p^4)$ Lagrangian has got four derivatives, and so on.

In order to incorporate into the ideal theory of massless Nambu-Goldstone bosons sources of explicit chiral symmetry breaking, such as quark masses and electroweak interactions, it is useful to introduce external classical fields coupled to the quark currents. As such, we introduce the extended QCD Lagrangian

$$\mathcal{L}_{\text{QCD}} = \mathcal{L}^0_{\text{QCD}} + \bar{q}\gamma^\mu(v_\mu + \gamma^5 a_\mu)q - \bar{q}(s - i\gamma^5 p)q \,, \tag{3.21}$$

where $\mathcal{L}^0_{\text{QCD}}$ is the massless QCD Lagrangian, and v_μ, a_μ, s and p are, respectively, the vector, axial-vector, scalar and pseudoscalar external Hermitian matrix-valued fields. By separating the quark fields into left and right chiralities [cf. Eq. (2.24)] and defining the

following left- and right-handed external fields

$$r_\mu \equiv v_\mu + a_\mu\,, \quad l_\mu \equiv v_\mu - a_\mu\,, \tag{3.22}$$

allows one to rewrite Eq. (3.21) as

$$\mathcal{L}_{\rm QCD} = \mathcal{L}^0_{\rm QCD} + \bar{q}_L\gamma^\mu l_\mu q_L + \bar{q}_R\gamma^\mu r_\mu q_R - \bar{q}_R(s+ip)q_L - \bar{q}_L(s-ip)q_R\,. \tag{3.23}$$

The external fields v_μ, a_μ, s and p can be used to parameterise different sources of chiral symmetry breaking. In fact, direct comparison between Eq. (3.23) and the electroweak part of the SM Lagrangian enables the following identifications

$$\begin{aligned} r_\mu &= -eQA_\mu\,, \quad l_\mu = -eQA_\mu - \frac{e}{\sqrt{2}\sin\theta_W}(W^\dagger_\mu T_+ + \text{h.c.})\,, \\ s &= M\,, \qquad\qquad p = 0\,, \end{aligned} \tag{3.24}$$

where θ_W is the Weinberg, Q and M are, respectively, the quark-charge and mass matrices for three light quark flavours (i.e. $n_f = 3$),

$$Q = \frac{1}{3}\text{diag}\{2,-1,-1\}\,, \quad M = \text{diag}\{m_u, m_d, m_s\}\,, \tag{3.25}$$

whilst T_+ is a 3×3 matrix carrying the relevant Cabibbo-Kobayashi-Maskawa (CKM) elements

$$\begin{pmatrix} 0 & V_{ud} & V_{us} \\ 0 & 0 & 0 \\ 0 & 0 & 0 \end{pmatrix}. \tag{3.26}$$

One could also include the Z boson interactions into v_μ and a_μ, the effects of the Higgs into s or other BSM quark couplings into the external fields should it be needed.

The Lagrangian in Eq. (3.23) respects the $SU(3)_L \times SU(3)_R$ chiral symmetry so long as the external fields transform as

$$\begin{aligned} q_L &\to\ g_L q_L\,, \qquad\qquad q_R \to g_R q_R\,, \\ s+ip &\to g_R(s+ip)g_L^\dagger\,, \quad s-ip \to g_L(s-ip)g_R^\dagger\,, \\ l_\mu &\to\ g_L l_\mu g_L^\dagger + ig_L\partial_\mu g_L^\dagger\,, \quad r_\mu \to g_R r_\mu g_R^\dagger + ig_R\partial_\mu g_R^\dagger\,. \end{aligned} \tag{3.27}$$

Furthermore, in order to respect local gauge invariance, the gauge fields v_μ and a_μ must be introduced through covariant derivatives

$$D_\mu U = \partial_\mu U - ir_\mu U + iUl_\mu\,, \quad D_\mu U^\dagger = \partial_\mu U^\dagger + iU^\dagger r_\mu - il_\mu U^\dagger\,, \tag{3.28}$$

and through field strength tensors

$$L^{\mu\nu} = \partial^\mu l^\nu - \partial^\nu l^\mu - i\left[l^\mu, l^\nu\right], \quad R^{\mu\nu} = \partial^\mu r^\nu - \partial^\nu r^\mu - i\left[r^\mu, r^\nu\right]. \tag{3.29}$$

Taking all this into account, the most general effective Lagrangian at LO in derivatives and number of external fields, consistent with Lorentz invariance and the local chiral symmetry, takes the form [42]

$$\mathcal{L}_2 = \frac{F^2}{4}\text{Tr}\left[D_\mu U^\dagger D^\mu U\right] + \frac{F^2}{4}\text{Tr}\left[U^\dagger\chi + \chi^\dagger U\right], \tag{3.30}$$

with

$$\chi = 2B_0(s+ip)\,. \tag{3.31}$$

The Green functions of quark currents can be obtained as functional derivatives of the generating functional $Z\,[v,a,s,p]$, which in turn is defined by

$$\exp\{iZ\} = \int [dq]\,[d\bar{q}]\,[dG_\mu] \exp\left\{ i \int d^4x\, \mathcal{L}_{\rm QCD} \right\} = \int [dU] \exp\left\{ i \int d^4x\, \mathcal{L}_{\rm eff} \right\}. \quad (3.32)$$

At lowest order, the generating functional reduces to the classical action, $S_2 = \int d^4x \mathcal{L}_2$, and the QCD currents can be calculated by taking derivatives with respect to the external fields

$$\begin{aligned} J^\mu_L = \bar{q}_L \gamma^\mu q_L \doteq \frac{\delta S_2}{\delta l_\mu} = \frac{i}{2} F^2 D_\mu U^\dagger U = \frac{F}{\sqrt{2}} D_\mu \Phi - \frac{i}{2} (\Phi \overset{\leftrightarrow}{D}_\mu \Phi) + \mathcal{O}(\Phi^3/F)\,, \\ J^\mu_R = \bar{q}_R \gamma^\mu q_R \doteq \frac{\delta S_2}{\delta r_\mu} = \frac{i}{2} F^2 D_\mu U U^\dagger = -\frac{F}{\sqrt{2}} D_\mu \Phi - \frac{i}{2} (\Phi \overset{\leftrightarrow}{D}_\mu \Phi) + \mathcal{O}(\Phi^3/F)\,, \end{aligned} \quad (3.33)$$

where $\Phi \overset{\leftrightarrow}{D}_\mu \Phi \equiv \Phi(D_\mu \Phi) - (D_\mu \Phi)\Phi$. From this, one immediately finds

$$J^\mu_V = J^\mu_R + J^\mu_L = -i\,(\Phi \overset{\leftrightarrow}{D}_\mu \Phi)\,, \quad J^\mu_A = J^\mu_R - J^\mu_L = -\sqrt{2} F D^\mu \Phi\,, \quad (3.34)$$

and by using the substitution $\Phi \to -\Phi$ or, equivalently, $U \to U^\dagger$ it becomes obvious that J^μ_V conserves parity, whilst J^μ_A violates it. Taking now derivatives with respect to the external scalar and pseudoscalar external sources, one finds

$$\begin{aligned} \bar{q}^j_L q^i_R \doteq -\frac{\delta S_2}{\delta (s - ip)^{ji}} = -\frac{F^2}{2} B_0\, U(\vec{\phi})_{ij}\,, \\ \bar{q}^j_R q^i_L \doteq -\frac{\delta S_2}{\delta (s + ip)^{ji}} = -\frac{F^2}{2} B_0\, U^\dagger(\vec{\phi})_{ij}\,. \end{aligned} \quad (3.35)$$

All the elements in the Lagrangian of Eq. (3.30) are determined by the chiral symmetry and its pattern of explicit breaking through the external sources with exception of F and B_0, which must be obtained from experiment. At order $\mathcal{O}(p^2)$, the fundamental chiral coupling F can be identified with the pion decay constant, f_π, defined as

$$F = \langle 0 |\, (J^\mu_A)^{12}\, | \pi^+ \rangle \equiv i\sqrt{2} f_\pi p^\mu\,, \quad (3.36)$$

whilst the coupling B_0 is related to the quark vacuum condensate through

$$\langle 0 |\, \bar{q}^j q^i\, | 0 \rangle = \langle 0 |\, \bar{q}^j_L q^i_R\, | 0 \rangle + \langle 0 |\, \bar{q}^j_R q^i_L\, | 0 \rangle = -F^2 B_0 \delta^{ij}\,. \quad (3.37)$$

By setting $s = M$ and $p = 0$, the non-derivative part of the Lagrangian in Eq. (3.30) generates the quadratic mass terms for the pseudoscalar mesons, as well as a tower of Φ^{2n} interactions proportional to the quark masses. Explicit evaluation of the quadratic mass terms gives rise to the following relations

$$\begin{aligned} M^2_{\pi^\pm} = 2\hat{m}\, B_0\,, \qquad M^2_{\pi^0} = 2\hat{m}\, B_0 - \epsilon + \mathcal{O}(\epsilon^2)\,, \\ M^2_{K^\pm} = (m_u + m_s) B_0\,, \quad M^2_{K^0} = (m_d + m_s) B_0\,, \\ M^2_{\eta_8} = \frac{2}{3} (\hat{m} + 2 m_s) B_0 + \epsilon + \mathcal{O}(\epsilon^2)\,, \end{aligned} \quad (3.38)$$

where[12]

$$\hat{m} = \frac{1}{2}(m_u + m_d)\,, \quad \epsilon = \frac{B_0}{4} \frac{(m_u - m_d)^2}{m_s - \hat{m}}\,. \quad (3.39)$$

[12]Note that isospin-breaking effects are of order $(m_d - m_u)/m_s$.

It is important to note from Eq. (3.38) that, as a result of the chiral symmetry, the squared pseudoscalar meson masses are proportional to a single power of the quark masses, with the constant of proportionality being related to the vacuum quark condensate through Eq. (3.37), which in effect is equivalent to the Gell-Mann-Oakes-Renner relation [43]

$$f_\pi^2 M_{\pi^\pm}^2 = -\hat{m}\,\langle 0|\,\bar{u}u + \bar{d}d\,|0\rangle\,. \tag{3.40}$$

Moreover, the expressions in Eq. (3.38) allow one to obtain the old current algebra mass ratios [43, 44]

$$\frac{M_{\pi^\pm}^2}{2\hat{m}} = \frac{M_{K^\pm}^2}{m_u + m_s} = \frac{M_{K^0}^2}{m_d + m_s} \approx \frac{3M_{\eta_8}^2}{2\hat{m} + 4m_s}\,, \tag{3.41}$$

and, up to $\mathcal{O}(m_u - m_d)$ corrections, the Gell-Mann-Okubo mass relation [45, 46]

$$3M_{\eta_8}^2 = 4M_K^2 - M_\pi^2\,. \tag{3.42}$$

To conclude, it is worth highlighting that the LO chiral Lagrangian in Eq. (3.30) encodes all the results from current algebra. That being said, the EFT formalism provides, in addition, a powerful framework to compute higher-order corrections in a systematic way.

3.2.1 Higher-order corrections

In Ref. [39] Weinberg proposed that the chiral dimension $\mathcal{D}$ of a connected Feynman diagram with L loops and N_{2k} vertices from $\mathcal{L}_{2k}$ is

$$\mathcal{D} = 2 + (d-2)L + \sum_{k=1}^{\infty} 2(k-1)N_{2k}\,. \tag{3.43}$$

where d is the number of space-time dimensions. All possible diagrams allowed by the symmetries of the theory with chiral dimension $\mathcal{D}$ have to be accounted for at order $\mathcal{O}(p^{\mathcal{D}})$. The ultraviolet divergences from loops must then be renormalised and this is done order by order in the momentum expansion by absorbing them through the appropriate redefinition of the low-energy constants (LECs).

In order to organise the chiral expansion, a well-defined power counting scheme for the external sources is needed. This turns out to be

$$U(\vec{\phi}) \sim \mathcal{O}(p^0)\,, \quad D_\mu, l_\mu, r_\mu \sim \mathcal{O}(p^1)\,, \quad L^{\mu\nu}, R^{\mu\nu}, \chi \sim \mathcal{O}(p^2)\,. \tag{3.44}$$

One can easily check that the LO Lagrangian with external sources from Eq. (3.30) is of order $\mathcal{O}(p^2)$, as expected, and that Weinberg's power counting remains valid in the presence of the symmetry-breaking terms. At $\mathcal{O}(p^4)$, the most general $SU(3)_L \times SU(3)_R$-invariant Lagrangian is given by [42]

$$\begin{aligned}
\mathcal{L}_4 = {} & L_1 \mathrm{Tr}\left[D_\mu U^\dagger D^\mu U\right]^2 + L_2 \mathrm{Tr}\left[D_\mu U^\dagger D_\nu U\right] \mathrm{Tr}\left[D^\mu U^\dagger D^\nu U\right] \\
& + L_3 \mathrm{Tr}\left[D_\mu U^\dagger D^\mu U D_\nu U^\dagger D^\nu U\right] + L_4 \mathrm{Tr}\left[D_\mu U^\dagger D^\mu U\right] \mathrm{Tr}\left[U^\dagger\chi + \chi^\dagger U\right] \\
& + L_5 \mathrm{Tr}\left[D_\mu U^\dagger D^\mu U \left(U^\dagger\chi + \chi^\dagger U\right)\right] + L_6 \mathrm{Tr}\left[U^\dagger\chi + \chi^\dagger U\right]^2 \\
& + L_7 \mathrm{Tr}\left[U^\dagger\chi - \chi^\dagger U\right]^2 + L_8 \mathrm{Tr}\left[\chi^\dagger U\chi^\dagger U + U^\dagger\chi U^\dagger\chi\right] \\
& - iL_9 \mathrm{Tr}\left[R^{\mu\nu} D_\mu U D_\nu U^\dagger + L^{\mu\nu} D_\mu U^\dagger D_\nu U\right] + L_{10} \mathrm{Tr}\left[U^\dagger R^{\mu\nu} U F_{L\mu\nu}\right] \\
& + H_1 \mathrm{Tr}\left[R_{\mu\nu}R^{\mu\nu} + L_{\mu\nu}L^{\mu\nu}\right] + H_2 \mathrm{Tr}\left[\chi^\dagger\chi\right]\,,
\end{aligned} \tag{3.45}$$

where the L_i and H_j (with $i = 1,...,10$ and $j = 1,2$) are LECs, whose numerical values are not determined by the chiral symmetry. These parameters are the equivalent to F and B_0 in $\mathcal{L}_2$ and contain information of the underlying short-distance dynamics. It should be noted that the structures in Eq. (3.45) proportional to H_1 and H_2, whilst needed for renormalisation purposes, only contain external sources and, thus, do not influence the pseudoscalar meson dynamics [19].

Employing dimensional regularisation and reabsorbing the one-loop divergences originating from $\mathcal{L}_2$ through the renormalisation of the $\mathcal{O}(p^4)$ LECs, one finds

$$L_i = L_i^r(\mu) + \Gamma_i \Delta, \quad H_j = H_j^r(\mu) + \widetilde{\Gamma}_j \Delta, \tag{3.46}$$

where

$$\Delta = \frac{\mu^{d-4}}{32\pi^2}\left[\frac{2}{d-4} - \log(4\pi) + \gamma_E - 1\right]. \tag{3.47}$$

The renormalised couplings $L_i^r(\mu)$ and $H_j^r(\mu)$ depend on the arbitrary scale μ of dimensional regularisation and their logarithmic running is dictated by

$$L_i^r(\mu_2) = L_i^r(\mu_1) + \frac{\Gamma_i}{(4\pi)^2}\log\left(\frac{\mu_1}{\mu_2}\right), \quad H_j^r(\mu_2) = H_j^r(\mu_1) + \frac{\widetilde{\Gamma}_j}{(4\pi)^2}\log\left(\frac{\mu_1}{\mu_2}\right), \tag{3.48}$$

where the chiral constants Γ_i and $\widetilde{\Gamma}_j$ are

$$\begin{aligned} &\Gamma_1 = \frac{3}{32}, \quad \Gamma_2 = \frac{3}{16}, \quad \Gamma_3 = 0, \quad \Gamma_4 = \frac{1}{8}, \quad \Gamma_5 = \frac{3}{8}, \quad \Gamma_6 = \frac{11}{144}, \\ &\Gamma_7 = 0, \quad \Gamma_8 = \frac{5}{48}, \quad \Gamma_9 = \frac{1}{4}, \quad \Gamma_{10} = -\frac{1}{4}, \quad \widetilde{\Gamma}_1 = -\frac{1}{8}, \quad \widetilde{\Gamma}_2 = \frac{5}{34}. \end{aligned} \tag{3.49}$$

All physical observables must be independent of the arbitrary scale μ and what one finds is that the scale dependence of the running parameters is cancelled by scale-dependent terms from non-local (non-polynomial) loop contributions in the perturbative series.

At order $\mathcal{O}(p^2)$, the χPT Lagrangian can describe all QCD Green functions with only two LECs (i.e. F and B_0), whilst, at $\mathcal{O}(p^4)$, one needs to fix 12 LECs (i.e. L_i and H_j) from phenomenology so as to be able to make predictions. At order $\mathcal{O}(p^6)$, the χPT Lagrangian contains 94 operators of even intrinsic parity and 23 independent chiral structures of odd intrinsic parity, with their corresponding LECs. We see that increasing the precision of the predictions by including higher-order corrections significantly reduces the predictive power of the EFT. Thus, the main limitation of EFTs is the proliferation of unknown LECs at higher orders. At LO, the symmetries of the theory severely restrict the number of allowed operators, enabling the derivation of many phenomenological results in terms of a small number of dynamical parameters. However, at higher orders in the chiral expansion the symmetries constraint significantly less the number of operators, being much more sensitive to the non-trivial aspects of the underlying QCD dynamics. All LECs are in principle calculable from QCD, though this first-principles computation cannot at present be analytically performed. In practice they are fixed using either empirical input[13] or QCD-inspired models, such as meson-resonance saturation or lattice QCD. Numerical lattice simulations provide a promising avenue to address this problem, though currently this technique is still far from being able to achieve a complete matching between QCD and its low-energy effective theory [19].

[13] At present, low-energy phenomenology is the main source of information for the $\mathcal{O}(p^4)$ LECs. In particular, the elastic $\pi\pi$ and πK scattering amplitudes are affected by $L_{1,2,3}$, the two-derivative couplings $L_{4,5}$ give rise to mass corrections to the meson decay constants, the pseudoscalar meson masses are sensitive to the non-derivative terms $L_{6,7,8}$, L_9 is associated to the meson electromagnetic radius, and L_{10} contributes to amplitudes with at least two external vector or axial-vector fields, such as the radiative semileptonic decay $\pi \to e\nu\gamma$ [19].

TABLE 3.1: Values for the renormalised couplings $L_i^r(M_\rho)$ from phenomenological analyses at orders $\mathcal{O}(p^4)$ and $\mathcal{O}(p^6)$ in χPT, and from lattice simulations [19].

	$L_i^r(M_\rho)\times 10^3$		
i	$\mathcal{O}(p^4)$ [47]	$\mathcal{O}(p^6)$ [47]	Lattice [48]
1	1.0 ± 0.1	0.53 ± 0.06	
2	1.6 ± 0.2	0.81 ± 0.04	
3	-3.8 ± 0.3	-3.07 ± 0.20	
4	0.0 ± 0.3	0.3 (fixed)	0.09 ± 0.34
5	1.2 ± 0.1	1.01 ± 0.06	1.19 ± 0.25
6	0.0 ± 0.4	0.14 ± 0.05	0.16 ± 0.20
7	-0.3 ± 0.2	-0.34 ± 0.09	
8	0.5 ± 0.2	0.47 ± 0.10	0.55 ± 0.15
9	6.9 ± 0.7	5.9 ± 0.4	
10	-5.2 ± 0.1	-4.1 ± 0.4	

Table 3.1 summarises our current knowledge on the $\mathcal{O}(p^4)$ renormalised couplings, L_i^r, from phenomenological analyses [47] performed at orders $\mathcal{O}(p^4)$ and $\mathcal{O}(p^6)$ in χPT at the scale $\mu = M_\rho$. In addition, we quote results from lattice simulations by the HPQCD Collaboration [48] for comparison. Note that the values obtained from the $\mathcal{O}(p^6)$ analysis need to be taken with caution as the theoretical procedure required the inclusion of some priors for the unknown LECs.

To conclude, it is worth highlighting that, since χPT is a polynomial expansion in powers of momenta over some typical hadronic scale $\Lambda_{\chi PT}$, the validity of the effective theory is expected to break around the mass of the lightest non-pseudo-Goldstone hadronic resonances, i.e. $\Lambda_{\chi PT} \lesssim M_\rho$, which is down to the fact that they induce poles in the S-matrix that cannot be reproduced by a power expansion.

3.2.2 The effective Wess-Zumino-Witten action

As discussed in Sec. 2.4, an anomaly arises when a symmetry of the classical Lagrangian is no longer valid at the quantum level. This usually occurs when one deals with theories that have different transformation properties for the right and left fermion chiralities and can be understood within the path integral formalism as the fermionic integration measure transforming non-trivially under those transformations associated to the symmetries that are destroyed by the quantum effects.

The low-energy effective chiral Lagrangians that we have discussed thus far in this section contain a larger symmetry than QCD. Assuming no external fields with exception of $\chi = 2B_0 M$ [cf. Eqs. (3.31) and (3.25)], both $\mathcal{L}_2$ and $\mathcal{L}_4$ are invariant under the $\Phi(x) \to -\Phi(x)$ substitution, which amounts to having interaction terms with only an even number of Nambu-Goldstone bosons and is equivalent to saying that these terms are of even intrinsic parity [28]. Thus, $\mathcal{L}_2$ and $\mathcal{L}_4$ cannot describe processes such as $K^+K^- \to \pi^+\pi^-\pi^0$ or the decay $\pi^0 \to \gamma\gamma$ (after including a coupling to electromagnetic fields).

Let us next consider the $n_f = 3$ QCD Lagrangian from Eq. (3.21), with external sources v_μ, a_μ, s and p, and local chiral transformations given by Eq. (3.27). The anomalous change in the generating functional due to the non-invariance of the fermionic integration measure under the $U(1)_A$ transformation is given by [49]

$$\delta Z\,[v,a,s,p] = -\frac{N_C}{16\pi^2}\int d^4x\,\mathrm{Tr}\,[\beta(x)\Omega(x)]\,, \tag{3.50}$$

where $N_C = 3$ is the number of QCD colours, $\beta = \beta_a T^a$ and

$$\begin{aligned}\Omega(x) = \epsilon^{\mu\nu\sigma\rho}\Big[& v_{\mu\nu}v_{\sigma\rho} + \frac{4}{3}\nabla_\mu a_\nu \nabla_\sigma a_\rho + \frac{2}{3} i \left\{ v_{\mu\nu}, a_\sigma a_\rho \right\} + \frac{8}{3} i\, a_\sigma v_{\mu\nu} a_\rho \\ & + \frac{4}{3} a_\mu a_\nu a_\sigma a_\rho \Big]\end{aligned} \tag{3.51}$$

with $\epsilon_{0123} = 1$ and

$$v_{\mu\nu} = \partial_\mu v_\nu - \partial_\nu v_\mu - i\left[v_\mu, v_\nu\right], \quad \nabla_\mu a_\nu = \partial_\mu a_\nu - i\left[v_\mu, a_\nu\right]. \tag{3.52}$$

Note, that the anomalous change in the generating functional $\delta Z\left[v,a,s,p\right]$ is an $\mathcal{O}(p^4)$ effect in the chiral counting. Since the $U(1)_A$ anomaly explicitly violates the chiral symmetry at the fundamental QCD level, one must include in the effective theory a functional Z_A with the property that its change under a chiral gauge transformation reproduces Eq. (3.50). This functional has the explicit form [50, 51]

$$\begin{aligned}S[U,l,r]_{\mathrm{WZW}} = & -\frac{i\,N_C}{240\pi^2}\int d\sigma^{ijklm}\,\mathrm{Tr}\Big[\Sigma_i^L\Sigma_j^L\Sigma_k^L\Sigma_l^L\Sigma_m^L\Big] \\ & -\frac{i\,N_C}{48\pi^2}\int d^4x\,\epsilon_{\mu\nu\alpha\beta}\Big\{W(U,l,r)^{\mu\nu\alpha\beta} - W(\mathbb{1},l,r)^{\mu\nu\alpha\beta}\Big\},\end{aligned} \tag{3.53}$$

where

$$\begin{aligned}W(U,l,r)_{\mu\nu\alpha\beta} = & \,\mathrm{Tr}\left[U l_\mu l_\nu l_\alpha U^\dagger r_\beta\right] + \frac{1}{4}\mathrm{Tr}\left[U l_\mu U^\dagger r_\nu U l_\alpha U^\dagger r_\beta\right] \\ & + i\,\mathrm{Tr}\left[U\partial_\mu l_\nu l_\alpha U^\dagger r_\beta\right] + i\,\mathrm{Tr}\left[\partial_\mu r_\nu U l_\alpha U^\dagger r_\beta\right] \\ & - i\,\mathrm{Tr}\left[\Sigma_\mu^L l_\nu U^\dagger r_\alpha U l_\beta\right] + \mathrm{Tr}\left[\Sigma_\mu^L U^\dagger \partial_\nu r_\alpha U l_\beta\right] \\ & - \mathrm{Tr}\left[\Sigma_\mu^L\Sigma_\nu^L U^\dagger r_\alpha U l_\beta\right] + \mathrm{Tr}\left[\Sigma_\mu^L l_\nu \partial_\alpha l_\beta\right] + \mathrm{Tr}\left[\Sigma_\mu^L \partial_\nu l_\alpha l_\beta\right] \\ & - i\,\mathrm{Tr}\left[\Sigma_\mu^L l_\nu l_\alpha l_\beta\right] + \frac{1}{2}\mathrm{Tr}\left[\Sigma_\mu^L l_\nu \Sigma_\alpha^L l_\beta\right] - i\,\mathrm{Tr}\left[\Sigma_\mu^L\Sigma_\nu^L\Sigma_\alpha^L l_\beta\right] \\ & - (L \leftrightarrow R),\end{aligned} \tag{3.54}$$

with

$$\Sigma_\mu^L = U^\dagger\partial_\mu U, \quad \Sigma_\mu^R = U\partial_\mu U^\dagger, \tag{3.55}$$

and $(L \leftrightarrow R)$ standing for the interchanges $U \leftrightarrow U^\dagger$, $l_\mu \leftrightarrow r_\mu$ and $\Sigma_\mu^L \leftrightarrow \Sigma_\mu^R$. Note that the first line of Eq. (3.53) corresponds to the effective Wess-Zumino-Witten (WZW) action in the absence of external fields, where the $d\sigma^{ijklm}$ integration is over a five-dimensional manifold whose boundary is a four-dimensional Minkowski space, whilst the second line contains the additional terms in the anomalous action associated to the presence of external fields. Both terms in S_{WZW} are of $\mathcal{O}(p^4)$ according to the chiral counting rules [19].

Let us now look into the special case with coupling to the external electromagnetic four-vector potential by inserting the external sources

$$r_\mu = l_\mu = -eQA_\mu, \tag{3.56}$$

where Q is the quark-charge matrix from Eq. (3.25). Operating, one finds from the WZW action, i.e. second line of Eq. (3.53), the following expression for the relevant part of the

lowest-order anomalous Lagrangian [28]

$$\begin{aligned}\mathcal{L}^{\rm ext}_{\rm WZW} = & -eA_\mu J^\mu + i\frac{e^2}{48\pi^2}\epsilon^{\mu\nu\rho\sigma}\partial_\nu A_\rho A_\sigma \\ & \times {\rm Tr}\left[2Q^2\left(U\partial_\mu U^\dagger - U^\dagger\partial_\mu U\right) - QU^\dagger Q\partial_\mu U + QUQ\partial_\mu U^\dagger\right],\end{aligned} \tag{3.57}$$

where the current is given by

$$J^\mu = \frac{\epsilon^{\mu\nu\sigma\rho}}{48\pi^2}{\rm Tr}\left[Q\partial_\nu UU^\dagger\partial_\rho UU^\dagger\partial_\sigma UU^\dagger + QU^\dagger\partial_\nu UU^\dagger\partial_\rho UU^\dagger\partial_\sigma U\right]. \tag{3.58}$$

With this equation, one can now calculate the decay rate $\pi^0 \to \gamma\gamma$, which is found to be

$$\Gamma(\pi^0 \to \gamma\gamma) = \left(\frac{N_C}{3}\right)^2 \frac{\alpha^2 M_\pi^3}{64\pi^3 F^2} = 7.7\ {\rm eV}, \tag{3.59}$$

where F is set to $F = f_\pi$. This result is in excellent agreement with the measured empirical value of (7.63 ± 0.16) eV for $N_C = 3$.

3.3 Large-N_C limit of QCD

The $1/N_C$ expansion of QCD is an attempt to create a perturbative framework where none exists otherwise [5]. The general idea is to extrapolate the physical value for the number of QCD colours from $N_C = 3$ to $N_C \to \infty$ [52], whilst scaling the strong coupling constant in such a way that $g_s^2 N_C$ remains finite. This enables the amplitudes in the theory to be analysed in powers of $1/N_C$ and the expectation is that significant dynamical insights can be drawn that may be relevant to the real world.

In going from colour $SU(3)$ to $SU(N_C)$, the quark and gluon representations are promoted from the original 3 and 8 to N_C and $N_C^2 - 1$, respectively. Consequently, at large N_C there are $N_C^2 - 1 \approx N_C^2$ gluons, whilst only N_C colours for a given quark, which means that the gluon dynamics becomes dominant in this limit. The perturbative analysis of large-N_C QCD becomes simpler by making use of the double-line notation in Feynman diagrams [52–54], where the colour flow becomes explicit as in $\bar{q}_i(G_\mu)^i_j q^j$, with $i, j = 1, ..., N_C$ being colour indices (see Fig. 3.1 where a few examples are explicitly shown). In this notation, quarks carry one colour label whilst gluons carry two (see, e.g., Refs. [5, 19, 54] for a pedagogical introduction to the topic). Several simple large N_C-counting rules emerge by examining the behaviour of Feynman diagrams in the large-N_C limit [54]: (i) the LO contributions are planar diagrams containing the minimum number of quark loops; (ii) non-planar diagrams are suppressed by factors of N_C^{-2}; and (iii) internal quark loops are suppressed by factors of $1/N_C$. Out of these rules, a general statement surfaces which is that in the large-N_C limit diagrams that are planar and with only a single quark running at the edge dominate.[14]

Assuming that colour confinement persists at $N_C \to \infty$, one expects that the particle spectrum continues to be divided into mesons and baryons. The wavefunction of a meson can be written as [5]

$$|\bar{q}^{(\alpha)} q^{(\beta)}\rangle_{\rm colour\ singlet} \sim \frac{1}{\sqrt{N_C}} d_i^{(\alpha)\dagger} b_i^{(\beta)\dagger} |0\rangle\,, \tag{3.60}$$

[14] One must note that, since the one-loop gluon vacuum polarisation is required to have a smooth limit at large N_C, the strong coupling constant g_s must scale as $\mathcal{O}(1/\sqrt{N_C})$; accordingly, adding an extra internal gluon propagator to a LO diagram effectively introduces an additional colour loop factor N_C that is cancelled by the additional two (gluon-quark-quark) vertex factors $(1/\sqrt{N_C})^2$ fulfilling, therefore, the above general statement.

(A) Propagators

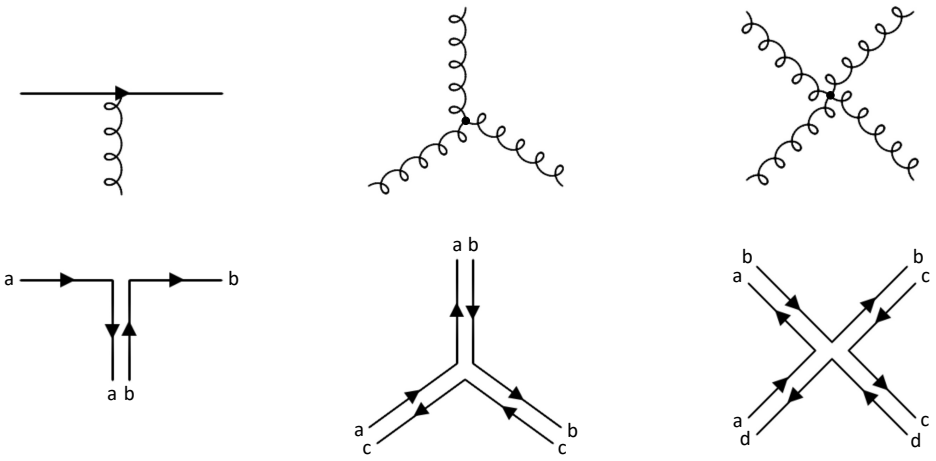

(B) Vertices

FIGURE 3.1: Propagators and vertices in the double line notation showing the colour flow.

where α and β are flavour labels, i is a colour index, $b^\dagger$ ($d^\dagger$) is the quark (antiquark) creation operator, and the $\sqrt{N_C}$ factor in the denominator is needed to normalise the wavefunction, as a sum over quark colours is required to form a colour singlet. It is not difficult to see that a meson propagator is, therefore, of order $\mathcal{O}(1)$ in N_C, since the $(1/\sqrt{N_C})^2$ factors from the wavefunction normalisation cancel the N_C factor from the quark loop. This in turn leads to meson masses, which appear in the denominator of propagators, being of $\mathcal{O}(1)$ in the large-N_C limit. Thus, meson masses remain close to their physical values at $N_C \to \infty$.

The two-body decay amplitude of a meson is of order $(1/\sqrt{N_C})^3 N_C = 1/\sqrt{N_C}$, where the factor $(1/\sqrt{N_C})^3$ comes from the three-meson wavefunction normalisation and the last N_C is the quark-loop colour factor, which renders the decay rate of order $1/N_C$. Consequently, the large-N_C limit involves narrow meson resonances, i.e. $\Gamma/M \to 0$. The rate of a meson decaying into three final states, by the same arguments, is further suppressed to order N_C^{-2} and, therefore, this provides a qualitative explanation for the two-body meson decay dominance in the real world. Likewise, meson-meson scattering amplitudes are of order $(1/\sqrt{N_C})^4 N_C = 1/N_C$, which suggests that mesons are stable and non-interacting at large N_C. Mixing of neutral mesons, including any number of gluons n_g, is of order[15] $(1/\sqrt{N_C})^2 (1/\sqrt{N_C})^{2n_g} N_C^{n_g} = 1/N_C$ and, therefore, suppressed in the $N_C \to \infty$ limit.

Moreover, the number of meson states is infinite in the large-N_C limit [54]. One way to see this is by noting that a generic n-point function of local quark bilinears $J = \bar{q}\Gamma q$,

$$\langle 0 | J_1(x_1) ... J_n(x_n) | 0 \rangle \,, \tag{3.61}$$

[15]The factor $(1/\sqrt{N_C})^2$ comes from the two-meson wavefunction normalisation, the factor $(1/\sqrt{N_C})^{2n_g}$ originates from the $2n_g$ gluon-quark-quark vertex factors and the $N_C^{n_g}$ factor arises from the additional colour loops associated to the n_g gluons.

is of order N_C. By inspecting two-point correlation function diagrams, one finds that at large N_C the only possible singularities correspond to one-meson poles.[16] Thus, a two-point function in momentum space can be written in the large-N_C limit as [54]

$$\langle 0|\, J_1(k) J_2(-k)\, |0\rangle = \sum_n \frac{a_n^2}{k^2 - M_n^2}\,. \tag{3.62}$$

From this, it is not difficult to see that the number of meson states must be infinite, since the left-hand side behaves logarithmically for large k^2 (down to asymptotic freedom) and the right-hand side would behave as $1/k^2$ for large k^2 should there be a finite number of states n. In addition to this, given that the one-particle poles must lay on the real axis for the spectral representation to hold, one can infer that the mesons are stable at $N_C \to \infty$.

A consequence of internal quark loops being suppressed by factors of $1/N_C$ in the large-N_C limit, which in turn is connected to the fact that there are N_C quark states whilst N_C^2 gluon states, is that the $\bar{q}q$ sea is virtually absent in the $N_C \to \infty$ limit. Similarly, $\bar{q}q\bar{q}q$ exotic states are heavily suppressed given that, in this limit, mesons do not interact with each other and, therefore, cannot merge to form an exotic. The large-N_C limit also provides a dynamical explanation for the OZI rule at low energies. In particular, for diagrams with n_m mesons and n_g gluons, the OZI-violating configurations are of order $N_C^{n_g - n_m}$, whilst OZI-allowed diagrams are of order $N_C^{n_g - n_m + 1}$, rendering the processes that do not respect the OZI rule comparatively suppressed by a factor of $1/N_C$.

An intriguing unity between the pseudoscalar singlet $\eta'(960)$ and the octet of Nambu-Goldstone bosons arises in massless QCD in the $N_C \to \infty$ limit. In order to understand this, let us first look into the matrix elements of the octet of axial currents from Eq. (2.35),

$$\langle 0|\, J_A^{\mu b}(0)\, |P_a(q)\rangle = i\, f_a q^\mu \delta_{ab}\,. \tag{3.63}$$

At large N_C, these matrix elements involve a meson normalisation factor and a quark-colour loop and, thus, they are of order $(1/\sqrt{N_C})N_C = \sqrt{N_C}$, which in turn implies $f_a \sim \mathcal{O}(\sqrt{N_C})$. The divergence of these matrix elements takes the form

$$\langle 0|\, \partial_\mu J_A^{\mu b}(0)\, |P_a(q)\rangle = f_a M_a^2 \delta_{ab}\,, \tag{3.64}$$

which, as discussed before, leads to the conservation of the octet of axial currents in the chiral limit, where the pseudoscalar mesons are massless Goldstone bosons. This is not the case for the singlet axial current due to the effect of the $U(1)_A$ anomaly, which leads to

$$\langle 0|\, \partial_\mu J_A^{\mu 0}(0)\, |\eta_1(q)\rangle = f_{\eta_1} M_{\eta_1}^2 = \left\langle 0 \left| \frac{3 g_s^2}{32\pi^2} G^a_{\mu\nu} \widetilde{G}_a^{\mu\nu} \right| \eta_1(q) \right\rangle . \tag{3.65}$$

Using the large-N_C counting rules, one finds that the above matrix element is of order $(1/\sqrt{N_C})(1/\sqrt{N_C})^2 N_C = 1/\sqrt{N_C}$, where the first factor comes from the meson wave-function normalisation, the second originates from the square of the strong coupling constant and the last corresponds to the quark-colour loop. Thus, one sees that the effect of the anomaly disappears in the large-N_C limit and the mass of the singlet state vanishes, i.e. $M_{\eta'} \sim 1/N_C \to 0$, which enables the $\eta'(958)$ to become the ninth pseudo-Goldstone boson.

The large-N_C counting rules are, of course, satisfied in χPT. As just shown above, F is of order $\mathcal{O}(\sqrt{N_C})$ in the $N_C \to \infty$ limit, which in turn cancels the $\mathcal{O}(\sqrt{N_C})$ dependence of

[16] Note that in a confining theory any intermediate state of a two-point function is a perturbative approximation to a single meson [19].

the field operators $\vec{\phi}$ in the $U(\vec{\phi})$ matrix [see Eq. (3.17)], rendering $U(\vec{\phi}) \sim \mathcal{O}(1)$.[17] Meson masses are of order $\mathcal{O}(1)$ at large N_C and, consequently, momenta and derivatives also scale as $\mathcal{O}(1)$. From Eq. (3.37), one can easily infer that B_0 is of order $\mathcal{O}(1)$. Next, by noting that the generating functional in Eq. (3.32) involves classical sources that are coupled to QCD quark bilinears and the fact that correlation functions of quark currents are of order $\mathcal{O}(N_C)$, then it is not difficult to see that the chiral Lagrangian in Eq. (3.19) must also scale as $\mathcal{O}(N_C)$ at large N_C, i.e. $\mathcal{L}_{\text{eff}} \sim \mathcal{O}(N_C)$. On the other hand, chiral loops get a suppression factor of $(4\pi F)^{-2} \sim \mathcal{O}(1/N_C)$ for each loop [19]. Similarly, a trace taken over flavour indices amounts to a sum over the quark flavours, which can only arise in a quark loop [5]; accordingly, any additional flavour trace in operators gets a $1/N_C$ suppression. Taking all this into account,[18] the large-N_C limit predicts the following ordering for the chiral coefficients in $\mathcal{L}_4$ [19]

$$\begin{aligned} L_1\,,\, L_2\,,\, L_3\,,\, L_5\,, L_8\,,\, L_9\,,\, L_{10} &= \mathcal{O}(N_C)\,, \\ 2L_1 - L_2\,,\, L_4\,,\, L_6\,,\, L_7 &= \mathcal{O}(1)\,, \end{aligned} \tag{3.66}$$

which is good agreement with phenomenological and lattice simulation results (see Tables 3.1 and 3.2).

It may be worth mentioning before concluding that baryons have a completely different behaviour in the large-N_C limit. In particular, given that to form a colour singlet one needs to combine N_C quarks in a totally colour-antisymmetric fashion, the mass of baryons grow as $\mathcal{O}(N_C)$ and, thus, become infinitely massive in the $N_C \to \infty$ limit [5]. For more details on baryons in the $1/N_C$ expansion, the reader is referred to [54].

Despite the explanatory power provided by the large-N_C framework, one must not forget that in the real world $N_C = 3$ and, thus, one finds experimental evidence for η-η' mixing, meson decays and scattering, finite masses for baryons, etc., which are forbidden in the $N_C \to \infty$ limit. In any case, the large-N_C limit of QCD provides a useful theoretical framework to qualitatively explain a number of dynamical effects that would otherwise remain unexplained.

3.3.1 Large-N_C chiral perturbation theory

Large-N_C χPT is the effective field theory of QCD in the chiral and large-N_C limits [57]. As seen in the previous subsection, in the large-N_C limit the $U(1)_A$ anomaly is absent and the pseudoscalar singlet η_1 becomes the ninth Nambu-Goldstone boson associated to the spontaneous breaking of $U(3)_L \times U(3)_R \to U(3)_V$. Both chiral and large-$N_C$ corrections are treated perturbatively in this framework [57, 58]. The effective Lagrangian is, thus, organised as a simultaneous expansion in powers of momenta, quark masses and $1/N_C$ [57, 59]

$$\mathcal{L}_{\text{eff}} = \mathcal{L}^{(0)} + \mathcal{L}^{(1)} + \mathcal{L}^{(2)} + \ldots\,, \tag{3.67}$$

where the superscripts arrange the perturbative expansion in contributions of order 1, δ, δ^2, ..., based on the following counting rules

$$\partial_\mu = \mathcal{O}(\sqrt{\delta})\,, \quad m_q = \mathcal{O}(\delta)\,, \quad 1/N_C = \mathcal{O}(\delta)\,. \tag{3.68}$$

[17] Note that each additional pseudoscalar meson state coupled to a current brings a suppression factor of $1/\sqrt{N_C}$ from the wavefunction normalisation.

[18] There are a few caveats associated to the operators O_1, O_2 and O_7 of the $\mathcal{O}(p^4)$ χPT Lagrangian that are explained in detail in Refs. [5, 19]. Without going into detail, it is worth highlighting that, since $M_{\eta'} \sim \mathcal{O}(1/N_C)$, the L_7 coupling could naively be considered of order $\mathcal{O}(N_C^2)$ [42]. However, the large-N_C counting is not consistent if one takes the limit of a heavy η' mass whilst keeping m_s small [55, 56].

At lowest order, $\mathcal{O}(\delta^0)$, the effective Lagrangian is given by

$$\mathcal{L}^{(0)} = \frac{F^2}{4}\mathrm{Tr}\left[D_\mu \widetilde{U}^\dagger D^\mu \widetilde{U}\right] + \frac{F^2}{4}\mathrm{Tr}\left[\widetilde{U}^\dagger \chi + \chi^\dagger \widetilde{U}\right] - \frac{1}{2}\tau(\psi+\theta)^2\,, \tag{3.69}$$

where $F \sim \sqrt{N_C}$ is the pion decay constant in the chiral limit, $\tau \sim \mathcal{O}(1)$ is the topological susceptibility of the purely gluonic theory [59] and $\chi = 2B_0(s+ip)$ [cf. Eq. (3.31)], with $B_0 \sim \mathcal{O}(1)$ being connected to the vacuum quark condensate. The unitary 3×3 matrix $\widetilde{U} = \exp\left\{i\sqrt{2}\widetilde{\Phi}/F\right\}$ collects the dynamical degrees of freedom, with

$$\widetilde{\Phi} \equiv \sum_{a=0}^{8}\frac{\lambda_a}{\sqrt{2}}\phi_a = \begin{pmatrix} \frac{1}{\sqrt{2}}\pi^0 + \frac{1}{\sqrt{6}}\eta_8 + \frac{1}{\sqrt{3}}\eta_1 & \pi^+ & K^+ \\ \pi^- & -\frac{1}{\sqrt{2}}\pi^0 + \frac{1}{\sqrt{6}}\eta_8 + \frac{1}{\sqrt{3}}\eta_1 & K^0 \\ K^- & \overline{K}^0 & -\frac{2}{\sqrt{6}}\eta_8 + \frac{1}{\sqrt{3}}\eta_1 \end{pmatrix}, \tag{3.70}$$

where the mathematical states $\eta_B^T \equiv (\eta_8, \eta_1)$ in the so-called octet-singlet basis are related to the physical states $\eta_P^T \equiv (\eta, \eta')$ by the following orthogonal transformation (see Appendix A)

$$\begin{pmatrix}\eta_8 \\ \eta_1\end{pmatrix} = \begin{pmatrix}\cos\theta_P & \sin\theta_P \\ -\sin\theta_P & \cos\theta_P\end{pmatrix}\begin{pmatrix}\eta \\ \eta'\end{pmatrix}, \tag{3.71}$$

with θ_P being the η-η' mixing angle in the octet-singlet basis at this order. Furthermore, $\psi = \sqrt{6}\eta_1/F$ is a dimensionless field variable defined such that $\det\{\widetilde{U}\} = \exp\{i\psi\}$ [42] and θ is a real field coupling to the winding number density.[19] Finally, D_μ is the covariant derivative defined in Eq. (3.28).

For completeness, we enumerate the remaining counting rules of large-N_C χPT: (i) the vacuum angle, θ, and the effective fields $\widetilde{U}(x)$ and $\psi(x)$ are treated as quantities of order 1; (ii) the vector and axial-vector external fields, $v_\mu(x)$ and $a_\mu(x)$, both used in the definition of D_μ count as small perturbations of the same order as derivatives; and (iii) the scalar and pseudoscalar external fields, $s(x)$ and $p(x)$, are of the same order as the quark masses [57]. This is,

$$(\widetilde{U}, \psi, \theta) = \mathcal{O}(1)\,, \quad (v_\mu, a_\mu) = \mathcal{O}(\sqrt{\delta})\,, \quad (s,p) = \mathcal{O}(\delta)\,. \tag{3.72}$$

With these counting rules, it is straightforward to see that the first term in $\mathcal{L}^{(0)}$ is of order $\mathcal{O}(N_C, p^2)$, the second term[20] is of order $\mathcal{O}(N_C, m_q)$ and the third is of order $\mathcal{O}(1)$. The LO effective Lagrangian contains, therefore, 3 LECs, namely, F, B_0 and τ.

The effective Lagrangian $\mathcal{L}^{(1)} = \mathcal{O}(\delta)$ contains the contributions of $\mathcal{O}(N_C, p^4)$, $\mathcal{O}(p^2)$ and $\mathcal{O}(1/N_C)$. The explicit expression for $\mathcal{L}^{(1)}$ is given by [57]

$$\begin{aligned}\mathcal{L}^{(1)} = {} & L_2\mathrm{Tr}\left[D_\mu\widetilde{U}^\dagger D_\nu\widetilde{U} D^\mu\widetilde{U}^\dagger D^\nu\widetilde{U}\right] + (2L_2+L_3)\mathrm{Tr}\left[D_\mu\widetilde{U}^\dagger D^\mu\widetilde{U} D_\nu\widetilde{U}^\dagger D^\nu\widetilde{U}\right] \\ & + L_5\mathrm{Tr}\left[D_\mu\widetilde{U}^\dagger D^\mu\widetilde{U}\left(\widetilde{U}^\dagger\chi + \chi^\dagger\widetilde{U}\right)\right] + L_8\mathrm{Tr}\left[\widetilde{U}^\dagger\chi\widetilde{U}^\dagger\chi + \chi^\dagger\widetilde{U}\chi^\dagger\widetilde{U}\right] \\ & - iL_9\mathrm{Tr}\left[R_{\mu\nu}D^\mu\widetilde{U}D^\nu\widetilde{U}^\dagger + L_{\mu\nu}D^\mu\widetilde{U}^\dagger D^\nu\widetilde{U}\right] + L_{10}\mathrm{Tr}\left[R_{\mu\nu}\widetilde{U}L^{\mu\nu}\widetilde{U}^\dagger\right] \\ & + \frac{1}{12}F^2\Lambda_1 D_\mu\psi D^\mu\psi - \frac{1}{12}iF^2\Lambda_2(\psi+\theta)\mathrm{Tr}\left[\widetilde{U}^\dagger\chi - \chi^\dagger\widetilde{U}\right] \\ & + \frac{1}{12}H_0\,D_\mu\theta D^\mu\theta + H_1\mathrm{Tr}\left[R_{\mu\nu}R^{\mu\nu} + L_{\mu\nu}L^{\mu\nu}\right] + H_2\mathrm{Tr}\left[\chi^\dagger\chi\right], \end{aligned} \tag{3.73}$$

[19] The winding number density or topological charge density can be written as $\omega = \frac{\alpha_s}{8\pi}G\widetilde{G}$.

[20] Note that here we have made the following assignments $s = M$ and $p = 0$, where the quark-mass matrix M is given in Eq. (3.25).

where $D_\mu \widetilde{U}$ and $D_\mu \widetilde{U}^\dagger$ are, once again, defined in Eq. (3.28), the field strength tensors $R_{\mu\nu}$ and $L_{\mu\nu}$ are given in Eq. (3.29), and the other covariant derivatives can be expressed as

$$D_\mu \psi = \partial_\mu \psi - 2\mathrm{Tr}\left[a_\mu\right], \qquad D_\mu \theta = \partial_\mu \theta + 2\mathrm{Tr}\left[a_\mu\right]. \tag{3.74}$$

It should be noted that the large-N_C χPT counting rules imply that the LECs L_2, L_3, L_5, L_8, L_9 and L_{10} represent quantities of order $\mathcal{O}(N_C)$, whilst Λ_1 and Λ_2 are of order $\mathcal{O}(1/N_C)$. Regarding the contact terms, H_0 is of order $\mathcal{O}(1)$, whilst H_1 and H_2 are of order $\mathcal{O}(N_C)$.

To conclude, it is worth noting that in large-N_C χPT the number of independent LECs entering the low-energy representation of the effective action at NLO is about the same as for the $SU(3)$ Lagrangian: whilst the four parameters $2L_1 - L_2$, L_4, L_6 and L_7 are relegated to NNLO, three new LECs appear, namely τ, Λ_1 and Λ_2 [57].

3.4 Resonance chiral theory

As already discussed, χPT is the low-energy effective field theory of QCD and is valid up to some energy scale $\Lambda_{\chi\mathrm{PT}}$ close to the mass of the lowest-lying resonances, e.g. M_ρ. Well below $\Lambda_{\chi\mathrm{PT}}$, the resonance propagator can be approximated by

$$\frac{1}{p^2 - M_R^2} = -\frac{1}{M_R^2}\sum_{n=0}\left(\frac{p^2}{M_R^2}\right)^n, \quad (p^2 \ll M_R^2), \tag{3.75}$$

which means that the exchange of virtual resonances generates derivative Nambu-Goldstone couplings proportional to powers of $1/M_R^2$. At energies close to $\Lambda_{\chi\mathrm{PT}}$, though, χPT is no longer expected to provide accurate predictions, as the perturbative expansion cannot account for resonance poles, and other effective field theories with new degrees of freedom are required. In this section, we follow the presentation from Ref. [19], chapter 3.

As a consequence of confinement, the QCD hadronic spectrum constitutes a dual asymptotic representation of the quark and gluon degrees of freedom. In effect, the hadronic resonances represent the most important feature of the non-perturbative strong dynamics of QCD. Accordingly, the chiral couplings receive significant contributions from the exchange of these resonances. In particular, one expects that at $\mathcal{O}(p^4)$ the χPT couplings, L_i, are saturated by the resonance exchange parameters (i.e. the masses and couplings).

A systematic analysis of the role of the QCD resonances can be performed within the framework of resonance chiral theory (RχT), which constitutes an interpolating representation, defined in the intermediate energy region (i.e. $\sim 1-2$ GeV), between the short-distance QCD and χPT. In RχT, one writes the most general chiral-invariant Lagrangian containing the resonances of the type $V(1^{--})$, $A(1^{++})$, $S(0^{++})$ and $P(0^{-+})$, as well as the Nambu-Goldstone modes, as degrees of freedom. The associated generating functional is given by

$$\exp\{iZ\} = \int [dU][dV][dA][dS][dP] \exp\left\{ i\int d^4x\, \mathcal{L}(U,V,A,S,P)\right\}, \tag{3.76}$$

where the coupling constants in the Lagrangian are to be extracted from phenomenology at the resonance mass scale. By integrating out the heavy degrees of freedom of RχT, one recovers the low-energy theory with only Nambu-Goldstone bosons, i.e. χPT. Of course, all the information from the short-distance physics remains encoded in the coupling constants of the low-energy EFT.

The resonance states in the hadronic spectrum have got definite transformation properties under the vacuum symmetry group $H \equiv SU(3)_V$. These states need to be coupled to the Nambu-Goldstone modes in a chiral-invariant manner and for that the compensating transformation $h(\vec{\phi}, g)$ in Eq. (3.15) can be employed. With the canonical choice of coset

representative $\xi_R(\vec{\phi}) = \xi_L^\dagger(\vec{\phi}) \equiv u(\vec{\phi})$, the action of G [cf. Eq. (3.12)] leads to [19]

$$u(\vec{\phi}) \xrightarrow{\mathrm{G}} g_R u(\vec{\phi}) h^\dagger(\vec{\phi}, g) = h(\vec{\phi}, g) u(\vec{\phi}) g_L^\dagger \,. \tag{3.77}$$

Thus, the chiral transformation $(g_L, g_R) \in G$ of the quark fields results in a transformation $h(\vec{\phi}, g) \in H$ acting on the hadronic states. Since we are interested in resonances transforming as octets or singlets under $SU(3)_V$, one can write

$$R_8 \xrightarrow{\mathrm{G}} h(\vec{\phi}, g) R_8 h^\dagger(\vec{\phi}, g) \,, \quad R_1 \xrightarrow{\mathrm{G}} R_1 \,, \tag{3.78}$$

where $R_8 = \vec{\lambda}\vec{R}/\sqrt{2}$ and R_1 are the resonance octet and singlet, respectively. The non-linear realisation of G acting on the octet field R_8 is local, which requires us to define the covariant derivative [60]

$$\nabla_\mu R_8 = \partial_\mu R_8 + [\Gamma_\mu, R_8] \,, \tag{3.79}$$

where the connection

$$\Gamma_\mu = \frac{1}{2}\left[u^\dagger(\partial_\mu - i r_\mu) u + u(\partial_\mu - i l_\mu) u^\dagger\right] \tag{3.80}$$

guarantees that

$$\nabla_\mu R_8 \xrightarrow{\mathrm{G}} h(\vec{\phi}, g) \nabla_\mu R_8 h^\dagger(\vec{\phi}, g) \,. \tag{3.81}$$

Let us define the following useful covariant parameters that shall be employed later

$$u_\mu \equiv i u^\dagger (D_\mu U) u^\dagger = u_\mu^\dagger \,, \quad \chi_\pm \equiv u^\dagger \chi u^\dagger \pm u \chi^\dagger u \,, \quad f_\pm^{\mu\nu} = u L^{\mu\nu} u^\dagger \pm u^\dagger R^{\mu\nu} u \,, \tag{3.82}$$

where u is the canonical coset representative that fulfils the condition $U = u^2$, and D_μ, χ, $L^{\mu\nu}$ and $R^{\mu\nu}$ are defined, respectively, in Eqs. (3.28), (3.31) and (3.29). All the quantities in Eq. (3.82) transform as $SU(3)_V$ octets, i.e. $X \xrightarrow{\mathrm{G}} h(\vec{\phi}, g) X h^\dagger(\vec{\phi}, g)$, and can easily be combined with the resonance fields to build chiral-invariant structures.

It is convenient to collect the octet and singlet resonances into a nonet multiplet, which can be done using the large-N_C limit whereby the resonances become degenerate in the chiral limit, such that

$$R \equiv R_8 + \frac{1}{\sqrt{3}} R_1 \mathbb{1} = \frac{1}{\sqrt{2}} \vec{\lambda}\vec{R} + \frac{1}{\sqrt{3}} R_1 \mathbb{1} \,. \tag{3.83}$$

Consequently, RχT employs the counting rules of large-N_C χPT to organise the perturbative expansion. Noting that the RχT couplings are of order $\mathcal{O}(\sqrt{N_C})$ [56], then the RχT Lagrangian can be systematically arranged according to the number of resonance fields in the interaction terms. In order to compute the resonance-exchange contributions to the $\mathcal{O}(p^4)$ χPT Lagrangian, it suffices to consider the LO couplings to the Nambu-Goldstone modes that are linear in the resonance fields [19]

$$\mathcal{L}_{\mathrm{R}\chi\mathrm{T}} \doteq \sum_R \mathcal{L}_R = \mathcal{L}_V + \mathcal{L}_A + \mathcal{L}_S + \mathcal{L}_P \,. \tag{3.84}$$

Let us investigate the different individual contributions to $\mathcal{L}_{\mathrm{R}\chi\mathrm{T}}$. In particular, the spin-0 Lagrangian, which caters for $R = S, P$, is given by

$$\mathcal{L}_R = \frac{1}{2}\mathrm{Tr}[\nabla^\mu R \nabla_\mu R - M_R^2 R^2] + \mathrm{Tr}[R \chi_R] \,, \tag{3.85}$$

where M_R is a common resonance multiplet mass, and the first and second traces correspond, respectively, to the kinetic and interaction terms. As it turns out, by invoking C and P invariance, it can be shown that the resonance interaction terms are governed by the $\mathcal{O}(p^2)$

chiral structures

$$\chi_S = c_d u_\mu u^\mu + c_m \chi_+ \,, \quad \chi_P = d_m \chi_- \,. \tag{3.86}$$

One can now express the solutions of the resonance equations of motion at low energies in terms of the local chiral operators, which contain light fields only, rendering

$$R = \frac{1}{M_R^2}\chi_R + \mathcal{O}\left(\frac{p^4}{M_R^4}\right). \tag{3.87}$$

By plugging Eqs. (3.87) and (3.86) into Eq. (3.85), one can find the LO contributions to the $\mathcal{O}(p^4)$ χPT Lagrangian, which take the form

$$\Delta\mathcal{L}_4^R = \sum_{R=S,P} \frac{1}{2M_R^2}\mathrm{Tr}[\chi_R \chi_R]\,. \tag{3.88}$$

This result can be expressed in the standard basis of χPT from Eq. (3.45), which in turn enables the identification of the following spin-0 resonance-exchange contributions to the $\mathcal{O}(p^4)$ χPT LECs [56, 60]

$$L_3^S = \frac{c_d^2}{2M_S^2}\,, \quad L_5^S = \frac{c_d c_m}{M_S^2}\,, \quad L_8^{S+P} = \frac{c_m^2}{2M_S^2} - \frac{d_m^2}{2M_P^2}\,. \tag{3.89}$$

As it can be seen, scalar exchanges contribute to L_3, L_5 and L_8, whilst the exchange of pseudoscalar resonances contribute to L_8 only.

Let us now look into the singlet η_1 resonance-exchange contribution to the $\mathcal{O}(p^4)$ χPT couplings. As it should clear, the singlet state has got a much larger mass than the octet of Nambu-Goldstone bosons due to the effect of the $U(1)_A$ anomaly, and, thus, this state is integrated out along with other massive resonances in the context of χPT. One can extract the LO effects, though, from the $U(3)_L \times U(3)_R$ chiral Lagrangian, which contains the matrix $\widetilde{U}(\vec{\phi})$ that collects the nonet of pseudoscalar fields

$$\mathcal{L}_2^{(U3)} \doteq \frac{F^2}{4}\mathrm{Tr}[\widetilde{U}^\dagger \chi + \chi^\dagger \widetilde{U}]\,. \tag{3.90}$$

From this, it can be shown that the exchange of the η_1 meson generates the following $\mathcal{O}(p^4)$ LEC contribution [19]

$$L_7^{\eta_1} = -\frac{F^2}{48M_{\eta_1}^2}\,. \tag{3.91}$$

It is important to note, however, that the singlet and octet contributions to L_7 exactly cancel each other at large N_C, which explains the result in Eq. (3.89).

Next, let us explore the $\mathcal{L}_V$ and $\mathcal{L}_A$ parts of $\mathcal{L}_{\mathrm{R}\chi\mathrm{T}}$ in Eq. (3.84). The spin-1 Lagrangian, with $R = V, A$, can more conveniently be written in terms of the anti-symmetric tensor fields $V_{\mu\nu}$ and $A_{\mu\nu}$ [60, 61], i.e.[21]

$$\mathcal{L}_R = -\frac{1}{2}\mathrm{Tr}[\nabla^\lambda R_{\lambda\mu}\nabla_\nu R^{\nu\mu} - \frac{M_R^2}{2}R_{\mu\nu}R^{\mu\nu}] + \mathrm{Tr}[R_{\mu\nu}\chi_R^{\mu\nu}]\,, \tag{3.92}$$

where the first and second traces correspond to the kinetic and interaction terms, respectively, and the $\mathcal{O}(p^2)$ chiral structures take the form

$$\chi_V^{\mu\nu} = \frac{F_V}{2\sqrt{2}}f_+^{\mu\nu} + \frac{iG_V}{\sqrt{2}}u^\mu u^\nu\,, \quad \chi_A^{\mu\nu} = \frac{F_A}{2\sqrt{2}}f_-^{\mu\nu}\,. \tag{3.93}$$

[21] Do not confuse $R_{\mu\nu}$ in Eq. (3.92) with the field strength tensor of right-handed external fields in Eq. (3.29).

Following the same procedure as for the spin-0 resonances, one can obtain the following vector and axial-vector contributions to the $\mathcal{O}(p^4)$ χPT LECs [60]

$$\begin{aligned} L_1^V &= \frac{G_V^2}{8M_V^2}\,, \qquad L_2^V = 2L_1^V\,, \qquad L_3^V = -6L_1^V\,, \\ L_9^V &= \frac{F_V G_V}{2M_V^2}\,, \qquad L_{10}^{V+A} = -\frac{F_V^2}{4M_V^2} + \frac{F_A^2}{4M_A^2}\,. \end{aligned} \tag{3.94}$$

Thus, vector-meson exchanges contribute to L_1, L_2, L_3, L_9 and L_{10}, whilst the exchange of axial-vector resonances contribute to L_{10} only.

It is important to highlight that the predicted contributions to the $\mathcal{O}(p^4)$ χPT LECs from the exchange of resonances provides a dynamical explanation to the phenomenological values shown in Table 3.1. As it can be seen in this table, the couplings L_4 and L_6 are consistent with zero and much smaller than the other LECs, which can be explained by the fact that they do not receive any contributions from the exchange resonances [cf. Eqs. (3.89) and (3.94)]. The coupling L_1 is predicted to be positive, in accordance with its phenomenological value, and the relation $L_2 = 2L_1$ is approximately satisfied. The prediction for L_7 being negative turns out to be also correct and of order $\mathcal{O}(1)$. All the other couplings are of order $\mathcal{O}(N_C)$.

By setting $F \approx f_\pi = 92.2$ MeV, which can be done at this order in the chiral expansion, and $M_V = M_\rho = 775$ MeV, one obtains the numerical result $|F_V| = 154$ MeV from $\Gamma(\rho^0 \to e^+e^-)$. As well as this, one can find $|G_V| = 53$ MeV from the experimental data on the electromagnetic pion radius, whilst $|G_V| \sim 69$ MeV is found from $\Gamma(\rho^0 \to 2\pi)$ [60]. For the axial parameters, use of Weinberg's sum rules [62],

$$F_V^2 - F_A^2 = F^2\,, \quad M_V^2 F_V^2 - M_A^2 F_A^2 = 0\,, \tag{3.95}$$

allows one to compute $F_A = 123$ MeV and $M_A = 968$ MeV.

There is, of course, more information that can be extracted from the short-distance properties of the underlying QCD dynamics, which can further constraint the RχT parameters [19, 63]. In particular, the matrix element of the vector current between two Nambu-Goldstone bosons can be parameterised by the vector form factor

$$F_V(t) = 1 + \frac{F_V G_V}{F^2}\frac{t}{M_V^2 - t}\,. \tag{3.96}$$

From this, one can easily extract the relation

$$F_V G_V = F^2\,, \tag{3.97}$$

which is found after imposing that $F_V(t)$ vanishes at infinite momentum transfer t.[22] Likewise, the matrix element of the axial current between a Nambu-Goldstone state and a photon is characterised by the axial form factor

$$G_A(t) = \frac{2F_V G_V - F_V^2}{M_V^2} + \frac{F_A^2}{M_A^2 - t}\,, \tag{3.98}$$

from which one obtains the condition

$$2F_V G_V = F_V^2, \tag{3.99}$$

[22] This is known as the Brodsky-Lepage asymptotic behaviour of the form factor, which in turn is a direct consequence of pQCD at large momentum transfers [64].

TABLE 3.2: Values for the renormalised couplings $L_i^r(M_\rho)$ from RχT predictions without (column 3) and with (column 4) short-distance information. Values labelled with † are used as inputs [19].

$L_i^r(M_\rho)\times 10^3$			
i	$\mathcal{O}(N_C)$	RχT [60]	RχT$_{\rm SD}$ [56, 63]
1	$\mathcal{O}(N_C)$	0.6	0.9
2	$\mathcal{O}(N_C)$	1.2	1.8
3	$\mathcal{O}(N_C)$	-2.8	-4.8
4	$\mathcal{O}(1)$	0.0	0.0
5	$\mathcal{O}(N_C)$	$1.2^\dagger$	1.1
6	$\mathcal{O}(1)$	0.0	0.0
7	$\mathcal{O}(1)$	-0.3	-0.3
8	$\mathcal{O}(N_C)$	$0.5^\dagger$	0.4
9	$\mathcal{O}(N_C)$	$6.9^\dagger$	7.1
10	$\mathcal{O}(N_C)$	-5.8	-5.3

after requiring that the axial form factor $G_A(t)$ vanishes at $t\to\infty$. Combining the relations from Eqs. (3.97) and (3.99), together with Weinberg's sum rules from Eq. (3.95), allows one to write

$$F_V = 2G_V = \sqrt{2}F\,,\quad F_A = F\,,\quad M_A = \sqrt{2}M_V\,. \tag{3.100}$$

We can also obtain similar constraints from the scalar sector. Specifically, the matrix element of the scalar current between a kaon and a pion is parameterised by the scalar form factor [65, 66]

$$F_S^{K\pi}(t) = 1 + \frac{4c_m}{F^2}\left[c_d + (c_m - c_d)\frac{M_K^2 - M_\pi^2}{M_S^2}\right]\frac{t}{M_S^2 - t}\,, \tag{3.101}$$

from which one gets

$$4c_d c_m = F^2\,,\quad c_m = c_d\,, \tag{3.102}$$

after imposing $F_S^{K\pi}(t)\to 0$ when $t\to\infty$. In addition, from the difference between the two-point correlation functions of two scalar and two pseudoscalar currents $\Pi_{SS-PP}(t)$, which should vanish if chirality were absolutely preserved [19], one finds the conditions [67]

$$c_m^2 - d_m^2 = \frac{F^2}{8}\,,\quad c_m^2 M_S^2 - d_m^2 M_P^2 = \frac{3\pi\alpha_s}{4}F^4\,, \tag{3.103}$$

after requiring that $\Pi_{SS-PP}(t)$ vanishes as $1/t^2$ when $t\to\infty$ [68–70]. Accordingly, the scalar and pseudoscalar parameters are found by combining the constraints from Eqs. (3.102) and (3.103) resulting in[23] [56]

$$c_m = c_d = \frac{F}{2}\,,\quad d_m = \frac{F}{2\sqrt{2}}\,,\quad M_P \approx \sqrt{2}M_S\,. \tag{3.104}$$

Finally, one can plug the results from Eqs. (3.100) and (3.104) into Eqs. (3.89) and (3.94) to obtain the following expressions for the $\mathcal{O}(p^4)$ χPT LECs in terms of just three parameters,

[23] The last relation actually contains a small correction, $M_P = \sqrt{2}M_S(1-\delta)^{1/2}$, with $\delta \approx 3\pi\alpha_s F^2/M_S^2 \sim 0.08\alpha_s$, which can be safely neglected [19].

i.e. F, M_V and M_S,

$$\begin{aligned} 2L_1 = L_2 = \frac{1}{4}L_9 = -\frac{1}{3}L_{10} = \frac{F^2}{8M_V^2}\,, \\ L_3 = -\frac{3F^2}{8M_V^2} + \frac{F^2}{8M_S^2}\,, \quad L_5 = \frac{F^2}{4M_S^2}\,, \quad L_8 = \frac{3F^2}{32M_S^2}\,. \end{aligned} \tag{3.105}$$

In Table 3.2, we summarise the numerical predictions for the $\mathcal{O}(p^4)$ χPT couplings from RχT with and without short-distance information [19]. The numerical values employed for the RχT input parameters are $M_V = 775$ MeV, $M_S = 1.4$ GeV and $F = f_\pi = 92.2$ MeV. In addition, $M_{\eta_1} = 804$ MeV is used for the L_7 prediction.

3.5 Vector meson dominance

Before QCD was discovered, the physics of hadrons was described using a variety of phenomenological models, which incorporated the approximate symmetries of the strong interactions. Some of these models still play an important role in our understanding of hadronic physics nowadays, which is down to the physical insight behind them, as well as our inability to solve QCD in the non-perturbative regime.

In particular, the interaction between hadronic matter and the photon is successfully described by the vector meson dominance (VMD) model, which posits that the hadronic components of the photon vacuum polarisation consists exclusively of vector mesons [71]. The prime ingredient of QCD at low energies appears to be the hadronic spectrum of the theory, which is supported by the fact that the χPT $\mathcal{O}(p^4)$ counterterms are saturated by the exchange of hadronic resonances, as we saw in Sec. 3.4. This idea puts VMD on firm footing at energies below ~ 1 GeV, where the main dynamical effect is associated to the exchange of vector mesons. Despite the fact that VMD enjoys considerable phenomenological support, it has never been formally derived from the SM [5].[24]

In the early 1960s, Sakurai proposed a theory of the strong interactions mediated by the exchange of intermediate vector mesons [72]. His theory was based on the ideas laid out by Yang and Mills on non-Abelian gauge theory [73]. Despite being able to generate the required interaction terms by minimal substitution in the Lagrangian, the mass term associated to the vector mesons destroyed the local gauge invariance. A few years later, Kroll et al. [74] attempted to derive VMD from field theory and found that the hadronic contribution to the polarisation of the photon takes the form of a propagating vector meson [71] (cf. Fig. 3.2). This in turn is directly linked to the idea that the hadronic electromagnetic current operator is proportional to the vector meson fields. For the neutral ρ^0 meson, this turns out to be[25]

$$J_\mu^{em}(x) = \frac{M_\rho^2}{\sqrt{2}g_\rho}\rho_\mu^0(x)\,, \tag{3.106}$$

which is known as the current-field identity and can be generalised to the isovector field $\vec{\rho}(x)$. The conservation of electromagnetic current in this equation implies that the $\vec{\rho}(x)$ field is divergenceless under the strong interactions, i.e.

$$\partial_\mu \vec{\rho}^{\,\mu} = 0\,, \tag{3.107}$$

[24] This is because, contrary to what happens in QED, high-order effects associated to the dressing of the $q\bar{q}$ quark-loop contribution to the photon propagator cannot be dismissed.

[25] Note that one could easily absorb the $\sqrt{2}$ in the denominator into the redefinition of the g coupling. However, we shall not do this in an effort to be consistent with the convention employed by Ref. [75], with the only caveat being that we use $f_\pi = 92.2$ MeV.

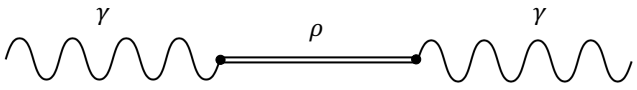

FIGURE 3.2: Hadronic contribution to the photon propagator in the VMD picture. Additional intermediate vector mesons are included in generalised VMD models.

which is, in fact, the usual Proca condition for a massive vector field coupling to a conserved current. The resulting Lagrangian for the hadronic sector obtained by Kroll et al. [74] also contained a mass term that violated the local (flavour) gauge symmetry.

Lurie managed to reproduce in Ref. [76] Sakurai's results employing conserved currents only. In this case, the Lagrangian is assumed to be invariant under global $SU(2)$ transformations and, thus, the presence of a mass term is innocuous. We start with the Lagrangian [71]

$$\mathcal{L} = -\frac{1}{4}\vec{\rho}_{\mu\nu}\cdot\vec{\rho}^{\mu\nu} + \frac{1}{2}M_\rho^2\vec{\rho}_\mu\cdot\vec{\rho}^\mu + \frac{1}{2}D_\mu\vec{\pi}\cdot D^\mu\vec{\pi} - \frac{1}{2}M_\pi^2\vec{\pi}\cdot\vec{\pi}\,, \tag{3.108}$$

where the vector meson field strength tensor takes the form

$$\vec{\rho}_{\mu\nu} = \partial_\mu\vec{\rho}_\nu - \partial_\nu\vec{\rho}_\mu - \sqrt{2}g\vec{\rho}_\mu\times\vec{\rho}_\nu \tag{3.109}$$

and the covariant derivative is defined as

$$D_\mu\vec{\pi} = \partial_\mu\vec{\pi} - \sqrt{2}g\vec{\rho}_\mu\times\vec{\pi}\,. \tag{3.110}$$

Note that the Lagrangian in Eq. (3.108) is invariant under the transformations

$$\vec{\rho}\to\vec{\rho}+\vec{\rho}\times\vec{\epsilon}, \quad \vec{\pi}\to\vec{\pi}+\vec{\pi}\times\vec{\epsilon}. \tag{3.111}$$

It is not difficult to find from Eq. (3.110) that

$$\frac{1}{2}D_\mu\vec{\pi}\cdot D^\mu\vec{\pi} = \frac{1}{2}\partial_\mu\vec{\pi}\cdot\partial^\mu\vec{\pi} - \sqrt{2}g\vec{\rho}_\mu\cdot(\vec{\pi}\times\partial^\mu\vec{\pi}) + g^2(\vec{\rho}_\mu\times\vec{\pi})^2\,, \tag{3.112}$$

which in turn can be plugged into Eq. (3.108) to obtain the equation of motion for the ρ field

$$\partial_\nu\vec{\rho}^{\mu\nu} + M_\rho^2\vec{\rho}^\mu = \sqrt{2}g\vec{J}_N^\mu\,, \tag{3.113}$$

where the Noether current turns out to be [71, 76]

$$\vec{J}_N^\mu = -\frac{\partial\mathcal{L}}{\partial(\partial_\mu\vec{\rho}_\nu)}\times\vec{\rho}_\nu - \frac{\partial\mathcal{L}}{\partial(\partial_\mu\vec{\pi})}\times\vec{\pi} = \vec{\rho}^{\mu\nu}\times\vec{\rho}_\nu + \vec{\pi}\times\partial^\mu\vec{\pi} + \sqrt{2}g(\vec{\rho}^\mu\times\vec{\pi})\times\vec{\pi}\,. \tag{3.114}$$

Since $\vec{J}_N^\mu$ must be conserved, Eq. (3.113) implies that the $\vec{\rho}_\mu$ field is necessarily divergenceless on account of $\vec{\rho}_{\mu\nu}$ being antisymmetric in its indices, as in Eq. (3.107). Expanding the field strength tensor in Eq. (3.113), moving the non-Abelian part of it to the right hand side and making use of the fact that the $\vec{\rho}$ field is divergenceless, allows one to write

$$(\partial^2 + M_\rho^2)\vec{\rho}^\mu = \sqrt{2}g\vec{J}^\mu\,, \tag{3.115}$$

with

$$\vec{J}^\mu = \vec{J}_N^\mu + \vec{\rho}^{\,\nu}\times\partial_\nu\vec{\rho}^\mu\,. \tag{3.116}$$

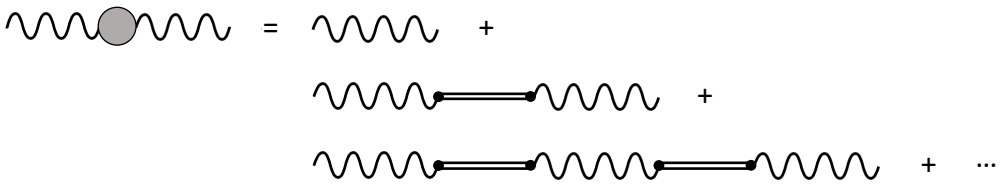

FIGURE 3.3: VMD dressing of the photon propagator.

In order to include the electromagnetic interactions into the model, we make use of Eqs. (3.106) and (3.115) to write a generic matrix element of the electromagnetic current J_μ^{em} as [71]

$$\begin{aligned}\langle B|\, eJ_\mu^{em}\,|A\rangle &= e\,\langle B|\,\frac{M_\rho^2}{\sqrt{2}g_\rho}\rho_\mu^0\,|A\rangle = \frac{eM_\rho^2}{\sqrt{2}g_\rho}\,\langle B|\,\frac{-\sqrt{2}gJ_\mu^0}{q^2-M_\rho^2}\,|A\rangle \\ &= \frac{-ieM_\rho^2}{\sqrt{2}g_\rho}\frac{-i}{q^2-M_\rho^2}\,\langle B|\,\sqrt{2}gJ_\mu^0\,|A\rangle\,,\end{aligned} \tag{3.117}$$

where the substitution $\partial_\mu \to iq_\mu$ has been employed and only the third component of the isotriplet has been considered for simplicity.[26] It is important to notice from Eq. (3.117) that the photon seems to couple to the hadronic matrix element with strength $eM_\rho^2/\sqrt{2}g_\rho$ via a ρ meson.

At this point, one can assume that the effects of the ρ self-interaction are negligible, which is a reasonable approximation considering that the ρ^0 decays almost exclusively via the two-pion channel. This allows writing the hadronic current of Eq. (3.116) as

$$J_\pi^\mu = (\vec{\pi}\times\partial^\mu\vec{\pi})_0\,, \tag{3.118}$$

which in the charge basis can be expressed as

$$J_\pi^\mu = i(\pi^-\partial^\mu\pi^+ - \pi^+\partial^\mu\pi^-)\,. \tag{3.119}$$

Accordingly, the associated part of the Lagrangian takes the simple form

$$\mathcal{L}_{\rho\pi} = -\sqrt{2}g_{\rho\pi\pi}\rho_\mu^0 J_\pi^\mu\,, \tag{3.120}$$

where we have chosen to write the coupling constant g as $g_{\rho\pi\pi}$.

It is worth noting that one may naively guess the interaction part of the electromagnetic Lagrangian by making use of Eq. (3.106) so that

$$\mathcal{L}_{\gamma\rho} = -eJ_\mu^{em}A_\mu = -\frac{eM_\rho^2}{\sqrt{2}g_\rho}\rho^0 A^\mu\,. \tag{3.121}$$

However, the addition of this term to the Lagrangian in Eq. (3.108), along with the associated kinetic term for the electromagnetic field, results in the photon acquiring an imaginary mass owing to the dressing of the photon propagator [72] (cf. Fig. 3.3). Instead, one must include the Lagrangian term

$$\mathcal{L}_{\gamma\rho} = -\frac{e}{2\sqrt{2}g_\rho}F_{\mu\nu}\rho^{\mu\nu}\,, \tag{3.122}$$

[26] Note that from this point forward we shall refer to the $\rho^0(x)$ meson only in the remaining calculations of this section.

which guarantees that the photon field remains massless. Note that in Eq. (3.122) $F_{\mu\nu}$ and $\rho^{\mu\nu}$ are, respectively, the field strength tensors for the electromagnetic and ρ^0 fields.[27] By expanding the product of field strength tensors, integrating by parts and substituting $\partial_\mu \to iq_\mu$, one finds that the above equation reduces in momentum space to

$$F_{\mu\nu}\rho^{\mu\nu} \to 2q^2 A^\mu \rho^0_\mu \,, \tag{3.123}$$

which can be interpreted as the photon decoupling from the ρ^0 (and, thus, from the hadronic matter) at $q^2 = 0$. This points towards the need for another term in the Lagrangian that directly couples the photon to hadronic matter. This happens to be

$$\mathcal{L}_{\gamma\pi} = -eA_\mu J^\mu_\pi \,, \tag{3.124}$$

which becomes dominant at $q^2 = 0$.

Summarising what we have discussed thus far, the full VMD Lagrangian can be expressed as [71]

$$\begin{aligned}\mathcal{L}_{\rm VMD} = &-\frac{1}{4}F_{\mu\nu}F^{\mu\nu} - \frac{1}{4}\rho_{\mu\nu}\rho^{\mu\nu} + \frac{1}{2}M^2_\rho \rho_\mu \rho^\mu - \sqrt{2}g_{\rho\pi\pi}\rho_\mu J^\mu_\pi \\ &- eA_\mu J^\mu_\pi - \frac{e}{2\sqrt{2}g_\rho}F_{\mu\nu}\rho^{\mu\nu} \,,\end{aligned} \tag{3.125}$$

where the shorthand notation $\rho_\mu \equiv \rho^0_\mu$ has been used. There is an alternative VMD formulation which has become the standard representation

$$\begin{aligned}\mathcal{L}'_{\rm VMD} = &-\frac{1}{4}F'_{\mu\nu}F'^{\mu\nu} - \frac{1}{4}\rho'_{\mu\nu}\rho'^{\mu\nu} + \frac{1}{2}M^2_\rho \rho'_\mu \rho'^\mu - \sqrt{2}g_{\rho\pi\pi}\rho'_\mu J^\mu_\pi \\ &- \frac{e' M^2_\rho}{\sqrt{2}g_\rho}\rho'_\mu A'^\mu + \frac{1}{2}\frac{e^2 M^2_\rho}{2g^2_\rho}A'_\mu A'^\mu \,.\end{aligned} \tag{3.126}$$

The two representation are equivalent to order $\mathcal{O}[(e/g_\rho)^3]$ in the limit of universality (i.e. $g_\rho = g_{\rho\pi\pi}$) and with the following substitutions [71]

$$\rho'_\mu = \rho_\mu + \frac{e}{\sqrt{2}g_\rho}A_\mu \,, \quad A'_\mu = A_\mu \sqrt{1 - \frac{e^2}{2g^2_\rho}} \,, \quad e' = e\sqrt{1 - \frac{e^2}{2g^2_\rho}} \,. \tag{3.127}$$

It is important to note that, whilst in Eq. (3.125) there is a direct coupling between the photon and hadronic matter, this term is missing in Eq. (3.126) and, instead, it contains a mass term for the photon.

One can compute the effect of the dressing of the photon propagator shown in Fig 3.3 using the standard representation of the VMD Lagrangian, which turns out to be

$$iD(q^2) = \frac{-i}{q^2 - \frac{e^2 M^2_\rho}{2g^2_\rho}} + \frac{-i}{q^2 - \frac{e^2 M^2_\rho}{2g^2_\rho}} \frac{-ieM^2_\rho}{\sqrt{2}g_\rho} \frac{-i}{q^2 - M^2_\rho} \frac{-ieM^2_\rho}{\sqrt{2}g_\rho} \frac{-i}{q^2 - \frac{e^2 M^2_\rho}{2g^2_\rho}} + \dots \,, \tag{3.128}$$

where the prime of the parameter e has been dropped for simplicity of notation. After resummation, one finds

$$iD(q^2) = \frac{-i}{q^2\left(1 + \frac{e^2}{2g^2_\rho}\frac{1}{1 - q^2/M^2_\rho}\right)} \,, \tag{3.129}$$

[27] Thus, the latter does not contain the non-Abelian cross product from Eq. (3.109).

which shows that the propagator has got the desired behaviour in the $q^2 \to 0$ limit, i.e.

$$iD(q^2) \to \frac{-i}{q^2(1+\frac{e^2}{2g_\rho^2})}\,. \tag{3.130}$$

It is worth noticing that the above equation appears to suggest a modification to the electromagnetic coupling constant of the form

$$e \to \frac{e}{\sqrt{1+\frac{e^2}{2g_\rho^2}}}\,. \tag{3.131}$$

Before concluding, we would like to highlight that, in the standard VMD representation, the pion form factor used for describing the process $\gamma \to \pi^+\pi^-$, which is the multiplicative deviation from a pointlike behaviour of the coupling of the photon to the pion field, can be written as

$$F_\pi(q^2) = -\frac{M_\rho^2}{q^2 - M_\rho^2}\frac{g_{\rho\pi\pi}}{g_\rho}\,. \tag{3.132}$$

At zero momentum transfer, the photon field sees only the charge of the pions and, therefore, the form factor should reduce to $F_\pi(0) = 1$ in the $q^2 \to 0$ limit. In order to fulfil this constraint, it is required that $g_{\rho\pi\pi} = g_\rho$, which is the basis for Sakurai's argument of universality, whereby it is assumed that all the interactions of the ρ meson are generated from the gauge principle through minimal substitution in the covariant derivative [72]. In this case, it is also a direct consequence of the ρ completely dominating the pion form factor [71].

3.5.1 Effective schemes for including vector mesons

In this subsection, we introduce the hidden symmetry scheme proposed by Bando et al. [77, 78] to explicitly incorporate the vector meson fields in the chiral Lagrangian. As well as this, we briefly present an alternative scheme known as the massive Yang-Mills approach put forward by Meissner, Schechter and other authors [79–82].

In the hidden symmetry (HS) scheme, the ρ-meson appears as the dynamical gauge boson of a hidden local symmetry in the non-linear chiral Lagrangian and its mass is generated by the Higgs mechanism associated to the partial spontaneous breaking of this local symmetry [71]. Let us start with the $SU(2)$ non-linear sigma-model Lagrangian [cf. Eq. (3.20)]

$$\mathcal{L} = \frac{f_\pi^2}{4}\mathrm{Tr}\left[\partial_\mu U^\dagger \partial^\mu U\right], \tag{3.133}$$

where $f_\pi = 92.2$ MeV is the pion decay constant and

$$U(x) = \exp\left\{i\sqrt{2}\,\frac{\pi(x)}{f_\pi}\right\}, \tag{3.134}$$

with $\pi(x) = \sqrt{2}\pi^a t^a$ and $t^a = \sigma^a/2$ being the generators of the $SU(2)$ symmetry group [cf. Eq. (2.21)]. Using Meissner's convention [79], the $U(x)$ field transforms under global chiral $SU(2)_L \times SU(2)_R$ as

$$U(x) \to g_L U(x) g_R^\dagger, \tag{3.135}$$

where $g_{L,R} \in SU(2)_{L,R}$. In addition to the chiral symmetry, we want to introduce a local hidden $SU(2)_V$ symmetry. In order to do this, let us first split the $U(x)$ field into two constituents that transform, respectively, under (left and right) $SU(2)_{L,R}$ so that

$$U(x) \equiv \xi_L^\dagger(x)\xi_R(x)\,, \tag{3.136}$$

where the $\xi_{L,R}(x)$ are $SU(2)$-valued entities transforming as

$$\xi_{L,R}(x) \to \xi_{L,R}(x) g^{\dagger}_{L,R} . \tag{3.137}$$

The crucial point here is that one assumes that, in addition, the components of the coset representative $\xi_{L,R}$ possess a local $SU(2)_V$ symmetry such that [79]

$$\xi_{L,R}(x) \to \lambda(x) \xi_{L,R}(x) g^{\dagger}_{R,L} , \tag{3.138}$$

with $\lambda(x) = e^{-i\alpha^a(x)t^a}$. It can immediately be seen that the $U(x)$ field is unaffected by this local $SU(2)_V$, although its components $\xi_{L,R}$ are not. Consequently, we say that it is a hidden symmetry [71].

One can now write the following $SU(2)_V$ invariant Lagrangians [75, 79]

$$\begin{aligned} \mathcal{L}_A = & -\frac{f_\pi^2}{4} \mathrm{Tr}[D_\mu \xi_L \xi_L^\dagger - D_\mu \xi_R \xi_R^\dagger]^2 , \\ \mathcal{L}_V = & -\frac{f_\pi^2}{4} \mathrm{Tr}[D_\mu \xi_L \xi_L^\dagger + D_\mu \xi_R \xi_R^\dagger]^2 , \end{aligned} \tag{3.139}$$

where the matrices ξ_L and ξ_R contain the pseudoscalar fields $\pi(x)$, as well as the unphysical fields $\tau(x)$ that will be absorbed to give mass to the vector mesons, i.e.

$$\xi_{L,R} = \exp\left\{ i \frac{\tau \mp \pi}{\sqrt{2} f_\pi} \right\} . \tag{3.140}$$

The covariant derivative takes the form

$$D_\mu \xi_{L,R} = \partial \xi_{L,R} - i g V_\mu \xi_{L,R} , \tag{3.141}$$

where we have introduced the gauge field

$$V_\mu(x) = \sqrt{2} V_\mu^a t^a . \tag{3.142}$$

Note that the Lagrangians in Eq. (3.139) are invariant under the local $SU(2)_V$ transformation $\lambda(x)$ so long as V_μ transforms as

$$V_\mu \to \lambda(x) V_\mu \lambda^\dagger(x) + \frac{i}{\sqrt{2} g} \lambda(x) \partial_\mu \lambda^\dagger(x) . \tag{3.143}$$

A kinetic term for the gauge field $V_\mu(x)$ is required so that $\mathcal{L}_V$ does not identically vanish when one uses the equation of motion (EOM) for V_μ [79]. Bando et al., thus, assumed that quantum mechanical effects at the composite level dynamically generate the corresponding kinetic term [71, 83]

$$-\frac{1}{4} \vec{G}_{\mu\nu} \cdot \vec{G}^{\mu\nu} , \tag{3.144}$$

where $G_{\mu\nu}$ is the non-Abelian field strength tensor associated to the vector meson

$$\vec{G}^i_{\mu\nu} = \partial_\mu \vec{V}^i_\nu - \partial_\nu \vec{V}^i_\mu - \sqrt{2} g \vec{V}_\mu \times \vec{V}_\nu . \tag{3.145}$$

Taking all this into account, we can construct the Lagrangian

$$\mathcal{L}_{\mathrm{HS}} = \mathcal{L}_A + a \mathcal{L}_V - \frac{1}{4} \vec{G}_{\mu\nu} \cdot \vec{G}^{\mu\nu} , \tag{3.146}$$

where a is an arbitrary parameter. The unphysical scalar degrees of freedom can be eliminated by choosing an appropriate $SU(2)_V$ gauge. This in turn is done by imposing the condition

$$\xi_L^\dagger = \xi_R = \exp\left\{ i\frac{\pi(x)}{\sqrt{2}f_\pi} \right\}. \tag{3.147}$$

To make further progress, we approximate $\xi_L^\dagger = \xi_R \approx 1 + i\pi(x)/\sqrt{2}f_\pi$, which allows the Lagrangian in Eq. (3.146) to be expressed as

$$\mathcal{L}_{\rm HS} = -\frac{1}{4}\vec{G}_{\mu\nu}\cdot\vec{G}^{\mu\nu} + \frac{f_\pi^2}{4}{\rm Tr}[\partial_\mu U^\dagger \partial^\mu U] + ag^2 f_\pi^2 \vec{V}_\mu \cdot \vec{V}^\mu - \frac{ag}{\sqrt{2}}\vec{V}^\mu \cdot (\vec{\pi}\times\partial_\mu\vec{\pi}), \tag{3.148}$$

where $\vec{\pi}\times\partial_\mu\vec{\pi}$ is the the hadronic current from Eqs. (3.114) and (3.118). Comparing this with Eq. (3.126), one can make the identifications $M_V^2 = 2ag^2 f_\pi^2$ and $g_{\rho\pi\pi} = \frac{1}{2}ag$.

Next, let us incorporate the electromagnetic interactions into the model. The photon field couples to the charge operator $Q = I_3^{(L+R)} + Y/2$, with $I_3^{(L+R)}$ and Y being, respectively, the global $SU(2)_L \times SU(2)_R$ isospins and hypercharge [79]. Note that these generators are independent of the ones associated to the hidden local $SU(2)_V$ to which the field V_μ couples. We can now extend the local gauge group $SU(2)_V \to SU(2)_V \times U(1)_Q$, where the $U(1)_Q$ is not a hidden symmetry. This in turn means that the $U(x)$ field must transform as [71]

$$U \to b(x) U b^\dagger(x), \tag{3.149}$$

where $b(x) = e^{-ie_0 Q\theta(x)}$, and Q and e_0 are, respectively, the generator and coupling constant of the $U(1)_Q$ group. This transformation demands that the ξ fields transform as

$$\xi_{L,R} \to \xi_{L,R} b^\dagger(x). \tag{3.150}$$

In addition, the covariant derivative in Eq. (3.141) must be redefined to include the new interaction term

$$D_\mu \xi_{L,R} = \partial\xi_{L,R} - i\sqrt{2}g\vec{V}_\mu\cdot\vec{t}\,\xi_{L,R} - ie_0\xi_{L,R}B_\mu t^3, \tag{3.151}$$

where B_μ is the new gauge field, which can be identified with the photon, and needs to transform as

$$B_\mu \to B_\mu - \frac{i}{e_0}\partial_\mu b^\dagger b, \tag{3.152}$$

to ensure invariance of the Lagrangians in Eq. (3.139) under $U(1)_Q$. Accordingly, Eq. (3.148) becomes

$$\begin{aligned}\mathcal{L}_{\rm HS} = & -\frac{1}{4}\vec{G}_{\mu\nu}\cdot\vec{G}^{\mu\nu} - \frac{1}{4}B_{\mu\nu}B^{\mu\nu} + \frac{f_\pi^2}{4}{\rm Tr}[\partial_\mu U^\dagger\partial^\mu U] \\ & + \frac{1}{2}M_\rho^2\vec{V}_\mu\cdot\vec{V}^\mu - \frac{e_0 M_\rho^2}{\sqrt{2}g}V_\mu^3 B^\mu + \frac{1}{2}\frac{e_0^2 M_\rho^2}{2g^2}B_\mu B^\mu \\ & - \frac{ag}{\sqrt{2}}\vec{V}^\mu\cdot(\partial_\mu\vec{\pi}\times\vec{\pi}) - e_0(1-\frac{a}{2})B^\mu(\partial^\mu\vec{\pi}\times\vec{\pi})_3,\end{aligned} \tag{3.153}$$

where $B_{\mu\nu}$ is the strength tensor of the field B_μ. The parameter a can be chosen to reproduce the standard VMD representation from Eq. (3.126). This is done with $a = 2$, which allows the direct coupling between the photon and the hadronic current [last term in Eq. (3.153)] to vanish, and imposes universality $g_{\rho\pi\pi} = ag/2 = g_\rho$. Furthermore, one can assume that the states V_μ^3 and B_μ mix in such a way that, after diagonalising the mass matrix, the physical

photon is massless [79]. Accordingly,

$$m_\gamma^2 = 0\,, \quad M_\rho^2 = a(2g^2 + e_0^2) f_\pi^2\,, \quad M_{\rho^\pm}^2 = 2ag^2 f_\pi^2\,, \tag{3.154}$$

and the mass eigenstates are given by

$$A_\mu = \frac{\sqrt{2}gB_\mu + e_0 V_\mu^3}{\sqrt{2g^2 + e_0^2}}\,, \quad V_\mu^0 = \frac{\sqrt{2}gV_\mu^3 - e_0 B_\mu^3}{\sqrt{2g^2 + e_0^2}}\,, \tag{3.155}$$

where the electromagnetic charge is given by

$$e = \frac{e_0}{\sqrt{1 + \frac{e_0^2}{2g^2}}} \approx e_0\,. \tag{3.156}$$

An alternative approach to the HS scheme just presented is the so-called massive Yang-Mills (YM) approach, in which the spin-1 fields are introduced in the ungauged Lagrangian through the covariant derivative. We start again with the non-linear sigma model from Eq. (3.133) and define the following covariant derivative

$$D_\mu U = \partial_\mu U + ig[V_\mu, U]\,, \tag{3.157}$$

where U and V_μ are given in Eqs. (3.134) and (3.142), respectively. From this, it is straightforward to find the lowest order Lagrangian [75]

$$\begin{aligned} \mathcal{L}_{\rm YM} = \frac{f_\pi^2}{4}{\rm Tr}[D_\mu U^\dagger D^\mu U] = i\sqrt{2}g\rho_\mu^0(\pi^+\partial^\mu\pi^- - \pi^-\partial^\mu\pi^+) \\ \times\left[1 - \frac{1}{3f_\pi^2}(\pi^0\pi^0 + 2\pi^+\pi^-)\right] + 2g^2\rho_\mu^0\rho^{0\mu}\pi^+\pi^- + \ldots\,, \end{aligned} \tag{3.158}$$

where only the terms involving interactions between the neutral ρ^0 and the pions are shown. In the massive YM approach, the vector-photon interaction is introduced through the corresponding Lagrangian term from the conventional VMD representation in Eq. (3.126)

$$\mathcal{L}_{\rho\gamma} = -2\sqrt{2}egf_\pi^2 A^\mu \rho_\mu^0\,, \tag{3.159}$$

where use of the relation $M_\rho^2 = 4g^2 f_\pi^2$ has been made [cf. Eq. (3.154)].

For completeness, we quote the $SU(3)$-extended non-anomalous Lagrangian terms that shall be used in subsequent chapters of this thesis. These are

$$\begin{aligned} \mathcal{L}_{VPP} &= ig{\rm Tr}[\widetilde{V}_\mu\widetilde{\Phi}\,\partial^\mu\widetilde{\Phi} - \widetilde{V}_\mu\partial^\mu\widetilde{\Phi}\,\widetilde{\Phi}]\,, \\ \mathcal{L}_{V\gamma} &= -4egf_\pi^2 A^\mu {\rm Tr}[Q\widetilde{V}_\mu]\,, \end{aligned} \tag{3.160}$$

where Q is the quark-charge matrix from Eq. (3.25), $\widetilde{\Phi}$ is nonet of pseudoscalar mesons defined in Eq. (3.70) and $\widetilde{V}_\mu$ can be written in the ideal-mixing limit as

$$\widetilde{V}_\mu \equiv \sum_{a=1}^{8}\frac{\lambda^a}{\sqrt{2}}V_\mu^a = \begin{pmatrix} \frac{1}{\sqrt{2}}\rho_\mu^0 + \frac{1}{\sqrt{2}}\omega_\mu & \rho_\mu^+ & K_\mu^{*+} \\ \rho_\mu^- & -\frac{1}{\sqrt{2}}\rho_\mu^0 + \frac{1}{\sqrt{2}}\omega_\mu & K_\mu^{*0} \\ K_\mu^{*-} & \overline{K}_\mu^{*0} & \phi_\mu \end{pmatrix}. \tag{3.161}$$

It is worth noting that the gauge coupling constant g can be determined using the experimental decay widths from the processes $\rho^0 \to \pi^+\pi^-$ and $\rho^0 \to e^+e^-$, yielding $g = 4.2 \pm 0.1$ and $g = 4.0 \pm 0.2$, respectively [75].

3.5.2 Inclusion of the anomalous term

The starting point for this discussion is the WZW anomalous Lagrangian from Sec. 3.2.2, Eq. (3.57). At order $\mathcal{O}(p^6)$ in the chiral expansion, the relevant part of the anomalous Lagrangian can be written as a linear combination of three independent terms with coefficients a_1, a_2 and a_3 (see Ref. [84] for details). For the present discussion, though, we are only interested in the Lagrangian terms associated to the $P\gamma\gamma$, $VP\gamma$ and VVP vertices and, as it turns out, they are proportional to the constants a_2 and a_3 only.[28] Thus, one can write [75, 85]

$$\begin{aligned}
\mathcal{L}_{P\gamma\gamma} &= \left(\frac{3}{4\pi^2} + 8a_3\right)\frac{e^2}{\sqrt{2}f_\pi}\epsilon^{\mu\nu\alpha\beta}\partial_\mu A_\nu \partial_\alpha A_\beta \mathrm{Tr}[Q^2\widetilde{\Phi}]\,, \\
\mathcal{L}_{VP\gamma} &= (a_2 - 2a_3)\frac{\sqrt{2}eg}{f_\pi}\epsilon^{\mu\nu\alpha\beta}\partial_\mu A_\nu \mathrm{Tr}[Q(\partial_\alpha \widetilde{V}_\beta\widetilde{\Phi} + \widetilde{\Phi}\partial_\alpha\widetilde{V}_\beta)]\,, \\
\mathcal{L}_{VVP} &= -2\sqrt{2}a_2\frac{g^2}{f_\pi}\epsilon^{\mu\nu\alpha\beta}\mathrm{Tr}[\partial_\mu\widetilde{V}_\nu\partial_\alpha\widetilde{V}_\beta\widetilde{\Phi}]\,,
\end{aligned} \tag{3.162}$$

where Q is, once again, the quark-charge matrix from Eq. (3.25), and $\widetilde{\Phi}$ and $\widetilde{V}_\mu$ are, respectively, the $U(3)$ matrices of pseudoscalar and vector meson fields defined in Eqs. (3.70) and (3.161). The characteristic feature of these anomalous terms is the appearance of the totally antisymmetric Levi-Civita tensor $\epsilon^{\mu\nu\alpha\beta}$, which indicates a mismatch of natural parity assignments in these processes [83].

It is interesting to note that the choice of coefficients $a_2 = 2a_3 = -3/16\pi^2$ in Eq. (3.162) leads to the vanishing of the direct $P\gamma\gamma$ and $VP\gamma$ couplings, which in turn allows recovering the conventional VMD model from Eq. (3.126), whereby pseudoscalar mesons do not couple directly to photons but through the exchange of intermediate vectors. Thus, $\mathcal{L}_{VVP}$ becomes

$$\mathcal{L}_{VVP} = \frac{3g^2}{4\sqrt{2}\pi^2 f_\pi}\epsilon^{\mu\nu\alpha\beta}\mathrm{Tr}[\partial_\mu\widetilde{V}_\nu\partial_\alpha\widetilde{V}_\beta\widetilde{\Phi}]\,, \tag{3.163}$$

It is important to highlight that any other choice for these parameters would give rise to deviations from the conventional VMD representation, with the possibility of direct $P\gamma\gamma$ and $VP\gamma$ vertices (see Ref. [75] and sources therein for a complete discussion).

3.6 $U(3)\times U(3)$ linear sigma model

Naive quark models (NQMs) (see Sec. 2.3) give predictions that are in qualitative agreement with the hadronic spectrum in the vector meson sector. However, they fail at providing an understanding of the spectrum of the lightest pseudoscalar and scalar meson sectors. For the former, though, the spontaneous breaking of the approximate chiral symmetry of QCD explains the lowest lying pseudoscalar mesons as pseudo-Goldstone modes and, thus, their smaller than expected masses; in addition, the effects of the $U(1)_A$ anomaly provide an explanation for the comparatively large mass of the pseudoscalar singlet state η'.

Contrary to this, the situation in the scalar sector has been far from clear [86–88], to the point where the $q\bar{q}$ structure for the $a_0(980)$ and $f_0(980)$ was at some stage put in doubt owing to the fact that the NQMs are unable to explain the very small coupling of these states to two photons [89, 90] and the quark content suggested by the mass spectrum is incompatible with their main decay channels [91, 92]. Similar to what happens in the pseudoscalar sector, there is an obvious reason as to why the NQMs fail at describing the scalar meson spectrum, which is the absence of the chiral symmetry within the model. As it turns out, the

[28] Note that all three coefficients enter in the analysis of processes such as $\omega \to 3\pi$.

approximate chiral symmetry of QCD is broken in the vacuum by the quark condensate, and the σ and f_0 have the same quantum numbers as the vacuum [87], rendering these features of the chiral symmetry as fundamental to understanding the scalar meson sector.

The well-known linear sigma model [93–95] can be generalised to three flavours by introducing *ab initio* and on the same footing the nonet of pseudoscalar mesons and its chiral partner, the scalar meson nonet. This effective theory contains the same flavour and chiral symmetries as massless QCD [87], incorporates the breaking of the $U(1)_A$ symmetry [88] and explicitly introduces the effect of the scalar meson poles, whilst keeping the correct behaviour as expected from χPT at low invariant masses [96]. Accordingly, the $U(3) \times U(3)$ linear sigma model (LσM) Lagrangian takes the form [86]

$$\mathcal{L}_{\mathrm{L}\sigma\mathrm{M}} = \frac{1}{2}\mathrm{Tr}\left[\partial_\mu \mathrm{M} \partial_\mu \mathrm{M}^\dagger\right] - V_{\mathrm{sym}} - V_{\mathrm{SB}}\,, \tag{3.164}$$

where V_{sym} is the $U(3) \times U(3)$ symmetric potential

$$V_{\mathrm{sym}} = \frac{\mu^2}{2}\mathrm{Tr}\left[\mathrm{M}\mathrm{M}^\dagger\right] + \frac{\lambda}{4}\mathrm{Tr}\left[\mathrm{M}\mathrm{M}^\dagger\mathrm{M}\mathrm{M}^\dagger\right] + \frac{\lambda'}{4}\mathrm{Tr}\left[\mathrm{M}\mathrm{M}^\dagger\right]\mathrm{Tr}\left[\mathrm{M}\mathrm{M}^\dagger\right], \tag{3.165}$$

and V_{SB} contains symmetry-breaking terms that explicitly break both the chiral and $U(1)_A$ symmetries

$$V_{\mathrm{SB}} = -\mathrm{Tr}\left[C\widetilde{\Sigma}\right] + \beta\left(\det\{\mathrm{M}\} + \det\left\{\mathrm{M}^\dagger\right\}\right). \tag{3.166}$$

The field matrix M is in turn written as

$$\mathrm{M} = \widetilde{\Sigma} + i\widetilde{\Phi}\,, \tag{3.167}$$

where

$$\widetilde{\Sigma} \equiv \frac{1}{\sqrt{2}}\lambda_i\sigma_i\,, \quad \widetilde{\Phi} \equiv \frac{1}{\sqrt{2}}\lambda_i\phi_i \tag{3.168}$$

are, respectively, the matrices for the nonet of scalar and pseudoscalar meson fields, with $i = 0, ..., 8$ [cf. Eq. (3.70)]. The coefficient matrix C in Eq. (3.166) is defined as

$$C \equiv \frac{1}{\sqrt{2}}\lambda_i c_i\,, \tag{3.169}$$

where the c_i are constants. The most general form that preserves isospin and gives rise to the partially conserved axial currents has c_0 and c_8 as the only two non-vanishing coefficients, with the former providing a common mass to the pseudoscalar nonet and the latter breaking the $SU(3)$ symmetry down to isospin [86]. On the other hand, the second term in Eq. (3.166) corresponds to the instanton induced quark interaction associated to the breaking of the $U(1)_A$ axial symmetry, which has the form of a determinant in flavour space that breaks the $U(3)_L \times U(3)_R$ symmetry group down to $SU(3)_L \times SU(3)_R \times U(1)_V$ [88].

Linear terms in the fields appearing in the Lagrangian, which originate from the linear $\widetilde{\Sigma}$ term in the symmetry breaking potential V_{SB}, can be eliminated from the theory by performing a shift to a new scalar field matrix $\widetilde{\Sigma} \to \widetilde{\Sigma} + V_0$. Thus, we introduce the $SU(3)$-violating isospin-conserving vacuum expectation value (VEV) matrix $V_0 = \mathrm{diag}\{a, a, b\}$, with a and b being related to the VEV of the scalar fields (denoted by $\{\,\}$) through [86, 88]

$$a = \frac{1}{\sqrt{3}}\{\sigma_0\} + \frac{1}{\sqrt{6}}\{\sigma_8\}\,, \quad b = \frac{1}{\sqrt{3}}\{\sigma_0\} - \frac{2}{\sqrt{6}}\{\sigma_8\}\,. \tag{3.170}$$

It is important to note that the shift in the $\widetilde{\Sigma}$ field gives rise to new three-meson interactions, as well as mass terms for the fields. To analyse this, it is convenient to write the shifted

Lagrangian as $\mathcal{L}_{\mathrm{L}\sigma\mathrm{M}} = \sum_n \mathcal{L}_n$, where terms containing products of n fields are collected in $\mathcal{L}_n$. The stability condition $\mathcal{L}_1 = 0$ sets the constraints [86]

$$\begin{aligned}\sqrt{\frac{2}{3}}c_0 + \sqrt{\frac{1}{3}}c_8 &= \sqrt{2}a(\xi + 2\beta b + \lambda a^2)\,,\\ \sqrt{\frac{2}{3}}c_0 - \frac{1}{2\sqrt{3}}c_8 &= \frac{1}{\sqrt{2}}(a+b)\left[\xi + 2\beta a + \lambda(a^2 - ab + b^2)\right],\end{aligned} \tag{3.171}$$

where we have defined the parameter $\xi \equiv \mu^2 + \lambda'(2a^2 + b^2)$ for convenience. The meson masses, on the other hand, are extracted from $\mathcal{L}_2$. For the non-mixed sector, one finds [88]

$$\begin{aligned}M_\pi^2 &= \xi + 2\beta b + \lambda a^2\,, \quad & M_K^2 &= \xi + 2\beta a + \lambda(a^2 - ab + b^2)\,,\\ M_a^2 &= \xi - 2\beta b + 3\lambda a^2\,, \quad & M_\kappa^2 &= \xi - 2\beta a + \lambda(a^2 + ab + b^2)\,,\end{aligned} \tag{3.172}$$

whereas the following relationships hold in the quark-flavour basis[29] for the mixed sector [86]

$$\begin{aligned}M_{\eta_{\mathrm{NS}}}^2 &= \xi - 2\beta b + \lambda a^2\,, \quad & M_{\sigma_{\mathrm{NS}}}^2 &= \xi + 2\beta b + 3\lambda a^2 + 4\lambda' a^2\,,\\ M_{\eta_{\mathrm{S}}}^2 &= \xi + \lambda b^2\,, & M_{\sigma_{\mathrm{S}}}^2 &= \xi + 3\lambda b^2 + 2\lambda' b^2\,,\\ M_{\eta_{\mathrm{S-NS}}}^2 &= -2\sqrt{2}\beta a\,, & M_{\sigma_{\mathrm{S-NS}}}^2 &= 2\sqrt{2}(\beta + \lambda' b)a\,.\end{aligned} \tag{3.173}$$

As it turns out, the $U(1)_A$ anomaly couples in this model to the scalar fields VEV by the spontaneous breaking of the chiral symmetry and contributes through this mechanism to the masses of all fields of the theory with exception of the strange mesons [88]. The masses for the physical fields, being linear combinations of the corresponding $|\mathrm{NS}\rangle$ and $|\mathrm{S}\rangle$ states, can be found by diagonalising the corresponding mass matrices yielding

$$\begin{aligned}M_\eta^2 &= \frac{1}{2}(M_{\eta_{\mathrm{NS}}}^2 + M_{\eta_{\mathrm{S}}}^2) - \frac{1}{2}\sqrt{(M_{\eta_{\mathrm{NS}}}^2 - M_{\eta_{\mathrm{S}}}^2)^2 + 4M_{\eta_{\mathrm{S-NS}}}^4}\,,\\ M_{\eta'}^2 &= \frac{1}{2}(M_{\eta_{\mathrm{NS}}}^2 + M_{\eta_{\mathrm{S}}}^2) + \frac{1}{2}\sqrt{(M_{\eta_{\mathrm{NS}}}^2 - M_{\eta_{\mathrm{S}}}^2)^2 + 4M_{\eta_{\mathrm{S-NS}}}^4}\,,\\ M_\sigma^2 &= \frac{1}{2}(M_{\sigma_{\mathrm{NS}}}^2 + M_{\sigma_{\mathrm{S}}}^2) - \frac{1}{2}\sqrt{(M_{\sigma_{\mathrm{NS}}}^2 - M_{\sigma_{\mathrm{S}}}^2)^2 + 4M_{\sigma_{\mathrm{S-NS}}}^4}\,,\\ M_{f_0}^2 &= \frac{1}{2}(M_{\sigma_{\mathrm{NS}}}^2 + M_{\sigma_{\mathrm{S}}}^2) + \frac{1}{2}\sqrt{(M_{\sigma_{\mathrm{NS}}}^2 - M_{\sigma_{\mathrm{S}}}^2)^2 + 4M_{\sigma_{\mathrm{S-NS}}}^4}\,,\end{aligned} \tag{3.174}$$

with mixing angles given by [86]

$$\sin 2\phi_P = -\frac{4\sqrt{2}\beta a}{m_{\eta'}^2 - m_\eta^2}\,, \quad \sin 2\phi_S = \frac{4\sqrt{2}(\beta + \lambda' b)a}{M_{f_0}^2 - M_\sigma^2}\,, \tag{3.175}$$

where ϕ_P and ϕ_S are, respectively, the pseudoscalar and scalar mixing angles in the quark-flavour basis. It is interesting to note from Eq. (3.174) that, according to this model, the η-η' mass splitting,

$$(m_{\eta'}^2 - m_\eta^2)^2 = [\lambda(a^2 - b^2) - 2\beta b]^2 + 32\beta^2 a^2\,, \tag{3.176}$$

is down to the breaking of the $SU(3)$ flavour symmetry and the effect of the $U(1)_A$ anomaly, as one would expect.

The $U(3) \times U(3)$ LσM has got six free parameters, i.e. a, b, μ, λ, λ' and β, which can be fixed from phenomenology. With exception of the mixed scalar meson masses, all the other

[29] See Appendix A for the definition of the basis states.

masses in Eqs. (3.172) and (3.173) depend on the parameters a, b, λ, β and the combination $\xi = \mu^2 + \lambda'(2a^2 + b^2)$. In order to extract the value of λ', though, one requires experimental information on the mixed scalar sector that still contains a significant amount of uncertainty. From the stability condition (i.e. $\mathcal{L}_1 = 0$), together with the definition of the divergence of the axial-vector currents in Eq. (2.36) and the meson mass relationships, one can obtain values for the VEV parameters [86]

$$a = \frac{f_\pi}{\sqrt{2}}, \quad b = \frac{2f_K - f_\pi}{\sqrt{2}}. \tag{3.177}$$

Likewise, one can use the expressions for $M^2_{\eta'}$, M^2_η and M^2_π to fix the values of β, λ and ξ. In particular, β is found as the solution to the second order equation[30]

$$8(a^2 + 2b^2)\beta^2 - 4b(2M^2_\pi - M^2_{\eta'} - M^2_\eta)\beta + (M^2_{\eta'} - M^2_\pi)(M^2_\eta - M^2_\pi) = 0\,, \tag{3.178}$$

whilst λ and ξ turn out to be

$$\lambda = \frac{2M^2_\pi - M^2_{\eta'} - M^2_\eta - 6b\beta}{a^2 - b^2}, \quad \xi = M^2_\pi - 2b\beta - \lambda a^2\,. \tag{3.179}$$

As it is discussed in Ref. [86], a mass of 980 MeV for the scalar singlet state f_0 requires a $\lambda' \approx 4$. This in turn leads to $M_\sigma \approx 400$ MeV, which is consistent with the range provided in Ref [1]. On the other hand, the scalar mixing angle ϕ_S can be extracted from Eq. (3.175) and several numerical values have been proposed by different authors, where $\phi_S \approx -14^\circ$ has been suggested in Ref. [86] and $\phi_S \approx -8^\circ$ in Ref. [96].

Next, the trilinear $\sigma_a \phi_b \phi_c$ coupling constants, which arise from the field shift $\widetilde{\Sigma} \to \widetilde{\Sigma} + V_0$, can be written in the isospin limit in terms of the predicted physical masses, mixing angles and decay constants (see Refs. [86, 87, 96] for details). As it turns out, they are given by

$$\begin{aligned}
g_{\sigma K^+K^-} &= g_{\sigma K^0 \overline{K}^0} = \frac{M^2_K - M^2_\sigma}{2f_K}(\cos\phi_S - \sqrt{2}\sin\phi_S)\,,\\
g_{f_0 K^+K^-} &= g_{f_0 K^0 \overline{K}^0} = \frac{M^2_K - M^2_{f_0}}{2f_K}(\sin\phi_S + \sqrt{2}\cos\phi_S)\,,\\
g_{a_0 K^+K^-} &= -g_{a_0 K^0 \overline{K}^0} = \frac{1}{\sqrt{2}} g_{a_0^\pm K^\mp K^{0(\overline{0})}} = \frac{M^2_K - M^2_{a_0}}{2f_K}\,,\\
g_{\sigma\pi^0\pi^0} &= g_{\sigma\pi^+\pi^-} = \frac{M^2_\pi - M^2_\sigma}{f_\pi}\cos\phi_S\,,\\
g_{f_0\pi^0\pi^0} &= g_{f_0\pi^+\pi^-} = \frac{M^2_\pi - M^2_{f_0}}{f_\pi}\sin\phi_S\,,\\
g_{\kappa^\mp K^\pm \pi^0} &= \frac{M^2_\pi - M^2_\kappa}{2f_K} = \frac{M^2_K - M^2_\kappa}{2f_\pi}\,,\\
g_{a_0\pi^0\eta^{(\prime)}} &= \frac{M^2_{\eta^{(\prime)}} - M^2_{a_0}}{f_\pi}\cos\phi_P\,,\\
g_{\kappa^\mp K^\pm \eta^{(\prime)}} &= \frac{M^2_{\eta^{(\prime)}} - M^2_\kappa}{2f_K}(\cos\phi_P - \sqrt{2}\sin\phi_P)\,.
\end{aligned} \tag{3.180}$$

Needless to say, the electromagnetic interactions are incorporated into the model through the usual procedure of promoting the partial derivatives in Eq. (3.164) to the gauge covariant

[30] It is worth highlighting that the β parameter is a direct measure of the $\eta_{\rm NS}$-π mass splitting [86].

derivative defined as

$$\partial_\mu \mathrm{M} \to D_\mu \mathrm{M} = \partial_\mu \mathrm{M} + ieA_\mu[Q, \mathrm{M}]\,, \tag{3.181}$$

with A_μ being the photon field and $Q = \mathrm{diag}\{2/3, -1/3, -1/3\}$ the quark-charge matrix.

Before concluding, a couple of points are worth highlighting: i) as it is done with VMD, one may invoke saturation by meson-resonance exchange to estimate the numerical values of some of the $\mathcal{O}(p^4)$ LECs using the $U(3) \times U(3)$ LσM but we shall not further pursue this topic here (the interested reader is referred to Ref. [86] for details); and ii) the $U(3) \times U(3)$ LσM appears to have fallen out of favour against dispersive methods to assess scalar exchange contributions (see, e.g., Refs. [97, 98]).

3.7 The Standard Model effective field theory

In the applications considered thus far in this chapter, the SM plays the role of the underlying UV theory whose low-energy limit is to be explored using the appropriate EFT. However, one can also regard the SM as an effective theory describing the low-energy limit of a presently unknown UV-completion theory that will ultimately replace the SM at much shorter distances [31], and this is known as the Standard Model effective field theory (SMEFT).

There are advantages in employing the EFT formalism in this context. First of all, the SMEFT allows describing new physics in a model-independent way, enabling the derivation of bounds on the parameters of the effective theory from experiments that can subsequently be recasted into bounds on the parameters of specific BSM models. As well as this, the SMEFT does not require defining concrete BSM schemes in order to parameterise potential deviations of experimental results from the SM. All in all, the SMEFT represents a powerful consistent field theory for characterising the low-energy limit of *any* new BSM physics.

Let us begin assuming that the separation of scales between the SM and the new physics is sufficiently large that a meaningful description of the SM as an EFT is possible.[31] Thus, the SMEFT Lagrangian takes the form

$$\begin{aligned}
\mathcal{L}_{\mathrm{SMEFT}} &= \mathcal{L}_{\mathrm{SM}} + \mathcal{L}^{(5)} + \mathcal{L}^{(6)} + ... \\
&= \mathcal{L}_{\mathrm{SM}} + \frac{1}{\Lambda}\sum_{k=1}^{n_{\mathcal{D}}} c_k^{(5)} \mathcal{Q}_k^{(5)} + \frac{1}{\Lambda^2}\sum_{k=1}^{n_{\mathcal{D}}} c_k^{(6)} \mathcal{Q}_k^{(6)} + ... \\
&= \mathcal{L}_{\mathrm{SM}} + \sum_{\mathcal{D}=5}^{\infty}\sum_{k=1}^{n_{\mathcal{D}}} \frac{c_k^{(\mathcal{D})}}{\Lambda^{\mathcal{D}-4}} \mathcal{Q}_k^{(\mathcal{D})}\,,
\end{aligned} \tag{3.182}$$

where the SM Lagrangian is the leading term in the EFT expansion, the $c_k^{(\mathcal{D})}$ are Wilson coefficients and Λ is the energy scale associated to the new physics in this context. The new operators $\mathcal{Q}_k^{(\mathcal{D})}$, with mass dimension $\mathcal{D}$, must respect the symmetries of the SM, such as Lorentz and gauge invariance, and are made of SM fields only, which means that the SM degrees of freedom are incorporated as fundamental or composite fields. The SMEFT Lagrangian contains an infinite set of operators although there are only a finite number of them at each dimension $\mathcal{D}$, with their contributions to any given observable being suppressed by powers of $(E/\Lambda)^{\mathcal{D}-4}$, where E represents the characteristic scale of the low-energy effective theory. In order to find a minimal set of independent operators at a given dimension, one may need to redefine the fields, use the equations of motion (EOMs) and apply other operator identities to eliminate the redundant operators [100].

[31] For a general renormalizable theory in the conventional sense, the heavy degrees of freedom decouple from the low-energy dynamics of the theory and can, therefore, be integrated out by virtue of the decoupling theorem by Appelquist and Carazzone [99].

As with any other EFT, one needs to include all possible operators at a given order in the power counting consistent with the symmetries of the theory for the SMEFT to be renormalisable order by order. The power counting scheme in the SMEFT is based on the mass dimension of the operators $\mathcal{Q}_k^{(\mathcal{D})}$. It must be noted that one can write

$$\mathcal{Q}_k^{(\mathcal{D})} = \overline{\psi}^a \psi^b \partial^c H^e (H^\dagger)^f A^g \,, \tag{3.183}$$

where ψ stands for a generic fermion field, H is the Higgs field and A is a generic gauge field. The mass dimension of this operator is

$$[\mathcal{Q}_k^{(\mathcal{D})}] \equiv \mathcal{D} = \frac{3}{2}(a+b) + c + e + f + g \,, \tag{3.184}$$

so that, in $d = 4$ spacetime dimensions, the condition

$$\left[\frac{\mathcal{Q}_k^{(\mathcal{D})}}{\Lambda^{\mathcal{D}-4}} \right] = 4 \tag{3.185}$$

is always fulfilled and the $c_k^{(\mathcal{D})}$ are, thus, dimensionless coefficients, as expected.

As indicated above, the leading term in the EFT expansion of the SMEFT is the SM Lagrangian. Consequently, it makes sense to provide a lightning summary of the SM here (cf. Refs. [3–6, 26] for a detailed account). The SM [101–103] is the most general renormalisable theory consistent with $SU(3)_C \times SU(2)_L \times U(1)_Y$ gauge invariance. The associated Lagrangian consists of the following parts

$$\mathcal{L}_{\rm SM} = \mathcal{L}_{\rm gauge} + \mathcal{L}_{\rm fermion} + \mathcal{L}_{\rm Higgs} + \mathcal{L}_{\rm Yukawa} \,, \tag{3.186}$$

where $\mathcal{L}_{\rm gauge}$ and $\mathcal{L}_{\rm fermion}$ contain, respectively, the kinetic terms for the gauge and fermion fields, $\mathcal{L}_{\rm Higgs}$ contains the kinetic and potential terms for the Higgs field, and $\mathcal{L}_{\rm Yukawa}$ contains the Yukawa sector of the SM. The gauge kinetic terms are

$$\mathcal{L}_{\rm gauge} = -\frac{1}{4} G^A_{\mu\nu} G^{A\mu\nu} - \frac{1}{4} W^I_{\mu\nu} W^{I\mu\nu} - \frac{1}{4} B_{\mu\nu} B^{\mu\nu} \,, \tag{3.187}$$

where $G^A_{\mu\nu}$ is the gluon field strength tensor, which is defined in Sec. 2.1, Eq. (2.2), whilst $W^I_{\mu\nu} = \partial_\mu W^I_\nu - \partial_\nu W^I_\mu - g \epsilon_{IJK} W^J_\mu W^K_\nu$ and $B_{\mu\nu} = \partial_\mu B_\nu - \partial_\nu B_\mu$ are, respectively, the corresponding $SU(2)_L$ and $U(1)_Y$ counterparts.

The fermion kinetic terms are given by

$$\mathcal{L}_{\rm fermion} = \bar{q} i \not{D} q + \bar{u} i \not{D} u + \bar{d} i \not{D} d + \bar{l} i \not{D} l + \bar{e} i \not{D} e \,, \tag{3.188}$$

where the matter content includes the left-handed[32] lepton weak doublet fields l_p^j, with weak hypercharge $\mathrm{Y}_l = -1$, the right-handed weak singlet lepton fields e_p, with $\mathrm{Y}_e = -2$, the left-handed quark weak doublet fields $q_p^{\alpha j}$, with $\mathrm{Y}_q = 1/3$, and the right-handed weak singlet up and down quark fields u_p^α and d_p^α, with $\mathrm{Y}_u = 4/3$ and $\mathrm{Y}_d = -2/3$, respectively (see summary of transformation properties of the SM fields under the Lorentz and gauge groups in Table 3.3). The matter field indices employed refer to weak isospin $j = 1, 2$, colour $\alpha = 1, 2, 3$ and generation $p = 1, 2, 3$, all of which have been suppressed in Eq. (3.188) for clarity of notation. The SM weak hypercharge assignment for the field i is related to the corresponding

[32] Remember that the chiral fermions are $\psi_{R/L} = P_{R/L}\psi$, where $P_{R/L} = (1 \pm \gamma^5)/2$ [cf. Eq. (2.23)].

TABLE 3.3: Transformation properties of the SM fields under the Lorentz $SU(2)_L \times SU(2)_R$ and gauge groups [19].

	Lorentz	$SU(3)_C$	$SU(2)_L$	$U(1)_Y$
$G_{\mu\nu}$	$(1,0)+(0,1)$	8	1	0
$W_{\mu\nu}$	$(1,0)+(0,1)$	1	3	0
$B_{\mu\nu}$	$(1,0)+(0,1)$	1	1	0
H	$(0,0)$	1	2	1
q	$(\frac{1}{2},0)$	3	2	$\frac{1}{3}$
u	$(0,\frac{1}{2})$	3	1	$\frac{4}{3}$
d	$(0,\frac{1}{2})$	3	1	$-\frac{2}{3}$
l	$(\frac{1}{2},0)$	1	2	-1
e	$(0,\frac{1}{2})$	1	1	-2

electric charge Q^i_{em} and diagonal $SU(2)_L$ generator t^i_3 by

$$Q^i_{em} = t^i_3 + \frac{\mathrm{Y}_i}{2}. \tag{3.189}$$

The fermion fields in Eq. (3.188) are in the weak eigenbasis, with

$$\begin{aligned} q_1 &= \begin{pmatrix} u_L \\ d'_L \end{pmatrix}, \quad q_2 = \begin{pmatrix} c_L \\ s'_L \end{pmatrix}, \quad q_3 = \begin{pmatrix} t_L \\ b'_L \end{pmatrix}, \\ l_1 &= \begin{pmatrix} \nu^{e\prime}_L \\ e_L \end{pmatrix}, \quad l_2 = \begin{pmatrix} \nu^{\mu\prime}_L \\ \mu_L \end{pmatrix}, \quad l_3 = \begin{pmatrix} \nu^{\tau\prime}_L \\ \tau_L \end{pmatrix}, \end{aligned} \tag{3.190}$$

where the down-type quark weak eigenstates (primed) can be expressed as linear combinations of the mass eigenstates (unprimed) through the CKM matrix (see Sec. 6.2 for further details). Similarly, in the lepton sector the neutrino weak eigenstates (primed) are related to the mass eigenstates (unprimed) by the PMNS matrix

$$\begin{pmatrix} d'_L \\ s'_L \\ b'_L \end{pmatrix} = V_{\mathrm{CKM}} \begin{pmatrix} d_L \\ s_L \\ b_L \end{pmatrix}, \quad \begin{pmatrix} \nu^{e\prime}_L \\ \nu^{\mu\prime}_L \\ \nu^{\tau\prime}_L \end{pmatrix} = U_{\mathrm{PMNS}} \begin{pmatrix} \nu^{e}_L \\ \nu^{\mu}_L \\ \nu^{\tau}_L \end{pmatrix}. \tag{3.191}$$

Furthermore, the covariant derivative acting on (left-handed) doublet fields is defined as[33]

$$D_\mu = \partial_\mu - (ig_s T^A G^A_\mu) - igt^I W^I_\mu - ig' \frac{\mathrm{Y}_i}{2} B_\mu, \tag{3.192}$$

whilst, when acting on (right-handed) singlet fields, it is given by

$$D_\mu = \partial_\mu - (ig_s T^A G^A_\mu) - ig' \frac{\mathrm{Y}_i}{2} B_\mu, \tag{3.193}$$

where the $T^A \equiv \lambda^A/2$ are the generators of $SU(3)$ transformations, with λ^A being the Gell-Mann matrices from Eq. (2.5), the $t^I \equiv \sigma^I/2$ are the generators of the $SU(2)$ group, with σ^I being the Pauli matrices from Eq. (2.21), and Y_i is the weak hypercharge of the i field.

[33] Note that leptons are singlets under the $SU(3)_C$ gauge symmetry group. Hence, the covariant derivative term containing the gluonic interaction vanishes when acting on leptons, which is indicated with the brackets in Eqs. (3.192) and (3.193).

The Higgs part of the SM Lagrangian takes the form

$$\mathcal{L}_{\text{Higgs}} = (D_\mu H)^\dagger (D^\mu H) - \lambda \left(H^\dagger H - \frac{1}{2} v^2 \right)^2 , \tag{3.194}$$

where H is the Higgs $SU(2)_L$ complex scalar doublet, with hypercharge $\mathrm{Y}_H = 1$. The associated VEV can be written as $\langle H^\dagger H \rangle = v^2/2$, with $v \sim 246$ GeV, which spontaneously breaks the gauge group $SU(2)_L \times U(1)_Y \to U(1)_Q$. With the above normalisation, the mass of the Higgs boson is $m_H^2 = 2\lambda v^2$.

Finally, the Yukawa sector of the SM is

$$-\mathcal{L}_{\text{Yukawa}} = Y^d_{mn} \bar{q}^m H d^n + Y^u_{mn} \bar{q}^m \widetilde{H} u^n + Y^e_{mn} \bar{l}^m H e^n + \text{h.c.} , \tag{3.195}$$

where the Y^p are the symmetric 3×3 (in generation space) Yukawa matrices of coupling constants (do not confuse these matrices with the hypercharge assignments Y_i). The conjugated Higgs field $\widetilde{H}$ is defined as $\widetilde{H} \equiv i\sigma_2 H^*$ and can be expressed in tensor notation as $\widetilde{H}^j = \epsilon_{jk} (H^k)^*$, where ϵ_{jk} is the totally antisymmetric tensor such that $\epsilon_{12} = +1$ and $\epsilon_{jk} = -\epsilon_{kj}$. After spontaneous symmetry breaking, the Higgs field acquires a VEV resulting in the generation of all quark and charged lepton masses. In the unitary gauge, one can write

$$H = \frac{1}{\sqrt{2}} \begin{pmatrix} 0 \\ v + h(x) \end{pmatrix} \tag{3.196}$$

and, after setting $h(x) \to 0$, it can be shown that the fermion mass matrices take the form $M^{u,d,e} = Y^{u,d,e} v/\sqrt{2}$ (cf. Sec. 6.2).

Let us now summarise the SM EOMs, which play a crucial role in the choice of SMEFT operator basis and the removal of redundant operators.[34] For the Higgs and gauge fields, one finds [100, 105]

$$\begin{aligned}
(D^\mu D_\mu H)^j &= \lambda v^2 H^j - 2\lambda (H^\dagger H) H^j + \epsilon_{jk} \bar{q}^k Y^u u - \bar{d} Y^{d\dagger} q^j - \bar{e} Y^{e\dagger} l^j , \\
(D^\mu G_{\mu\nu})^A &= g_s (\bar{q} \gamma_\nu T^A q + \bar{u} \gamma_\nu T^A u + \bar{d} \gamma_\nu T^A d) , \\
(D^\mu W_{\mu\nu})^I &= \frac{g}{2} (H^\dagger i \overleftrightarrow{D}^I_\nu H + \bar{l} \gamma_\nu \sigma^I l + \bar{q} \gamma_\nu \sigma^I q) , \\
\partial^\mu B_{\mu\nu} &= g' \mathrm{Y}_H H^\dagger i \overleftrightarrow{D}_\nu H + g' \sum_{f=l,e,q,u,d} \mathrm{Y}_f \bar{f} \gamma_\nu f ,
\end{aligned} \tag{3.197}$$

where the hermitian derivative notation, defined as

$$\begin{aligned}
H^\dagger i \overleftrightarrow{D}_\mu H &= i H^\dagger (D_\mu H) - i (D_\mu H)^\dagger H , \\
H^\dagger i \overleftrightarrow{D}^I_\nu H &= i H^\dagger \sigma^I (D_\mu H) - i (D_\mu H)^\dagger \sigma^I H ,
\end{aligned} \tag{3.198}$$

has been used. The fermion field EOMs are in turn given by

$$\begin{gathered}
i \not{D} q_j = Y^d H_j \, d + Y^u \widetilde{H}_j \, u , \quad i \not{D} d = Y^{d\dagger} H^\dagger q , \quad i \not{D} u = Y^{u\dagger} \widetilde{H}^\dagger q , \\
i \not{D} l_j = Y^e H_j \, e , \qquad i \not{D} e = Y^{e\dagger} H^\dagger l .
\end{gathered} \tag{3.199}$$

[34] It is worth noting that one can generally apply the EOMs to the Lagrangian without changing the observables, as it was shown in Ref. [104].

TABLE 3.4: Operators with H^n, sets X^3, H^6, H^4D^2 and ψ^2H^3 [100]. See main text for the operator naming conventions.

X^3		H^6 and H^4D^2		$\psi^2H^3+\text{h.c.}$	
$\mathcal{Q}_G$	$f^{ABC}G^{A\nu}_{\mu}G^{B\rho}_{\nu}G^{C\mu}_{\rho}$	$\mathcal{Q}_H$	$(H^\dagger H)^3$	$\mathcal{Q}_{eH}$	$(H^\dagger H)(\bar{l}_p e_r H)$
$\mathcal{Q}_{\widetilde{G}}$	$f^{ABC}\widetilde{G}^{A\nu}_{\mu}G^{B\rho}_{\nu}G^{C\mu}_{\rho}$	$\mathcal{Q}_{H\Box}$	$(H^\dagger H)\Box(H^\dagger H)$	$\mathcal{Q}_{uH}$	$(H^\dagger H)(\bar{q}_p u_r \widetilde{H})$
$\mathcal{Q}_W$	$\epsilon^{IJK}W^{I\nu}_{\mu}W^{J\rho}_{\nu}W^{K\mu}_{\rho}$	$\mathcal{Q}_{HD}$	$(H^\dagger D^\mu H)^*(H^\dagger D_\mu H)$	$\mathcal{Q}_{dH}$	$(H^\dagger H)(\bar{q}_p d_r H)$
$\mathcal{Q}_{\widetilde{W}}$	$\epsilon^{IJK}\widetilde{W}^{I\nu}_{\mu}W^{J\rho}_{\nu}W^{K\mu}_{\rho}$				

TABLE 3.5: Operators with H^n, sets X^2H^2, ψ^2XH and ψ^2H^2D [100]. See main text for the operator naming conventions.

X^2H^2		$\psi^2XH+\text{h.c.}$		ψ^2H^2D	
$\mathcal{Q}_{HG}$	$H^\dagger H G^A_{\mu\nu}G^{A\mu\nu}$	$\mathcal{Q}_{eW}$	$(\bar{l}_p\sigma^{\mu\nu}e_r)\sigma^I H W^I_{\mu\nu}$	$\mathcal{Q}^{(1)}_{Hl}$	$(H^\dagger i\overleftrightarrow{D}_\mu H)(\bar{l}_p\gamma^\mu l_r)$
$\mathcal{Q}_{H\widetilde{G}}$	$H^\dagger H \widetilde{G}^A_{\mu\nu}G^{A\mu\nu}$	$\mathcal{Q}_{eB}$	$(\bar{l}_p\sigma^{\mu\nu}e_r)H B_{\mu\nu}$	$\mathcal{Q}^{(3)}_{Hl}$	$(H^\dagger i\overleftrightarrow{D}^I_\mu H)(\bar{l}_p\sigma^I\gamma^\mu l_r)$
$\mathcal{Q}_{HW}$	$H^\dagger H W^I_{\mu\nu}W^{I\mu\nu}$	$\mathcal{Q}_{uG}$	$(\bar{q}_p\sigma^{\mu\nu}T^A u_r)\widetilde{H}G^A_{\mu\nu}$	$\mathcal{Q}_{He}$	$(H^\dagger i\overleftrightarrow{D}_\mu H)(\bar{e}_p\gamma^\mu e_r)$
$\mathcal{Q}_{H\widetilde{W}}$	$H^\dagger H \widetilde{W}^I_{\mu\nu}W^{I\mu\nu}$	$\mathcal{Q}_{uW}$	$(\bar{q}_p\sigma^{\mu\nu}u_r)\sigma^I\widetilde{H}W^I_{\mu\nu}$	$\mathcal{Q}^{(1)}_{Hq}$	$(H^\dagger i\overleftrightarrow{D}_\mu H)(\bar{q}_p\gamma^\mu q_r)$
$\mathcal{Q}_{HB}$	$H^\dagger H B_{\mu\nu}B^{\mu\nu}$	$\mathcal{Q}_{uB}$	$(\bar{q}_p\sigma^{\mu\nu}u_r)\widetilde{H}B_{\mu\nu}$	$\mathcal{Q}^{(3)}_{Hq}$	$(H^\dagger i\overleftrightarrow{D}^I_\mu H)(\bar{q}_p\sigma^I\gamma^\mu q_r)$
$\mathcal{Q}_{H\widetilde{B}}$	$H^\dagger H \widetilde{B}_{\mu\nu}B^{\mu\nu}$	$\mathcal{Q}_{dG}$	$(\bar{q}_p\sigma^{\mu\nu}T^A d_r)H G^A_{\mu\nu}$	$\mathcal{Q}_{Hu}$	$(H^\dagger i\overleftrightarrow{D}_\mu H)(\bar{u}_p\gamma^\mu u_r)$
$\mathcal{Q}_{HWB}$	$H^\dagger\sigma^I H W^I_{\mu\nu}B^{\mu\nu}$	$\mathcal{Q}_{dW}$	$(\bar{q}_p\sigma^{\mu\nu}d_r)\sigma^I H W^I_{\mu\nu}$	$\mathcal{Q}_{Hd}$	$(H^\dagger i\overleftrightarrow{D}_\mu H)(\bar{d}_p\gamma^\mu d_r)$
$\mathcal{Q}_{H\widetilde{W}B}$	$H^\dagger\sigma^I H \widetilde{W}^I_{\mu\nu}B^{\mu\nu}$	$\mathcal{Q}_{dB}$	$(\bar{q}_p\sigma^{\mu\nu}d_r)H B_{\mu\nu}$	$\mathcal{Q}_{Hud}$	$(\widetilde{H}^\dagger i D_\mu H)(\bar{u}_p\gamma^\mu d_r)$

3.7.1 SMEFT operators

In this subsection, we summarise the SMEFT operators up to mass dimension 6. By noticing that in $d=4$ spacetime dimensions scalar fields have mass dimension 1, field strength tensors have mass dimension 2, fermion fields have mass dimension $3/2$ and derivatives have mass dimension 1, one can already constrain the combinations of fields and derivatives in operators of a given mass dimension based on dimensional-analysis grounds only.

At mass dimension 5, there is a single operator that is consistent with the SM field content and gauge symmetries [106], and takes the form

$$\mathcal{Q}^{(5)} = \epsilon_{jk}\epsilon_{mn}H^j H^m (l_p^k)^T C l_r^n \equiv (\widetilde{H}^\dagger l_p)^T C (\widetilde{H}^\dagger l_r)\,, \tag{3.200}$$

where p,r are generation indices, j,k,m,n are weak $SU(2)_L$ indices and C is the charge-conjugation operator, which can be expressed as $C=i\gamma^2\gamma^0$ in the Dirac representation of gamma matrices. Note that this operator violates lepton number by two units, i.e. $\Delta L=\pm 2$, and an experimental consequence of it is the generation of Majorana neutrino masses when the weak interactions are spontaneously broken.[35] Since neutrino masses are very small, it is assumed that this operator may be generated at a very high scale (e.g. the grand unification energy scale) [19]. Accordingly, the first new-physics corrections are expected to be parameterised by operators of mass dimension 6.

[35] Note that the minimal SM contains only left-handed neutrinos. If one postulates, though, the existence of non-interacting right-handed neutrino fields, then the Higgs mechanism could be extended to generate neutrino Dirac masses. However, there is an alternative whereby neutrinos are their own antiparticles, i.e. they are Majorana fermions. In this scenario, it is possible to write a mass term out of left-handed neutrino fields only, which takes the form

$$\mathcal{L}_\nu = m_\nu \bar{\nu}^c_L \nu_L + \text{h.c.}\,, \tag{3.201}$$

where $\bar{\nu}^c_L$ is the charge-conjugated neutrino field.

TABLE 3.6: Four-fermion operators, sets $(\bar{L}L)(\bar{L}L)$, $(\bar{R}R)(\bar{R}R)$ and $(\bar{L}L)(\bar{R}R)$ [100]. See main text for the operator naming conventions.

$(\bar{L}L)(\bar{L}L)$		$(\bar{R}R)(\bar{R}R)$		$(\bar{L}L)(\bar{R}R)$	
$\mathcal{Q}_{ll}$	$(\bar{l}_p\gamma^\mu l_r)(\bar{l}_s\gamma^\mu l_t)$	$\mathcal{Q}_{ee}$	$(\bar{e}_p\gamma^\mu e_r)(\bar{e}_s\gamma^\mu e_t)$	$\mathcal{Q}_{le}$	$(\bar{l}_p\gamma^\mu l_r)(\bar{e}_s\gamma^\mu e_t)$
$\mathcal{Q}_{qq}^{(1)}$	$(\bar{q}_p\gamma^\mu q_r)(\bar{q}_s\gamma^\mu q_t)$	$\mathcal{Q}_{uu}$	$(\bar{u}_p\gamma^\mu u_r)(\bar{u}_s\gamma^\mu u_t)$	$\mathcal{Q}_{lu}$	$(\bar{l}_p\gamma^\mu l_r)(\bar{u}_s\gamma^\mu u_t)$
$\mathcal{Q}_{qq}^{(3)}$	$(\bar{q}_p\gamma^\mu\sigma^I q_r)(\bar{q}_s\gamma^\mu\sigma^I q_t)$	$\mathcal{Q}_{dd}$	$(\bar{d}_p\gamma^\mu d_r)(\bar{d}_s\gamma^\mu d_t)$	$\mathcal{Q}_{ld}$	$(\bar{l}_p\gamma^\mu l_r)(\bar{d}_s\gamma^\mu d_t)$
$\mathcal{Q}_{lq}^{(1)}$	$(\bar{l}_p\gamma^\mu l_r)(\bar{q}_s\gamma^\mu q_t)$	$\mathcal{Q}_{eu}$	$(\bar{e}_p\gamma^\mu e_r)(\bar{u}_s\gamma^\mu u_t)$	$\mathcal{Q}_{qe}$	$(\bar{q}_p\gamma^\mu q_r)(\bar{e}_s\gamma^\mu e_t)$
$\mathcal{Q}_{lq}^{(3)}$	$(\bar{l}_p\gamma^\mu\sigma^I l_r)(\bar{q}_s\gamma^\mu\sigma^I q_t)$	$\mathcal{Q}_{ed}$	$(\bar{e}_p\gamma^\mu e_r)(\bar{d}_s\gamma^\mu d_t)$	$\mathcal{Q}_{qu}^{(1)}$	$(\bar{q}_p\gamma^\mu q_r)(\bar{u}_s\gamma^\mu u_t)$
		$\mathcal{Q}_{ud}^{(1)}$	$(\bar{u}_p\gamma^\mu u_r)(\bar{d}_s\gamma^\mu d_t)$	$\mathcal{Q}_{qu}^{(8)}$	$(\bar{q}_p\gamma^\mu T^A q_r)(\bar{u}_s\gamma^\mu T^A u_t)$
		$\mathcal{Q}_{ud}^{(8)}$	$(\bar{u}_p\gamma^\mu T^A u_r)(\bar{d}_s\gamma^\mu T^A d_t)$	$\mathcal{Q}_{qd}^{(1)}$	$(\bar{q}_p\gamma^\mu q_r)(\bar{d}_s\gamma^\mu d_t)$
				$\mathcal{Q}_{qd}^{(8)}$	$(\bar{q}_p\gamma^\mu T^A q_r)(\bar{d}_s\gamma^\mu T^A d_t)$

TABLE 3.7: Four-fermion operators, sets $(\bar{L}R)(\bar{R}L)$ and baryon-number violating [100]. See main text for the operator naming conventions.

$(\bar{L}R)(\bar{R}L)$		B-violating	
$\mathcal{Q}_{ledq}$	$(\bar{l}_p^j e_r)(\bar{d}_s q_t^j)$	$\mathcal{Q}_{duq}$	$\epsilon^{\alpha\beta\gamma}\epsilon_{jk}[(d_p^\alpha)^T C u_r^\beta][(q_s^{\gamma j})^T C l_t^k]$
$\mathcal{Q}_{quqd}^{(1)}$	$(\bar{q}_p^j u_r)\epsilon_{jk}(\bar{q}_s^k d_t)$	$\mathcal{Q}_{qqu}$	$\epsilon^{\alpha\beta\gamma}\epsilon_{jk}[(q_p^{\alpha j})^T C q_r^{\beta k}][(u_s^\gamma)^T C e_t]$
$\mathcal{Q}_{quqd}^{(8)}$	$(\bar{q}_p^j T^A u_r)\epsilon_{jk}(\bar{q}_s^k T^A d_t)$	$\mathcal{Q}_{qqq}^{(1)}$	$\epsilon^{\alpha\beta\gamma}\epsilon_{jk}\epsilon_{mn}[(q_p^{\alpha j})^T C q_r^{\beta k}][(q_s^{\gamma m})^T C l_t^n]$
$\mathcal{Q}_{lequ}^{(1)}$	$(\bar{l}_p^j e_r)\epsilon_{jk}(\bar{q}_s^k u_t)$	$\mathcal{Q}_{qqq}^{(3)}$	$\epsilon^{\alpha\beta\gamma}(\sigma^I\epsilon)_{jk}(\sigma^I\epsilon)_{mn}[(q_p^{\alpha j})^T C q_r^{\beta k}][(q_s^{\gamma m})^T C l_t^n]$
$\mathcal{Q}_{lequ}^{(3)}$	$(\bar{l}_p^j\sigma_{\mu\nu} e_r)\epsilon_{jk}(\bar{q}_s^k\sigma^{\mu\nu} u_t)$	$\mathcal{Q}_{duu}$	$\epsilon^{\alpha\beta\gamma}[(d_p^\alpha)^T C u_r^\beta][(u_s^\gamma)^T C e_t]$

The first step towards constructing a complete set of operators for $\mathcal{L}^{(6)}$ satisfying invariance under the $SU(3)_C \times SU(2)_L \times U(1)_Y$ gauge group was reported in Ref. [107]. However, this operator basis was overcomplete, that is, there were operators whose Wilson coefficients vanished when observables were calculated, which occurs when the EOMs relate the field variables as the external states go on-shell [105]. One can make field redefinitions of the SM fields so that redundant combinations of $\mathcal{Q}^{(6)}$ operators vanish at the Lagrangian level instead of cancelling at the S-matrix-element level, resulting in a non-redundant basis for the SMEFT after making use of the EOMs. Although the first step in this direction was carried out by Buchmüller and Wyler [108] in the mid-1980s, a complete set of non-redundant dimension-6 operators was not found until more than two decades later through the works of Grzadkowski et al. in Ref. [109], and Giudice et al. in Ref. [110] and others [111–115]. It is important to highlight that there is not a unique way of redefining the SM model fields, which means that different operator bases are allowed and that SM fields become contextual in the SMEFT. All operator bases, though, are equivalent up to operator redefinitions, Fierz transformations, EOMs and other operator identities [100].

At dimension 6, one can have four-fermion interaction terms without bosons or derivatives. There can also be operators with two fermion fields, and a combination of scalar fields, derivatives and a field strength tensor with a total mass dimension of 3. The last possible class of operators are purely bosonic terms, such as a combination of field strength tensors, scalar fields and derivatives. In this thesis, we employ the so-called Warsaw basis [109], which contains 59 baryon-number conserving and 5 baryon-number violating operators. These in turn can be organised in twelve subsets (see Tables 3.4, 3.5, 3.6 and 3.7). Among these subsets, there are five that contain various four-fermion operators (cf. Tables 3.6 and 3.7).

The naming conventions in these tables are as follows: p, r, s, t are generation indices;

α, β, γ are fundamental-representation $SU(3)_C$ indices; A, B, C are adjoint-representation $SU(3)_C$ indices; j, k, m, n are fundamental-representation $SU(2)_L$ indices; and I is an adjoint-representation $SU(2)_L$ index. In addition, T^A are the generators of the $SU(3)_C$ group; and σ^I are the Pauli matrices. Moreover, $\widetilde{H}$ is the conjugated Higgs field; $\widetilde{G}^A_{\mu\nu}$ is the dual of the gluon field strength tensor (i.e. $\widetilde{G}^A_{\mu\nu} \equiv \frac{1}{2}\epsilon_{\mu\nu\sigma\rho}G^{A\sigma\rho}$); and $\widetilde{W}^I_{\mu\nu}$ is the corresponding dual weak field strength tensor. Finally, C is the charge-conjugation operator; ϵ is the totally antisymmetric tensor; $\sigma^{\mu\nu} \equiv \frac{i}{2}(\gamma^\mu\gamma^\nu - \gamma^\nu\gamma^\mu)$ is the Dirac antisymmetric tensor; and $\Box$ is the d'Alambertian operator. Taking into account all the different flavours of quarks and leptons results in a total of 2499 baryon-number conserving operators [100].

Chapter 4

The η-η' mixing

The mixing of states is a quantum-mechanical feature that is closely related to the symmetries of the underlying dynamics and the specific mechanisms that lead to their breaking [116]. In particular, one finds numerous examples of mixing phenomena in the field of high energy physics, such as K^0-$\overline{K}^0$, D^0-$\overline{D}^0$ and B^0-$\overline{B}^0$ mixing, neutrino oscillations, quark mixing through the Cabibbo-Kobayashi-Maskawa mechanism, and the Weinberg angle [1].

In the non-perturbative regime of QCD, there is a very rich phenomenology arising from the dynamical (spontaneous) breaking of the chiral symmetry, its explicit breaking by the quark masses and the axial $U(1)_A$ anomaly [116]. In this context, the η and η' phenomenology has stablished itself as a fruitful arena to investigate many aspect of low-energy QCD.

In this chapter, we analyse in detail the mixing of the η and η' mesons within the framework of large-N_C χPT, which allows the η' meson to become the ninth pseudo-Goldstone boson of the spontaneously broken $U(3)_L \times U(3)_R \to U(3)_V$ chiral symmetry of QCD.

4.1 Leading order in large-N_C χPT

As shown in Chapter 3.3, the axial $U(1)_A$ anomaly vanishes within the large-N_C χPT framework in the $N_C \to \infty$ limit, which in turn enables the inclusion of the pseudoscalar singlet within the nonet of Nambu-Goldstone bosons associated to the spontaneous breaking of the flavour $U(3)_L \times U(3)_R \to U(3)_V$ chiral symmetry. In this setting, let us consider the two-dimensional space of isoscalar (pseudoscalar) mesons, where the $SU(3)$ octet and singlet fields are grouped in the doublet $\eta_B^T \equiv (\eta_8, \eta_1)$. Accordingly, the quadratic term in the Lagrangian takes the form [58, 65]

$$\mathcal{L} = \frac{1}{2}\partial_\mu \eta_B^T \mathcal{K} \partial^\mu \eta_B - \frac{1}{2}\eta_B^T \mathcal{M}^2 \eta_B \,, \tag{4.1}$$

where

$$\mathcal{K} = \begin{pmatrix} 1+\delta_8 & \delta_{81} \\ \delta_{81} & 1+\delta_1 \end{pmatrix}, \quad \mathcal{M}^2 = \begin{pmatrix} M_8^2 & M_{81}^2 \\ M_{81}^2 & M_1^2 \end{pmatrix}, \tag{4.2}$$

with the following definitions for the mass matrix elements

$$\begin{aligned} M_8^2 &= \overset{\circ}{M}{}_8^2 + \Delta M_8^2 \,, \\ M_1^2 &= \overset{\circ}{M}{}_1^2 + \Delta M_1^2 + M_0^2 \,, \\ M_{81}^2 &= \overset{\circ}{M}{}_{81}^2 + \Delta M_{81}^2 \,. \end{aligned} \tag{4.3}$$

Note that $M_0^2 = 6\tau/F^2$ stands for the $U(1)_A$ anomaly contribution to the η_1 mass, with τ being the topological susceptibility of the purely gluonic theory (see Sec. 3.3.1), whilst the $\overset{\circ}{M}{}_i^2$ $(i = 8, 1)$ are the $\mathcal{O}(\delta^0)$ quark-mass contributions to the octet and singlet isoscalar masses, which can be obtained from the second term in Eq. (3.69), and in the isospin limit

read [58]

$$\begin{aligned}
\overset{\circ}{M}{}_8^2 &= \frac{2}{3}B_0(\hat{m}+2m_s) = \frac{1}{3}(4\overset{\circ}{M}{}_K^2 - \overset{\circ}{M}{}_\pi^2)\,,\\
\overset{\circ}{M}{}_1^2 &= \frac{2}{3}B_0(2\hat{m}+m_s) = \frac{1}{3}(2\overset{\circ}{M}{}_K^2 + \overset{\circ}{M}{}_\pi^2)\,,\\
\overset{\circ}{M}{}_{81}^2 &= \frac{2\sqrt{2}}{3}B_0(\hat{m}-m_s) = -\frac{2\sqrt{2}}{3}(\overset{\circ}{M}{}_K^2 - \overset{\circ}{M}{}_\pi^2)\,,
\end{aligned} \tag{4.4}$$

where the m_a ($a=u,d,s$) are the masses of the three light quarks, $\hat{m}\equiv(m_u+m_d)/2$, and $\overset{\circ}{M}{}_K^2$ and $\overset{\circ}{M}{}_\pi^2$ are the kaon and pion masses at $\mathcal{O}(\delta^0)$ in the combined chiral and $1/N_C$ expansion.

The parameters δ_8, δ_1 and δ_{81} in Eq. (4.2), and ΔM_8^2, ΔM_1^2 and ΔM_{81}^2 in Eq. (4.3) correspond to NLO corrections, which means that they vanish at LO. Accordingly, the LO mass eigenstates of the physical states η and η' are obtained by simply diagonalising the mass matrix $\mathcal{M}^2$ by means of the orthogonal transformation (cf. Appendix A)

$$R \equiv \begin{pmatrix} \cos\theta_P & -\sin\theta_P \\ \sin\theta_P & \cos\theta_P \end{pmatrix}, \tag{4.5}$$

such that

$$\eta_B = R^T\cdot\eta_P \equiv R^T\cdot\begin{pmatrix}\eta\\ \eta'\end{pmatrix}, \quad \mathcal{M}^2_{\rm diag} = R\cdot\mathcal{M}^2\cdot R^T\,. \tag{4.6}$$

Operating, one finds the following LO large-N_C results for the η and η' masses, and mixing angle θ_P [117, 118]

$$\begin{aligned}
\overset{\circ}{M}{}_\eta^2 &= \frac{1}{2}M_0^2 + \overset{\circ}{M}{}_K^2 - \frac{1}{2}\sqrt{M_0^4 - \frac{4}{3}M_0^2\Delta + 4\Delta^2}\,,\\
\overset{\circ}{M}{}_{\eta'}^2 &= \frac{1}{2}M_0^2 + \overset{\circ}{M}{}_K^2 + \frac{1}{2}\sqrt{M_0^4 - \frac{4}{3}M_0^2\Delta + 4\Delta^2}\,,\\
\sin\theta_P &= -\frac{1}{\sqrt{1+\left(3M_0^2 - 2\Delta + \sqrt{9M_0^4 - 12M_0^2\Delta + 36\Delta^2}\right)^2/32\Delta^2}}\,,
\end{aligned} \tag{4.7}$$

with $\Delta \equiv \overset{\circ}{M}{}_K^2 - \overset{\circ}{M}{}_\pi^2$. It is worth highlighting that the mathematical parameterisation that has been employed in this subsection is the octet-singlet basis but others, such as the quark-flavour basis (cf. Appendix A), are also widely used.

4.2 Next-to-leading order in large-N_C χPT

To first order in δ_8, δ_1 and δ_{81}, the kinetic matrix $\mathcal{K}$ in Eq. (4.1) can be diagonalised through the following matrix field redefinition [58]

$$\eta_B = Z^{1/2^T}\cdot\hat{\eta} \equiv Z^{1/2^T}\cdot\begin{pmatrix}\hat{\eta}_8\\ \hat{\eta}_1\end{pmatrix}, \quad Z^{1/2}\cdot\mathcal{K}\cdot Z^{1/2^T} = \mathbb{1}\,, \tag{4.8}$$

which is satisfied for

$$Z^{1/2} = \begin{pmatrix} 1-\delta_8/2 & -\delta_{81}/2 \\ -\delta_{81}/2 & 1-\delta_1/2 \end{pmatrix}. \tag{4.9}$$

Using this field redefinition, the mass matrix can be written in the $\hat{\eta}$ basis as

$$\widehat{\mathcal{M}}^2 = Z^{1/2}\cdot\mathcal{M}^2\cdot Z^{1/2^T}\,, \tag{4.10}$$

where, to first order in ΔM_i^2 and $\delta_i \times M_j^2$ products ($i,j = 8,1,81$), one finds

$$\begin{aligned}
\widehat{M}_8^2 &= \overset{\circ}{M}{}_8^2(1-\delta_8) - \overset{\circ}{M}{}_{81}^2\,\delta_{81} + \Delta M_8^2\,,\\
\widehat{M}_1^2 &= (M_0^2 + \overset{\circ}{M}{}_1^2)(1-\delta_1) - \overset{\circ}{M}{}_{81}^2\,\delta_{81} + \Delta M_1^2\,,\\
\widehat{M}_{81}^2 &= \overset{\circ}{M}{}_{81}^2\Big[1-(\delta_8+\delta_1)/2\Big] - (M_0^2 + \overset{\circ}{M}{}_8^2 + \overset{\circ}{M}{}_1^2)\delta_{81}/2 + \Delta M_{81}^2\,.
\end{aligned} \tag{4.11}$$

As before, one must diagonalise the mass matrix $\widehat{\mathcal{M}}^2$ by means of an orthogonal transformation in order to obtain the physical mass eigenstates. To that end, one employs Eq. (4.5) so that

$$\hat{\eta} = R^T\cdot\eta_P \equiv R^T\cdot\begin{pmatrix}\eta\\ \eta'\end{pmatrix}\,,\quad \mathcal{M}^2_{\rm diag} = R\cdot\widehat{\mathcal{M}}^2\cdot R^T\,, \tag{4.12}$$

and finds the following non-trivial relations [58]

$$M_\eta^2 + M_{\eta'}^2 = \widehat{M}_8^2 + \widehat{M}_1^2\,,\quad M_{\eta'}^2 - M_\eta^2 = \sqrt{\left(\widehat{M}_8^2 - \widehat{M}_1^2\right)^2 + 4\widehat{M}_{81}^2}\,, \tag{4.13}$$

and

$$\tan\theta_P = \frac{\widehat{M}_8^2 - M_\eta^2}{\widehat{M}_{81}^2} = \frac{M_{\eta'}^2 - \widehat{M}_1^2}{\widehat{M}_{81}^2} = \frac{\widehat{M}_{81}^2}{M_{\eta'}^2 - \widehat{M}_8^2} = \frac{\widehat{M}_{81}^2}{\widehat{M}_1^2 - M_\eta^2}\,. \tag{4.14}$$

It follows from Eqs. (4.8) and (4.12) that the transformation matrix from the bare to the physical basis takes the form $\eta_B = (R\cdot Z^{1/2})^T\cdot\eta_P$, with

$$R\cdot Z^{1/2} = \begin{pmatrix}\cos\theta_P(1-\delta_8/2) + \sin\theta_P\delta_{81}/2 & -\sin\theta_P(1-\delta_1/2) - \cos\theta_P\delta_{81}/2\\ \sin\theta_P(1-\delta_8/2) - \cos\theta_P\delta_{81}/2 & \cos\theta_P(1-\delta_1/2) - \sin\theta_P\delta_{81}/2\end{pmatrix}. \tag{4.15}$$

At $\mathcal{O}(\delta)$ in large-N_C χPT, a shift in the kinetic matrix can only come from the terms associated to L_5 and Λ_1 in Eq. (3.73). Accordingly, it is straightforward to find the following expressions

$$\delta_8 = \frac{8L_5}{F^2}\overset{\circ}{M}{}_8^2\,,\quad \delta_1 = \frac{8L_5}{F^2}\overset{\circ}{M}{}_1^2 + \Lambda_1\,,\quad \delta_{81} = \frac{8L_5}{F^2}\overset{\circ}{M}{}_{81}^2\,. \tag{4.16}$$

Likewise, a shift in the mass matrix can only come from the terms associated to L_8 and Λ_2 in Eq. (3.73). Thus, one obtains

$$\begin{aligned}
\Delta M_8^2 &= \frac{16L_8}{F^2}(\overset{\circ}{M}{}_8^4 + \overset{\circ}{M}{}_{81}^4)\,,\\
\Delta M_1^2 &= \frac{16L_8}{F^2}(\overset{\circ}{M}{}_1^4 + \overset{\circ}{M}{}_{81}^4) + 2\Lambda_2\overset{\circ}{M}{}_1^2\,,\\
\Delta M_{81}^2 &= \overset{\circ}{M}{}_{81}^2\left(\frac{32L_8}{F^2}\overset{\circ}{M}{}_K^2 + \Lambda_2\right).
\end{aligned} \tag{4.17}$$

Making use now of some of the RχT results from Sec. 3.4, in particular the relations from Eq. (3.89)

$$L_5 = \frac{c_d c_m}{M_S^2}\,,\quad L_8 = \frac{c_m^2}{2M_S^2}\,, \tag{4.18}$$

one can rewrite the expressions from Eqs. (4.16) and (4.17) as

$$\delta_8 = \frac{8c_d c_m}{M_S^2}\frac{\overset{\circ}{M}{}_8^2}{F^2}\,, \quad \delta_1 = \frac{8c_d c_m}{M_S^2}\frac{\overset{\circ}{M}{}_1^2}{F^2}\,, \quad \delta_{81} = \frac{8c_d c_m}{M_S^2}\frac{\overset{\circ}{M}{}_{81}^2}{F^2} \tag{4.19}$$

and

$$\begin{aligned}
\Delta M_8^2 =& \frac{8c_m^2}{M_S^2 F^2}(\overset{\circ}{M}{}_8^4 + \overset{\circ}{M}{}_{81}^4)\,,\\
\Delta M_1^2 =& \frac{8c_m^2}{M_S^2 F^2}(\overset{\circ}{M}{}_1^4 + \overset{\circ}{M}{}_{81}^4)\,,\\
\Delta M_{81}^2 =& \frac{16c_m^2}{M_S^2 F^2}\overset{\circ}{M}{}_{81}^2\overset{\circ}{M}{}_K^2\,,
\end{aligned} \tag{4.20}$$

where M_S is the mass of a generic octet scalar resonance.

4.3 Decay constants in the η-η' sector

The decay constants in the η-η' system are defined as in Eq. (2.35), that is, as the matrix elements of the axial currents [58]

$$\langle 0|\, J_A^{\mu a}(0)\,|P(p)\rangle = i p_\mu f_P^a\,, \tag{4.21}$$

where the $J_A^{\mu a} \equiv \bar{q}\gamma^\mu\gamma_5\lambda^a q$ are the axial currents defined at the quark level, $a = 8, 1$ and $P = \eta, \eta'$. Since the physical η and η' mesons have octet and singlet components, Eq. (4.21) defines four independent decay constants, f_P^a. These can be expressed as [119]

$$\{f_P^a\} = \begin{pmatrix} f_\eta^8 & f_\eta^1 \\ f_{\eta'}^8 & f_{\eta'}^1 \end{pmatrix} = \begin{pmatrix} f_8\cos\theta_8 & -f_1\sin\theta_1 \\ f_8\sin\theta_8 & f_1\cos\theta_1 \end{pmatrix} \tag{4.22}$$

in what is known as the two-angle parameterisation scheme [119–122]. The physical decay constants are given by [42]

$$f_P^a = F\left[(\mathcal{T}^\dagger)^{-1}\mathcal{K}\right]_P^a\,, \tag{4.23}$$

where $F = f_\pi$ at $\mathcal{O}(\delta^0)$ and $\mathcal{T}$ is the matrix that simultaneously diagonalises the kinetic and mass matrices of the Lagrangian in Eq. (4.1)

$$\mathcal{K} = \mathcal{T}^\dagger\mathcal{T}\,, \quad \mathcal{M}^2 = \mathcal{T}^\dagger\mathcal{M}^2_{\text{diag}}\mathcal{T}\,. \tag{4.24}$$

Of course, the transformation matrix $\mathcal{T}$ that diagonalises both $\mathcal{K}$ and $\mathcal{M}^2$ is the one that relates the physical and bare fields, i.e. $\eta_P = R\cdot(Z^{1/2^T})^{-1}\cdot\eta_B$, and, therefore, one is allowed to write $f_P^a = F\left[R\cdot(Z^{1/2^T})^{-1}\right]_P^a$. Accordingly, to first order in δ_8, δ_1 and δ_{81}, the decay constants f_P^a can be expressed as

$$\begin{aligned}
f_\eta^8/F &= \cos\theta_P\left(1+\frac{\delta_8}{2}\right) - \sin\theta_P\frac{\delta_{81}}{2}\,,\\
f_\eta^1/F &= -\sin\theta_P\left(1+\frac{\delta_1}{2}\right) + \cos\theta_P\frac{\delta_{81}}{2}\,,\\
f_{\eta'}^8/F &= \sin\theta_P\left(1+\frac{\delta_8}{2}\right) + \cos\theta_P\frac{\delta_{81}}{2}\,,\\
f_{\eta'}^1/F &= \cos\theta_P\left(1+\frac{\delta_1}{2}\right) + \sin\theta_P\frac{\delta_{81}}{2}\,.
\end{aligned} \tag{4.25}$$

Employing the relationships

$$f_8 = \sqrt{(f_\eta^8)^2 + (f_{\eta'}^8)^2}\,, \quad f_1 = \sqrt{(f_\eta^1)^2 + (f_{\eta'}^1)^2} \tag{4.26}$$

and

$$\tan\theta_8 = \frac{f_{\eta'}^8}{f_\eta^8}\,, \quad \tan\theta_1 = -\frac{f_\eta^1}{f_{\eta'}^1}\,, \tag{4.27}$$

one can easily find the following NLO results for the two basic decay constants

$$f_8 = F\left(1 + \frac{\delta_8}{2}\right), \quad f_1 = F\left(1 + \frac{\delta_1}{2}\right), \tag{4.28}$$

and mixing angles

$$\theta_8 = \theta_P + \arctan\frac{\delta_{81}}{2}\,, \quad \theta_1 = \theta_P - \arctan\frac{\delta_{81}}{2}\,. \tag{4.29}$$

4.4 η and η' admixtures with the π^0

In order to study the mixing between the η, η' and π^0, one must incorporate isospin-breaking effects, which are induced by the difference in mass of the u and d quarks, as well as the difference in electric charge once QED is taken into account. Some of the results from this subsection are relevant for Chapter 11.

For the analysis that follows, we perform the calculations in the quark-flavour basis (see Appendix A for details). One can easily change basis by means of the following substitutions

$$|\pi^0\rangle \to |\pi_3\rangle\,, \quad |\eta_8\rangle \to \frac{1}{\sqrt{3}}\,|\eta_{\rm NS}\rangle - \sqrt{\frac{2}{3}}\,|\eta_{\rm S}\rangle\,, \quad |\eta_1\rangle \to \sqrt{\frac{2}{3}}\,|\eta_{\rm NS}\rangle + \frac{1}{\sqrt{3}}\,|\eta_{\rm S}\rangle\,, \tag{4.30}$$

where $|\pi_3\rangle = \frac{1}{\sqrt{2}}\,|\bar{u}u - \bar{d}d\rangle$ is the pure isospin triplet state, and $|\eta_{\rm NS}\rangle = \frac{1}{\sqrt{2}}\,|\bar{u}u + \bar{d}d\rangle$ and $|\eta_{\rm S}\rangle = |\bar{s}s\rangle$ are the non-strange and strange mathematical states, respectively. Using the above substitutions, Eq. (3.70) becomes

$$\widetilde{\Phi} = \begin{pmatrix} \frac{1}{\sqrt{2}}\pi_3 + \frac{1}{\sqrt{2}}\eta_{\rm NS} & \pi^+ & K^+ \\ \pi^- & -\frac{1}{\sqrt{2}}\pi_3 + \frac{1}{\sqrt{2}}\eta_{\rm NS} & K^0 \\ K^- & \overline{K}^0 & \eta_{\rm S} \end{pmatrix}. \tag{4.31}$$

In order to make progress, Eqs. (4.1) and (4.2) must be enlarged so as to include the π_3 state. This is

$$\mathcal{L} = \frac{1}{2}\partial_\mu \phi_B^T \widetilde{\mathcal{K}} \partial^\mu \phi_B - \frac{1}{2}\phi_B^T \widetilde{\mathcal{M}}^2 \phi_B\,, \tag{4.32}$$

where $\phi_B^T \equiv (\pi_3, \eta_{\rm NS}, \eta_{\rm S})$ and

$$\widetilde{\mathcal{K}} = \begin{pmatrix} 1+\delta_3 & \delta_{\rm NS3} & \delta_{\rm S3} \\ \delta_{\rm NS3} & 1+\delta_{\rm NS} & \delta_{\rm SNS} \\ \delta_{\rm S3} & \delta_{\rm SNS} & 1+\delta_{\rm S} \end{pmatrix}, \quad \widetilde{\mathcal{M}}^2 = \begin{pmatrix} M_3^2 & M_{\rm NS3}^2 & M_{\rm S3}^2 \\ M_{\rm NS3}^2 & M_{\rm NS}^2 & M_{\rm SNS}^2 \\ M_{\rm S3}^2 & M_{\rm SNS}^2 & M_{\rm S}^2 \end{pmatrix}, \tag{4.33}$$

with definitions for the mass matrix elements similar to those from Eq. (4.3)

$$\begin{gathered} M_3^2 = \overset{\circ}{M}{}_3^2 + \Delta M_3^2\,, \quad M_{\rm NS}^2 = \overset{\circ}{M}{}_{\rm NS}^2 + \Delta M_{\rm NS}^2\,, \quad M_{\rm S}^2 = \overset{\circ}{M}{}_{\rm S}^2 + \Delta M_{\rm S}^2 + M_0^2\,, \\ M_{\rm NS3}^2 = \overset{\circ}{M}{}_{\rm NS3}^2 + \Delta M_{\rm NS3}^2\,, \quad M_{\rm S3}^2 = \overset{\circ}{M}{}_{\rm S3}^2 + \Delta M_{\rm S3}^2\,, \quad M_{\rm SNS}^2 = \overset{\circ}{M}{}_{\rm SNS}^2 + \Delta M_{\rm SNS}^2\,. \end{gathered} \tag{4.34}$$

As before, from the second term in Eq. (3.69) one finds at LO

$$\begin{aligned}
\overset{\circ}{M}{}^2_3 &= B_0(m_u+m_d) = \overset{\circ}{M}{}^2_{\pi^\pm}\,,\\
\overset{\circ}{M}{}^2_{\rm NS} &= B_0(m_u+m_d) = \overset{\circ}{M}{}^2_{\pi^\pm}\,,\\
\overset{\circ}{M}{}^2_{\rm S} &= 2B_0 m_s = \overset{\circ}{M}{}^2_{K^0} + \overset{\circ}{M}{}^2_{K^\pm} - \overset{\circ}{M}{}^2_{\pi^\pm}\,,\\
\overset{\circ}{M}{}^2_{\rm NS3} &= B_0(m_u-m_d) = \overset{\circ}{M}{}^2_{K^\pm} - \overset{\circ}{M}{}^2_{K^0}\,,\\
\overset{\circ}{M}{}^2_{\rm SNS} &= 0\,, \quad \overset{\circ}{M}{}^2_{\rm S3} = 0\,.
\end{aligned} \tag{4.35}$$

Drawing a parallel with Eqs. (4.8) and (4.9), at NLO the kinetic matrix $\widetilde{\mathcal{K}}$ is diagonalised with the field redefinition

$$\phi_B = \widetilde{Z}^{1/2^T}\cdot\hat{\phi}\,, \quad \widetilde{Z}^{1/2}\cdot\widetilde{\mathcal{K}}\cdot\widetilde{Z}^{1/2^T} = \mathbb{1}\,, \tag{4.36}$$

where

$$\widetilde{Z}^{1/2} = \begin{pmatrix} 1-\delta_3/2 & -\delta_{\rm NS3}/2 & -\delta_{\rm S3}/2 \\ -\delta_{\rm NS3}/2 & 1-\delta_{\rm NS}/2 & -\delta_{\rm SNS}/2 \\ -\delta_{\rm S3}/2 & -\delta_{\rm SNS}/2 & 1-\delta_{\rm S}/2 \end{pmatrix}. \tag{4.37}$$

After some algebra, one arrives at the following large-N_C χPT expressions for the kinetic shifts from the terms associated to L_5 and Λ_1 in Eq. (3.73)

$$\begin{aligned}
\delta_3 &= \frac{8L_5}{F^2}\overset{\circ}{M}{}^2_3\,, \quad \delta_{\rm NS} = \frac{8L_5}{F^2}\overset{\circ}{M}{}^2_{\rm NS} + \frac{2}{3}\Lambda_1\,, \quad \delta_{\rm S} = \frac{8L_5}{F^2}\overset{\circ}{M}{}^2_{\rm S} + \frac{1}{3}\Lambda_1\,,\\
\delta_{\rm NS3} &= -\frac{8L_5}{F^2}\overset{\circ}{M}{}^2_{\rm NS3}\,, \quad \delta_{\rm SNS} = \frac{\sqrt{2}}{3}\Lambda_1\,, \quad \delta_{\rm S3} = 0\,.
\end{aligned} \tag{4.38}$$

To diagonalise the mass matrix, we employ the following orthogonal transformation [see Eq. (7.9)]

$$\widetilde{R} \equiv \begin{pmatrix} 1 & \epsilon_{12} & \epsilon_{13} \\ -\epsilon_{12}\cos\phi_{23} + \epsilon_{13}\sin\phi_{23} & \cos\phi_{23} & -\sin\phi_{23} \\ -\epsilon_{12}\sin\phi_{23} - \epsilon_{13}\cos\phi_{23} & \sin\phi_{23} & \cos\phi_{23} \end{pmatrix}, \tag{4.39}$$

where ϕ_{23} is the mixing angle in the η-η' sector, and ϵ_{12} and ϵ_{13} are first order approximations to the mixing angles in the π^0-η and π^0-η' systems, respectively. The shifts in the masses, which are associated to the L_8 and Λ_2 terms in Eq. (3.73), are

$$\begin{aligned}
\Delta M^2_3 &= \frac{16L_8}{F^2}(\overset{\circ}{M}{}^4_3 + \overset{\circ}{M}{}^4_{\rm NS3})\,, \quad \Delta M^2_{\rm NS} = \frac{16L_8}{F^2}(\overset{\circ}{M}{}^4_{\rm NS} + \overset{\circ}{M}{}^4_{\rm NS3}) + \frac{4}{3}\Lambda_2\overset{\circ}{M}{}^2_{\rm NS}\,,\\
\Delta M^2_{\rm S} &= \frac{16L_8}{F^2}\overset{\circ}{M}{}^4_{\rm S} + \frac{2}{3}\Lambda_2\overset{\circ}{M}{}^2_{\rm S}\,, \quad \Delta M^2_{\rm S3} = -\frac{\sqrt{2}}{3}\Lambda_2(\overset{\circ}{M}{}^2_{\rm S} + \overset{\circ}{M}{}^2_3 - 2\overset{\circ}{M}{}^2_{\rm K^\pm})\,,\\
\Delta M^2_{\rm NS3} &= \frac{32L_8}{F^2}\overset{\circ}{M}{}^2_{\rm NS3}\overset{\circ}{M}{}^2_{\rm NS} - \frac{2}{3}\Lambda_2(\overset{\circ}{M}{}^2_{\rm S} + \overset{\circ}{M}{}^2_3 - 2\overset{\circ}{M}{}^2_{\rm K^\pm})\,,\\
\Delta M^2_{\rm SNS} &= -\frac{\sqrt{2}}{3}\Lambda_2(\overset{\circ}{M}{}^2_{\rm S} + \overset{\circ}{M}{}^2_{\rm NS})\,,
\end{aligned} \tag{4.40}$$

where $\overset{\circ}{M}{}^2_{\rm K^\pm} = B_0(m_u+m_s)$. As before, the R$\chi$T results can be obtained by using the identities from Eq. (4.18).

For completeness, we provide the theoretical expressions for the mathematical states π_3, $\eta_{\rm NS}$ and $\eta_{\rm S}$ as functions of the physical states π^0, η and η' at NLO in large-N_C χPT in Appendix B.

Chapter 5

The complex plane in elementary particle physics

In this chapter, we explore one of the most important discoveries in elementary particle physics, which is that of the existence of the complex plane [123]. We begin by reviewing some basic features of the scattering matrix (S-matrix), including unitarity, analyticity and crossing symmetry. Next, we briefly cover the topic of resonances and some Breit-Wigner-like parameterisations. We conclude the chapter by discussing dispersion relations and some of the associated basic results.

5.1 The S-matrix

The superposition principle in quantum mechanics allows for a generic state $|\psi\rangle$ to be written as

$$|\psi\rangle = \sum_n a_n |n\rangle \,, \tag{5.1}$$

where the set of basis states $|n\rangle$ is assumed to be orthonormal and complete, i.e.

$$\langle m|n\rangle = \delta_{mn} \,, \quad \sum_m |m\rangle \langle m| = \mathbb{1} \,. \tag{5.2}$$

The probability that a final state $|f\rangle$ is measured can be calculated from squaring the modulus of the matrix element $\langle f|U|i\rangle$, where $|i\rangle$ is some initial state and U is assumed to be a linear operator. In addition, one requires that, after normalisation of the quantum states, the total probability of a system to end up in any other state to be unity, which in turn can be expressed by the condition $\sum_n |a_n|^2 = 1$. Thus, one is allowed to write [123]

$$\begin{aligned} 1 &= \sum_m |\langle m|U|\psi\rangle|^2 = \sum_m \langle\psi|U^\dagger|m\rangle \langle m|U|\psi\rangle \\ &= \langle\psi|U^\dagger U|\psi\rangle = \sum_{n,n'} a^*_{n'} a_n \langle n'|U^\dagger U|n\rangle \,. \end{aligned} \tag{5.3}$$

For Eq. (5.3) to hold for any choice of a_n, it is necessary that $U^\dagger U = 1$. Accordingly, the condition that the total probability be unity for some initial state to end up in some other arbitrary final state is equivalent to requiring the operator U to be unitary.

The unitary operator that connects asymptotic *in* and *out* states is known as the S-matrix, and the scattering amplitude is defined as the interacting part of the S-matrix [1]

$$(2\pi)^4 \delta^4(p_i - p_f) \mathcal{M}_{i\to f} = {}_{\text{out}}\langle f|S - \mathbb{1}|i\rangle_{\text{in}} \,, \tag{5.4}$$

where $|i\rangle$ and $|f\rangle$ are asymptotic states of non-interacting particles with four-momenta p_i and p_f, respectively. Note that the usual relativistic normalisation for single particle states is employed

$$\langle p_f|p_i\rangle = (2\pi)^3 2E_{p_i} \delta^3(\vec{p}_f - \vec{p}_i) \,, \tag{5.5}$$

with $E_{p_i} = \sqrt{\vec{p}_i^{\,2} + m^2}$. The transfer matrix ($\mathcal{T}$-matrix), defined such that $S = \mathbb{1} + i\mathcal{T}$, is the non-trivial part of the S-matrix and, as a consequence of the unitarity of the latter, i.e. $S^\dagger S = 1$, one can write [4]

$$i(\mathcal{T}^\dagger - \mathcal{T}) = \mathcal{T}^\dagger \mathcal{T} \,. \tag{5.6}$$

Sandwiching the left-hand side of Eq. (5.6) between $\langle f|$ and $|i\rangle$ gives

$$\begin{aligned} \langle f| \, i(\mathcal{T}^\dagger - \mathcal{T}) \, |i\rangle &= i \, \langle i| \, \mathcal{T} \, |f\rangle^* - i \, \langle f| \, \mathcal{T} \, |i\rangle \\ &= i(2\pi)^4 \delta^4(p_i - p_f) \left(\mathcal{M}^*_{f\to i} - \mathcal{M}_{i\to f} \right) , \end{aligned} \tag{5.7}$$

whilst on the right hand side one gets

$$\begin{aligned} \langle f| \, \mathcal{T}^\dagger \mathcal{T} \, |i\rangle &= \sum_X \int d\Pi_X \, \langle f| \, \mathcal{T}^\dagger \, |X\rangle \, \langle X| \, \mathcal{T} \, |i\rangle \\ &= \sum_X (2\pi)^4 \delta^4(p_f - p_X)(2\pi)^4 \delta^4(p_i - p_X) \int d\Pi_X \mathcal{M}_{i\to X} \mathcal{M}^*_{f\to X} \,, \end{aligned} \tag{5.8}$$

after making use of the completeness relation

$$\mathbb{1} = \sum_X \int d\Pi_X \, |X\rangle \, \langle X| \,, \tag{5.9}$$

where the sum is over any single- and multi-particle states $|X\rangle$, and

$$d\Pi_X \equiv \prod_{j\in X} \frac{d^3 p_j}{(2\pi)^3} \frac{1}{2E_j} \,. \tag{5.10}$$

Therefore, unitarity implies [4]

$$\mathcal{M}_{i\to f} - \mathcal{M}^*_{f\to i} = i \sum_X \int d\Pi_X (2\pi)^4 \delta^4(p_i - p_X) \mathcal{M}_{i\to X} \mathcal{M}^*_{f\to X} \,, \tag{5.11}$$

which is known as the generalised optical theorem. The above relation must hold order-by-order in perturbation theory and, since the left-hand side has matrix elements whilst the right-hand side has matrix elements squared, implies that, for example at order Λ^2 in some coupling, the left-hand side must be a loop to match a tree-level contribution on the right-hand side. Consequently, imaginary parts of loop amplitudes are determined by tree-level amplitudes and, therefore, an interacting theory must contain loops to satisfy the unitarity requirement [4].

A particularly important special case of this theorem is when $|i\rangle = |f\rangle = |A\rangle$, for some state $|A\rangle$. In particular, Eq. (5.11) takes now the form

$$2\mathrm{Im}\mathcal{M}_{A\to A} = \sum_X \int d\Pi_X (2\pi)^4 \delta^4(p_A - p_X) |\mathcal{M}_{A\to X}|^2 \,. \tag{5.12}$$

By noting that when $|A\rangle$ is a one-particle state the decay rate may be written as

$$\Gamma_{A\to X} = \frac{1}{2m_A} \int d\Pi_X (2\pi)^4 \delta^4(p_A - X) |\mathcal{M}_{A\to X}|^2 , \tag{5.13}$$

then one finds from Eqs. (5.12) and (5.13) that

$$\mathrm{Im}\mathcal{M}_{A\to A} = m_A \sum_X \Gamma_{A\to X} = m_A \Gamma_{\mathrm{tot}}\,, \tag{5.14}$$

where Γ_{tot} is the total decay rate of the particle. The above expression states that the imaginary part of the amplitude associated to the exact propagator is equal to the mass times the total decay rate of the particle [4]. Similarly, if $|A\rangle$ is a two-particle state, the cross section in the centre-of-mass (CM) frame can be expressed as

$$\sigma_{A\to X} = \frac{1}{4E_{\mathrm{CM}}|\vec{p}_i|}\int d\Pi_X (2\pi)^4 \delta^4(p_A - X)|\mathcal{M}_{A\to X}|^2\,, \tag{5.15}$$

and, thus,

$$\mathrm{Im}\mathcal{M}_{A\to A} = 2E_{\mathrm{CM}}|\vec{p}_i| \sum_X \sigma_{A\to X}\,, \tag{5.16}$$

which is known as the optical theorem.

Notice from Eqs. (5.14) and (5.16) that, when an energy threshold for particle production is crossed from below, then new additional intermediate states are allowed in $|X\rangle$. This in turn implies *sudden* changes in the left-hand side of these equations, suggesting that the matrix elements have singularities in the complex plane at each threshold. These singularities are branch points of the amplitude $\mathcal{M}$. In order for the amplitude to be single-valued, Riemann surfaces are employed and, by convention, one draws branch cuts in the complex energy-squared plane from branch points to infinity along the (positive) real axis. This is an example of the effect of unitarity on analyticity of the S-matrix.

It is generally believed that causality requires transition amplitudes to be the real-boundary values of analytic functions of complex variables [123]. The causality condition in QFT is usually assumed to correspond to the commutativity[1] (anticommutativity) of integer (half-integer) spin field operators for spacelike separations

$$\begin{aligned} [\phi(x),\phi(y)] &= 0\,, \quad (x-y)^2 < 0\,, \\ \{\bar{\psi}(x),\psi(y)\} &= 0\,, \quad (x-y)^2 < 0\,. \end{aligned} \tag{5.17}$$

The above condition is only physically meaningful for the electromagnetic field and it can only have an indirect application for other fields. Even if the condition in Eq. (5.17) is accepted, it is difficult to use it to rigorously prove any analytic properties of transition amplitudes, though an heuristic derivation was provided in Ref. [124]. The reader is referred to Ref. [123] for an in-depth discussion.

The scattering amplitude is effectively an analytic function of the Mandelstam variables s, t and u barring poles and kinematic singularities. The Mandelstam variables are Lorentz-invariant quantities used in $2\to 2$ scattering and $1\to 3$ decays. For a $2\to 2$ scattering process with matrix element $\langle p_3, p_4|\, S\, |p_1, p_2\rangle$, they are given by

$$\begin{aligned} s &\equiv (p_1+p_2)^2 = (p_3+p_4)^2\,, \\ t &\equiv (p_1-p_3)^2 = (p_2-p_4)^2\,, \\ u &\equiv (p_1-p_4)^2 = (p_2-p_3)^2\,. \end{aligned} \tag{5.18}$$

As a consequence of total energy-momentum conservation and the on-shell mass condition for each particle, these variables are related by $s+t+u = \sum_{i=1}^4 m_i^2$.

[1] Remember that commutativity and anticommutativity of integer and half-integer spin operators, respectively, imply that they are simultaneously observable, and that they are uncorrelated and cannot influence each other for spacelike separations.

Branch points, thus, appear when particle-production channels open, forcing the number of Riemann sheets to double at each massive two-particle threshold. With branch cuts on the real axis of the s-complex plane, one must decide which side of the branch cut provides the physical amplitude. This is directly connected to the Feynman prescription (also known as the $i\varepsilon$-prescription) for obtaining physical amplitudes, which consists of giving a small negative imaginary part, $-i\varepsilon$, to the mass of each particle in any internal line of a Feynman diagram. This is nothing but a trick for representing the time ordering of causal processes. From perturbation theory one finds that the physical amplitude is given by the limit on the (right-hand) branch cut from the upper-half of the s-plane [123]

$$\mathcal{M}(\text{physical}) = \lim_{\varepsilon \to 0^+} \mathcal{M}(s + i\varepsilon, t_0)\,. \tag{5.19}$$

Poles in the scattering amplitude refer to either bound states, which are located on the physical sheet (specifically on the real s-axis below the lowest threshold), or resonances, which are located on the unphysical sheets [1]. Resonances are covered in more detail in Sec. 5.2.

Let us now consider the consequences of relativistic invariance of the S-matrix. If Λ is any proper Lorentz transformation, such that $|m'\rangle = \Lambda\,|m\rangle$, then we require any observable quantities to be independent of the Lorentz frame, which is expressed by the condition

$$|\langle m'|\,S\,|n'\rangle|^2 = |\langle m|\,S\,|n\rangle|^2\,. \tag{5.20}$$

The definition of the S-matrix elements given above does not specify the phase uniquely. This in turn allows us to replace Eq. (5.20) by the stronger condition [123]

$$\langle m'|\,S\,|n'\rangle = \langle m|\,S\,|n\rangle\,. \tag{5.21}$$

For spinless particles this entails that the matrix elements depend on the external four-momenta through their invariant scalar products only, i.e. the Mandelstam variables. For the case of elastic scattering of two spinless particles, the requirement of Lorentz invariance in Eq. (5.21) has the direct consequence of the symmetry of the matrix element

$$\langle m|\,S\,|n\rangle = \langle n|\,S\,|m\rangle\,, \tag{5.22}$$

that is

$$\langle p_1, p_2|\,S\,|p_3, p_4\rangle = \langle p_3, p_4|\,S\,|p_1, p_2\rangle\,, \tag{5.23}$$

where a rotation of π about the bisector of the angle between p_1 and p_3 in the CM frame interchanges these momenta, as well as p_2 and p_4. Note that this result does not necessarily stand for other amplitudes, although it sometimes can be derived from the C invariance of the strong interactions. This appears to suggest that, in this general case, the left-hand side of Eq. (5.11) is not the imaginary part of the amplitude. However, it can be shown [123] that the matrix element $\langle p_1, p_2|\,\mathcal{T}\,|p_3, p_4\rangle^*$ is related to $\langle p_3, p_4|\,\mathcal{T}\,|p_1, p_2\rangle$ by analytic continuation, where the latter is the limit onto the real axis of the complex s-plane from above and the former is the limit from below of the same analytic function. Therefore, the left-hand side of Eq. (5.11) is the discontinuity of the analytic function across the branch cut.

Crossing symmetry is, therefore, the property whereby transition amplitudes of processes that differ only by particles being replaced by their antiparticles on the other side of the interaction (and vice versa) are related by analytic continuation of the kinematic variables. The interpretation of this statement is that particles are indistinguishable from antiparticles traveling back in time. This effectively entails that the same analytic function for the scattering amplitude of a process can be used to describe the amplitude of other channels associated to the original process. It is, thus, possible to deduce the existence of additional singularities from

crossing symmetry [123]. Since $\sqrt{t}$ and $\sqrt{u}$ represent the energies in the t- and u-channels, they yield further branch points at the corresponding particle-production thresholds.

In order to calculate the discontinuity associated to the branch cut of a transition amplitude, one normally has to carry out a Feynman integral, which is usually a complicated task. There are, however, alternative techniques that can facilitate this by making use of the analytic properties of the amplitude. To demonstrate the idea, let us take a simple theory with two scalar fields ϕ and π, with Lagrangian

$$\mathcal{L} = -\frac{1}{2}\phi(\Box + M^2)\phi - \frac{1}{2}\pi(\Box + m^2)\pi - \frac{\lambda}{2}\phi\pi^2\,, \tag{5.24}$$

where $\Box$ is the d'Alembertian operator, i.e. $\Box = \partial_\mu\partial\mu$. The imaginary part of a propagator can be evaluated by noting that [4]

$$\mathrm{Im}\frac{1}{p^2 - m^2 + i\varepsilon} = \frac{1}{2i}\left(\frac{1}{p^2 - m^2 + i\varepsilon} - \frac{1}{p^2 - m^2 - i\varepsilon}\right) = \frac{-\varepsilon}{(p^2 - m^2) + \varepsilon^2}\,, \tag{5.25}$$

which vanishes as $\varepsilon \to 0$ except when $p^2 \approx m^2$. By integrating over p^2, one obtains

$$\int_0^\infty dp^2 \frac{-\varepsilon}{(p^2 - m^2) + \varepsilon^2} = -\pi\,, \tag{5.26}$$

which in turn implies

$$\mathrm{Im}\frac{1}{p^2 - m^2 + i\varepsilon} = -\pi\delta(p^2 - m^2)\,. \tag{5.27}$$

Thus, the propagator is real except when the particle goes on-shell [4].

The imaginary part of a loop amplitude can also be calculated using similar manipulations. As it turns out (see Ref.[4] for a detailed derivation), this is given by

$$2\mathrm{Im}\mathcal{M}_{\mathrm{loop}}(p^2) = -\frac{\lambda^2}{2}\int \frac{d^4k}{(2\pi)^4}(-2\pi i)\delta\left[(p-k)^2 - m^2\right](-2\pi i)\delta(k^2 - m^2)\,. \tag{5.28}$$

It is important to note that Eq. (5.28) indicates that the imaginary part of the loop amplitude can be calculated by putting the intermediate virtual particles on-shell. This result is valid for any amplitude and the generalisation of the procedure is known as the cutting rules [125]. They can be summarised as follows [4]:

- cut through the diagram in all possible ways that put the propagators on-shell, respecting momentum conservation;[2]
- for each cut, replace $\frac{1}{p^2 - m^2 + i\varepsilon} \to -2i\pi\delta(p^2 - m^2)\theta(p^0)$;
- sum over all the cuts;
- finally, the result is the discontinuity across the branch cut of the diagram, where $\mathrm{Disc}(i\mathcal{M}) \equiv i\mathcal{M}(p^0 + i\varepsilon) - i\mathcal{M}(p^0 - i\varepsilon) = -2\mathrm{Im}\mathcal{M}$.

At this point, one can employ dispersive techniques (cf. Sec. 5.3) to calculate the real part of the amplitude from its imaginary part (which can in turn be computed using the cutting rules, as just shown). It is remarkable that complicated Feynman integrals can be evaluated in a relatively easy manner by making use of the analytic properties of the scattering amplitudes.

[2] Note that cuts are directional, meaning that "cut" particles should have positive energy when flowing from left to right (i.e. the time direction) in Feynman diagrams.

5.2 Resonances

Resonances are extremely short lived particles whose presence is inferred from the peak located around certain energies in differential cross sections of scattering experiments and widths of decaying particles.

Resonance particles can be produced in resonance formation experiments [1]

$$A + B \to \mathbf{R} \to C_1 + ... + C_n \,, \tag{5.29}$$

and resonance production experiments

$$\begin{aligned} A + B \to \mathbf{R} + \mathrm{S} \to [C_1 + ... + C_n] + \mathrm{S} \,, \\ Z \to \mathbf{R} + \mathrm{S} \to [C_1 + ... + C_n] + \mathrm{S} \,, \end{aligned} \tag{5.30}$$

where S symbolises a spectator particle. The first reaction in Eq. (5.30) corresponds to an associated production and the second to a decay.

The most important characteristic of a resonance is its pole position, s_p, in the complex s-plane, which is defined as

$$s_p \equiv \left(M_p - \frac{i}{2}\Gamma_p \right)^2 \approx M_p^2 - i M_p \Gamma_p \,, \tag{5.31}$$

and is independent of the reaction analysed. In addition to the pole position, a resonance is also characterised by its residues, which quantify its couplings to the various channels. Close to the resonance pole, the scattering matrix $\mathcal{M}$ can be written as [1]

$$\lim_{s \to s_p} (s - s_p) \mathcal{M}_{ba} = -\mathcal{R}_{ba} \,, \tag{5.32}$$

where the residues may be calculated using the closed contour integral around the pole

$$\mathcal{R}_{ba} = -\frac{1}{2\pi i} \oint ds \mathcal{M}_{ba} \,, \tag{5.33}$$

with s being the CM energy squared.

Different approaches to extracting the intrinsic properties of a resonance, in general, lead to parameterisations that deviate from each other.[3] For instance, the standard Breit-Wigner parameters M_{BW} and Γ_{BW} do not correspond to the M_p and Γ_p from the pole position in the complex s-plane [cf. Eq. (5.31)], and this is down to the effects of the finite width and the influence of thresholds.[4] In the following discussion, we restrict the scope to Breit-Wigner-like descriptions of resonances. For details on other formalisms, see for example

[3] There are two well-known definitions of mass and width for a given resonance that are commonly used in the hadron physics literature. In the conventional approach, which we only mention here for completeness but we shall not further discuss in this thesis, the mass and width of the resonance are defined in terms of the phase shift δ as

$$\delta(s = M_\delta^2) = 90^\circ \,, \quad \Gamma_\delta = \frac{1}{M_\delta} \left[\frac{d\delta(s)}{ds} \right]^{-1}_{s = M_\delta^2} \,. \tag{5.34}$$

The interested reader may check Refs. [126, 127] and sources therein for details. The second definition makes use of the position of the resonance pole in the complex s-plane. The different formalisms associated to this are discussed in the main text.

[4] In general, the use of the simple Breit-Wigner parameterisation with constant width is only applicable to narrow resonances far from thresholds. One could improve on this by using an energy-dependent width, which incorporates a kinematic dependence on the energy, but this amounts to including only the imaginary part of the self-energy. Thus, there is a strong case for using the fully corrected one-loop propagator, which includes both the real and imaginary parts of the self-energy, ensuring in this way that the analytical properties of the amplitude where the propagator is used are preserved [126, 128].

Refs. [1, 129] and references therein.

The *standard perturbative formalism* for calculating the decay width of an unstable particle is an extension of the formalism used for calculating the S-matrix of stable particles, despite the fact that unstable particles are not asymptotic states. If the particle is long-lived, the general expectation is for this formalism to be approximately valid, though not necessarily to all orders in perturbation theory. Let us demonstrate the procedure for the particular case of a scalar particle. The two-point Green's function after Dyson summation takes the form [130]

$$D(s) = \frac{i}{s - M_0^2 + \Pi(s)}\,, \tag{5.35}$$

where $\Pi(s)$ is the sum of one-particle irreducible graphs and M_0 is the bare mass of the scalar particle. One can now Taylor expand the real part of $\Pi(s)$ around M_R^2,

$$\mathrm{Re}\Pi(s) = \mathrm{Re}\Pi(M_R^2) + \left.\frac{d\mathrm{Re}\Pi(s)}{ds}\right|_{s=M_R^2} (s - M_R^2) + \ldots\,, \tag{5.36}$$

and plug it into Eq. (5.35). Rearranging, one finds

$$D(s) = \frac{iZ}{s - M_R^2 + iZ\mathrm{Im}\Pi(s) + \ldots}\,, \tag{5.37}$$

where the renormalised mass and wavefunction renormalisation factor are defined as

$$M_R^2 \equiv M_0^2 - \mathrm{Re}\Pi(M_R^2)\,, \quad Z^{-1} \equiv 1 + \left.\frac{d\mathrm{Re}\Pi(s)}{ds}\right|_{s=M_R^2}\,. \tag{5.38}$$

The parameter M_R is known as the *on-shell mass* and, by comparison with a Breit-Wigner resonance, the *on-shell width* is given by[5]

$$\Gamma_R = \frac{1}{M_R} Z\mathrm{Im}\Pi(M_R^2)\,, \tag{5.39}$$

which is equivalent to the standard perturbative definition [cf. Eq. (5.14)]. The *on-shell* formalism breaks down when the mass of the unstable particle is close to the opening of a two-body threshold. This is because when the real part of $\Pi(s)$ was Taylor expanded in the above derivation, it was assumed that the function is analytic near M_R^2. However, when s is at a threshold, $\Pi(s)$ has a branch point on the real axis. If this is a two-body threshold, then one can write [130]

$$\Pi(s) = ik^{2L+1} f(s) + g(s)\,, \tag{5.40}$$

where L is the orbital angular momentum of the particles, and the functions f and g are regular, non-vanishing at threshold and real. Furthermore, k is the common momentum of the threshold particles of mass M_1 and M_2 in the CM frame

$$k = \frac{1}{2\sqrt{s}} \sqrt{[s - (M_1 + M_2)^2][s - (M_1 - M_2)^2]}\,. \tag{5.41}$$

Accordingly, when a two-particle s-wave threshold is approached from below, $d\mathrm{Re}\Pi(s)/ds|_{s=M_R^2}$ diverges like k^{-1}, and so does Z^{-1}. The *on-shell width*, thus, vanishes as these type of thresholds are approached. One arrives at the conclusion that a width

[5] As noted in Ref. [126], this definition applies only to narrow resonances, i.e. $\Gamma \ll M_R$, where $\mathrm{Im}\Pi(s)$ can be approximated by $\mathrm{Im}\Pi(M_R^2)$ over the width of the resonance. If this is not the case, then the full energy dependence of $\Pi(s)$ ought to be taken into account.

that is not based on the Breit-Wigner analogy [cf. Eq. (5.39)] and that behaves sensibly in the threshold region is required.

An alternative approach to the one just presented is proposed in Ref. [130] where the definitions of the width and mass of a particle are extracted directly from the position of the pole in the particle's propagator. In this so-called *pole approach*, a consistent definition of the resonance width that behaves sensibly in the threshold region is found by not performing a Taylor expansion of the real part of $\Pi(s)$. Instead, the scalar propagator is expressed as [126, 130]

$$D(s) = \frac{i}{s - M_0^2 + \Pi(s)} = \frac{i}{s - M_R^2 + \mathrm{Re}\Pi(s) - \mathrm{Re}\Pi(M_R^2) + i\mathrm{Im}\Pi(s)}\,, \tag{5.42}$$

where M_R is defined in Eq. (5.38). The *pole mass* and *pole width* of the resonance, M_p and Γ_p, are found from the pole equation [126]

$$\Delta(s_p) = s_p - M_R^2 + \mathrm{Re}\Pi_+(s_p) - \mathrm{Re}\Pi_+(M_R^2) + i\mathrm{Im}\Pi_+(s_p) = 0\,, \tag{5.43}$$

where s_p is defined in Eq. (5.31) and $\Pi_+(s) \equiv \Pi(s + i\varepsilon)$. The pole equation involves a complex function of a complex variable. Accordingly, noting that for real s one has got $\Pi_+(s) = R(s) + iI(s)$, then for an arbitrary complex s one finds

$$\Pi_+(s) = \mathrm{Re}R(s) - \mathrm{Im}I(s) + i[\mathrm{Im}R(s) + \mathrm{Re}I(s)]\,. \tag{5.44}$$

For the general case where the resonance is coupled to several channels, one must look for the poles of Eq. (5.43) in all Riemann sheets,[6] which in turn are defined by the corresponding complex channel momenta. For the particular case of a resonance coupled to channels a and b, one must look for the poles in the four Riemann sheets enumerated according to the signs of $(\mathrm{Im}p_a, \mathrm{Im}p_b)$ [126, 131]

$$\begin{aligned}
&\text{sheet I} \quad (+\,+): \quad (\mathrm{Im}p_a > 0, \mathrm{Im}p_b > 0)\,,\\
&\text{sheet II} \quad (-\,+): \quad (\mathrm{Im}p_a < 0, \mathrm{Im}p_b > 0)\,,\\
&\text{sheet III} \quad (-\,-): \quad (\mathrm{Im}p_a < 0, \mathrm{Im}p_b < 0)\,,\\
&\text{sheet IV} \quad (+\,-): \quad (\mathrm{Im}p_a > 0, \mathrm{Im}p_b < 0)\,.
\end{aligned} \tag{5.45}$$

To conclude, it is worth highlighting that the physically relevant poles are the ones that lie closest to the physical axis. For a resonance coupled to a single channel, one finds that, below threshold, this pole is on the first sheet; above threshold, it is on the second sheet, since the lower half plane of the second sheet is connected to the physical axis without crossing the branch cut [130].

5.3 Dispersion relations

Dispersive methods are powerful, model-independent techniques based on the fundamental principles of analyticity and unitarity. By exploiting non-perturbative relations between amplitudes, a resummation of rescattering effects between final-states particles is possible, in contrast to the usual perturbative expansion in which these effects are treated order-by-order only [14].

A dispersion relation is a formula that gives the real part of a scattering amplitude in terms of an integral over its imaginary part [6]. In its original formulation, it was derived from the analyticity property of the index of refraction as a function of frequency, which in turn followed from the condition that electromagnetic waves in a medium cannot travel faster than

[6] Remember that for each threshold that is crossed, the number of Riemann sheets duplicates.

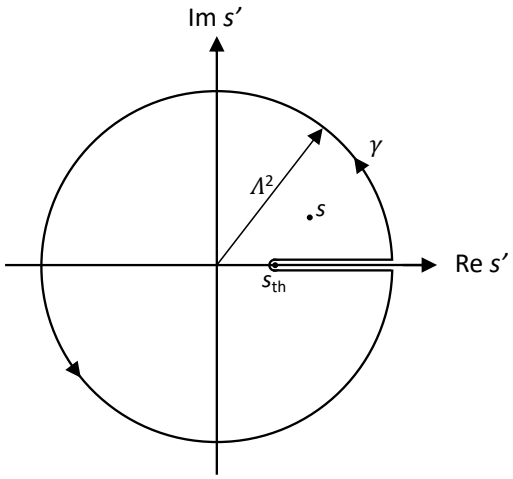

FIGURE 5.1: Integration contour γ in the complex s-plane.

light in the vacuum. The modern approach to dispersion relations [124] considers instead the condition of microscopic causality to derive the analyticity property of scattering amplitudes. The precise statement of this condition is, as discussed before, that the commutator of observables vanishes for spacelike separations.

It is useful to consider a two-meson form factor $F(s)$ as an example to develop the main ideas and features of dispersion relations. It turns out that $F(s)$ is an analytic function of the Mandelstam variable s across the entire s-complex plane, except for a branch cut along the positive real axis, originating at the first two-particle intermediate state threshold $s_{\rm th}$. In general, these form factors are real below threshold, $s < s_{\rm th}$, and they acquire an imaginary part above threshold, $s > s_{\rm th}$, which in turn is linked to the propagation of on-shell intermediate states. Analyticity allows one to relate the real part of the form factor to the discontinuity across the branch cut and this is done by analytically continuing s into the complex plane so that $F(s)$ becomes a complex-valued function of the complex variable s.

Using Cauchy's integral formula

$$F(s) = \frac{1}{2\pi i} \oint_\gamma ds' \frac{F(s')}{s'-s}\,, \tag{5.46}$$

and performing the integration along the closed contour shown in Fig. 5.1, one finds

$$F(s) = \frac{1}{2\pi i}\left[\int_{s_{\rm th}}^{\Lambda^2} ds' \frac{F(s'+i\varepsilon)-F(s'-i\varepsilon)}{s'-s} + \oint_{|s'|=\Lambda^2} ds' \frac{F(s')}{s'-s} + \oint_{|s'|=\varepsilon} ds' \frac{F(s')}{s'-s}\right], \tag{5.47}$$

where ε is a positive infinitesimal quantity and Λ^2 is the infinite radius of a contour circle. The definition of the discontinuity across the branch cut,

$$\mathrm{Disc}F(s) = F(s+i\varepsilon) - F(s-i\varepsilon) = F(s+i\varepsilon) - F^*(s+i\varepsilon) = 2i\mathrm{Im}F(s+i\varepsilon)\,, \tag{5.48}$$

where the second equality follows from Schwartz's reflection principle, i.e. $F(z^*) = F^*(z)$, allows writing the first term in Eq. (5.47) as

$$\frac{1}{\pi}\int_{s_{\rm th}}^{\Lambda^2} ds' \frac{\mathrm{Im}F(s')}{s'-s-i\varepsilon}\,. \tag{5.49}$$

In addition, one can show that the second and third integrals in Eq. (5.47) vanish, respectively, in the limits $\Lambda^2 \to \infty$, if $F(s)$ decreases fast enough as $|s| \to \infty$, and $\varepsilon \to 0$. Therefore, we arrive at the following expression for the unsubtracted dispersion relation

$$F(s) = \frac{1}{\pi} \int_{s_{\rm th}}^{\infty} ds' \frac{{\rm Im}F(s')}{s' - s - i\varepsilon} \,. \tag{5.50}$$

The above relation, which is a direct consequence of analyticity, implies that the form factor $F(s)$ can be reconstructed anywhere in the complex plane provided one knows its absorptive part along the branch cut, which is in turn given by unitarity and the optical theorem [14].

If the function $F(s)$ does not approach zero quickly enough for $|s| \to \infty$, one can still write a dispersion relation with subtractions points s_0 located on the real axis and to the left of the first threshold. To show this, note that the following identity

$$\frac{1}{s' - s} = \frac{1}{s' - s_0} + \frac{s - s_0}{(s' - s_0)(s' - s)} \tag{5.51}$$

enables Eq. (5.46) to take the form

$$F(s) = \frac{1}{2\pi i} \oint_{\gamma} ds' \frac{F(s')}{s' - s_0} + \frac{s - s_0}{2\pi i} \oint_{\gamma} ds' \frac{F(s')}{(s' - s_0)(s' - s)} \,, \tag{5.52}$$

where the first term is the subtraction constant $F(s_0)$. By following the same steps as in the derivation of the unsubtracted version of the dispersion relation, we obtain the once-subtracted dispersion relation

$$F(s) = F(s_0) + \frac{s - s_0}{\pi} \int_{s_{\rm th}}^{\infty} ds' \frac{{\rm Im}F(s')}{(s' - s_0)(s' - s - i\varepsilon)} \,, \tag{5.53}$$

where the integrand of the second term is suppressed by an additional power of s in the denominator, which helps improve the convergence of the integral and reduce the dependence of the dispersion relation on the knowledge of ${\rm Im}F(s)$ at large s. This procedure can be generalised to an n-times subtracted dispersion relation at $s = s_0$ [132]

$$F(s) = \sum_{k=0}^{n-1} \frac{(s - s_0)^k}{k!} \frac{d^k F(s)}{ds^k}\bigg|_{s=s_0} + \frac{(s - s_0)^n}{\pi} \int_{s_{\rm th}}^{\infty} ds' \frac{{\rm Im}F(s')}{(s' - s_0)^n (s' - s - i\varepsilon)} \,. \tag{5.54}$$

Note that the subtractions can be performed at different points so long as they are located on the real axis and to the left of the branch cut.

It is important to highlight that one can still perform subtractions even when it is not strictly necessary, that is, even if $F(s)$ has the desired asymptotic behaviour, i.e. $F(s) = 0$ as $|s| \to \infty$. The reason for this is that the unsubtracted dispersion relation in Eq. (5.50) requires complete knowledge of the discontinuity across the branch cut up to arbitrarily large energies, which is, of course, not realistic. By introducing subtractions, one reduces the importance of the contribution from the high energy region of the integral. Note that, by doing this, the information from this region of the integral becomes encoded in the subtraction constants instead. Thus, there is a clear parallelism between the subtraction constants from dispersion relations and the low-energy constants from EFTs, as they both contain short-distance information [19, 132].

Unitarity imposes additional strong constraints on the form factors. Let us consider the scattering of two incoming and two outgoing particles, and assume that the energy region of interest only allows elastic final-state rescattering, which in turn means that in Eq. (5.11) the

only intermediate state is $|X\rangle = |f\rangle$. Accordingly,

$$\mathrm{Im}\mathcal{M}_{i\to f} = \frac{(2\pi)^4}{2S}\int \frac{d^3q_1 d^3q_2}{2E_1(2\pi)^3 2E_2(2\pi)^3}\delta^4(p_i - q_1 - q_2)\mathcal{M}_{i\to f}\mathcal{M}^*_{f\to f}\,, \tag{5.55}$$

where $S = 2$ is a symmetry factor required to avoid double counting when the final state particles are indistinguishable, $S = 1$ otherwise. Furthermore, $q_1 = (E_1, \mathbf{q}_1)$ and $q_2 = (E_2, \mathbf{q}_2)$ are the on-shell four-momenta of the two intermediate particles, and $p_i = k + k' = (\sqrt{s}, \mathbf{0})$ and $p_f = p + p' = (\sqrt{s}, \mathbf{0})$ are the total initial and final four-momenta in the CM frame, respectively. Next, let us define the angles $\theta = \measuredangle(\mathbf{k}, \mathbf{p})$, $\theta' = \measuredangle(\mathbf{k}, \mathbf{q}_1)$ and $\theta'' = \measuredangle(\mathbf{q}_1, \mathbf{p})$, and integrate over the delta function to find [14]

$$\mathrm{Im}\mathcal{M}_{i\to f}(s,\theta) = \frac{1}{32\pi^2 S}\frac{|\mathbf{q}_1|}{\sqrt{s}}\int d\Omega\, \mathcal{M}_{i\to f}(s,\theta'')\mathcal{M}^*_{f\to f}(s,\theta')\,, \tag{5.56}$$

where $d\Omega \equiv \sin\theta' d\theta' d\phi$ and $|\mathbf{q}_1| = \frac{1}{2}\sqrt{s - s_{\mathrm{th}}}$.

One can now particularise the above discussion to the pion vector form factor, which is defined as

$$\langle \pi^+(p')\pi^-(p)|\, J^{em}_\mu(0)\,|0\rangle = (p' - p)_\mu F^V_\pi(s)\,, \tag{5.57}$$

where

$$J^{em}_\mu = \frac{2}{3}\bar{u}\gamma_\mu u - \frac{1}{3}\bar{d}\gamma_\mu d - \frac{1}{3}\bar{s}\gamma_\mu s \tag{5.58}$$

is the electromagnetic vector current for the light quarks. After performing a partial-wave projection of the integrand,[7] the unitary relation of Eq. (5.56) becomes [14]

$$\mathrm{Im}F^V_\pi(s) = \sigma(s)F^V_\pi(s)[t^{I=1}_{J=1}(s)]^*\theta(s - s_{\mathrm{th}})\,, \tag{5.60}$$

where $\sigma(s) \equiv \sqrt{1 - s_{\mathrm{th}}/s} = \frac{2|\mathbf{q}_1|}{\sqrt{s}}$, $t^{I=1}_{J=1}(s)$ is the $\pi\pi$ P-wave isospin $I = 1$ scattering amplitude and the two-pion threshold is $s_{\mathrm{th}} = 4M_\pi^2$. The unitary relation in Eq. (5.60) can also be applied to the elastic partial-wave amplitude $t^1_1(s)$ rendering

$$\mathrm{Im}t^1_1(s) = \sigma(s)|t^1_1(s)|^2\theta(s - s_{\mathrm{th}})\,. \tag{5.61}$$

After rewriting $t^1_1(s) = |t^1_1(s)|e^{i\delta^1_1}(s)$, one finds

$$|t^1_1(s)| = \frac{\sin\delta^1_1(s)}{\sigma(s)}\,, \tag{5.62}$$

where $\delta^1_1(s)$ is the elastic scattering phase shift. Plugging Eq. (5.62) into the form factor unitary relation of Eq. (5.60) results in

$$\mathrm{Im}F^V_\pi(s) = \sin\delta^1_1(s)e^{-i\delta^1_1(s)}F^V_\pi(s)\theta(s - s_{\mathrm{th}})\,. \tag{5.63}$$

Noting that the form factor can also be expressed as $F^V_\pi(s) = |F^V_\pi(s)|e^{i\phi(s)}$, Eq. (5.63) becomes

$$\mathrm{Im}F^V_\pi(s) = \sin\delta^1_1(s)|F^V_\pi(s)|e^{i[\phi(s) - \delta^1_1(s)]}\theta(s - s_{\mathrm{th}})\,, \tag{5.64}$$

[7] The partial-wave projection of a scattering amplitude can be expressed as [4]

$$\mathcal{M}(s,z) = 16\pi\sum_{L=0}^{\infty} t_L(s)(2L+1)\mathcal{P}_L(z)\,, \tag{5.59}$$

where $\mathcal{P}_L(z)$ is the Legendre polynomial of degree L, with L being the orbital angular momentum, and $t_L(s)$ is the amplitude of the L-th partial wave.

which fixes the phase $\phi(s) = \delta_1^1(s)$ since the left-hand side is real. This result is known as Watson's theorem, which holds only in the elastic region.

Next, since $\ln F_\pi^V(s)$ is an analytic function in the complex plane, one can make use of the once-subtracted dispersion relation from Eq. (5.53) so that

$$\ln F_\pi^V(s) = \ln F_\pi^V(s_0) + \frac{s-s_0}{\pi}\int_{s_\text{th}}^\infty ds' \frac{\text{Im}\ln F_\pi^V(s')}{(s'-s_0)(s'-s-i\varepsilon)}\,. \tag{5.65}$$

Using Watson's theorem, the form factor can be expressed as $F_\pi^V(s) = |F_\pi^V(s)|e^{i\delta_1^1(s)}$, which in turn allows writing [cf. Eq. (5.48)]

$$\text{Im}\ln F_\pi^V(s) = \frac{\ln F_\pi^V(s) - \ln F_\pi^V(s)^*}{2i} = \delta_1^1(s)\,. \tag{5.66}$$

This can be plugged into Eq. (5.65) to give

$$\ln F_\pi^V(s) = \ln F_\pi^V(s_0) + \frac{s-s_0}{\pi}\int_{s_\text{th}}^\infty ds' \frac{\delta_1^1(s')}{(s'-s_0)(s'-s-i\varepsilon)}\,. \tag{5.67}$$

Exponentiating both sides leads to the following solution[8] to the unitary relation from Eq. (5.60)

$$F_\pi^V(s) = F_\pi^V(s_0)\exp\left\{\frac{s-s_0}{\pi}\int_{s_\text{th}}^\infty ds' \frac{\delta_1^1(s')}{(s'-s_0)(s'-s-i\varepsilon)}\right\} = F_\pi^V(s_0)\Omega_1^1(s)\,, \tag{5.68}$$

where $\Omega_1^1(s)$ is the so-called Omnès function [133]

$$\Omega_1^1(s) = \exp\left\{\frac{s-s_0}{\pi}\int_{s_\text{th}}^\infty ds' \frac{\delta_1^1(s')}{(s'-s_0)(s'-s-i\varepsilon)}\right\}. \tag{5.69}$$

Note that by using the Sokhotski–Plemelj theorem,[9] the solution from Eq. (5.68) can be re-expressed as

$$F_\pi^V(s) = F_\pi^V(s_0)\exp\left\{\mathcal{P}\frac{s-s_0}{\pi}\int_{s_\text{th}}^\infty ds' \frac{\delta_1^1(s')}{(s'-s_0)(s'-s)}\right\}e^{i\delta_1^1(s)}\,, \tag{5.71}$$

which enables the easy extraction of the real and imaginary parts, as well as the absolute value, of the form factor.

To conclude, the result from Eq. (5.68) can be generalised to n subtractions [132]

$$F_\pi^V(s) = Q_n(s)\exp\left\{\frac{(s-s_0)^n}{\pi}\int_{s_\text{th}}^\infty ds' \frac{\delta_1^1(s')}{(s'-s_0)^n(s'-s-i\varepsilon)}\right\}, \tag{5.72}$$

where

$$Q_n(s) = \exp\left\{\sum_{k=0}^{n-1}\frac{1}{k!}\frac{d^k \ln F_\pi^V(s)}{ds^k}\bigg|_{s=s_0}(s-s_0)^k\right\}. \tag{5.73}$$

[8] It is worth noting that, since $\delta_1^1(s)$ asymptotically approaches a constant value at large s, one subtraction point suffices for good convergence.

[9] This theorem states that, under the integral sign, the following relationship holds

$$\lim_{\varepsilon\to 0^+}\frac{1}{x'-x-i\varepsilon} = \mathcal{P}\frac{1}{x'-x} + i\pi\delta(x'-x)\,, \tag{5.70}$$

where $\mathcal{P}$ denotes the Cauchy principal value and δ stands for the Dirac delta function.

Chapter 6

CP violation in the Standard Model

CP violation plays a crucial role in our current understanding of particle physics as well as the evolution of the early Universe. In order to explain the observed dominance of matter over antimatter in the Universe, the so-called baryon asymmetry, CP violation is required. However, the only place where CP violating effects can be accommodated within the SM is in the weak interactions of quarks and leptons [134], which is insufficient to generate the observed baryon asymmetry in Universe, suggesting that other sources of CP violation beyond the SM may be at play.

In this chapter we provide a brief introduction to discrete symmetries, to then focus on the quark-mixing matrix and CP violation in the quark sector, which is the dominant source of CP-violating effects in the SM.

6.1 Introduction to discreet symmetries

As it is well known, the invariance of a system under a continuous symmetry transformation leads to a conservation law by Noethers' theorem. In addition to the familiar continuous symmetries, there are discrete symmetries that also play an important role in modern particle physics: parity inversion, charge conjugation and time reversal.

The parity transformation P is a unitary operator that reverses the momentum of a particle without flipping its spin. In other words, it reverses the handedness of space, $\vec{x} \to -\vec{x}$. Mathematically, it can be expressed as [3, 5]

$$P\psi(t,\vec{x})P^{-1} = \gamma^0\psi(t,-\vec{x})\,. \tag{6.1}$$

Under the charge conjugation operation C, particles and antiparticles are interchanged by conjugating all internal quantum numbers. In particular, C is a unitary linear operator that takes a fermion with a given spin orientation into an antifermion with the same spin orientation. In the Dirac representation of the gamma matrices,[1] C can be written as

$$C\psi(x)C^{-1} = i\gamma^2\gamma^0\overline{\psi}^T(x)\,. \tag{6.3}$$

Last but not least, the time reversal transformation T is an antiunitary operator that reverses momentum and flips the spin of a particle. The expression that allows computing the action of T on a fermion field using the same Dirac basis for the γ matrices is

$$T\psi(t,\vec{x})T^{-1} = i\gamma^1\gamma^3\psi(-t,\vec{x})\,. \tag{6.4}$$

[1] The Dirac basis that we employ is given by [5]

$$\gamma^0 = \begin{pmatrix} 1 & 0 \\ 0 & -1 \end{pmatrix}, \quad \gamma^i = \begin{pmatrix} 0 & \sigma^i \\ -\sigma^i & 0 \end{pmatrix}, \quad \gamma^5 = \begin{pmatrix} 0 & -1 \\ -1 & 0 \end{pmatrix}, \tag{6.2}$$

where the σ^i (with $i = 1,2,3$) are the Pauli matrices from Eq. (2.21). These Dirac matrices, of course, obey the anticommutation relations $\{\gamma^\mu,\gamma^\nu\} = 2g^{\mu\nu}$, as it can easily be checked.

TABLE 6.1: Transformation properties of the various fermion bilinears under P, C, T and CPT [3]. Note that the shorthand $(-1)^\mu \equiv 1$ for $\mu = 0$ and $(-1)^\mu \equiv -1$ for $\mu = 1,2,3$ is used.

	$\overline{\psi}\psi$	$i\overline{\psi}\gamma^5\psi$	$\overline{\psi}\gamma^\mu\psi$	$\overline{\psi}\gamma^\mu\gamma^5\psi$	$\overline{\psi}\sigma^{\mu\nu}\psi$	∂_μ
P	$+1$	-1	$(-1)^\mu$	$-(-1)^\mu$	$(-1)^\mu(-1)^\nu$	$(-1)^\mu$
C	$+1$	$+1$	-1	$+1$	-1	$+1$
T	$+1$	-1	$(-1)^\mu$	$(-1)^\mu$	$-(-1)^\mu(-1)^\nu$	$-(-1)^\mu$
CPT	$+1$	$+1$	-1	-1	$+1$	-1

An important result in quantum field theory, known as the CPT theorem, states that one cannot build a locally Lorentz-invariant QFT with a Hermitian Hamiltonian that violates CPT [3] and, at the time of writing this, all observations to date indicate that CPT is indeed a symmetry of Nature [1]. A summary of how the various Dirac field bilinears transform under P, C, T and CPT is given in Table 6.1.

A CP transformation combines the charge conjugation with parity operations, and takes a specially simple form in the Majorana representation of the γ matrices,[2] where the charge conjugation operator is just the complex conjugation of the fermion field. Thus, the CP transformation takes the form [135]

$$\begin{aligned} &\psi(t,\vec{x}) \to \gamma^0\psi^*(t,-\vec{x}) = -\overline{\psi}^T(t,-\vec{x})\,, \\ &\overline{\psi}(t,-\vec{x}) \to \psi^T(t,-\vec{x})\,. \end{aligned} \tag{6.6}$$

From Eq. (6.6) one can see that the CP transformation interchanges ψ and $\overline{\psi}$ with a minus sign to make up for Fermi statistics. In effect, a CP transformation takes, for example, a left-handed electron e^-_L into a right-handed positron e^+_R.

If CP were an exact symmetry of Nature, its laws would be identical for matter and antimatter. The electromagnetic, strong and gravitational interactions respect P and C separately and, therefore, any phenomena mediated by these interactions is also CP-symmetric. The weak interactions, on the other hand, violate separately P and C maximally, though CP is still preserved in most processes mediated by this force. CP is violated in some rare weak-interaction processes such as in neutral K decays, as well as in B and D decays.

Experimentally, one finds that a K_L meson decays more often into $\pi^- e^+ \nu_e$ than into $\pi^+ e^- \overline{\nu}_e$, which allows electrons and positrons to be unambiguously distinguished, although the asymmetry is very small, at the 0.003 level only. CP-violating effects within the B system are significantly larger, with the asymmetry associated to the $B_0/\overline{B}^0$ decaying into CP eigenstates such as $J/\psi\, K_S$ being at the 0.7 level. The above observations arise from mixing effects in the K^0-$\overline{K}^0$ and B^0-$\overline{B}^0$ sectors, but CP violation has also been detected originating directly from decay amplitudes in $K \to \pi\pi$, subsequently in B^0, B^+ and B^0_s decays, and most recently in charm decays (see Ref. [1] for an in-depth review of the experimental status of CP violation in meson decays). Similar CP-violating effects are also expected in baryon decays, although they have not yet been observed. Contrary to this, should any CP violation be detected in processes involving the top quark or in flavour-conserving processes, such as electric dipole moments, or in the lepton sector would be a clear indication of BSM physics.

[2] A Majorana representation is one in which the γ matrices are imaginary. For example, one can take

$$\gamma^0 = \begin{pmatrix} 0 & \sigma_2 \\ \sigma_2 & 0 \end{pmatrix}, \quad \gamma^1 = \begin{pmatrix} i\sigma_3 & 0 \\ 0 & i\sigma_3 \end{pmatrix}, \quad \gamma^2 = \begin{pmatrix} 0 & -\sigma_2 \\ \sigma_2 & 0 \end{pmatrix}, \quad \gamma^3 = \begin{pmatrix} -i\sigma_1 & 0 \\ 0 & -i\sigma_1 \end{pmatrix}. \tag{6.5}$$

6.2 CKM quark-mixing matrix

The quark masses and mixing arise in the SM from the Yukawa interactions between the quark fields and the Higgs condensate (see Sec. 3.7 for a quick introduction to the SM). Including three generations of quarks, indexed by i and j, the Yukawa terms in the Lagrangian are [1]

$$-\mathcal{L}_{\text{mass}} = Y^d_{ij}\bar{q}^i_L H d^j_R + Y^u_{ij}\bar{q}^i_L \widetilde{H} u^j_R + \text{h.c.}\,, \tag{6.7}$$

where $q^i_L \equiv (u^i_L, d^i_L)^T$ are left-handed quark doublets, and d^i_R and u^i_R are right-handed down- and up-type quark singlets, respectively, in the weak-eigenstate basis.[3] Furthermore, H is the complex scalar $SU(2)$ Higgs-doublet field and $\widetilde{H} \equiv i\sigma_2 H^*$ is its conjugate, which also transforms in the fundamental representation of $SU(2)$. In addition, $\mathcal{L}_{\text{mass}}$ contains two 3×3 (in generation space) Yukawa matrices, i.e. Y^d and Y^u, which need to be diagonalised in order to yield the physical masses of the quarks. The Yukawa matrices, being general complex matrices, consist of many parameters for just a few masses but, in spite of the structure imposed by the gauge interactions, they embody enough redundancy so that most of the complex phases can be rotated away by redefinitions of the fields. It is important to note that each term in Eq. (6.7) is invariant under the set of $SU(3)_C \times SU(2)_L \times U(1)_Y$ gauge transformations [4].

After spontaneous breaking of the electroweak symmetry, H acquires a vacuum expectation value that, without loss of generality, can be expressed as

$$\langle H \rangle = \sqrt{\frac{1}{2}} \begin{pmatrix} 0 \\ v \end{pmatrix}. \tag{6.8}$$

By plugging $\langle H \rangle$ into Eq. (6.7), the quark mass terms in the Lagrangian become

$$\mathcal{L}_{\text{mass}} = -\frac{v}{\sqrt{2}}(Y^d_{ij}\bar{d}^i_L d^j_R + Y^u_{ij}\bar{u}^i_L u^j_R) + \text{h.c.} = -\frac{v}{\sqrt{2}}(\bar{d}_L Y_d d_R + \bar{u}_L Y_u u_R) + \text{h.c.}\,, \tag{6.9}$$

where in the last expression we are employing matrix notation. Next, we diagonalise the Yukawa matrices to extract the physical masses. To that end, we make use of the fact that the matrix $YY^\dagger$ is Hermitian and, thus, has real eigenvalues. Accordingly, one may write [4]

$$Y_d Y_d^\dagger = U_d M_d^2 U_d^\dagger\,, \quad Y_u Y_u^\dagger = U_u M_u^2 U_u^\dagger\,, \tag{6.10}$$

where $M_{d,u}$ are diagonal mass matrices and $U_{d,u}$ are unitary matrices. Therefore, the Yukawa matrices can in general be expressed as

$$Y_d = U_d M_d K_d^\dagger\,, \quad Y_u = U_u M_u K_u^\dagger\,, \tag{6.11}$$

where additional unitary matrices, $K_{d,u}$, have been employed. The Lagrangian, thus, takes the form

$$\mathcal{L}_{\text{mass}} = -\frac{v}{\sqrt{2}}(\bar{d}_L U_d M_d K_d^\dagger d_R + \bar{u}_L U_u M_u K_u^\dagger u_R) + \text{h.c.} \tag{6.12}$$

Note that we are free to change the basis of the right-handed fields using the substitutions $d_R \to K_d d_R$ and $u_R \to K_u u_R$, as well as the left-handed fields using $d_L \to U_d d_L$ and $u_L \to U_u u_L$. These substitutions have the effect of removing the $U_{d,u}$ and $K_{d,u}$ unitary matrices from the Yukawa couplings, leaving just the diagonal $M_{u,d}$ mass matrices. Accordingly, we arrive at

$$\mathcal{L}_{\text{mass}} = -m^d_j \bar{d}^j_L d^j_R - m^u_j \bar{u}^j_L u^j_R + \text{h.c.}\,, \tag{6.13}$$

[3] In this section, as opposed to what was done in Sec. 3.7, we shall keep the L and R subindices to denote left- and right-handed fields to avoid any potential ambiguity.

where m_j^d and m_j^u are the diagonal elements associated to $\frac{v}{\sqrt{2}}M_d$ and $\frac{v}{\sqrt{2}}M_u$, respectively. The basis employed in Eq. (6.13) is known as the mass-eigenstate basis. It must be noted that the Lagrangian still contains a residual $U(1)^6$ global symmetry [4].

Let us now look at how the kinetic terms are affected by the above change of basis. The Lagrangian in the flavour basis can be written as

$$\begin{aligned}
\mathcal{L}_{\text{flavour}-\text{basis}} = \; & \bar{q}_L^i i\left(\not{\partial} - ig\frac{\sigma^a}{2}\not{W}^a - ig'\frac{\mathrm{Y}_L^q}{2}\not{B}\right)q_L^i + \bar{u}_R^i i\left(\not{\partial} - ig'\frac{\mathrm{Y}_R^u}{2}\not{B}\right)u_R^i \\
& + \bar{d}_R^i i\left(\not{\partial} - ig'\frac{\mathrm{Y}_R^d}{2}\not{B}\right)d_R^i - \frac{v}{\sqrt{2}}\left(Y_{ij}^d \bar{d}_L^i d_R^j - Y_{ij}^u \bar{u}_L^i u_R^j + \text{h.c.}\right) \\
= \; & (\bar{u}_L \;\; \bar{d}_L)^i \left[i\not{\partial} + \begin{pmatrix} \frac{g'}{6}\not{B} + \frac{g}{2}\not{W}^3 & \frac{g}{\sqrt{2}}\not{W}^+ \\ \frac{g}{\sqrt{2}}\not{W}^- & \frac{g'}{6}\not{B} - \frac{g}{2}\not{W}^3 \end{pmatrix}\right]\begin{pmatrix} u_L \\ d_L \end{pmatrix}^i \\
& + \bar{u}_R^i\left(i\not{\partial} + g'\frac{2}{3}\not{B}\right)u_R^i + \bar{d}_R^i\left(i\not{\partial} - g'\frac{1}{3}\not{B}\right)d_R^i \\
& - \frac{v}{\sqrt{2}}\left[\bar{d}_L^i\left(U_d M_d K_d^\dagger\right)_{ij} d_R^j + \bar{u}_L^i\left(U_u M_u K_u^\dagger\right)_{ij} u_R^j + \text{h.c.}\right],
\end{aligned} \tag{6.14}$$

where i and j are flavour indices, σ^a are the Pauli matrices, and the weak hypercharges used in the second equality are $\mathrm{Y}_L^q = 1/3$, $\mathrm{Y}_R^u = 4/3$ and $\mathrm{Y}_R^d = -2/3$ (not to be confused with the Yukawa matrices Y_{ij}^d and Y_{ij}^u). From Eq. (6.14) it is straightforward to see that the matrices K_d and K_u drop out once the $d_R \to K_d d_R$ and $u_R \to K_u u_R$ rotations are performed. Similarly, after rotating $d_L \to U_d d_L$ and $u_L \to U_u u_L$, the B_μ and W_μ^3 couplings are not affected, as they do not mix up- and down-type quarks, and the only couplings affected by the flavour rotations are those associated to the $W_\mu^\pm$ gauge bosons. Thus, one obtains [4]

$$\begin{aligned}
\mathcal{L}_{\text{mass}-\text{basis}} = \; & \mathcal{L}_{\text{kin}} + \frac{e}{\sin\theta_w} Z^\mu J_\mu^Z + eA^\mu J_\mu em - m_j^d(\bar{d}_L^j d_R^j + \bar{d}_R^j d_L^j) - m_j^u(\bar{u}_L^j u_R^j + \bar{u}_R^j u_L^j) \\
& + \frac{e}{\sqrt{2}\sin\theta_w}\left[W_\mu^+ \bar{u}_L^i \gamma^\mu (V_{\text{CKM}})_{ij} d_L^j + W_\mu^- \bar{d}_L^i \gamma^\mu (V_{\text{CKM}}^\dagger)_{ij} u_L^j\right],
\end{aligned} \tag{6.15}$$

where the photon and neutral weak gauge boson fields are defined as

$$\begin{aligned}
A_\mu &\equiv \sin\theta_w W_\mu^3 + \cos\theta_w B_\mu \,, \\
Z_\mu &\equiv \cos\theta_w W_\mu^3 - \sin\theta_w B_\mu \,,
\end{aligned} \tag{6.16}$$

J_μ^Z and J_μ^{em} are the neutral and electromagnetic currents, respectively, and θ_w is the Weinberg or weak mixing angle. Moreover, $V_{\text{CKM}} \equiv U_u^\dagger U_d$, known as the Cabibbo-Kobayashi-Maskawa (CKM) matrix, contains all the quark mixing effects and takes the form

$$V_{\text{CKM}} \equiv U_u^\dagger U_d = \begin{pmatrix} V_{ud} & V_{us} & V_{ub} \\ V_{cd} & V_{cs} & V_{cb} \\ V_{td} & V_{ts} & V_{tb} \end{pmatrix}. \tag{6.17}$$

Fundamentally, the V_{CKM} matrix is the unitary transformation that relates the weak down-type eigenstates (primed) with the corresponding physical mass down-type eigenstates (unprimed). That is [see Eqs. (3.190) and (3.191)],

$$\begin{pmatrix} d'_L \\ s'_L \\ b'_L \end{pmatrix} = V_{\text{CKM}} \begin{pmatrix} d_L \\ s_L \\ b_L \end{pmatrix}. \tag{6.18}$$

In general, an $n \times n$ unitary matrix contains n^2 degrees of freedom (i.e. n real numbers for the diagonal elements and two real numbers for each element above the main diagonal). Since a real unitary matrix is an orthogonal matrix and orthogonal matrices have got $\frac{1}{2}n(n-1)$ independent parameters, it follows that, out of the n^2 elements that parameterise the unitary matrix, $\frac{1}{2}n(n-1)$ elements can be represented by real mixing angles. The remaining $\frac{1}{2}n(n+1)$ parameters are complex phases [9]. However, some of these can be absorbed into arbitrary phase rotations of the quark fields. For n generations of quarks, there are $2n$ arbitrary phase rotations available (one for each up- and down-type quark) but, noting that changing all the quark phases by the same amount would have no effect on the mixing matrix, it tuns out that in general $2n-1$ complex phases can be absorbed into the redefinition of the fields, leaving $\frac{1}{2}(n-1)(n-2)$ complex phases that cannot be removed.

As far as we know, there are three generation of quarks in Nature and, thus, $n = 3$ for the CKM matrix. Consequently, it may be parameterised by means of three real mixing angles, θ_{12}, θ_{23} and θ_{13} (which correspond to rotations in the ij-flavour planes [4]), and six phases out of which five can be eliminated by a redefinition of the quark fields, leaving just one phase, δ, that cannot be removed. Accordingly, the most general CKM matrix, using the standard parameterisation, is [1]

$$\begin{aligned} V_{\rm CKM} &= \begin{pmatrix} 1 & 0 & 0 \\ 0 & c_{23} & s_{23} \\ 0 & -s_{23} & c_{23} \end{pmatrix} \begin{pmatrix} c_{13} & 0 & s_{13}e^{i\delta/2} \\ 0 & 1 & 0 \\ -s_{13}e^{i\delta/2} & 0 & c_{13} \end{pmatrix} \begin{pmatrix} c_{13} & 0 & s_{13} \\ 0 & 1 & 0 \\ -s_{13} & 0 & c_{13} \end{pmatrix} \\ &= \begin{pmatrix} c_{12}c_{13} & s_{12}c_{13} & s_{13}e^{-i\delta} \\ -s_{12}c_{23} - c_{12}s_{23}s_{13}e^{i\delta} & c_{12}c_{23} - s_{12}s_{23}s_{13}e^{i\delta} & s_{23}c_{13} \\ s_{12}s_{23} - c_{12}c_{23}s_{13}e^{i\delta} & -c_{12}s_{23} - s_{12}c_{23}s_{13}e^{i\delta} & c_{23}c_{13} \end{pmatrix}, \end{aligned} \tag{6.19}$$

where $c_{ij} = \cos\theta_{ij}$ and $s_{ij} = \sin\theta_{ij}$.[4] It is important to highlight that the phase δ is responsible for all CP-violating effects in quark flavour-changing processes in the SM. Accordingly, unless all the elements of the CKM matrix can be made real, the quark sector of the SM is not invariant under CP and, with the parameterisation from Eq. (6.19), this would require the phase angle $\delta = 0$ [135]. Interestingly, if there were only two generations of quarks in the SM, there would be enough redundancy available in the quark mixing matrix to make all its elements real and the electroweak $SU(2)_L \times U(1)_Y$ interactions would respect the CP symmetry.

The most up-to-date experimental values for the four parameters in Eq. (6.19) are [1]

$$\begin{aligned} &\sin\theta_{12} = 0.22650 \pm 0.00048\,, \quad \sin\theta_{13} = 0.00361^{+0.00011}_{-0.00009}\,, \\ &\sin\theta_{23} = 0.04053^{+0.00083}_{-0.00061}\,, \qquad\qquad \delta = 1.196^{+0.045}_{-0.043}\,. \end{aligned} \tag{6.20}$$

As it can be seen, the mixing angles are small, which means that the mass and flavour basis are reasonably close, and that the CKM matrix is nearly diagonal. As well as this, the mixing angles satisfy the hierarchy $\theta_{13} \ll \theta_{23} \ll \theta_{12} \ll 1$ and, therefore, it makes sense to use a small-angle approximation to the general mixing matrix from Eq. (6.19), which leads to the widely used Wolfestein parameterisation. Identifying $V_{us} \simeq s_{12} = \lambda$, then one can write $V_{cb} \simeq s_{23} = A\lambda^2$ and $V_{ub} = s_{13}e^{-i\delta} = A\lambda^3(\rho - i\eta)$, where $A \simeq 1$ and $|\rho - i\eta| < 1$ [9]. Thus, the CKM matrix can be expressed to $\mathcal{O}(\lambda^3)$ as

$$V_{\rm CKM} = \begin{pmatrix} 1 - \lambda^2/2 & \lambda & A\lambda^3(\rho - i\eta) \\ -\lambda & 1 - \lambda^2/2 & A\lambda^2 \\ A\lambda^3(1 - \rho - i\eta) & -A\lambda^2 & 1 \end{pmatrix} + \mathcal{O}(\lambda^4)\,. \tag{6.21}$$

[4] Note that the three real mixing angles can be chosen to lie in the first quadrant (i.e. $s_{ij}, c_{ij} \geq 0$).

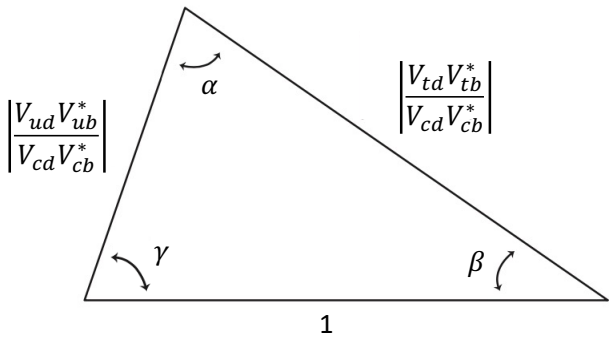

FIGURE 6.1: Graphical representation of CKM elements by means of the unitarity triangle.

The unitarity condition of the CKM matrix implies that its rows, as well as its columns, are orthonormal, i.e. $\sum_i V_{ij}V_{ik}^* = \delta_{jk}$ and $\sum_j V_{ij}V_{kj}^* = \delta_{ik}$. There are six vanishing combinations that can be represented as closed triangles in the complex plane. The most interesting and commonly used unitarity triangle, down to the fact that the V_{td} and V_{ub} elements are poorly determined, comes from the condition

$$V_{ud}V_{ub}^* + V_{cd}V_{cb}^* + V_{td}V_{tb}^* = 0\,. \tag{6.22}$$

After dividing each side by the best measured term, i.e. $V_{cd}V_{cb}^*$, we arrive at

$$\frac{V_{ud}V_{ub}^*}{V_{cd}V_{cb}^*} + \frac{V_{td}V_{tb}^*}{V_{cd}V_{cb}^*} + 1 = 0\,, \tag{6.23}$$

which is graphically represented in Fig. 6.1. The angles of the unitarity triangle can be expressed as [1]

$$\begin{aligned}
\alpha &= \arg\left(-\frac{V_{td}V_{tb}^*}{V_{ud}V_{ub}^*}\right) \simeq \arg\left(-\frac{1-\rho-i\eta}{\rho+i\eta}\right)\,,\\
\beta &= \arg\left(-\frac{V_{cd}V_{cb}^*}{V_{td}V_{tb}^*}\right) \simeq \arg\left(\frac{1}{1-\rho-i\eta}\right)\,,\\
\gamma &= \arg\left(-\frac{V_{ud}V_{ub}^*}{V_{cd}V_{cb}^*}\right) \simeq \arg\left(\rho+i\eta\right)\,,
\end{aligned} \tag{6.24}$$

where η represents the CP-violating phase. It is important to note that the length of the sides of the unitarity triangle quantify the amount of quark-flavour mixing in the SM, whilst its angles are sensitive to CP violation. In fact, the unitarity triangle would collapse to a line if all the elements of $V_{\rm CKM}$ were real [4]. Many measurements of CP-violating observables can be used to constrain these angles (cf. [1] for details).

It is interesting to note that, without loss of generality, one could have assumed that the Yukawa matrices are Hermitian and, thus, they may be written as $Y_d = U_d M_d U_d^\dagger$ and $Y_u = U_u M_u U_u^\dagger$, which is accomplished by rotating $d_R \to K_d U_d^\dagger d_R$ and $u_R \to K_u U_u^\dagger u_R$. Now, if Y_d and Y_u could be simultaneously diagonalised, then $V_{\rm CKM} = \mathbb{1}$ and there would be no CP violation in the SM. Accordingly, CP-violating effects are encoded in the commutator [4]

$$-iC = [Y_u, Y_d] = \left[U_u M_u U_u^\dagger, U_d M_d U_d^\dagger\right] = U_u\left[M_u, V_{\rm CKM} M_d V_{\rm CKM}^\dagger\right] U_u^\dagger\,, \tag{6.25}$$

where the matrix C is traceless and Hermitian due to both Y_u and Y_d being Hermitian. One can use its determinant as a basis-independent quantity

$$\det C = -\frac{16}{v^6}(m_t - m_c)(m_t - m_u)(m_c - m_u)(m_b - m_s)(m_b - m_d)(m_s - m_d)J\,, \quad (6.26)$$

where J is known as the Jarlskog invariant and is defined such that

$$\mathrm{Im}\left[(V_{\mathrm{CKM}})_{ij}\,(V_{\mathrm{CKM}})_{kl}\,(V_{\mathrm{CKM}})^*_{il}\,(V_{\mathrm{CKM}})^*_{kj}\right] = J\sum_{m,n}\epsilon_{ikm}\epsilon_{jln}\,, \quad (6.27)$$

with ϵ_{ijk} being the Levi-Civita symbol. In terms of the standard parameterisation from Eq. (6.19), the Jarlskog invariant can be expressed as

$$J = s_{12}s_{23}s_{31}c_{12}c_{23}c^2_{31}\sin\delta\,. \quad (6.28)$$

As it turns out, the Jarlskog invariant has a geometrical interpretation whereby it is equal to twice the area of the unitarity triangle and, thus, the condition for the reality of the CKM matrix is contained in the requirement $J = 0$. On that account, CP-violating effects in the SM are proportional to J (or, equivalently, they are proportional to $\mathrm{Im}\det[Y_u, Y_d]$), and their presence is subject to the conditions $\theta_{ij} \neq 0$ and $\delta \neq 0$, as it can be seen from Eq. (6.28).

It should be noted that the origin of CP violation in the quark sector through the CKM mechanism is the dominant source of CP-violating effects in the SM. However, despite the large range of phenomenological successes, this mechanism fails to accommodate the cosmologically[5] observed baryon asymmetry by several orders of magnitude [1]. The evidence for neutrino masses points towards the possibility of an additional source of CP violation in the lepton sector through the complex phase of the Pontecorvo–Maki–Nakagawa–Sakata (PMNS) matrix but CP violation in the neutrino sector has yet to be experimentally observed.

Before concluding, it is important to highlight that neutral mesons that do not carry flavour quantum numbers, such as the η and η' states, are their own antiparticles and have definite CP eigenvalues. In particular, the decays of these states are mediated by the electromagnetic and strong[6] forces, which in principle respect the CP symmetry.[7] Accordingly, an observation of CP-violating effects in these processes would be an unequivocal signature of physics beyond the SM.

[5] Of course, this refers to baryogenesis, which is the proposed process through which the matter-antimatter asymmetry of the Universe was dynamically generated. It requires CP violation as a necessary condition, as well as C and baryon-number violations, and interactions out of equilibrium, all collectively known as the Sakharov conditions [136].

[6] Note that, in this instance, the processes mediated by the strong interactions are OZI-suppressed.

[7] The signature of CP violation in these decays is the presence of particles with opposite CP in the final state.

Part II

CONTRIBUTION TO KNOWLEDGE

Chapter 7

π^0-η-η' mixing from $V \to P\gamma$ and $P \to V\gamma$ decays[1]

An enhanced phenomenological model that includes isospin-symmetry breaking is presented in this chapter. This model is then used in a number of statistical fits to the most recent experimental data for the radiative transitions $VP\gamma$ ($V = \rho$, K^*, ω, ϕ and $P = \pi$, K, η, η') and estimations for the mixing angles amongst the three neutral pseudoscalar states with vanishing third-component of isospin are obtained. The quality of the performed fits is good, e.g. $\chi^2_{\text{min}}/\text{d.o.f} = 1.9$. The current experimental uncertainties allow for isospin-symmetry violations with a confidence level of approximately 2.5σ.

7.1 Introduction

The $SU(3)$-flavour symmetry is broken by the strange quark being significantly heavier than the up and down quarks [116, 122, 138]. As a result of this, the physical states η and η' become a mixture of the pure octet $|\eta_8\rangle$ and singlet $|\eta_1\rangle$ mathematical states. Through an orthogonal transformation with mixing angle θ_P (see Appendix A), the mass eigenstates $|\eta\rangle$ and $|\eta'\rangle$ can be expressed as a linear combination of $|\eta_8\rangle$ and $|\eta_1\rangle$ [116, 138],

$$\begin{aligned} |\eta\rangle &= \cos\theta_P\,|\eta_8\rangle - \sin\theta_P\,|\eta_1\rangle\,, \\ |\eta'\rangle &= \sin\theta_P\,|\eta_8\rangle + \cos\theta_P\,|\eta_1\rangle\,, \end{aligned} \tag{7.1}$$

with $|\eta_8\rangle = \frac{1}{\sqrt{6}}\,|u\bar{u}+d\bar{d}-2s\bar{s}\rangle$ and $|\eta_1\rangle = \frac{1}{\sqrt{3}}\,|u\bar{u}+d\bar{d}+s\bar{s}\rangle$. Another commonly used basis for the description of the η-η' mixing is the quark-flavour basis, which becomes exact in the limit $m_s \to \infty$ [139],

$$\begin{aligned} |\eta\rangle &= \cos\phi_P\,|\eta_{\text{NS}}\rangle - \sin\phi_P\,|\eta_{\text{S}}\rangle\,, \\ |\eta'\rangle &= \sin\phi_P\,|\eta_{\text{NS}}\rangle + \cos\phi_P\,|\eta_{\text{S}}\rangle\,, \end{aligned} \tag{7.2}$$

where $|\eta_{\text{NS}}\rangle = \frac{1}{\sqrt{2}}\,|u\bar{u}+d\bar{d}\rangle$ and $|\eta_{\text{S}}\rangle = |s\bar{s}\rangle$. The mixing angles θ_P and ϕ_P are related by $\theta_P = \phi_P - \arctan\sqrt{2} \simeq \phi_P - 54.7^\circ$.

The mixing of the η and η' mesons is heavily influenced by the $U(1)_A$ anomaly of QCD [120], which induces a significant amount of mixing in the η-η' sector [122]. The $U(1)_A$ anomaly forces the $|\eta\rangle$ and $|\eta'\rangle$ mass eigenstates, which one would naively expect to be almost *ideally mixed*, to be nearly flavour octet and singlet states. In addition, the $U(1)_A$ anomaly is responsible for the non-Goldstone nature of the singlet state, forcing it to be massive even in the chiral limit. As a result of the mixing, the $U(1)_A$ anomaly is transferred to both the η and η' mesons [116].

In the vector meson sector, where the spins of the quark-antiquark bound states are parallel, the mixing between the ω and ϕ mesons is usually described using the quark-flavour basis, as there is no anomaly affecting this sector [122, 140]. Accordingly, the mixing angle ϕ_V is small (about 3° to 4°), which is consistent with the OZI-rule and becomes rigorous in the limit $N_C \to \infty$ [122].

[1] This chapter is based on Ref. [137].

Early phenomenological studies on the η-η' mixing used experimental data to perform statistical fits in terms of the mixing angles. One significant contribution was made by Gilman et al. in the late 1980s [141], which provided an estimation of $\theta_P \simeq -20^\circ$ after a complete review of the empirical data available at the time. Subsequently, Bramon et al. [138, 142] introduced in their phenomenological model corrections due to non-ideal mixing in the vector meson nonet and obtained a somewhat less negative mixing angle, i.e. $\theta_P = (-16.9 \pm 1.7)^\circ$ and $\theta_P = (-15.5 \pm 1.3)^\circ$, respectively, where the former was deduced from the rich set of J/ψ decays into a vector and a pseudoscalar meson, whilst the latter came from a thorough analysis of many different decay channels. In Ref. [138], the flavour $SU(3)$-breaking corrections were introduced in terms of constituent quark mass differences, whilst mixing with other pseudoscalar states like glueballs was neglected. Benayoun et al. proposed in Ref. [143] an approach based on a hidden local symmetry model, supplemented with nonet symmetry breaking in the pseudoscalar sector. This approach achieved good agreement with experimental data, with exception of the $K^{*\pm}$ radiative decays, and found a pseudoscalar mixing angle $\theta_P \simeq -11^\circ$, which is consistent with the quadratic Gell-Mann-Okubo mass formula but in conflict with χPT. A value of $\phi_V \simeq 3^\circ$ was found in the vector meson sector.

In 2001, Bramon et al. [140] introduced an additional source of flavour $SU(3)$-symmetry breaking by including a quantum mechanical extension for the $VP\gamma$ radiative decays. The phenomenological model assumed isospin symmetry and the expectation that, even though gluon annihilation channels induce η-η' mixing, they play a negligible role in $VP\gamma$ transitions respecting, therefore, the OZI-rule [140]. The $VP\gamma$ decay couplings were expressed in terms of the mixing angles and relative spatial wavefunction overlaps; then, using experimental estimations for the decay couplings, the best fit values for the free parameters of the model were obtained. The quality of their fits was very good (e.g. $\chi^2_{\text{min}}/\text{d.o.f.} = 0.7$) and the estimations for the mixing angles were found to be $\phi_P = (37.7 \pm 2.4)^\circ$ and $\phi_V = (3.4 \pm 0.2)^\circ$ using the experimental data available at the time. An important conclusion that was drawn is that the $SU(3)$-breaking effects originated from flavour dependence through the relative spatial wavefunction overlaps cannot be neglected.

Ball et al. presented in Ref. [144] (see also Ref. [145]) a different approach by assuming that the meson decay constants follow the pattern of particle state mixing, connecting the short-distance properties of mesons, i.e. decay constants, with long-distance phenomena, i.e. mass eigenstates mixing [139]. In particular, the $VP\gamma$ radiative decays were directly linked to the anomaly of the AVV triangle diagram and the $SU(3)$-breaking effects were introduced by means of leptonic decay constants. A fit using experimental data for several $VP\gamma$ decay channels enabled an estimation for θ_P between -20° and -17°. This strategy and subsequent enhancements introduced by others have been ubiquitous in the literature (e.g. [120, 122, 139, 146–149]). In this context, phenomenological studies have confirmed that a two mixing angle scheme is required to properly describe the experimental data in the octet-singlet basis [120, 121, 150–152], whilst a single mixing angle suffices to achieve good agreement in the quark-flavour basis [120, 121, 150, 153–155], which is supported by large-N_C χPT [57, 119] at next-to-leading order. This appears to indicate that the difference between the two mixing angles in the octet-singlet basis is produced by an $SU(3)$-breaking effect, whereas in the quark-flavour basis the difference comes from an OZI-rule violating effect [120, 122]. In addition, at lowest order in χPT, one only requires a single mixing angle, which endorses Eqs. (7.1) and (7.2).

Using this approach, Feldmann et al. [121] provided theoretical (to first order in flavour symmetry breaking) and phenomenological estimations for θ_P of -12.3° (no error provided) and $(-15.4 \pm 1.0)^\circ$, respectively. Likewise, Escribano et al. [120] found phenomenological values for $\theta_P = (-14.3 \pm 1.0)^\circ$ and $\phi_V = (4.1 \pm 2.2)^\circ$ using one mixing angle in the quark-flavour basis. As well as this, Kroll obtained in Ref. [156] values for θ_P of $(-13.2 \pm 2.2)^\circ$ and $(-13.5 \pm 1.1)^\circ$, employing two different sources of empirical data available at the time,

i.e. the PDG 2004 and KLOE Collaboration, respectively.

The gluonic content of the η and η' wavefunctions was analysed using empirical data from $VP\gamma$ decays in Refs. [157, 158] and the model that was employed followed Ref. [140]. It was found that the gluonic content for the η and η' wavefunctions is consistent with zero, using the most up-to-date data at the time. Furthermore, it was once again emphasised the importance of the secondary source of flavour $SU(3)$-symmetry breaking to achieve good agreement with experimental data.

Feldmann et al. discussed in Ref. [153] the effects of isospin-symmetry breaking, which is induced by the mass difference between the u and d quarks, as well as QED effects, using the theoretical framework first presented in Ref. [159]. Mathematically, they expressed the admixtures of the η and η' to the physical π^0 as [153]

$$|\pi^0\rangle = |\pi_3\rangle + \epsilon\,|\eta\rangle + \epsilon'\,|\eta'\rangle\,, \tag{7.3}$$

where $|\pi_3\rangle$ denotes the $I_3 = 0$ state of the pseudoscalar isospin triplet. By assuming a mixing angle of $\phi = 39.3^\circ$ for the η-η' system, they found through the diagonalisation of the associated mass matrix that the mixing between the π^0 and η mesons was $\epsilon = 1.4\%$, whilst the π^0-η' mixing was $\epsilon' = 0.37\%$ (no errors associated to these theoretical estimations were provided).

Kroll, as a continuation of the previous work, highlighted in Ref. [156] that isospin-symmetry breaking is of order $(m_d - m_u)/m_s$ due to the effect of the $U(1)_A$ anomaly, which is embodied in the divergence of the singlet axial-vector current [42, 160]. As a result of the mixing, the $U(1)_A$ anomaly is transferred to the π^0, η and η' physical states. A simple generalisation of the quark-flavour mixing scheme (e.g. [122, 148, 153]) allowed him to write the following theoretical expressions for the mixing parameters ϵ and ϵ' [156],

$$\begin{aligned} \epsilon(z) &= \cos\phi \left[\frac{1}{2} \frac{m_{dd}^2 - m_{uu}^2}{m_\eta^2 - m_{\pi^0}^2} + z \right], \\ \epsilon'(z) &= \sin\phi \left[\frac{1}{2} \frac{m_{dd}^2 - m_{uu}^2}{m_{\eta'}^2 - m_{\pi^0}^2} + z \right], \end{aligned} \tag{7.4}$$

where the parameter z is the quotient of decay constants $z = (f_u - f_d)/(f_u + f_d)$ and the quark mass difference $m_{dd}^2 - m_{uu}^2$ was estimated from the K^0-K^+ mass difference. Assuming again a mixing angle in the η-η' sector of $\phi = 39.3^\circ$ and making use of the $f_u = f_d$ limit, he found the following numerical estimations for the mixing parameters ϵ and ϵ',

$$\begin{aligned} \hat{\epsilon} &= \epsilon(z=0) = (1.7 \pm 0.2)\%\,, \\ \hat{\epsilon}' &= \epsilon'(z=0) = (0.4 \pm 0.1)\%\,. \end{aligned} \tag{7.5}$$

Escribano et al. analysed in Ref. [161] the second-class current decays $\tau^- \to \pi^- \eta^{(\prime)} \nu_\eta$ and found estimations for the π^0-η and π^0-η' mixing parameters from theory, making use of scalar and vector form factors at next-to-leading order in χPT. The analytic expressions that they found are consistent with those from Kroll shown in Eq. (7.4) up to higher-order isospin corrections. The numerical estimations that they obtained are

$$\begin{aligned} \epsilon_{\pi\eta} &= c\phi_{\eta\eta'} \frac{m_{K^0}^2 - m_{K^+}^2 - m_{\pi^0}^2 + m_{\pi^+}^2}{m_\eta^2 - m_{\pi^-}^2} \left[1 - \frac{m_\eta^2 - m_{\pi^-}^2}{M_S^2} \right] = (9.8 \pm 0.3) \times 10^{-3}\,, \\ \epsilon_{\pi\eta'} &= s\phi_{\eta\eta'} \frac{m_{K^0}^2 - m_{K^+}^2 - m_{\pi^0}^2 + m_{\pi^+}^2}{m_{\eta'}^2 - m_{\pi^-}^2} \left[1 - \frac{m_{\eta'}^2 - m_{\pi^-}^2}{M_S^2} \right] = (2.5 \pm 1.5) \times 10^{-4}\,, \end{aligned} \tag{7.6}$$

TABLE 7.1: Comparison between estimations for the seven free parameters from the model presented in Ref. [140], using the PDG 2000 and the most up-to-date experimental data.

Parameter	Estimation from [140]	Current Estimation
g	0.70 ± 0.02 GeV^{-1}	0.70 ± 0.01 GeV^{-1}
$\frac{m_s}{\overline{m}}$	1.24 ± 0.07	1.17 ± 0.06
ϕ_P	$(37.7 \pm 2.4)^\circ$	$(41.4 \pm 0.5)^\circ$
ϕ_V	$(3.4 \pm 0.2)^\circ$	$(3.3 \pm 0.1)^\circ$
$z_{\rm NS}$	0.91 ± 0.05	0.84 ± 0.02
$z_{\rm S}$	0.89 ± 0.07	0.76 ± 0.04
z_K	0.91 ± 0.04	0.89 ± 0.03
$\chi^2_{\rm min}$/d.o.f.	0.7	4.6

where $c\phi_{\eta\eta'}$ and $s\phi_{\eta\eta'}$ stand for $\cos\phi_{\eta\eta'}$ and $\sin\phi_{\eta\eta'}$, respectively; also, an η-η' mixing angle of $\phi_{\eta\eta'} = (41.4 \pm 0.5)^\circ$ was assumed, together with a scalar mass of $M_S = 980$ MeV.

It must be noted that Kroll's mixing parameters ϵ and ϵ' in Ref. [156] [cf. Eq. (7.3)] were defined in the quark-flavour basis whilst Escribano et al.'s $\epsilon_{\pi\eta}$ and $\epsilon_{\pi\eta'}$ in Ref. [161] were defined in the octet-singlet basis. Despite this difference, it can be easily shown that, since both authors used the same $SO(3)$ rotation matrix *structure*, one can write $\epsilon = \epsilon_{\pi\eta}$ and $\epsilon' = \epsilon_{\pi\eta'}$, which are valid as first order approximations.

7.2 Methodology

From the effective Lagrangian that is commonly used to describe $VP\gamma$ radiative decays, a set of expressions for the theoretical decay couplings is found in terms of the free parameters of the model. Next, using experimental data from Ref. [1], the corresponding experimental decay couplings are calculated and, finally, an optimisation fit is performed.

In the framework of the conventional quark model, the flavour symmetry-breaking mechanism associated to differences in the effective magnetic moments of light and strange quarks in magnetic dipolar transitions is introduced via constituent quark mass differences. This is implemented by means of a multiplicative $SU(3)$-breaking term, i.e. $1 - s_e \equiv \overline{m}/m_s$, in the s-quark entry of the quark-charge matrix Q [138]. A second source of flavour symmetry breaking, connected to the differences in the spatial extensions of the meson state wavefunctions, is also considered [140]. This symmetry-breaking mechanism is introduced through additional multiplicative factors in the theoretical coupling constants, accounting for the corresponding relative wavefunction overlaps, and are left as free parameters in the fit.

The isospin violation in the pseudoscalar sector is investigated in this framework. The mixing in this case requires an $SO(3)$ rotation matrix relating the π^0, η and η' mass eigenstates to the $SU(3)$ mathematical states, with three mixing angles. Additional wavefunction overlap factors are introduced to the model and gluon annihilation channels, which might contribute to the mixing, are neglected.[2]

7.3 The mixing of the η-η' revisited

The analysis carried out in Ref. [140] for the estimation of the mixing angle in the η-η' sector is reproduced in this section using the most up-to-date experimental data [1]. The theoretical

[2]This is a necessary simplification to reduce the number of free parameters in the model; otherwise, the statistical fit would not be possible given the limited number of available decay channels.

$VP\gamma$ decay couplings are confirmed to be those presented in Ref. [140]. The relationship between the decay couplings and the decay widths is given by

$$\Gamma(V \to P\gamma) = \frac{1}{3}\frac{g_{VP\gamma}^2}{4\pi}|\mathbf{p}_\gamma|^3 = \frac{1}{3}\Gamma(P \to V\gamma)\,, \tag{7.7}$$

where $\mathbf{p}_\gamma$ is the linear momentum of the outgoing photon. Using Eq. (7.7) together with the experimental data for the total decay widths, branching ratios and meson masses from Ref. [1], one can obtain experimental values for the decay couplings. From these and the corresponding theoretical counterparts, an optimisation fit can be performed. Making use of a standard minimisation software package, the optimal values for the seven free parameters of the model are presented in Table 7.1. One can see that the fitted values obtained in this chapter are in good agreement with those found by Bramon et al. in Ref. [140]. The current associated standard errors are smaller, which is due to the fact that the uncertainties associated to the experimental measurements have decreased over the years. The most recent empirical data seems to favour a somewhat bigger η-η' mixing angle ϕ_P, which is consistent with other recent results (e.g. Refs. [154, 162–164]). As well as this, the most up-to-date experimental data grants more relevance to the secondary source of flavour $SU(3)$-symmetry breaking, as the z_{NS} and z_{S} spatial wavefunction overlap factors are further from unity.

That being said, the quality of the fit for the current estimations is poor with a $\chi^2_{\text{min}}/\text{d.o.f.} \simeq 23.1/5 \simeq 4.6$, while in Ref. [140], using the data available at the time, the quality of the fit was excellent, i.e. $\chi^2_{\text{min}}/\text{d.o.f.} = 0.7$. This, again, is connected to the improved quality of the most recent data [1]. Based on this goodness-of-fit test, one ought to come to the conclusion that the current experimental data no longer supports the model presented in Ref. [140].

7.4 Enhanced model for the π^0-η-η' mixing

The phenomenological model presented above is enhanced in this section by incorporating isospin-breaking effects, enabling the investigation of the mixing phenomena between the π^0, η and η' pseudoscalar mesons. This improved model considers that the physical pseudoscalar mesons with vanishing third-component of isospin are an admixture of some pure mathematical states and the mixing is, thus, implemented by a three-dimensional rotation amongst them. In addition, the mechanisms of flavour $SU(3)$-symmetry breaking that have been discussed in Sec. 7.2 are enhanced to account for violations of isospin. In the vector meson sector, a single mixing angle is still considered, as this sector is anomaly-free.

In order to find the theoretical decay couplings associated to the different $VP\gamma$ radiative transitions, one starts with the effective Lagrangian that is usually used to calculate amplitudes in $V \to P\gamma$ and $P \to V\gamma$ decay processes [138],

$$\mathcal{L}_{VP\gamma} = g_e \epsilon_{\mu\nu\alpha\beta}\partial^\mu A^\nu \text{Tr}[Q(\partial^\alpha V^\beta P + P\partial^\alpha V^\beta)]\,, \tag{7.8}$$

where g_e is a generic electromagnetic coupling constant, $\epsilon_{\mu\nu\alpha\beta}$ is the totally antisymmetric tensor, A_μ is the electromagnetic field, V_μ and P are, respectively, the matrices for the vector and pseudoscalar meson fields, and Q is the quark-charge matrix in Eq. (3.25), i.e. $Q = \text{diag}\{2/3, -1/3, -1/3\}$.

Next, the following $SO(3)$ rotation matrix correlating the pseudoscalar $I_3 = 0$ physical states with the pure quark-flavour basis states is selected

$$\begin{pmatrix} \pi^0 \\ \eta \\ \eta' \end{pmatrix} = \begin{pmatrix} 1 & \epsilon_{12} & \epsilon_{13} \\ -\epsilon_{12}c\phi_{23} + \epsilon_{13}s\phi_{23} & c\phi_{23} & -s\phi_{23} \\ -\epsilon_{13}c\phi_{23} - \epsilon_{12}s\phi_{23} & s\phi_{23} & c\phi_{23} \end{pmatrix} \begin{pmatrix} \pi_3 \\ \eta_{\text{NS}} \\ \eta_{\text{S}} \end{pmatrix}, \tag{7.9}$$

where ϵ_{12} and ϵ_{13} are first order approximations to the corresponding ϕ_{12} and ϕ_{13} mixing angles, as isospin-breaking corrections are small [159]. It must be stressed that the particular *structure* that we have selected for the $SO(3)$ rotation matrix is down to the fact that it enables an enhanced *resolution* against the statistical uncertainties associated to both mixing parameters ϵ_{12} and ϵ_{13} simultaneously, once the optimisation fits are performed.[3]

The transformations that map Kroll's ϵ and ϵ' in the quark-flavour basis (cf. Eq. (7.3) and Ref. [156]) and Escribano et al.'s $\epsilon_{\pi\eta}$ and $\epsilon_{\pi\eta'}$ in the octet-singlet basis (cf. Ref. [161]) to the ϵ_{12} and ϵ_{13} in the quark-flavour basis used in this chapter [cf. Eq. (7.9)] are[4]

$$\begin{pmatrix}\epsilon_{12}\\ \epsilon_{13}\end{pmatrix} = \begin{pmatrix} c\phi_P & s\phi_P \\ -s\phi_P & c\phi_P\end{pmatrix}\begin{pmatrix}\epsilon\\ \epsilon'\end{pmatrix}, \tag{7.10}$$

and

$$\begin{pmatrix}\epsilon_{12}\\ \epsilon_{13}\end{pmatrix} = \frac{1}{\sqrt{3}}\begin{pmatrix} c\theta_P-\sqrt{2}\,s\theta_P & s\theta_P+\sqrt{2}\,c\theta_P \\ -s\theta_P-\sqrt{2}\,c\theta_P & c\theta_P-\sqrt{2}\,s\theta_P\end{pmatrix}\begin{pmatrix}\epsilon_{\pi\eta}\\ \epsilon_{\pi\eta'}\end{pmatrix}. \tag{7.11}$$

At this point, one can obtain the expressions for the theoretical decay couplings of the enhanced phenomenological model. These are

$$\begin{aligned}
g_{\rho^0\pi^0\gamma} &= g\Big(\frac{1}{3}+\epsilon_{12}z_{\rm NS}\Big), \quad g_{\rho^+\pi^+\gamma} = g\frac{z_+}{3},\\
g_{\rho^0\eta\gamma} &= g\Big[\Big(z_{\rm NS}-\frac{\epsilon_{12}}{3}\Big)c\phi_{23}+\frac{\epsilon_{13}}{3}s\phi_{23}\Big],\\
g_{\omega\pi^0\gamma} &= g\Big[\Big(1+\frac{\epsilon_{12}}{3}z_{\rm NS}\Big)c\phi_V+\frac{2}{3}z_{\rm S}\frac{\overline{m}}{m_s}\epsilon_{13}s\phi_V\Big],\\
g_{\eta'\rho^0\gamma} &= g\Big[\Big(z_{\rm NS}-\frac{\epsilon_{12}}{3}\Big)s\phi_{23}-\frac{\epsilon_{13}}{3}c\phi_{23}\Big],\\
g_{\omega\eta\gamma} &= g\left\{\Big[\Big(\frac{z_{\rm NS}}{3}-\epsilon_{12}\Big)c\phi_{23}+\epsilon_{13}s\phi_{23}\Big]c\phi_V-\frac{2}{3}z_{\rm S}\frac{\overline{m}}{m_s}s\phi_{23}s\phi_V\right\},\\
g_{\eta'\omega\gamma} &= g\left\{\Big[\Big(\frac{z_{\rm NS}}{3}-\epsilon_{12}\Big)s\phi_{23}-\epsilon_{13}c\phi_{23}\Big]c\phi_V+\frac{2}{3}z_{\rm S}\frac{\overline{m}}{m_s}c\phi_{23}s\phi_V\right\},\\
g_{\phi\pi^0\gamma} &= g\Big[\Big(1+\frac{\epsilon_{12}}{3}z_{\rm NS}\Big)s\phi_V-\frac{2}{3}z_{\rm S}\frac{\overline{m}}{m_s}\epsilon_{13}c\phi_V\Big],\\
g_{\phi\eta\gamma} &= g\left\{\Big[\Big(\frac{z_{\rm NS}}{3}-\epsilon_{12}\Big)c\phi_{23}+\epsilon_{13}s\phi_{23}\Big]s\phi_V+\frac{2}{3}z_{\rm S}\frac{\overline{m}}{m_s}s\phi_{23}c\phi_V\right\},\\
g_{\phi\eta'\gamma} &= g\left\{\Big[\Big(\frac{z_{\rm NS}}{3}-\epsilon_{12}\Big)s\phi_{23}-\epsilon_{13}c\phi_{23}\Big]s\phi_V-\frac{2}{3}z_{\rm S}\frac{\overline{m}}{m_s}c\phi_{23}c\phi_V\right\},\\
g_{K^{*0}K^0\gamma} &= -\frac{1}{3}g\Big(1+\frac{\overline{m}}{m_s}\Big)z_{K^0} = -\frac{1}{3}g\Big(1+z_{\rm S}\frac{\overline{m}}{m_s}\Big)z'_{K^0},\\
g_{K^{*+}K^+\gamma} &= \frac{1}{3}g\Big(2-\frac{\overline{m}}{m_s}\Big)z_{K^+} = \frac{1}{3}g\Big(2-z_{\rm S}\frac{\overline{m}}{m_s}\Big)z'_{K^+},
\end{aligned} \tag{7.12}$$

where the wavefunction overlap parameters have been redefined as relative overlap factors [140]: $z_{\rm NS}\equiv Z_{\rm NS}/Z_3$, $z_{\rm S}\equiv Z_{\rm S}/Z_3$, $z_+\equiv Z_+/Z_3$, $z_{K^0}\equiv Z_{K^0}/Z_3$ and $z_{K^+}\equiv Z_{K^+}/Z_3$. The generic electromagnetic coupling constant g_e in Eq. (7.8) has been replaced by $g=Z_3g_e$ on the right hand side equalities of Eq. (7.12). In some instances, the overlap factors in the strange sector have been redefined to $z'_{K^0}=z_{K^0}(1+\overline{m}/m_s)/(1+z_{\rm S}\overline{m}/m_s)$ and

[3] This point will become clearer later when the results are discussed.

[4] Given that these are orthogonal transformations, to move from one definition to the other in the opposite direction, one only needs to multiply by the transposed matrices.

$z'_{K^+} = z_{K^+}(2-\overline{m}/m_s)/(2-z_{\rm S}\overline{m}/m_s)$ in order to avoid redundant free parameters. It is worth highlighting that Eq. (7.12) reduce to the expressions shown in Ref. [140] in the good $SU(2)$ limit, as expected.

A fit of the theoretical decay couplings from Eq. (7.12) to the experimental data for ten free parameters provides the following estimations

$$\begin{aligned} g &= 0.69 \pm 0.01 \text{ GeV}^{-1}, & z_+ &= 0.95 \pm 0.05, \\ \phi_{23} &= (41.5 \pm 0.5)^\circ, & \phi_V &= (4.0 \pm 0.2)^\circ, \\ \epsilon_{12} &= (2.3 \pm 1.0)\ \%, & \epsilon_{13} &= (2.5 \pm 0.9)\ \%, \\ z_{\rm NS} &= 0.89 \pm 0.03, & z_{\rm S}\overline{m}/m_s &= 0.65 \pm 0.01, \\ z'_{K^0} &= 1.01 \pm 0.04, & z'_{K^+} &= 0.76 \pm 0.04\ . \end{aligned} \tag{7.13}$$

The quality of the fit is relatively good, with $\chi^2_{\rm min}/\text{d.o.f.} \simeq 4.6/2 = 2.3$. The fitted values for the mixing angles ϕ_{23} and ϕ_V are in very good agreement with recent published results (e.g. [120, 157, 163]). The g and $m_s/\overline{m}$ [see Eq. (7.14) below for an estimation of the latter] are also consistent with those from other studies but, as highlighted by Bramon et al. in Ref. [140], these parameters are largely dependent on the particular model used; hence, comparison provides limited value.

An important point to notice from Eq. (7.13) is that the estimations for ϵ_{12} and ϵ_{13} are very small but not compatible with zero with a confidence level of 2.3σ and 2.8σ, respectively, assuming a Gaussian distribution for the error. The ϵ_{12} and ϵ_{13} values from our fit can be translated to Kroll's and Escribano et al.'s definitions for their $SO(3)$ rotation matrix yielding $\epsilon = \epsilon_{\pi\eta} = (0.1 \pm 0.9)\ \%$ and $\epsilon' = \epsilon_{\pi\eta'} = (3.4 \pm 0.9)\ \%$. It can be observed that our mixing parameters ϵ and $\epsilon_{\pi\eta}$ are compatible with zero, whilst our parameters ϵ' and $\epsilon_{\pi\eta'}$ are not consistent with zero with a confidence level of 3.8σ. Clearly, all mathematical representations for the physical states are equivalent; however, the specific rotation matrix selected in Eq. (7.9) enables the simultaneous determination that *both* parameters controlling the mixing in the π^0-η and π^0-η' sectors are incompatible with zero.

In addition, it is worth noting from our results that the contribution to the physical state $|\pi^0\rangle$ from the mathematical state $|\eta_8\rangle$ is significantly smaller (in fact, consistent with zero) than that from the pure singlet state $|\eta_1\rangle$. This is an interesting result as one would naively expect the amount of mixing in the π^0-η system to be larger than the one found in the π^0-η' sector, based on mass arguments. This can be explained, though, by the fact that the $U(1)_A$ anomaly mediates $\eta_1 \leftrightarrow \pi_3$ transitions and, therefore, provides an additional contribution to the associated mixing. Note that Escribano et al. [161] made use of the large-N_C limit in their calculations, which effectively rids the theory of the chiral anomaly; hence, the effect mentioned above does not surface in their estimations for the mixing parameters. On the other hand, Kroll obtained in Ref. [156] first order theoretical results for the mixing parameters, neglecting, thus, any high-order symmetry breaking corrections; this is a sound approximation for the η-η' system but might potentially compromise the results for the π^0-η and π^0-η' sectors where the mixing parameters are very small.

Another fit is carried out fixing $\epsilon_{12} = \epsilon_{13} = 0$ and leaving all the other parameters free. The quality of the fit is significantly decreased with $\chi^2_{\rm min}/\text{d.o.f.} \simeq 21.3/4 \simeq 5.3$, highlighting the fact that a certain amount of mixing between the neutral π^0 with the η and η' mesons different from zero is required to correctly describe the data.

Fixing the parameters $z_+ = 1$ and $z_{K^0} = z_{K^+}$, which accounts for *turning off* the secondary mechanism of isospin-symmetry breaking, and performing a fit with all the other

parameters left free, we find

$$\begin{aligned} g &= 0.69 \pm 0.01 \text{ GeV}^{-1}, \quad m_s/\overline{m} = 1.17 \pm 0.06, \\ \phi_{23} &= (41.5 \pm 0.5)^\circ, \qquad \phi_V = (4.0 \pm 0.2)^\circ, \\ \epsilon_{12} &= (2.4 \pm 1.0)\ \%, \qquad \epsilon_{13} = (2.5 \pm 0.9)\ \%, \\ z_{\text{NS}} &= 0.89 \pm 0.03, \qquad z_{\text{S}} = 0.77 \pm 0.04, \\ z_K &= 0.90 \pm 0.03, \end{aligned} \tag{7.14}$$

where the quality of the fit is better, i.e. $\chi^2_{\text{min}}/\text{d.o.f.} \simeq 5.6/3 \simeq 1.9$. The z's in Eq. (7.14) are different from unity, signalling that the secondary mechanism of flavour $SU(3)$-symmetry breaking is still required for the correct description of the experimental data. This statement can be tested by performing a fit where all the z's are fixed to one and it is found that the quality of the fit is substantially decreased, i.e. $\chi^2_{\text{min}}/\text{d.o.f.} \simeq 41.8/6 \simeq 7.0$.

The estimates for ϵ_{12} and ϵ_{13} in Eq. (7.14) are, again, not compatible with zero with a confidence level of 2.4σ and 2.8σ, respectively. In general, the estimations from Eq. (7.14) are very approximate to the ones shown in Eq. (7.13). It is interesting to see that reducing the number of free parameters in the last fit leads to a sizeable increase in the quality of the fit. This is related to the fact that, despite the residual χ^2_{min} being smaller when ten free parameters are employed, this reduction does not compensate for the loss of one degree of freedom. Accordingly, it appears that the introduction of the secondary mechanism of isospin-symmetry breaking is not required to reproduce the experimental data. For this reason, the degrees of freedom z_+, z_{K^0} and z_{K^+} will be fixed to $z_+ = 1$ and $z_{K^0} = z_{K^+}$ for any subsequent fits.

Two more statistical fits using the estimated values for ϵ_{12} and ϵ_{13} from Kroll [156] and Escribano et al. [161] can be performed. Starting with Kroll's estimations $\epsilon_{12} = (1.6 \pm 0.2)\ \%$ and $\epsilon_{13} = (-0.8 \pm 0.1)\ \%$ we obtain

$$\begin{aligned} g &= 0.69 \pm 0.01 \text{ GeV}^{-1}, \quad m_s/\overline{m} = 1.17 \pm 0.06, \\ \phi_{23} &= (41.4 \pm 0.5)^\circ, \qquad \phi_V = (3.1 \pm 0.1)^\circ, \\ z_{\text{NS}} &= 0.86 \pm 0.0, \qquad z_{\text{S}} = 0.77 \pm 0.04, \\ z_K &= 0.90 \pm 0.03, \end{aligned} \tag{7.15}$$

where the quality of the fit is significantly poorer, i.e. $\chi^2_{\text{min}}/\text{d.o.f.} \simeq 22.0/5 = 4.4$. Likewise, using Escribano et al.'s $\epsilon_{12} = (7.5 \pm 0.2) \times 10^{-3}$ and $\epsilon_{13} = (-6.3 \pm 0.2) \times 10^{-3}$ and performing the fit once more, the following results are found

$$\begin{aligned} g &= 0.70 \pm 0.01 \text{ GeV}^{-1}, \quad m_s/\overline{m} = 1.17 \pm 0.06, \\ \phi_{23} &= (41.4 \pm 0.5)^\circ, \qquad \phi_V = (3.2 \pm 0.1)^\circ, \\ z_{\text{NS}} &= 0.85 \pm 0.02, \qquad z_{\text{S}} = 0.77 \pm 0.04, \\ z_K &= 0.90 \pm 0.03, \end{aligned} \tag{7.16}$$

where the quality of the fit is similar to the previous one, i.e. $\chi^2_{\text{min}}/\text{d.o.f.} \simeq 24.0/5 = 4.8$. This shows that the theoretical estimations for the mixing parameters ϵ_{12} and ϵ_{13} provided by Kroll [156] and Escribano et al. [161] do not appear to agree with the most recent experimental data [1]. It must be stressed, though, that the phenomenological model presented in this chapter is based on the relatively simple standard quark model with a quantum mechanical extension, whilst Refs. [156] and [161] used more sophisticated theoretical approaches. Having said this, those estimations had limited numerical input from experiment due to their intrinsic theoretical nature.

TABLE 7.2: Summary of fitted values for the Fit 1, Fit 2, Fit 3, Fit 4 and Fit 5, corresponding to Eqs. (7.13), (7.14), (7.15), (7.16) and (7.17), respectively.

Parameter	Fit 1	Fit 2	Fit 3	Fit 4	Fit 5
g (GeV^{-1})	0.69 ± 0.01	0.69 ± 0.01	0.69 ± 0.01	0.70 ± 0.01	0.69 ± 0.01
ϵ_{12}	(2.3 ± 1.0) %	(2.4 ± 1.0) %	-	-	(2.4 ± 1.0) %
ϵ_{13}	(2.5 ± 0.9) %	(2.5 ± 0.9) %	-	-	(2.5 ± 0.9) %
ϕ_{23} ($^\circ$)	41.5 ± 0.5	41.5 ± 0.05	41.4 ± 0.5	41.4 ± 0.5	41.5 ± 0.5
ϕ_V ($^\circ$)	4.0 ± 0.2	4.0 ± 0.2	3.1 ± 0.1	3.2 ± 0.1	4.0 ± 0.2
$m_s/\overline{m}$	-	1.17 ± 0.06	1.17 ± 0.06	1.17 ± 0.06	-
$z_{\rm S}\overline{m}/m_s$	0.65 ± 0.01	-	-	-	0.65 ± 0.01
$z_{\rm NS}$	0.89 ± 0.03	0.89 ± 0.03	0.86 ± 0.02	0.85 ± 0.02	0.89 ± 0.03
z_+	0.95 ± 0.05	-	-	-	-
$z_{\rm S}$	-	0.77 ± 0.04	0.77 ± 0.04	0.77 ± 0.04	-
z_K	-	0.90 ± 0.03	0.90 ± 0.03	0.90 ± 0.03	-
z'_{K^0}	1.01 ± 0.04	-	-	-	-
z'_{K^+}	0.76 ± 0.04	-	-	-	-
$\chi^2_{\rm min}$/d.o.f.	2.3	1.9	4.4	4.8	1.9

A final fit is carried out where the experimental points associated to the neutral and charged $K^* \to K\gamma$ transitions are not considered.[5] Accordingly, the free parameters z_K, or z'_{K^0} and z'_{K^+}, are not included in this fit, and the parameters $m_s/\overline{m}$ and $z_{\rm S}$ are considered jointly again. The estimated values from the fit are

$$\begin{aligned} g &= 0.69 \pm 0.01 \text{ GeV}^{-1}, \quad z_{\rm S}\overline{m}/m_s = 0.65 \pm 0.01, \\ \phi_{23} &= (41.5 \pm 0.5)^\circ, \qquad \phi_V = (4.0 \pm 0.2)^\circ, \\ \epsilon_{12} &= (2.4 \pm 1.0)\ \%, \qquad \epsilon_{13} = (2.5 \pm 0.9)\ \%, \\ z_{\rm NS} &= 0.89 \pm 0.03\ . \end{aligned} \tag{7.17}$$

The quality of the fit is good, $\chi^2_{\rm min}/\text{d.o.f.} \simeq 5.6/3 \simeq 1.9$. The estimates for ϵ_{12} and ϵ_{13} are again incompatible with zero at a confidence level of 2.4σ and 2.8σ, respectively.

A summary of all the fitted parameters is shown in Table 7.2. The robustness of the fitted values for the parameters g, ϵ_{12}, ϵ_{13}, ϕ_{23} and ϕ_V across Fits 1, 2 and 5 is remarkable. In addition, the consistency of the z parameters across all the fits is also very good. As well as this, a comparison between the calculated decay widths and the experimental decay widths obtained directly from [1] is presented in Table 7.3. The agreement is very good for the estimated values from $\Gamma_{\rm fit1}$, $\Gamma_{\rm fit2}$ and $\Gamma_{\rm fit5}$. The decay width estimations $\Gamma_{\rm fit3}$ and $\Gamma_{\rm fit4}$ are not as good as the others, implying again that the experimental data seems to favour different values for ϵ_{12} and ϵ_{13} than those suggested by Kroll [156] and Escribano et al. [161].

It is worth highlighting that the biggest contribution to the residual $\chi^2_{\rm min}$ in $\Gamma_{\rm fit1}$, $\Gamma_{\rm fit2}$ and $\Gamma_{\rm fit5}$ consistently comes from the neutral $\rho^0 \to \pi^0\gamma$ decay. This might be related to the fact that the measurement associated to this decay channel has relatively small experimental uncertainty. However, it might also be pointing to limitations directly connected to the assumptions that have been taken in the phenomenological model presented in this chapter, such as, for example, potential gluonic content of the mesonic wavefunctions or contributions to the mixing from gluonic annihilation channels.

[5] Note that, traditionally, strange decay width measurements have suffered from larger uncertainties than the other radiative decays.

TABLE 7.3: Comparison between the experimental decay widths $\Gamma_{\rm exp}$ for the various radiative decay channels, and the $\Gamma_{\rm fit1}$, $\Gamma_{\rm fit2}$, $\Gamma_{\rm fit3}$, $\Gamma_{\rm fit4}$ and $\Gamma_{\rm fit5}$ predictions from the enhanced model associated to the fit values from Eqs. (7.13), (7.14), (7.15), (7.16) and (7.17), respectively.

Transition	$\Gamma_{\rm exp}$ [keV]	$\Gamma_{\rm fit1}$ [keV]	$\Gamma_{\rm fit2}$ [keV]	$\Gamma_{\rm fit3}$ [keV]	$\Gamma_{\rm fit4}$ [keV]	$\Gamma_{\rm fit5}$ [keV]
$\rho^0 \to \eta\gamma$	44 ± 3	41 ± 3	41 ± 3	38 ± 2	38 ± 2	41 ± 3
$\rho^0 \to \pi^0\gamma$	69 ± 9	85 ± 5	85 ± 5	82 ± 2	79 ± 2	85 ± 5
$\rho^+ \to \pi^+\gamma$	67 ± 7	67 ± 8	74 ± 2	75 ± 2	75 ± 2	74 ± 2
$\omega \to \eta\gamma$	3.8 ± 0.3	4.0 ± 0.5	4.0 ± 0.5	3.4 ± 0.2	3.5 ± 0.2	4.0 ± 0.5
$\omega \to \pi^0\gamma$	713 ± 20	705 ± 21	701 ± 20	703 ± 19	704 ± 19	701 ± 20
$\phi \to \eta\gamma$	55.4 ± 1.1	55 ± 3	55 ± 8	54 ± 8	54 ± 8	55 ± 3
$\phi \to \eta'\gamma$	0.26 ± 0.01	0.27 ± 0.01	0.27 ± 0.04	0.28 ± 0.05	0.27 ± 0.05	0.27 ± 0.01
$\phi \to \pi^0\gamma$	5.5 ± 0.2	5.5 ± 1.0	5.5 ± 1.1	5.5 ± 0.3	5.5 ± 0.3	5.5 ± 1.0
$\eta' \to \rho^0\gamma$	57 ± 3	57 ± 4	57 ± 4	56 ± 3	55 ± 3	57 ± 4
$\eta' \to \omega\gamma$	5.1 ± 0.3	5.2 ± 0.2	5.2 ± 0.2	6.4 ± 0.1	6.5 ± 0.1	5.2 ± 0.2
$K^{*0} \to K^0\gamma$	116 ± 10	116 ± 11	116 ± 10	116 ± 10	116 ± 10	-
$K^{*+} \to K^+\gamma$	46 ± 4	46 ± 5	46 ± 5	46 ± 5	46 ± 5	-
$\chi^2_{\rm min}$/d.o.f.	-	2.3	1.9	4.4	4.8	1.9

7.5 Conclusions

The phenomenological model based on the standard quark model with two sources of flavour $SU(3)$-symmetry breaking proposed by Bramon et al. in Ref. [140] has been tested using the most up-to-date $VP\gamma$ experimental data [1] in Sec. 7.3. It has been shown that the quality of the most recent empirical data is sufficiently good to see that the model struggles to accurately reproduce experiment. Consequently, the objective in this chapter has been to enhance this phenomenological model to reconcile it with experiment. This has been achieved by introducing isospin symmetry-breaking effects in the model.

The main result from the present investigation is that the quality of the most up-to-date experimental data [1] enables a small amount of isospin-symmetry breaking that is inconsistent with zero, with a confidence level of approximately 2.5σ, using the enhanced phenomenological model. The quality of the performed fits is good, with e.g. $\chi^2_{\rm min}/\text{d.o.f.} \simeq 1.9$. In addition, the estimations for the fit parameters appear to be very robust across the fits that have been performed. The fitted values for $g = 0.69 \pm 0.01$ GeV^{-1}, $\phi_{23} = (41.5 \pm 0.5)^\circ$, $\phi_V = (4.0 \pm 0.2)^\circ$ and $m_s/\overline{m} = 1.17 \pm 0.06$ are in good agreement with those from other analyses available in the published literature (e.g. [120, 157, 163]). Contrary to this, our estimates for the parameters controlling the mixing in the π^0-η and π^0-η' sectors, i.e. $\epsilon_{12} = (2.4 \pm 1.0)$ % and $\epsilon_{13} = (2.5 \pm 0.9)$ % —using the mathematical definition for the rotation matrix from Eq. (7.9)— or $\epsilon = \epsilon_{\pi\eta} = (0.1 \pm 0.9)$ % and $\epsilon' = \epsilon_{\pi\eta'} = (3.5 \pm 0.9)$ % —once translated into Kroll's [156] and Escribano et al.'s [161] definitions—, are not in accordance with the estimations that were provided by these authors in Refs. [156] and [161], respectively.

To conclude, it is worth highlighting that all the results from the present investigation appear to indicate that the enhanced phenomenological model, which is based on simple quark model concepts and implements isospin-violating effects, is sufficient to describe to a large degree of accuracy the radiative decays, and the rich and complex mixing phenomenology in the pseudoscalar meson sector.

Chapter 8

A theoretical analysis of the doubly radiative decays $\eta^{(\prime)} \to \pi^0\gamma\gamma$ and $\eta' \to \eta\gamma\gamma$[1]

The scalar and vector meson exchange contributions to the doubly radiative decays $\eta^{(\prime)} \to \pi^0\gamma\gamma$ and $\eta' \to \eta\gamma\gamma$ are analysed within the $U(3) \times U(3)$ LσM and VMD frameworks, respectively. Predictions for the diphoton invariant mass distributions and the associated integrated branching ratios are given, and compared with current experimental data. Whilst a satisfactory description of the shapes of the $\eta^{(\prime)} \to \pi^0\gamma\gamma$ diphoton spectra and the $\eta' \to \pi^0(\eta)\gamma\gamma$ branching ratios is obtained —thus, supporting the validity of our approach—, the situation is unclear for the normalisation of the $\eta \to \pi^0\gamma\gamma$ as there are significant discrepancies in the measurements from different experimental collaborations. The theoretical predictions for the $\eta' \to \eta\gamma\gamma$ presented in this chapter are the first that have been published.

8.1 Introduction

Measurements of η and η' decays have reached unprecedented precision over the years placing new demands on the accuracy of the corresponding theoretical descriptions [14]. Amongst them, the radiative decay $\eta \to \pi^0\gamma\gamma$ has attracted much interest as this process is the perfect laboratory for testing χPT and its natural extensions, but also down to decades of tension between the associated theoretical predictions and the experimental measurements.

Likewise, the study of the $\eta' \to \pi^0\gamma\gamma$ and $\eta' \to \eta\gamma\gamma$ decay processes are of interest for a number of reasons. First, they complete existing calculations of the sister process $\eta \to \pi^0\gamma\gamma$, which has been studied in many different frameworks, ranging from the seminal works based on VMD [166, 167] and χPT [168] to more modern treatments based on the unitarisation of the chiral amplitudes [97, 98] or dispersive approaches [169]. At present, whilst there is only a course estimation for the branching ratio (BR) of the $\eta' \to \pi^0\gamma\gamma$ decay [170, 171], there is no calculation or theoretical prediction for the $\eta' \to \eta\gamma\gamma$. Second, the BESIII Collaboration has recently reported the first measurements for the decays $\eta' \to \pi^0\gamma\gamma$ [172] and $\eta' \to \eta\gamma\gamma$ [173], thus, making the topic of timely interest [174]. Third, the analysis of these decays could help extract relevant information on the properties of the lowest-lying scalar resonances; in particular, the isovector $a_0(980)$ from the two $\eta^{(\prime)} \to \pi^0\gamma\gamma$ processes, and the isoscalars $\sigma(500)$ and $f_0(980)$ from the $\eta' \to \eta\gamma\gamma$ decay, thus, complementing other investigations such as the studies of $V \to P^0P^0\gamma$ decays ($V = \rho^0, \omega, \phi$ and $P^0 = \pi^0, \eta$) [96], D and J/ψ decays, central production, etc. (see note on scalar mesons in Ref. [1]). For all these reasons, our aim here is to provide a first detailed evaluation of the invariant mass spectra and integrated BRs for the three doubly radiative decays $\eta^{(\prime)} \to \pi^0\gamma\gamma$ and $\eta' \to \eta\gamma\gamma$.

On the experimental front, the BR of the $\eta \to \pi^0\gamma\gamma$ decay has been measured by GAMS-2000 [175], BR $= (7.1 \pm 1.4) \times 10^{-4}$, Crystal Ball@AGS in 2005 [176], BR $= (3.5 \pm 0.7 \pm 0.6) \times 10^{-4}$, and 2008 [177], BR $= (2.21 \pm 0.24 \pm 0.47) \times 10^{-4}$, where the latter also included an invariant mass spectrum for the two outgoing photons. An independent analysis of the last Crystal Ball data resulted in BR $= (2.7 \pm 0.9 \pm 0.5) \times 10^{-4}$ [178].

[1] This chapter is based on Ref. [165].

Early results are summarised in the review of Ref. [179]. Surprisingly low in comparison with all previous measurements is the 2006 result reported by the KLOE Collaboration [180], BR $= (0.84 \pm 0.27 \pm 0.14) \times 10^{-4}$, based on a sample of 68 ± 23 events. More recent measurements of the diphoton energy spectrum, $\Gamma(\eta \to \pi^0\gamma\gamma) = (0.330 \pm 0.030)$ eV and BR $= (2.54 \pm 0.27) \times 10^{-4}$ were released by the A2 Collaboration at the Mainz Microtron (MAMI) [181], based on the analysis of 1.2×10^3 $\eta \to \pi^0\gamma\gamma$ decay events. Very recently, a (preliminary) value with significantly smaller uncertainties has been found by the KLOE Collaboration, BR $= (1.23 \pm 0.14) \times 10^{-4}$, and has been published in a conference proceedings [182]; the associated diphoton spectrum has not yet been published, although it was presented at The 10^{th} International Workshop on Chiral Dynamics 2021 [183]. The latest PDG states a fit value of BR $= (2.55 \pm 0.22) \times 10^{-4}$ [1]. For the $\eta' \to \pi^0\gamma\gamma$ decay, the BESIII Collaboration has recently reported for the first time the associated $m^2_{\gamma\gamma}$ invariant mass distribution [172]. The measured branching fraction is BR $= (3.20 \pm 0.07 \pm 0.23) \times 10^{-3}$, superseding the upper limit BR $< 8 \times 10^{-4}$ at 90% CL determined by the GAMS-2000 experiment [184]. Finally, for the $\eta' \to \eta\gamma\gamma$ decay, a measurement of BR $< 1.33 \times 10^{-4}$ at 90% CL has been provided, again for the first time, by the BESIII Collaboration [173].

On the theoretical front, the $\eta \to \pi^0\gamma\gamma$ decay has been a stringent test for the predictive power of χPT. Within this framework, the tree-level contributions at $\mathcal{O}(p^2)$ and $\mathcal{O}(p^4)$ vanish because the pseudoscalar mesons involved are neutral. The first non-vanishing contribution comes at $\mathcal{O}(p^4)$, either from kaon loops, largely suppressed by their mass, or from pion loops, also suppressed since they violate G-parity and, therefore, are proportional to $m_u - m_d$. Quantitatively, Ametller et al. found in Ref. [168] that $\Gamma^{(4)}_\pi = 0.84 \times 10^{-3}$ eV, $\Gamma^{(4)}_K = 2.45 \times 10^{-3}$ eV and $\Gamma^{(4)}_{\pi,K} = 3.89 \times 10^{-3}$ eV for the π, K and π+K loop contributions to the decay width, which turns out to be two orders of magnitude smaller than the PDG fit value $\Gamma^{\text{exp}}_{\eta\to\pi^0\gamma\gamma} = 0.334 \pm 0.029$ eV [1]. The first sizeable contribution comes at $\mathcal{O}(p^6)$, but the associated low-energy constants are not well defined and one must resort to phenomenological models to fix them. To this end, for instance, VMD has been used to determine these coefficients by expanding the vector meson propagators and keeping the lowest term. Assuming equal contributions from the ρ^0 and ω mesons, the authors of Ref. [168] found that $\Gamma^{(6)}_{\rho+\omega} = 0.18$ eV, which was about two times smaller than their "all-order" estimation with the full vector meson propagator $\Gamma_{\text{VMD}} = 0.31$ eV, and in reasonable agreement with older VMD estimates [166, 167], as well as Refs. [185, 186]. The contributions of the scalar $a_0(980)$ and tensor $a_2(1320)$ resonances to the $\mathcal{O}(p^6)$ chiral coefficients were also assessed in Ref. [168] following the same procedure but no "all-order" estimates were provided. Contrary to the VMD contribution where the coupling constants appear squared, the signs of the a_0 and a_2 contributions are not unambiguously fixed [168]. At order $\mathcal{O}(p^8)$, a new type of loop effects taking two vertices from the anomalous chiral Lagrangian appear. Pion loops are no longer suppressed since the associated vertices do not violate G-parity and the kaon-loop suppression does not necessarily occur. Numerically, the contributions from these loops were $\Gamma^{(8)}_\pi = 5.2 \times 10^{-5}$eV, $\Gamma^{(8)}_K = 2.2 \times 10^{-3}$ eV and $\Gamma^{(8)}_{\pi,K} = 2.5 \times 10^{-3}$ eV [168]. Summing up all the effects that were not negligible and presented no sign ambiguities, i.e. the non-anomalous pion and kaon loops at $\mathcal{O}(p^4)$, the corresponding loops at $\mathcal{O}(p^8)$ with two anomalous vertices, and the "all-order" VMD estimate, resulted in $\Gamma^{\chi+\text{VMD}}_{\eta\to\pi^0\gamma\gamma} = 0.42$ eV [168]. Including the contributions from the a_0 and a_2 exchanges with sign ambiguities, which did not represent an "all-order" estimate of these effects, they conservatively concluded that $\Gamma^{\chi+\text{VMD}+a_0+a_2}_{\eta\to\pi^0\gamma\gamma} = 0.42 \pm 0.20$ eV [168]. The further inclusion of C-odd axial-vector resonances raised this value to 0.47 ± 0.20 eV [187] (see also Ref. [188]). Other determinations of the $\mathcal{O}(p^6)$ low-energy constants in the early and extended Nambu–Jona-Lasinio models led to 0.11–0.35 eV [189], 0.58 ± 0.30 eV [190] and $0.27^{+0.18}_{-0.07}$ eV [191]. A different approach based on quark-box diagrams [192, 193] yielded values of 0.70 eV and 0.58–0.92 eV,

respectively. In the most recent analyses, the $\eta \to \pi^0\gamma\gamma$ process has been considered within a chiral unitary approach for the meson-meson interaction, thus generating the a_0 resonance and fixing the sign ambiguity of its contribution. Using this approach, Oset et al. found a decay width of 0.47 ± 0.10 eV and 0.33 ± 0.08 eV in their 2003 [97] and 2008 [98] works, respectively, and the discrepancy may be down to differences in the radiative decay widths of the vector mesons used as input in their calculations. In any case, both estimations appear to be in good agreement with the empirical value $\Gamma^{\rm exp}_{\eta\to\pi^0\gamma\gamma} = 0.334 \pm 0.029$ eV [1]. On the other hand, there is only a rough estimation for the $\eta' \to \pi^0\gamma\gamma$ decay width [170, 171] and no theoretical analysis for the $\eta' \to \eta\gamma\gamma$ process.

The methodology in this chapter can be summarised as follows. First, we begin calculating the dominant chiral-loop contribution, that is, the $\mathcal{O}(p^4)$ diagrams containing two vertices of the lowest order Lagrangian and one loop of charged pions or kaons. We employ the large-N_C limit of χPT and regard the singlet state η_1 as the ninth pseudo-Goldstone boson of the theory. In addition, we simplify the calculations by assuming the isospin limit, which allows one to consider only the kaon loops for the two $\eta^{(\prime)} \to \pi^0\gamma\gamma$ decays. The $\mathcal{O}(p^8)$ loop corrections from diagrams with two anomalous vertices are very small [168] and, therefore, not considered. The explicit contributions of intermediate vector and scalar mesons are accounted for by means of the VMD and LσM frameworks. Accordingly, we compute the dominant contribution, i.e. the exchange of intermediate vector mesons, through the decay chain $P^0 \to V\gamma \to P^0\gamma\gamma$. Next, we consider the scalar meson contributions, providing an "all-order" estimate of the scalar effects through a calculation performed within the LσM, which enables us to, first, fix the sign ambiguity and, second, assess the relevance of the full scalar meson propagators, as opposed to integrating them out.

The structure of this chapter is as follows. In Sec. 8.2, we review the χPT calculation for the $\eta \to \pi^0\gamma\gamma$ and provide theoretical expressions for the $\eta' \to \pi^0\gamma\gamma$ and $\eta' \to \eta\gamma\gamma$ decays. In Sec. 8.3, we calculate the effects of intermediate vector meson exchanges, which represent the dominant contribution, using the VMD model. In Sec. 8.4, the chiral-loop prediction is substituted by a LσM calculation, where the effects of scalar meson resonances are taken into account explicitly. In Sec. 8.5, theoretical results for the decay widths and associated diphoton energy spectra are presented for the three decay processes, and a detailed discussion of the results is given. Some final remarks and conclusions are presented in Sec. 8.6.

8.2 Chiral-loop calculation

Let us first focus our attention on the $\eta \to \pi^0\gamma\gamma$ process. At order $\mathcal{O}(p^2)$, there are no contributions to this process and, at $\mathcal{O}(p^4)$, the contributions come from diagrams with two vertices from the lowest order chiral Lagrangian and a loop of charged pions and kaons. However, as discussed in Sec. 8.1, the contribution from kaon loops is dominant and the pion loops vanish in the isospin limit. The invariant amplitude can, thus, be written as follows

$$\mathcal{A}^{\chi\rm PT}_{\eta\to\pi^0\gamma\gamma} = \frac{2\alpha}{\pi}\frac{1}{M^2_{K^+}} L(s_K)\{a\} \times \mathcal{A}^{\chi}_{K^+K^-\to\pi^0\eta}\,, \tag{8.1}$$

where α is the fine-structure constant, M_{K^+} is the mass of the charged kaon, $L(\hat{s})$ is the loop integral

$$\begin{aligned} L(z) &= -\frac{1}{2z} - \frac{2}{z^2} f\left(\frac{1}{z}\right), \\ f(z) &= \begin{cases} \frac{1}{4}\left(\log\frac{1+\sqrt{1-4z}}{1-\sqrt{1-4z}} - i\pi\right)^2 & \text{for } z < \frac{1}{4} \\ -\left[\arcsin\left(\frac{1}{2\sqrt{z}}\right)\right]^2 & \text{for } z > \frac{1}{4} \end{cases}, \end{aligned} \tag{8.2}$$

and $s_K = s/M_{K^+}^2$, with $s = (q_1+q_2)^2 = 2q_1\cdot q_2$ being the invariant mass of the two outgoing photons. The Lorentz structure $\{a\}$ in Eq. (8.1) is defined as

$$\{a\} = (\epsilon_1\cdot\epsilon_2)(q_1\cdot q_2) - (\epsilon_1\cdot q_2)(\epsilon_2\cdot q_1)\,, \tag{8.3}$$

where $\epsilon_{1,2}$ and $q_{1,2}$ are the polarisation and four-momentum vectors of the final photons and $\mathcal{A}^{\chi}_{K^+K^-\to\pi^0\eta}$ is the four-pseudoscalar amplitude, which can be expressed as follows[2]

$$\begin{aligned}\mathcal{A}^{\chi\mathrm{PT}}_{K^+K^-\to\pi^0\eta} =& \frac{1}{4f_\pi^2}\left[\left(s - \frac{M_\eta^2}{3} - \frac{8M_K^2}{9} - \frac{M_\pi^2}{9}\right)(\cos\phi_P + \sqrt{2}\sin\phi_P)\right.\\ &\left. + \frac{4}{9}(2M_K^2 + M_\pi^2)\left(\cos\phi_P - \frac{\sin\phi_P}{\sqrt{2}}\right)\right],\end{aligned} \tag{8.4}$$

where f_π is the pion decay constant and ϕ_P is the η-η' pseudoscalar mixing angle in the quark-flavour basis at lowest order in χPT defined as [142]

$$\begin{aligned}|\eta\rangle &= \cos\phi_P\,|\eta_{\mathrm{NS}}\rangle - \sin\phi_P\,|\eta_{\mathrm{S}}\rangle\,,\\ |\eta'\rangle &= \sin\phi_P\,|\eta_{\mathrm{NS}}\rangle + \cos\phi_P\,|\eta_{\mathrm{S}}\rangle\,,\end{aligned} \tag{8.5}$$

with $|\eta_{\mathrm{NS}}\rangle = \frac{1}{\sqrt{2}}|u\bar{u}+d\bar{d}\rangle$ and $|\eta_{\mathrm{S}}\rangle = |s\bar{s}\rangle$ (cf. Appendix A).

It must be noted that, in the seminal work of Ref. [168], the chiral-loop prediction was computed taking only into account the η_8 contribution and the mixing angle was fixed to $\theta_P = \phi_P - \arctan\sqrt{2} = \arcsin(-1/3) \simeq -19.5^\circ$. As explained before, in this chapter the singlet contribution is also considered and the dependence on the mixing angle is made explicit.

For the $\eta' \to \pi^0\gamma\gamma$ process, the associated amplitude is that of Eq. (8.1) with the replacements $M_\eta \to M_{\eta'}$, $(\cos\phi_P + \sqrt{2}\sin\phi_P) \to (\sin\phi_P - \sqrt{2}\cos\phi_P)$ and $(\cos\phi_P - \sin\phi_P/\sqrt{2}) \to (\sin\phi_P + \cos\phi_P/\sqrt{2})$ in Eq. (8.4). Finally, for the $\eta' \to \eta\gamma\gamma$ decay, two types of amplitudes contribute, one associated to a loop of charged kaons, as in the former two cases, and the other to a loop of charged pions, which in this case is not suppressed by G-parity. Again, the corresponding amplitudes have the same structure as Eq. (8.1) but replacing $s_K \to s_\pi$ and $M_{K^+} \to M_{\pi^+}$ for the pion loop, and, instead of Eq. (8.4), one must make use of

$$\begin{aligned}\mathcal{A}^{\chi\mathrm{PT}}_{K^+K^-\to\eta\eta'} =& -\frac{1}{4f_\pi^2}\left[\left(s - \frac{M_\eta^2 + M_{\eta'}^2}{3} - \frac{8M_K^2}{9} - \frac{2M_\pi^2}{9}\right)\left(\sqrt{2}\cos 2\phi_P + \frac{\sin 2\phi_P}{2}\right)\right.\\ &\left. + \frac{4}{9}(2M_K^2 - M_\pi^2)\left(2\sin 2\phi_P - \frac{\cos 2\phi_P}{\sqrt{2}}\right)\right],\end{aligned} \tag{8.6}$$

$$\mathcal{A}^{\chi\mathrm{PT}}_{\pi^+\pi^-\to\eta\eta'} = \frac{M_\pi^2}{2f_\pi^2}\sin 2\phi_P\,, \tag{8.7}$$

for the loop of kaons and pions, respectively.

To the best of our knowledge, the amplitudes for the $\eta' \to \pi^0\gamma\gamma$ and $\eta' \to \eta\gamma\gamma$ constitute the first chiral-loop predictions for these processes.

[2] This amplitude should not be confused with the four-pseudoscalar scattering amplitude calculated in χPT at lowest order.

8.3 VMD calculation

As discussed in Sec. 8.1, VMD can be used to calculate an "all-order" estimate for the contribution of intermediate vector meson exchanges to the processes of interest in this chapter. In Ref. [168], for example, it was found that the VMD amplitude represents the dominant contribution to the $\eta \to \pi^0\gamma\gamma$ decay, and, as it will be shown in Sec. 8.5, this is also the case for the $\eta' \to \pi^0\gamma\gamma$ and $\eta' \to \eta\gamma\gamma$ processes.

There is a total of six Feynman diagrams contributing to each one of the three decay processes, corresponding to the exchange of the three neutral vector mesons ρ^0, ω and ϕ. After some algebra, one arrives at the following expression for the invariant amplitude of the $\eta \to \pi^0\gamma\gamma$ decay

$$\mathcal{A}^{\rm VMD}_{\eta\to\pi^0\gamma\gamma} = \sum_{V=\rho^0,\omega,\phi} g_{V\eta\gamma} g_{V\pi^0\gamma} \left[\frac{(P\cdot q_2 - M_\eta^2)\{a\} - \{b\}}{D_V(t)} + \left\{ \begin{array}{c} q_2 \leftrightarrow q_1 \\ t \leftrightarrow u \end{array} \right\} \right], \tag{8.8}$$

where $t, u = (P - q_{2,1})^2 = M_\eta^2 - 2P\cdot q_{2,1}$ are the Mandelstam variables, and the Lorentz structures $\{a\}$ and $\{b\}$ are defined as

$$\begin{aligned} \{a\} &= (\epsilon_1\cdot\epsilon_2)(q_1\cdot q_2) - (\epsilon_1\cdot q_2)(\epsilon_2\cdot q_1)\,, \\ \{b\} &= (\epsilon_1\cdot q_2)(\epsilon_2\cdot P)(P\cdot q_1) + (\epsilon_2\cdot q_1)(\epsilon_1\cdot P)(P\cdot q_2) - (\epsilon_1\cdot\epsilon_2)(P\cdot q_1)(P\cdot q_2) \\ &\quad - (\epsilon_1\cdot P)(\epsilon_2\cdot P)(q_1\cdot q_2)\,, \end{aligned} \tag{8.9}$$

where P is the four-momentum of the decaying particle, and $\epsilon_{1,2}$ and $q_{1,2}$ are the polarisation and four-momentum vectors of the final photons, respectively. The denominator $D_V(t) = M_V^2 - t - iM_V\Gamma_V$ is the vector meson propagator, with $V = \rho^0$, ω and ϕ. Note, though, that for the ρ^0 propagator we make use of an energy-dependent decay width

$$\Gamma_{\rho^0}(t) = \Gamma_{\rho^0} \left(\frac{t - 4M_\pi^2}{M_{\rho^0}^2 - 4M_\pi^2} \right)^{3/2} \theta(t - 4M_\pi^2)\,. \tag{8.10}$$

The amplitudes for the $\eta' \to \pi^0\gamma\gamma$ and $\eta' \to \eta\gamma\gamma$ decays have a similar structure to that of Eq. (8.8), with the replacements $M_\eta^2 \to M_{\eta'}^2$, and $g_{V\eta\gamma}g_{V\pi^0\gamma} \to g_{V\eta'\gamma}g_{V\pi^0\gamma}$ for the $\eta' \to \pi^0\gamma\gamma$ and $g_{V\eta\gamma}g_{V\pi^0\gamma} \to g_{V\eta'\gamma}g_{V\eta\gamma}$ for the $\eta' \to \eta\gamma\gamma$ case.

To parameterise the $VP\gamma$ coupling constants, $g_{VP\gamma}$, one can make use of a simple phenomenological quark-based model first presented in Ref. [140], which was initially developed to describe $V \to P\gamma$ and $P \to V\gamma$ radiative decays. The coupling constants can, thus, be written as [137, 140]

$$\begin{aligned} g_{\rho^0\pi^0\gamma} &= \frac{1}{3}g\,, \quad g_{\omega\pi^0\gamma} = g\cos\phi_V\,, \quad g_{\phi\pi^0\gamma} = g\sin\phi_V\,, \\ g_{\rho^0\eta\gamma} &= g z_{\rm NS}\cos\phi_P\,, \qquad g_{\rho^0\eta'\gamma} = g z_{\rm NS}\sin\phi_P\,, \\ g_{\omega\eta\gamma} &= \frac{1}{3}g\Big(z_{\rm NS}\cos\phi_P\cos\phi_V - 2\frac{\overline{m}}{m_s} z_{\rm S}\sin\phi_P\sin\phi_V \Big)\,, \\ g_{\omega\eta'\gamma} &= \frac{1}{3}g\Big(z_{\rm NS}\sin\phi_P\cos\phi_V + 2\frac{\overline{m}}{m_s} z_{\rm S}\cos\phi_P\sin\phi_V \Big)\,, \\ g_{\phi\eta\gamma} &= \frac{1}{3}g\Big(z_{\rm NS}\cos\phi_P\sin\phi_V + 2\frac{\overline{m}}{m_s} z_{\rm S}\sin\phi_P\cos\phi_V \Big)\,, \\ g_{\phi\eta'\gamma} &= \frac{1}{3}g\Big(z_{\rm NS}\sin\phi_P\sin\phi_V - 2\frac{\overline{m}}{m_s} z_{\rm S}\cos\phi_P\cos\phi_V \Big)\,, \end{aligned} \tag{8.11}$$

where g is a generic electromagnetic constant, ϕ_P is the pseudoscalar η-η' mixing angle in the quark-flavour basis, ϕ_V is the vector ω-ϕ mixing angle in the same basis, $\overline{m}/m_s$ is the quotient of constituent quark masses,[3] and $z_{\rm NS}$ and $z_{\rm S}$ are the *non-strange* and *strange* multiplicative factors accounting for the relative meson wavefunction overlaps (cf. Chapter 7).

It is important to note that in Ref. [168], the VMD prediction for the $\eta \to \pi^0\gamma\gamma$ process was calculated assuming equal ρ^0 and ω contributions and without including the decay widths in the propagators. These approximations were valid in this particular case, since the phase space available prevents the vector mesons to resonate. However, for the $\eta' \to \pi^0\gamma\gamma$ case, the available phase space allows these vectors to be on-shell and the introduction of their decay widths is mandatory. For consistency, we include the decay widths in the vector meson propagators of the three decays of interest.

8.4 LσM calculation

An all-order estimate for the contribution of scalar meson exchanges to the processes under study can be obtained by means of the LσM, where the complementarity between this model and χPT can be used to include the scalar meson poles at the same time as keeping the correct low-energy behaviour expected from chiral symmetry. This procedure was applied with success to the related $V \to P^0P^0\gamma$ decays [96].

Within this framework, the two $\eta^{(\prime)} \to \pi^0\gamma\gamma$ processes proceed through kaon loops, and by exchanging the $a_0(980)$ in the s-channel and the κ in the t- and u-channels. The $\eta' \to \eta\gamma\gamma$ decay is more complex as it proceeds through both kaon and pion loops; the $\sigma(600)$ and the $f_0(980)$ are exchanged in the s-channel for both types of loops, whilst, in the u- and t-channels, the κ is exchanged for kaon loops and the $a_0(980)$ for pion loops.

The loop contributions take place through combinations of three diagrams for each one of the intermediate states, which added together give finite results. The amplitudes for the three $\eta^{(\prime)} \to \pi^0\gamma\gamma$ and $\eta' \to \eta\gamma\gamma$ processes in the LσM can, thus, be expressed as follows

$$\mathcal{A}^{\rm L\sigma M}_{\eta\to\pi^0\gamma\gamma} = \frac{2\alpha}{\pi}\frac{1}{M^2_{K^+}} L(s_K)\{a\} \times \mathcal{A}^{\rm L\sigma M}_{K^+K^-\to\pi^0\eta}\,, \tag{8.12}$$

$$\mathcal{A}^{\rm L\sigma M}_{\eta'\to\pi^0\gamma\gamma} = \frac{2\alpha}{\pi}\frac{1}{M^2_{K^+}} L(s_K)\{a\} \times \mathcal{A}^{\rm L\sigma M}_{K^+K^-\to\pi^0\eta'}\,, \tag{8.13}$$

$$\mathcal{A}^{\rm L\sigma M}_{\eta'\to\eta\gamma\gamma} = \frac{2\alpha}{\pi}\frac{1}{M^2_{\pi}} L(s_\pi)\{a\} \times \mathcal{A}^{\rm L\sigma M}_{\pi^+\pi^-\to\eta\eta'} + \frac{2\alpha}{\pi}\frac{1}{M^2_{K^+}} L(s_K)\{a\} \times \mathcal{A}^{\rm L\sigma M}_{K^+K^-\to\eta\eta'}\,, \tag{8.14}$$

where $L(z)$, $s_{\pi,K}$ and $\{a\}$ are the same as in Sec. 8.2. The four-pseudoscalar amplitudes $\mathcal{A}^{\rm L\sigma M}_{\eta^{(\prime)}\pi^0\to K^+K^-}$ and $\mathcal{A}^{\rm L\sigma M}_{\eta'\eta\to K^+K^-(\pi^+\pi^-)}$ in Eqs. (8.12-8.14) turn out to be s, t and u dependent and can be expressed in terms of the pion and kaon decay constants, f_π and f_K, the masses of the scalar and pseudoscalar mesons involved in the processes, and the scalar and pseudoscalar mixing angles in the quark-flavour basis, ϕ_S and ϕ_P, where ϕ_S is defined as

$$\begin{aligned} |\sigma\rangle &= \cos\phi_S\,|\sigma_{\rm NS}\rangle - \sin\phi_S\,|\sigma_{\rm S}\rangle\,, \\ |f_0\rangle &= \sin\phi_S\,|\sigma_{\rm NS}\rangle + \cos\phi_S\,|\sigma_{\rm S}\rangle\,, \end{aligned} \tag{8.15}$$

[3] As explained in Chapter 7, the flavour symmetry-breaking mechanism associated to differences in the effective magnetic moments of light (i.e. up and down) and strange quarks in magnetic dipolar transitions is implemented via constituent quark mass differences. Specifically, one introduces a multiplicative $SU(3)$-breaking term, i.e. $1 - s_e \equiv \overline{m}/m_s$, in the s-quark entry of the quark-charge matrix Q.

with $|\sigma_{\rm NS}\rangle = \frac{1}{\sqrt{2}}|u\bar{u}+d\bar{d}\rangle$ and $|\sigma_{\rm S}\rangle = |s\bar{s}\rangle$ (cf. Appendix A). For our analysis, the procedure outlined in Ref. [96] is applied in order to obtain a consistent full s-dependent amplitude. In essence, this involves replacing the t- and u-channel contributions by the result of subtracting from the chiral-loop amplitude, i.e. Eqs. (8.4-8.7), the infinite mass limit of the s-channel scalar contribution.[4] We refer the interested reader to Ref. [96] for further details. After performing these replacements, one finally obtains the following scalar amplitudes

$$\begin{aligned}\mathcal{A}^{\rm L\sigma M}_{K^+K^-\to\pi^0\eta} =& \frac{1}{2f_\pi f_K}\Bigg\{(s-M_\eta^2)\frac{M_K^2-M_{a_0}^2}{D_{a_0}(s)}\cos\phi_P + \frac{1}{6}\Big[(5M_\eta^2+M_\pi^2-3s)\cos\phi_P \\ & -\sqrt{2}(M_\eta^2+4M_K^2+M_\pi^2-3s)\sin\phi_P\Big]\Bigg\},\end{aligned} \tag{8.16}$$

$$\begin{aligned}\mathcal{A}^{\rm L\sigma M}_{K^+K^-\to\pi^0\eta'} =& \frac{1}{2f_\pi f_K}\Bigg\{(s-M_{\eta'}^2)\frac{M_K^2-M_{a_0}^2}{D_{a_0}(s)}\sin\phi_P + \frac{1}{6}\Big[(5M_{\eta'}^2+M_\pi^2-3s)\sin\phi_P \\ & +\sqrt{2}(M_{\eta'}^2+4M_K^2+M_\pi^2-3s)\cos\phi_P\Big]\Bigg\},\end{aligned} \tag{8.17}$$

$$\begin{aligned}\mathcal{A}^{\rm L\sigma M}_{K^+K^-\to\eta\eta'} =& \frac{s-M_K^2}{2f_K}\left[\frac{g_{\sigma\eta\eta'}}{D_\sigma(s)}\left(\cos\phi_S-\sqrt{2}\sin\phi_S\right)+\frac{g_{f_0\eta\eta'}}{D_{f_0}(s)}\left(\sin\phi_S+\sqrt{2}\cos\phi_S\right)\right] \\ & -\frac{s-M_K^2}{4f_\pi f_K}\left[1-2\left(\frac{2f_K}{f_\pi}-1\right)\right]\sin(2\phi_P) \\ & -\frac{1}{4f_\pi^2}\Bigg[\left(s-\frac{M_\eta^2+M_{\eta'}^2}{3}-\frac{8M_K^2}{9}-\frac{2M_\pi^2}{9}\right)\left(\sqrt{2}\cos 2\phi_P+\frac{\sin 2\phi_P}{2}\right) \\ & +\frac{4}{9}(2M_K^2-M_\pi^2)\left(2\sin 2\phi_P-\frac{\cos 2\phi_P}{\sqrt{2}}\right)\Bigg],\end{aligned} \tag{8.18}$$

$$\mathcal{A}^{\rm L\sigma M}_{\pi^+\pi^-\to\eta\eta'} = \frac{s-M_\pi^2}{f_\pi}\left[\frac{g_{\sigma\eta\eta'}}{D_\sigma(s)}\cos\phi_S+\frac{g_{f_0\eta\eta'}}{D_{f_0}(s)}\sin\phi_S\right]+\frac{2M_\pi^2-s}{2f_\pi^2}\sin 2\phi_P\,, \tag{8.19}$$

where $D_S(s)$ are the $S=\sigma$, f_0 and a_0 propagators defined in Appendix C. Note that they are complete one-loop propagators, as the usual Breit-Wigner description is not adequate in this case due to either the presence of thresholds or a very wide decay width. The required couplings in Eqs. (8.18) and (8.19) are given by

$$\begin{aligned}g_{\sigma\eta\eta'} =& \frac{\sin 2\phi_P}{2f_\pi}\Bigg\{(M_\eta^2\cos^2\phi_P+M_{\eta'}^2\sin^2\phi_P-M_{a_0}^2)\left[\cos\phi_S+\sqrt{2}\sin\phi_S\left(2\frac{f_K}{f_\pi}-1\right)\right] \\ & -(M_{\eta'}^2-M_\eta^2)\left(\cos\phi_S\cos 2\phi_P-\frac{1}{2}\sin\phi_S\sin 2\phi_P\right)\Bigg\},\end{aligned} \tag{8.20}$$

$$\begin{aligned}g_{f_0\eta\eta'} =& \frac{\sin 2\phi_P}{2f_\pi}\Bigg\{(M_\eta^2\cos^2\phi_P+M_{\eta'}^2\sin^2\phi_P-M_{a_0}^2)\left[\sin\phi_S-\sqrt{2}\cos\phi_S\left(2\frac{f_K}{f_\pi}-1\right)\right] \\ & -(M_{\eta'}^2-M_\eta^2)\left(\sin\phi_S\cos 2\phi_P+\frac{1}{2}\cos\phi_S\sin 2\phi_P\right)\Bigg\}.\end{aligned} \tag{8.21}$$

These couplings can be written in different equivalent forms; here, the ones involving the a_0

[4] It is important to note that this approximation is possible due to the fact that, in the t- and u-channels, the exchanged scalar mesons do not resonate.

Decay	BR [1]	$\lvert g_{VP\gamma}\rvert$ GeV^{-1}
$\rho^0 \to \pi^0\gamma$	$(4.7 \pm 0.6) \times 10^{-4}$	$0.22(1)$
$\rho^0 \to \eta\gamma$	$(3.00 \pm 0.21) \times 10^{-4}$	$0.48(2)$
$\eta' \to \rho^0\gamma$	$(28.9 \pm 0.5)\%$	$0.40(1)$
$\omega \to \pi^0\gamma$	$(8.40 \pm 0.22)\%$	$0.70(1)$
$\omega \to \eta\gamma$	$(4.5 \pm 0.4) \times 10^{-4}$	$0.135(6)$
$\eta' \to \omega\gamma$	$(2.62 \pm 0.13)\%$	$0.127(4)$
$\phi \to \pi^0\gamma$	$(1.30 \pm 0.05) \times 10^{-3}$	$0.041(1)$
$\phi \to \eta\gamma$	$(1.303 \pm 0.025)\%$	$0.2093(20)$
$\phi \to \eta'\gamma$	$(6.22 \pm 0.21) \times 10^{-5}$	$0.216(4)$

TABLE 8.1: PDG values for the branching ratios of the $V(P) \to P(V)\gamma$ transitions and the calculated $g_{VP\gamma}$ couplings directly from experiment [cf. Eq. (8.23)].

mass and the pion decay constant have been chosen for the sake of clarity. We can anticipate that taking into account the effects of scalar meson exchanges in an explicit way does not provide a noticeable improvement with respect to the chiral-loop prediction, except for the $\eta' \to \eta\gamma\gamma$ case, where the σ contribution turns out to be significant (see Sec. 8.5).

8.5 Results and discussion

In this section, we use the theoretical expressions developed in this chapter to present quantitative results. The decay widths for the processes of interest are calculated using the standard formula for the three-body decay [1], with the squared amplitude given by

$$|\mathcal{A}|^2 = |\mathcal{A}^{\rm VMD}|^2 + |\mathcal{A}^{\rm L\sigma M}|^2 + 2{\rm Re}\mathcal{A}^{*\rm VMD}\mathcal{A}^{\rm L\sigma M}\,, \tag{8.22}$$

where the vector ($\mathcal{A}^{\rm VMD}$) and scalar ($\mathcal{A}^{\rm L\sigma M}$) exchange contributions have been presented in Secs. 8.3 and 8.4, respectively. The last term in Eq. (8.22) represents the interference between the scalar and vector effects.

For the numerical values of the masses and decay widths of the participating resonances, we use the most up-to-date experimental data from the PDG [1], whilst for the pion and kaon decay constants we employ $f_\pi = 92.1$ MeV and $f_K = 110.1$ MeV, repectively. For the VMD couplings[5] [cf. Eq. (8.8)], we follow two different approaches: $i)$ the $g_{VP\gamma}$ are obtained directly from the experimental decay widths of the $V \to P\gamma$ and $P \to V\gamma$ ($P = \pi^0, \eta, \eta'$ and $V = \rho^0, \omega, \phi$) radiative transitions [1] by making use of

$$\begin{aligned}\Gamma_{V\to P\gamma} &= \frac{1}{3}\frac{g^2_{VP\gamma}}{32\pi}\left(\frac{M_V^2 - M_P^2}{M_V}\right)^3\,,\\ \Gamma_{P\to V\gamma} &= \frac{g^2_{VP\gamma}}{32\pi}\left(\frac{M_P^2 - M_V^2}{M_P}\right)^3\,,\end{aligned} \tag{8.23}$$

and are summarised in Table 8.1; $ii)$ the phenomenological model from Ref. [140] is employed to parameterise the VMD couplings [cf. Eq. (8.11)], and, by performing an optimisation fit to the most up-to-date $VP\gamma$ experimental data [1], one can find preferred values for

[5]Note that, for the LσM couplings, i.e. $g_{\sigma\eta\eta'}$ and $g_{f_0\eta\eta'}$, the current experimental state-of-the-art does not allow obtaining the associated numerical values directly from the empirical data. Therefore, one must resort to theoretical or phenomenological models to estimate them [cf. Eqs. (8.20) and (8.21)]. Likewise, the mixing angle in the scalar sector is fixed in our calculations to $\phi_S = -8^\circ$ following Ref. [96].

Decay	Couplings	Chiral-loop	LσM	VMD	Γ	$\mathrm{BR}_{\mathrm{th}}$	$\mathrm{BR}_{\mathrm{exp}}$ [1]
$\eta \to \pi^0\gamma\gamma$ (eV)	Empirical	1.87×10^{-3}	5.0×10^{-4}	0.16(1)	0.18(1)	$1.35(8) \times 10^{-4}$	$2.56(22) \times 10^{-4}$
	M-B	1.87×10^{-3}	5.0×10^{-4}	0.16(1)	0.17(1)	$1.30(1) \times 10^{-4}$	
$\eta' \to \pi^0\gamma\gamma$ (keV)	Empirical	1.1×10^{-4}	1.3×10^{-4}	0.57(3)	0.57(3)	$2.91(21) \times 10^{-3}$	$3.20(7)(23) \times 10^{-3}$
	M-B	1.1×10^{-4}	1.3×10^{-4}	0.70(4)	0.70(4)	$3.57(25) \times 10^{-3}$	
$\eta' \to \eta\gamma\gamma$ (eV)	Empirical	1.4×10^{-2}	3.29	21.2(1.2)	23.0(1.2)	$1.17(8) \times 10^{-4}$	$8.25(3.41)(0.72) \times 10^{-5}$
	M-B	1.4×10^{-2}	3.29	19.1(1.0)	20.9(1.0)	$1.07(7) \times 10^{-4}$	

TABLE 8.2: Chiral-loop, LσM and VMD predictions for the $\eta \to \pi^0\gamma\gamma$, $\eta' \to \pi^0\gamma\gamma$ and $\eta' \to \eta\gamma\gamma$ decays with empirical and model-based VMD couplings. The total decay widths are calculated from the coherent sum of the LσM and VMD contributions.

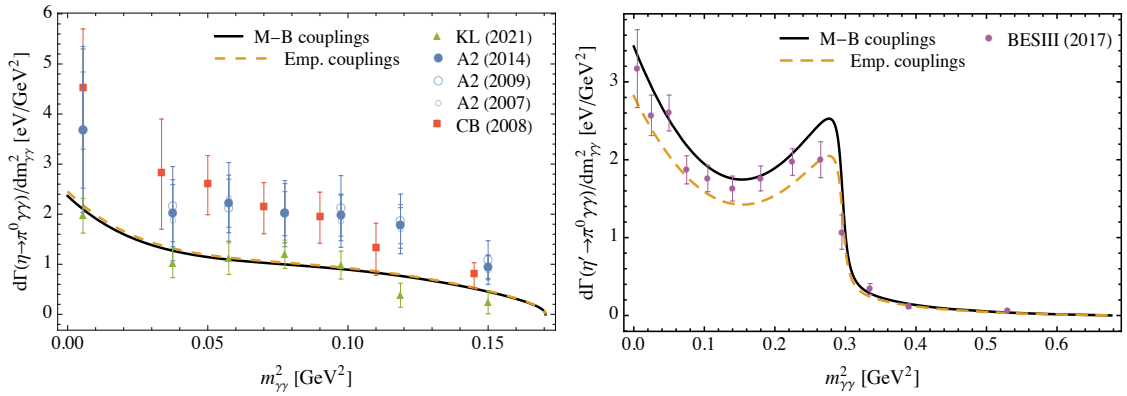

(A) $\eta \to \pi^0\gamma\gamma$ decay. (B) $\eta' \to \pi^0\gamma\gamma$ decay.

FIGURE 8.1: Comparison between the experimental diphoton energy spectra for the $\eta \to \pi^0\gamma\gamma$ and $\eta' \to \pi^0\gamma\gamma$ and our theoretical predictions using the empirical and model-based VMD couplings. The experimental data is taken from Refs. [182, 183] (KLOE), Ref. [181] (A2), Ref. [177] (Crystal Ball) and Ref. [172] (BESIII).

these parameters[6]

$$g = 0.70 \pm 0.01 \text{ GeV}^{-1}, \quad z_S\overline{m}/m_s = 0.65 \pm 0.01,$$
$$\phi_P = (41.4 \pm 0.5)^\circ, \qquad \phi_V = (3.3 \pm 0.1)^\circ, \tag{8.24}$$
$$z_{NS} = 0.83 \pm 0.02.$$

Hereafter, we refer to the former couplings as empirical and the latter as model-based couplings.

The numerical results obtained using both the empirical and model-based VMD couplings are summarised in Table 8.2. There, we show the contributions from χPT, the LσM, which replaces χPT when scalar meson poles are incorporated explicitly, and VMD. In addition, the theoretical decay widths and corresponding branching ratios are presented, together with the associated experimental values. Note that the quoted errors in the theoretical predictions come from the uncertainties associated to the VMD couplings. Using

[6]Note that this phenomenological model, contrary to the one presented in Chapter 7 and Ref. [137], does not take into account isospin-violating effects and this is reflected in the quality of the fit, which is far from ideal, $\chi^2/\text{d.o.f.} = 5.3$. However, in this study we are working in the isospin limit and, therefore, this simplified version of the model suffices for our purposes. Should one have used more simplified models by setting, for example, $z_{NS} = 1$ and $z_S = 1$, or $z_{NS} = 1$ and $z_S\overline{m}/m_s = 1$, would lead to qualities of fits of $\chi^2/\text{d.o.f.} = 18.3$ and $\chi^2/\text{d.o.f.} = 110.4$, respectively, which are clearly not acceptable.

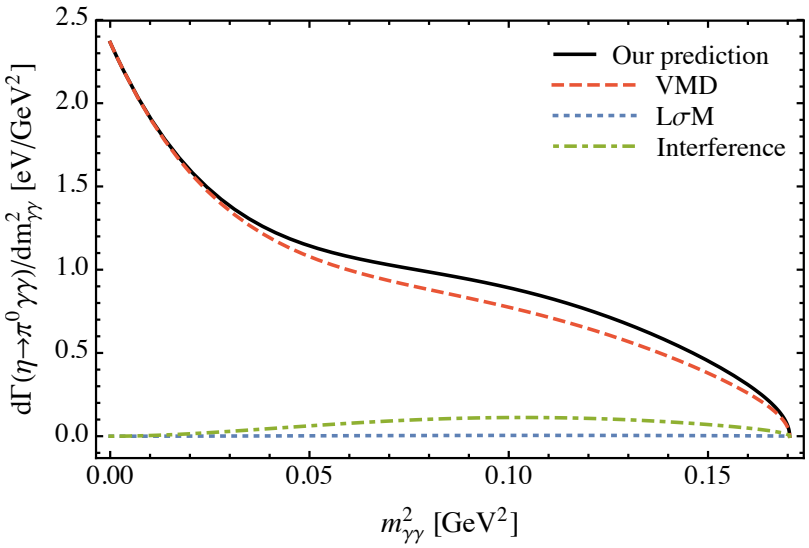

FIGURE 8.2: Contributions to the $\eta \to \pi^0\gamma\gamma$ diphoton energy spectrum (solid black), using the model-based VMD couplings, from intermediate vector (dashed red), scalar (dotted blue) meson exchanges and their interference (dot-dashed green).

the empirical VMD couplings, one finds that, whilst our prediction for the $\eta \to \pi^0\gamma\gamma$ process, $\mathrm{BR} = 1.35(8) \times 10^{-4}$, is approximately a factor of two smaller than the PDG reported value[7] [1] $\mathrm{BR} = 2.55(22) \times 10^{-4}$, our theoretical estimates for the $\eta' \to \pi^0\gamma\gamma$ and $\eta' \to \eta\gamma\gamma$, $\mathrm{BR} = 2.91(21) \times 10^{-3}$ and $\mathrm{BR} = 1.17(8) \times 10^{-4}$, are consistent with the BESIII experimental measurements $\mathrm{BR} = 3.20(7)(23) \times 10^{-3}$ [172] and $\mathrm{BR} = 8.25(3.41)(72) \times 10^{-5}$ [173], respectively. Employing, instead, the model-based VMD couplings from Eq. (8.11) and making use of the fit values for the model parameters shown in Eq. (8.24), we find that the branching ratio for the $\eta \to \pi^0\gamma\gamma$ decay, $\mathrm{BR} = 1.30(8) \times 10^{-4}$, is very much in line with that obtained using the empirical couplings and approximately half the corresponding PDG experimental value.[8] Thus, our theoretical results for this reaction appear to be robust against small variations of the VMD couplings. For the $\eta' \to \pi^0\gamma\gamma$ and $\eta' \to \eta\gamma\gamma$ processes, we obtain $\mathrm{BR} = 3.57(25) \times 10^{-3}$ and $\mathrm{BR} = 1.07(8) \times 10^{-4}$, which, once again, are in agreement with the values reported by BESIII [172, 173]. The branching ratio for the latter process turns out to be $\mathrm{BR} = 1.11(8) \times 10^{-4}$ and $\mathrm{BR} = 1.00(7) \times 10^{-4}$ for the empirical and model-based couplings using a Breit-Wigner propagator for the σ meson, where the pole parameters quoted in Ref. [1] have been utilised, instead of the complete one-loop propagator. As it can be seen, the use of either propagator provides very approximate results, with the differences surfacing in the associated energy spectra.

Our predictions for the diphoton invariant mass distributions are compared with the corresponding experimental data in Fig. 8.1. One can see from both plots that the shape of the spectra is captured well by our theoretical predictions. The energy spectrum of the $\eta \to \pi^0\gamma\gamma$ decay (Fig. 8.1a) appears to have a normalisation offset with respect to the measurements

[7] It is important to note that this prediction is in excellent agreement with the recently measured $\mathrm{BR} = (1.23 \pm 0.14) \times 10^{-4}$ by the KLOE Collaboration [182].

[8] Oset et al. considered additional contributions in Ref. [98], such as axial exchanges in the chiral loops and VMD loop contributions, where the associated amplitudes had been unitarised by making use of the Bethe-Salpenter equation for the resummation of the meson-meson scattering amplitudes, as well as contributions from the three-meson axial anomaly; all this allowed them to raise their prediction up to $\Gamma_{\eta\to\pi^0\gamma\gamma} = 0.33 \pm 0.08$ eV.

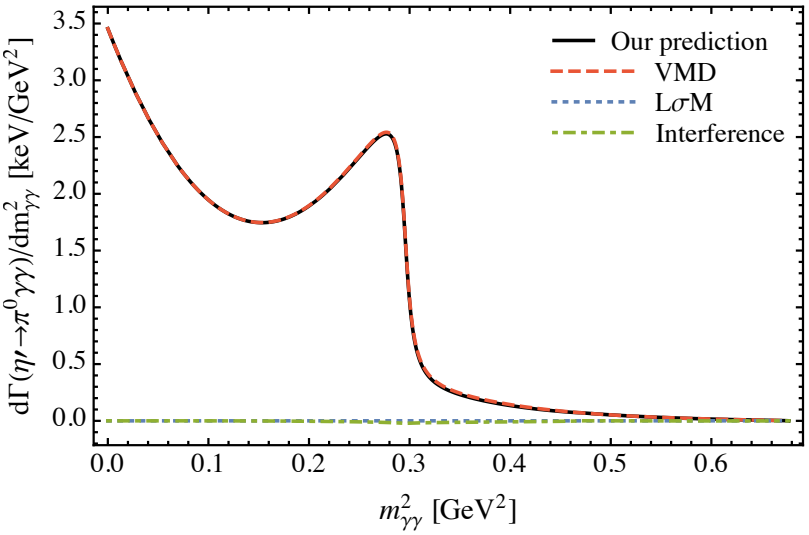

FIGURE 8.3: Contributions to the $\eta' \to \pi^0\gamma\gamma$ diphoton energy spectrum (solid black), using the model-based VMD couplings, from intermediate vector (dashed red), scalar (dotted blue) meson exchanges and their interference (dot-dashed green).

from A2 [181] and Crystal Ball [177], but it is in excellent agreement with the latest measurement by KLOE [182, 183]. In addition, our predictions for the $\eta' \to \pi^0\gamma\gamma$ spectrum, using either set of VMD couplings, shows very good agreement with the experimental measurement by BESIII [172]. In addition, the use of one set of couplings or the other makes little difference for the $\eta \to \pi^0\gamma\gamma$, though, it appears that the model-based couplings capture slightly better the experimental data for the $\eta' \to \pi^0\gamma\gamma$. For this reason, as well as down to its intrinsic aesthetic appeal and the fact that it highlights the power of the theoretical treatment, from this point onwards we adhere to the use of the model-based VMD couplings for any subsequent calculation.

The different contributions to the $\gamma\gamma$ invariant mass distribution of the $\eta \to \pi^0\gamma\gamma$ decay are shown in Fig. 8.2. As it can be seen, the spectrum is dominated by the exchange of vector mesons, accounting for 93%, out of which, the weights for the ρ^0, ω and ϕ are 25%, 20% and 0%, respectively; the remaining 48% comes from the interference between the three participating vector mesons. The contribution of the scalar exchanges accounts for less than 1%, making it very difficult to isolate the effect of individual scalar mesons even with the advent of more precise experimental data. The interference between the intermediate scalar and vector exchanges is constructive and accounts for about 7%. The contributions to the energy spectrum of the $\eta' \to \pi^0\gamma\gamma$ process are displayed in Fig. 8.3. Once again, the exchange of vector mesons completely dominate the spectrum contributing approximately with the 100.4% to the total signal, whilst the effects of scalar meson exchanges and their interference with the formers are negligible with 0% and -0.4% (destructive interference), respectively. As well as this, the ω contribution prevails with the 79% of the total VMD signal, whilst the ρ^0 and ϕ account for the 5% and 0%, respectively; the remaining 16% comes from the interference between the vector resonances. Finally, the different contributions to the $\eta' \to \eta\gamma\gamma$ energy spectrum are presented in Fig. 8.4. As expected, the contribution to the total signal from the exchange of vector mesons dominates again with about the 91%, with the ρ^0, ω and ϕ accounting for 54%, 14% and 1% of the VMD signal, respectively, and the remaining 22% being the result of their interference; interestingly, the scalar meson effects turn out to be sizeable in this process, weighing approximately 16%, with the exchange

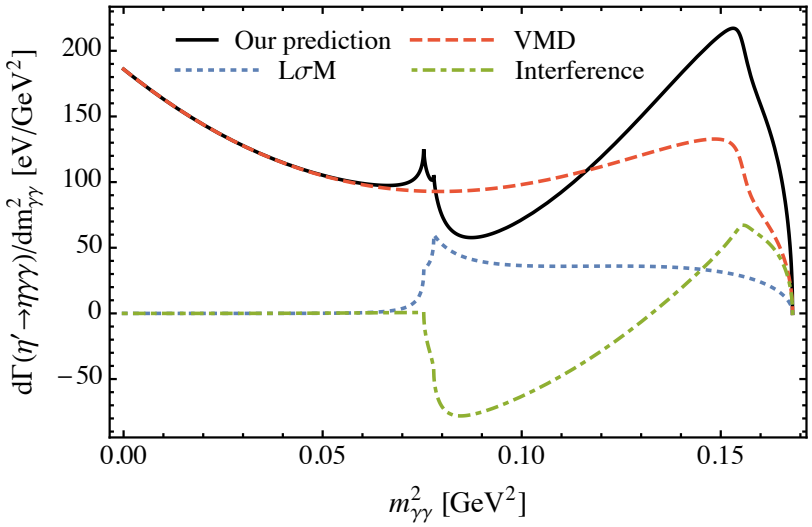

FIGURE 8.4: Contributions to the $\eta' \to \eta\gamma\gamma$ diphoton energy spectrum (solid black), using the model-based VMD couplings, from intermediate vector (dashed red), scalar (dotted blue) meson exchanges and their interference (dot-dashed green).

of σ mesons dominating the scalar signal.[9] The interference between the scalar and vector mesons is destructive and accounts for around the 7% and significantly influences the shape of the spectrum. It is worth noting the effect of using the complete one-loop propagator for the σ exchange, which manifests itself at the $m^2_{\gamma\gamma} = 0.078$ GeV peak and is associated to the $\pi^+\pi^-$ threshold. This peak, of course, is absent when the Breit-Wigner propagator for the σ exchange is used.

8.6 Conclusions

In this chapter, we have presented a thorough theoretical analysis of the doubly radiative decays $\eta^{(\prime)} \to \pi^0\gamma\gamma$ and $\eta' \to \eta\gamma\gamma$, and provided theoretical results for the associated decay widths and diphoton energy spectra in terms of intermediate scalar and vector meson exchange contributions using the LσM and VMD frameworks, respectively.

A complete set of theoretical expressions for the transition amplitudes from χPT, VMD and the LσM have been given for the three decay processes. Some of these expressions constitute, to the best of our knowledge, the first predictions of its kind. In addition, we have provided quantitative results by making use of numerical input from the PDG [1]. In particular, for the estimation of the VMD coupling constants, $g_{VP\gamma}$, two different routes have been followed: on the one hand, we have extracted them directly from the experimental $V(P) \to P(V)\gamma$ decay widths, and, on the other hand, we have obtained them from a phenomenological quark-based model and a fit to experimental data. A summary of the predicted decay widths, theoretical branching ratios and contributions to the total signals for the three doubly radiative decays $\eta^{(\prime)} \to \pi^0\gamma\gamma$ and $\eta' \to \eta\gamma\gamma$ is shown in Table 8.2, and a discussion of the results obtained and how they compare to available experimental data has been carried out in Sec. 8.5. As well as this, the diphoton invariant mass distributions associated to these

[9] A possible improvement to our prediction for the scalar meson contribution may be possible by considering a more sophisticated scalar scattering amplitude $\mathcal{A}_{\pi^+\pi^-\to\eta'\eta}$ [cf. Eq. (8.19)] as has successfully been done for the associated $\eta' \to \eta\pi\pi$ decay process in Ref. [194].

processes are shown in Figs. 8.2, 8.3 and 8.4, respectively, using the model-based VMD couplings. It is worth highlighting that, whilst vector meson exchanges vastly dominate over the scalar contributions for the $\eta^{(\prime)} \to \pi^0\gamma\gamma$ decays, we find that for the $\eta' \to \eta\gamma\gamma$ the scalar meson effects turn out to be substantial, specially that of the σ meson, and this represents an opportunity for learning details about this still poorly understood scalar state. In particular, we look forward to the release of the energy spectrum data for the $\eta' \to \eta\gamma\gamma$ process by the BESIII Collaboration to assess the robustness of our theoretical approach.

It is important to highlight that our theoretical predictions for the $\eta \to \pi^0\gamma\gamma$ appear to agree very well with the latest measurements from KLOE [182, 183], although they are found to be approximately a factor of two smaller than the experimental measurements from A2 [181] and Crystal Ball [177]. In addition, our predictions for the $\eta' \to \pi^0\gamma\gamma$ and $\eta' \to \eta\gamma\gamma$ are in good agreement with recent measurements performed by BESIII [172, 173].

As a final remark, we would very much like to encourage experimental groups to measure these decays again, first, to try to resolve and settle the inconsistency in the measurements from different experimental collaborations for the $\eta \to \pi^0\gamma\gamma$ decay and, second, to confirm whether a more refined theoretical treatment to describe the three processes simultaneously is required.

Chapter 9

Sensitivity of the $\eta^{(\prime)} \to \pi^0\gamma\gamma$ and $\eta' \to \eta\gamma\gamma$ decays to a sub-GeV leptophobic $U(1)_B$ boson[1]

The sensitivity of the doubly radiative decays $\eta^{(\prime)} \to \pi^0\gamma\gamma$ and $\eta' \to \eta\gamma\gamma$ to signatures of a leptophobic B boson in the MeV–GeV mass range is analysed in this chapter. By adding an explicit B-boson resonance exchange, $\eta \to B\gamma \to \pi^0\gamma\gamma$, to the SM contributions from vector and scalar meson exchanges, and employing experimental data for the associated branching ratios, it allows us to improve the current constraints on the B-boson mass m_B and coupling to SM particles α_B. From these constraints and the analysis of the available experimental $\gamma\gamma$ invariant mass distribution, we show that a B-boson signature in the resonant mass range $M_{\pi^0} \lesssim m_B \lesssim M_\eta$ is strongly suppressed and would be very difficult to experimentally identify, assuming that the leptophobic B boson only decays to SM particles. In contrast, the limits outside this mass window are less stringent and the corresponding t- and u-channel signatures may still be observable in the data, as it occurs with the non-resonant SM ρ, ω and ϕ meson exchanges. In addition, we make use of experimental data from the $\eta' \to \pi^0\gamma\gamma$ and $\eta' \to \eta\gamma\gamma$ decays to explore larger B-boson masses. The results of this chapter are relevant for the B-boson search programmes at existing and forthcoming light-meson facilities, such as KLOE(-II) and Jefferson Lab Eta Factory experiments.

9.1 Introduction

An increasingly ubiquitous strategy to search for physical phenomena beyond the Standard Model (BSM) is to test fundamental symmetries such as C, P, T, CP, and CPT in different processes. Specifically, decays of the neutral pseudoscalar mesons η and η' constitute a particularly suited playground to look for new physics [14, 15]. This is because these two mesons are special, as they are eigenstates of the C, P, CP and G-parity operators, and all their strong and electromagnetic decays are either anomalous or forbidden at lowest order due to the conservation of fundamental symmetries of QCD. Consequently, higher-order contributions are expected to become relevant, rendering the η/η' decays sensitive hadronic probes to test discrete symmetries and to search for undiscovered fundamental BSM particles, such as dark photons or leptophobic $U(1)_B$ bosons (see Refs. [14, 15] and references therein). Examples of this are the rare $\eta^{(\prime)} \to \pi^0\gamma\gamma$ and $\eta' \to \eta\gamma\gamma$ decays which, as they are highly suppressed in the SM [97, 98, 165, 168, 196], have been put forward as fine probes to search for MeV–GeV signatures of a new leptophobic B boson [197] arising from a new $U(1)_B$ gauge symmetry that couples predominantly to quarks over leptons [198–202].

Experimental searches for leptophobic B bosons depend on the mass m_B and the associated decay channels, and have placed constraints on the coupling for masses that span from below the MeV scale, obtained from long-range nuclear forces [203] and low-energy neutron scattering [204–206], to above the GeV scale, obtained at high-energy hadron colliders in dijet resonance searches, as well as in heavy quarkonia and Z decays [207–212]. The intermediate MeV–GeV mass range has been less explored thus far [197, 199], which

[1] This chapter is based on Ref. [195].

is down to this being the region of non-perturbative QCD, and has often been considered as a challenging blindspot for experiment in the past. However, searches for leptophobic B bosons are gaining traction in this intermediate mass range given the potential signatures that can be looked for in decays of light mesons, such as η, η', ω, and ϕ [197], after years of sterile sub-GeV dark-photon searches most of them relying on the coupling of this new force to leptons in decays to e^+e^- and $\mu^+\mu^-$ pairs [213–223]. Indeed, the search for leptophobic B bosons has been incorporated into the physics programmes of existing light-meson factories such as the KLOE-II experiment [182, 224], which is searching for B bosons by looking for enhancements in the $\pi^0\gamma$ invariant mass spectrum of the $\phi \to \eta B \to \eta\pi^0\gamma$ process, and is a top priority physics goal for the recently approved Jefferson Lab Eta Factory (JEF) experiment [225], which promises a new and exciting era for η and η' physics, with the $\eta \to \pi^0\gamma\gamma$ decay being their key signal channel. The Belle Collaboration has also pursued searches for a B boson decaying into $\pi^+\pi^-$ using $\eta \to \pi^+\pi^-\gamma$ decays [226] but have found no signal and, since $B \to \pi^+\pi^-$ is suppressed by G-parity conservation, the limits on the B-boson parameters are not as stringent as the constraints coming from other decays, such as the $\eta \to \pi^0\gamma\gamma$. B-boson searches may also be carried out at future η/η' factories, such as the proposed REDTOP experiment [15],[2] or in direct photoproduction $\gamma p \to Bp \to \pi^+\pi^-\pi^0 p$ at the GlueX experiment at Jefferson Lab [227], which will probe B-boson masses above 0.5 GeV. Alternatively, signals of $U(1)_B$ leptophobic B bosons decaying into invisible particles, i.e. dark matter, have also been pursued at neutrino factories [228] and at the LHC [229].

The model that we consider in this chapter for a $U(1)_B$ leptophobic gauge boson B that couples to the baryon number has the following interaction Lagrangian [197, 199]

$$\mathcal{L}_{\rm int} = \left(\frac{1}{3}g_B + \varepsilon Q_q e\right)\bar{q}\gamma^\mu q B_\mu - \varepsilon e \bar{\ell}\gamma^\mu \ell B_\mu \,, \tag{9.1}$$

where B_μ is the new gauge boson field and g_B is the new gauge coupling, with $\alpha_B = g_B^2/4\pi$ being the fine structure constant associated to the baryonic force. This interaction structure is gauge invariant and preserves the low-energy symmetries of QCD, namely C, P and T invariance, as well as isospin and $SU(3)$ flavour symmetry.

Partial widths for B-boson decays in the MeV–GeV mass range have been calculated in [197] using the hidden local symmetry framework for VMD. Above the single-pion threshold, $M_{\pi^0} \lesssim m_B \lesssim 1$ GeV, the B boson decays predominantly to $\pi^0\gamma$, or to $\pi^0\pi^+\pi^-$ when kinematically allowed, very much like the ω meson. Indeed, the B boson is assigned the same quantum numbers as those from the ω, i.e. $I^G(J^{PC}) = 0^-(1^{--})$. It must be noted that the interaction Lagrangian in Eq. (9.1) is not completely decoupled from leptons as it contains subleading photon-like couplings to leptons proportional to $\varepsilon = eg_B/(4\pi)^2$ via kinetic mixing. This effect allows the purely leptonic decay $B \to e^+e^-$, which dominates below single-pion threshold $m_B \lesssim M_{\pi^0}$. There are other allowed decay channels such as $B \to \eta\gamma$ and $B \to \pi^+\pi^-$; however, these are subleading [197] and, in particular, the latter, which is forbidden by G-parity conservation, arises via ρ-ω mixing.

At present, conservative constraints from η and η' decays on the B-boson parameters α_B and m_B are based on total rates by setting the SM contribution to zero [197], or using different words, by assuming the B-boson intermediate states $\eta^{(\prime)} \to B\gamma \to \pi^0\gamma\gamma$, $\eta' \to B\gamma \to \pi^+\pi^-\pi^0\gamma$ and $\eta' \to B\gamma \to \eta\gamma\gamma$, and making use of the narrow width approximation (NWA), e.g. $\text{BR}(\eta \to \pi^0\gamma\gamma) = \text{BR}(\eta \to B\gamma) \times \text{BR}(B \to \pi^0\gamma)$. It must be stressed, though, that the SM contribution to these decays is not negligible [98, 165, 169, 230] and, therefore, it should not be disregarded in exclusion analyses of B bosons. Thus, one of the goals of this chapter is to take into account SM effects in these analyses. To that effect, we

[2] The current detector layout at REDTOP is non-sensitive to neutral final states [15], but an improved version of REDTOP is planned where the η will be tagged and final states with π^0's and photons could be detected.

employ our controlled SM contributions, i.e. the VMD and LσM amplitudes from Chapter 8 (cf. Ref. [165]), we supplement them with the explicit inclusion of an intermediate B boson and use the most up-to-date experimental data.

Significantly greater sensitivity to the B-boson model could be obtained from the analysis of the invariant mass distributions. Provided that $M_{\pi^0} \leq m_B \leq M_{\eta^{(\prime)}}$, the B-boson mediated decay $\eta^{(\prime)} \to B\gamma \to \pi^0\gamma\gamma$ would reveal a peak around m_B in the $\pi^0\gamma$ invariant mass spectrum. Searches for a $\pi^0\gamma$ resonance within this mass region in $\eta \to \pi^0\gamma\gamma$ decays are the main physics goal of the JEF experiment [225], which plans to improve the total rate limit by two orders of magnitude, and is being searched for by KLOE-II [182, 224] via $\phi \to \eta B \to \eta\pi^0\gamma$ and $\eta \to B\gamma \to \pi^0\gamma\gamma$. Accordingly, we aim to perform a detailed analysis of the $\gamma\gamma$ and $\pi^0\gamma$ invariant mass distributions. In particular, using the available experimental diphoton spectra, together with our SM and B-boson amplitudes, we determine which regions of the α_B-m_B plane are preferred by the data and assess the B-boson contribution. It can be anticipated that, whilst the constraint from the $\eta \to \pi^0\gamma\gamma$ process in the resonant mass range $M_{\pi^0} \lesssim m_B \lesssim M_\eta$ is so strong that it makes it very difficult to identify any B-boson signatures (assuming that the B boson only decays into SM particles), its imprint in the t- and u-channels may be noticeable in the invariant mass distributions when $m_B \lesssim M_{\pi^0}$ and $m_B \gtrsim M_\eta$, as it occurs with the non-resonant SM ρ, ω and ϕ exchanges [165].

The chapter is structured as follows. In Sec. 9.2.1, we summarise the vector and scalar meson resonance exchange contributions to the amplitudes of the three $\eta^{(\prime)} \to \pi^0\gamma\gamma$ and $\eta' \to \eta\gamma\gamma$ decays (cf. Chapter 8). In Sec. 9.2.2, we present the framework to include the contribution of intermediate B-boson exchanges to the amplitudes. We then use these amplitudes in Sec. 9.3 to, first, set limits on the B-boson parameters α_B and m_B from the experimental branching ratios, and, second, to study the effect of the B-boson on the $m^2_{\gamma\gamma}$ and $m^2_{\pi^0\gamma}$ invariant mass distributions. We conclude this chapter with some conclusions in Sec. 9.4.

9.2 Theoretical Framework

9.2.1 Standard Model: vector and scalar contributions

VMD and the LσM can be used to calculate the SM contributions from vector and scalar meson resonance exchanges to the $\eta^{(\prime)} \to \pi^0\gamma\gamma$ and $\eta' \to \eta\gamma\gamma$ decay processes. In Ref. [168], it was found that the VMD amplitude represents the dominant contribution to the $\eta \to \pi^0\gamma\gamma$ decay, whilst in Chapter 8 and Ref. [165] we showed that this is also the case for the $\eta' \to \pi^0\gamma\gamma$ and $\eta' \to \eta\gamma\gamma$ processes.

In the VMD picture, the decay $\eta \to \pi^0\gamma\gamma$ proceeds through the transition $\eta \to V\gamma$ followed by $V \to \pi^0\gamma$, resulting in a total of six diagrams contributing to the amplitude of the process, which corresponds to the exchange of the three neutral vector mesons $V = \rho^0, \omega$ and ϕ in the t- and u-channels. By combining the $V\eta\gamma$ and $V\pi^0\gamma$ interacting terms with the propagator of the exchanged vector mesons, one can calculate the vector meson contributions to the $\eta \to \pi^0\gamma\gamma$ decay. We found in Eq. (8.8)

$$\mathcal{A}^{\rm VMD}_{\eta\to\pi^0\gamma\gamma} = \sum_{V=\rho^0,\omega,\phi} g_{V\eta\gamma} g_{V\pi^0\gamma} \left[\frac{(P\cdot q_2 - M_\eta^2)\{a\} - \{b\}}{D_V(t)} + \left\{ \begin{array}{c} q_2 \leftrightarrow q_1 \\ t \leftrightarrow u \end{array} \right\} \right], \quad (9.2)$$

where $t, u = (P - q_{2,1})^2 = M_\eta^2 - 2P\cdot q_{2,1}$ are Mandelstam variables, $\{a\}$ and $\{b\}$ are the Lorentz structures defined in Eq. (8.9)

$$\begin{aligned} \{a\} &= (\epsilon_1\cdot\epsilon_2)(q_1\cdot q_2) - (\epsilon_1\cdot q_2)(\epsilon_2\cdot q_1)\,, \\ \{b\} &= (\epsilon_1\cdot q_2)(\epsilon_2\cdot P)(P\cdot q_1) + (\epsilon_2\cdot q_1)(\epsilon_1\cdot P)(P\cdot q_2) \\ &\quad - (\epsilon_1\cdot\epsilon_2)(P\cdot q_1)(P\cdot q_2) - (\epsilon_1\cdot P)(\epsilon_2\cdot P)(q_1\cdot q_2)\,, \end{aligned} \quad (9.3)$$

with P being in this context the four-momentum of the decaying η meson, and $\epsilon_{1,2}$ and $q_{1,2}$ the polarisation and four-momentum vectors of the final photons, respectively. The denominator $D_V(q^2) = M_V^2 - q^2 - iM_V\Gamma_V$ is the vector meson propagator, with $V = \rho^0$, ω and ϕ. Due to the fact the the ρ^0 meson has got a very large decay width, the use of the usual Breit-Wigner prescription is not justified and, thus, one must employ the energy-dependent decay width from Eq. (8.10)

$$\Gamma_{\rho^0}(q^2) = \Gamma_{\rho^0}\left(\frac{q^2 - 4M_\pi^2}{M_{\rho^0}^2 - 4M_\pi^2}\right)^{3/2}\theta(q^2 - 4M_\pi^2)\,. \tag{9.4}$$

The amplitudes for the decays $\eta' \to \pi^0\gamma\gamma$ and $\eta' \to \eta\gamma\gamma$ have a similar structure to that of Eq. (9.2) with the replacements $M_\eta^2 \to M_{\eta'}^2$, and $g_{V\eta\gamma}g_{V\pi^0\gamma} \to g_{V\eta'\gamma}g_{V\pi^0\gamma}$ for the $\eta' \to \pi^0\gamma\gamma$ case and $g_{V\eta\gamma}g_{V\pi^0\gamma} \to g_{V\eta'\gamma}g_{V\eta\gamma}$ for the $\eta' \to \eta\gamma\gamma$ one.

For our analysis, we fix the $g_{VP\gamma}$ couplings in Eq. (9.2) from experiment as follows: we first calculate the decay widths for the radiative transitions $V \to P\gamma$ and $P \to V\gamma$, and find the relationships presented in Eq. (8.23)

$$\begin{aligned}\Gamma_{V\to P\gamma} &= \frac{1}{3}\frac{g_{VP\gamma}^2}{32\pi}\left(\frac{M_V^2 - M_P^2}{M_V}\right)^3,\\ \Gamma_{P\to V\gamma} &= \frac{g_{VP\gamma}^2}{32\pi}\left(\frac{M_P^2 - M_V^2}{M_P}\right)^3,\end{aligned} \tag{9.5}$$

which then are used in combination with the experimental decay widths from the PDG [1] to obtain the empirical $g_{VP\gamma}$ couplings provided in Table 8.1.

It is important to note that the most general $VP\gamma$ couplings in Eq. (9.2) are energy dependent, i.e. $g_{VP\gamma}(q^2)$. In the conventional VMD model, pseudoscalar mesons do not couple directly to photons but through the exchange of intermediate vectors; thus, in this framework, a particular $VP\gamma$ coupling constant times its normalised form factor is given by[3]

$$g_{VP\gamma}\,\hat{F}_{VP\gamma}(q^2) = \sum_{V'}\frac{g_{VV'P}\,g_{V'\gamma}}{M_{V'}^2 - q^2}\,, \tag{9.6}$$

where $g_{VV'P}$ are the vector-vector-pseudoscalar couplings, $g_{V'\gamma}$ the vector-photon conversion couplings and $M_{V'}$ the intermediate vector masses. In the $SU(3)$-flavour symmetry and OZI-rule respecting limits, one could express all the $g_{VP\gamma}$ in terms of a single coupling constant g and $SU(3)$-group factors [231]. On the other hand, in the context of RχT, for instance, the $VP\gamma$ effective vertex is made of a local $VP\gamma$ vertex weighted by a coupling constant, h_V, and a non-local one built from the exchange of an intermediate vector weighted by a second coupling constant, σ_V, times the vector-photon conversion factor f_V [232]

$$g_{VP\gamma}\,\hat{F}_{VP\gamma}(q^2) = C_{VP\gamma}|e|\frac{4\sqrt{2}\,h_V}{f_\pi}\left(1 + \frac{\sigma_V f_V}{\sqrt{2}\,h_V}\frac{q^2}{M_{V'}^2 - q^2}\right), \tag{9.7}$$

where $C_{VP\gamma}$ are $SU(3)$-group factors. Notwithstanding this, and down to the fact that the outgoing photons in $\eta^{(\prime)} \to \pi^0\gamma\gamma$ and $\eta' \to \eta\gamma\gamma$ are on-shell, the energy dependence of the vertex form factors vanish in either model and the corresponding couplings become just constants [233]. As has just been explained, in the approach followed in this chapter we extract the values for these coupling constants directly from experiment not relying on any specific model [231, 232], rendering our theoretical treatment of vector exchanges rather model independent.

[3] Should q^2 be timelike, that is $q^2 > 0$, then an imaginary part would need to be added to the propagator; this introduces the associated resonance width effects and rids the propagator from its divergent behaviour.

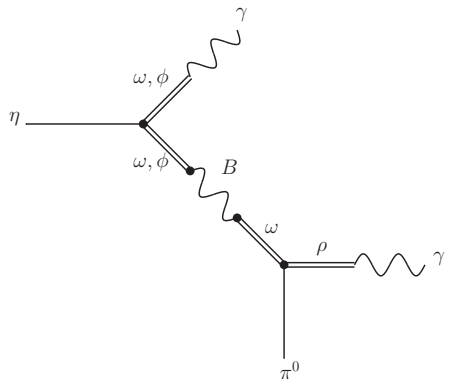

FIGURE 9.1: Schematic diagram of the B-boson exchange mechanism for the decay $\eta \to \pi^0\gamma\gamma$.

Moving on to the effects of scalar resonance exchanges on the decays under study, they were explicitly assessed in Chapter 8 making use of the LσM, and it was found that the scalar contributions are subdominant, whilst the exchange of vector resonances largely dominate. Accordingly, it has been deemed not necessary to employ a more sophisticated theoretical treatment, such as dispersive methods (see e.g. Refs. [97, 98]), to analyse the effect of the scalar exchanges. This, of course, would not be possible for processes where the contribution from scalar resonances is dominant, for instance in $\phi \to \eta\pi^0\gamma$ [96, 234], and an improved theoretical treatment would, therefore, be required in these cases.

9.2.2 Beyond the Standard Model: B-boson contribution

In analogy to the VMD contributions summarised in the previous subsection, we next define the framework to include intermediate B-boson exchanges to the decay amplitude.

The diagrammatic representation of the decay process is depicted in Fig. 9.1 for the $\eta \to \pi^0\gamma\gamma$ case.[4] This contribution can be assessed from the conventional VMD VVP and $V\gamma$ Lagrangians (cf. Secs. 3.5.1 and 3.5.2)

$$\begin{aligned} \mathcal{L}_{VVP} &= \frac{G}{\sqrt{2}}\epsilon^{\mu\nu\alpha\beta}\mathrm{Tr}\left[\partial_\mu V_\nu \partial_\alpha V_\beta P\right], \\ \mathcal{L}_{V\gamma} &= -4egf_\pi^2 A^\mu \mathrm{Tr}\left[QV_\mu\right], \end{aligned} \tag{9.8}$$

where $G = 3g^2/4\pi^2 f_\pi$, V^μ and P are the matrices for the nonet of vector and pseudoscalar meson fields, respectively, A^μ is the photon field, and $Q = \mathrm{diag}\{2/3, -1/3, -1/3\}$ is the quark-charge matrix, supplemented by an effective Lagrangian that describes the VB interaction. The latter is formally identical to the $V\gamma$ Lagrangian in Eq. (9.8) with the substitutions $A^\mu \to B^\mu$, $e \to g_B$ and $Q \to \mathrm{diag}\{1/3, 1/3, 1/3\}$, and it is given by

$$\mathcal{L}_{VB} = -4\frac{1}{3}g_B g f_\pi^2 B^\mu \mathrm{Tr}\left[V_\mu\right]. \tag{9.9}$$

From the VVP and VB Lagrangians in Eqs. (9.8) and (9.9), respectively, along with the corresponding V-meson propagators, it is straightforward to obtain expressions for the $g_{BP\gamma}$ couplings in terms of the generic B-boson coupling g_B. The $g_{BP\gamma}$ couplings are energy

[4] It should be mentioned that the same diagram where the B boson is replaced by a photon also exists. However, this is not considered in the present analysis given that this contribution is highly suppressed with respect to the intermediate vector exchanges that has already been considered in Sec. 9.2.1 and introduces unnecessary complexity.

dependent and read

$$\begin{aligned} g_{B\pi^0\gamma}(q^2) &= \frac{eg_B}{4\pi^2 f_\pi} F_\omega(q^2)\,, \\ g_{B\eta\gamma}(q^2) &= \frac{eg_B}{12\pi^2 f_\pi}\left[c\phi_P F_\omega(q^2) + \sqrt{2}s\phi_P F_\phi(q^2)\right], \\ g_{B\eta'\gamma}(q^2) &= \frac{eg_B}{12\pi^2 f_\pi}\left[s\phi_P F_\omega(q^2) - \sqrt{2}c\phi_P F_\phi(q^2)\right], \end{aligned} \tag{9.10}$$

where ϕ_P is the η-η' mixing angle in the quark-flavour basis [138] and the abbreviations $c\phi_P \equiv \cos\phi_P$ and $s\phi_P \equiv \sin\phi_P$ have been employed. The functions $F_V(q^2)$ in the previous equations are form factors that account for the ω and ϕ propagation, and are given by

$$F_V(q^2) = \frac{M_V^2}{M_V^2 - q^2 - iM_V\Gamma_V}\,. \tag{9.11}$$

Combining the $g_{B\pi^0\gamma}$ and $g_{B\eta\gamma}$ couplings from Eq. (9.10) with the propagator of the B-boson, allows one to find the B-boson exchange contribution to the $\eta \to \pi^0\gamma\gamma$ amplitude

$$\mathcal{A}^{B\,\text{boson}}_{\eta\to\pi^0\gamma\gamma} = g_{B\eta\gamma}(t)g_{B\pi^0\gamma}(t)\left[\frac{(P\cdot q_2 - M_\eta^2)\{a\} - \{b\}}{D_B(t)} + \left\{ \begin{array}{c} q_2 \leftrightarrow q_1 \\ t \leftrightarrow u \end{array} \right\}\right], \tag{9.12}$$

where $D_B(q^2) = m_B^2 - q^2 - im_B\Gamma_B$ is the B-boson propagator. The B-boson contribution to the amplitudes of the $\eta' \to \pi^0\gamma\gamma$ and $\eta' \to \eta\gamma\gamma$ decays have a similar structure to that of Eq. (9.12) with the replacements $M_\eta^2 \to M_{\eta'}^2$, and $g_{B\eta\gamma}g_{B\pi^0\gamma} \to g_{B\eta'\gamma}g_{B\pi^0\gamma}$ for the $\eta' \to \pi^0\gamma\gamma$ and $g_{B\eta\gamma}g_{B\pi^0\gamma} \to g_{B\eta'\gamma}g_{B\eta\gamma}$ for the $\eta' \to \eta\gamma\gamma$.

The decay widths for the radiative transitions $\eta^{(\prime)} \to B\gamma$ and $B \to \pi^0\gamma, \eta^{(\prime)}\gamma$ can be calculated from Eq. (9.10) and the analogous to Eq. (9.5). They are given by

$$\begin{aligned} \Gamma_{\eta\to B\gamma} &= \frac{\alpha_{em}\alpha_B M_\eta^3}{288\pi^3 f_\pi^2}\left(1 - \frac{m_B^2}{M_\eta^2}\right)^3 \times \left[c\phi_P F_\omega(m_B^2) + \sqrt{2}s\phi_P F_\phi(m_B^2)\right]^2, \\ \Gamma_{\eta'\to B\gamma} &= \frac{\alpha_{em}\alpha_B M_{\eta'}^3}{288\pi^3 f_\pi^2}\left(1 - \frac{m_B^2}{M_{\eta'}^2}\right)^3 \times \left[s\phi_P F_\omega(m_B^2) - \sqrt{2}c\phi_P F_\phi(m_B^2)\right]^2, \end{aligned} \tag{9.13}$$

for the B production from $\eta^{(\prime)}$ decays and

$$\begin{aligned} \Gamma_{B\to\pi^0\gamma} &= \frac{\alpha_{em}\alpha_B m_B^3}{96\pi^3 f_\pi^2}\left(1 - \frac{M_\pi^2}{m_B^2}\right)^3 |F_\omega(m_B^2)|^2, \\ \Gamma_{B\to\eta\gamma} &= \frac{\alpha_{em}\alpha_B m_B^3}{864\pi^3 f_\pi^2}\left(1 - \frac{M_\eta^2}{m_B^2}\right)^3 \times \left[c\phi_P F_\omega(m_B^2) + \sqrt{2}s\phi_P F_\phi(m_B^2)\right]^2, \\ \Gamma_{B\to\eta'\gamma} &= \frac{\alpha_{em}\alpha_B m_B^3}{864\pi^3 f_\pi^2}\left(1 - \frac{M_{\eta'}^2}{m_B^2}\right)^3 \times \left[s\phi_P F_\omega(m_B^2) - \sqrt{2}c\phi_P F_\phi(m_B^2)\right]^2, \end{aligned} \tag{9.14}$$

for the B-boson decays. The leptonic decays arise from the kinetic mixing of the B boson with the photon, cf. Eq. (9.1), and read [197]

$$\Gamma_{B\to\ell^+\ell^-} = \frac{\alpha_{em}\varepsilon^2 m_B}{3}\left(1 + \frac{2m_\ell^2}{m_B^2}\right)\sqrt{1 - \frac{4m_\ell^2}{m_B^2}}, \tag{9.15}$$

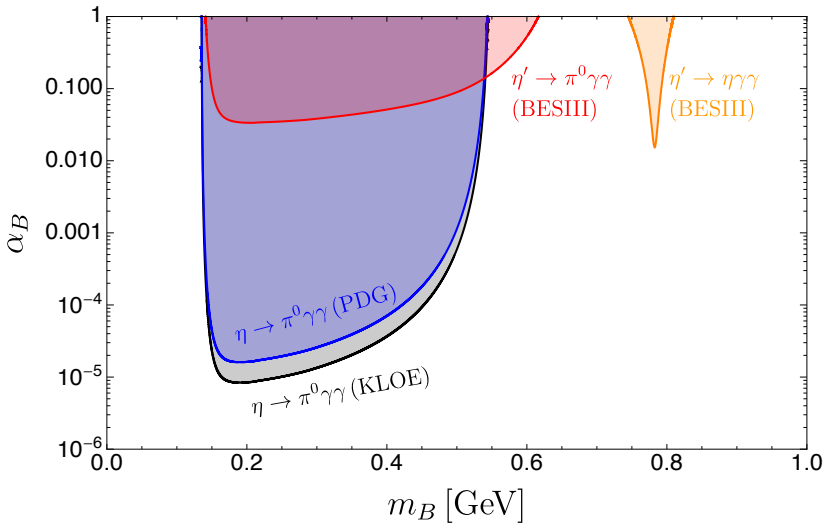

FIGURE 9.2: Limits on the leptophobic $U(1)_B$-boson parameters α_B and m_B from the $\eta \to \pi^0\gamma\gamma$ BR measured by KLOE [182] (black line) and the value reported by the PDG [1] (blue line). Also shown are the limits from the BESIII measurements of $\eta' \to \pi^0\gamma\gamma$ (red line) [172] and $\eta' \to \eta\gamma\gamma$ (orange line) [173]. Following the approach of Ref. [197], the SM contribution is set to zero in all cases and the NWA is applied. The shaded regions are excluded.

whilst the B-boson decay to $\pi^+\pi^-$, which also depends on ε, is given by [197]

$$\Gamma_{B\to\pi^+\pi^-} = \frac{\alpha_{em}\varepsilon^2 m_B}{12}\left(1-\frac{4M_\pi^2}{m_B^2}\right)^{3/2}|F_\pi(m_B^2)|^2\,, \tag{9.16}$$

where $F_\pi(q^2)$ is the pion vector form factor. Finally, for the three-body decay $\Gamma_{B\to\pi^+\pi^-\pi^0}$ we make use of the following amplitude

$$\mathcal{A}^{B\,\text{boson}}_{B\to\pi^+\pi^-\pi^0} = \frac{g^2 g_B}{\pi^2 f_\pi}\epsilon_{\mu\nu\alpha\beta}\left(\frac{p_+^\mu p_-^\nu p_0^\alpha}{D_{\rho^0}(s)}+\frac{p_-^\mu p_0^\nu p_+^\alpha}{D_{\rho^-}(t)}+\frac{p_0^\mu p_+^\nu p_-^\alpha}{D_{\rho^+}(u)}\right)\varepsilon^\beta F_\omega(m_B^2)\,, \tag{9.17}$$

where ε_β is the polarisation vector of the B boson, $D_\rho(q^2)$ is the ρ propagator with energy-dependent width defined in Eq. (9.4), p_+, p_- and p_0 are the four-momentum vectors associated to the π^+, π^- and π^0, respectively, and the Mandelstam variables s, t and u are defined, in this instance, as $s=(p_++p_-)^2$, $t=(p_-+p_0)^2$ and $u=(p_++p_0)^2$.

9.3 Limits on α_B and m_B

In this section, we make use of the theoretical expressions from Secs. II A and II B, along with the available experimental data, to place limits on the B-boson parameters α_B and m_B.

As a preliminary step, we adopt the approach presented in Ref. [197] with the most up-to-date experimental data to generate limits on the B-boson parameters from the decays under study, $\eta^{(\prime)} \to \pi^0\gamma\gamma$ and $\eta' \to \eta\gamma\gamma$, which are shown in the form of exclusion plots in Fig. 9.2. That approach neglects the SM contribution and uses the NWA to place limits upon requiring that the B-boson contribution does not exceed the total observed branching ratio (BR) at 2σ. The curves for the $\eta \to \pi^0\gamma\gamma$ process come from the (preliminary) value found by the KLOE Collaboration, BR $= (1.23 \pm 0.14) \times 10^{-4}$ [182] (black line), and the BR reported by the PDG, BR $= (2.55 \pm 0.22) \times 10^{-4}$ [1] (blue line); we also show the traces obtained from the BESIII Collaboration measurements for

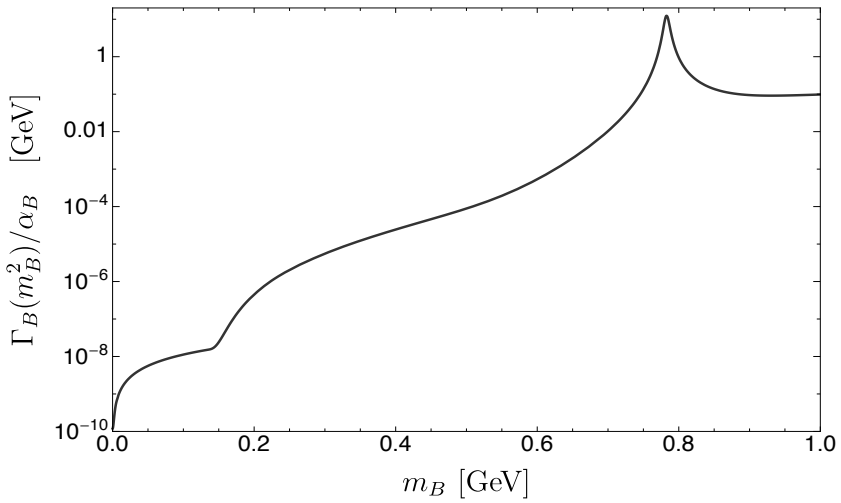

FIGURE 9.3: Normalised width of the B boson, $\Gamma_B(m_B^2)/\alpha_B$, as a function of m_B from Eq. (9.19).

the decays $\eta' \to \pi^0\gamma\gamma$, BR $= (3.20 \pm 0.07 \pm 0.23) \times 10^{-3}$ [172] (red line), and $\eta' \to \eta\gamma\gamma$, BR $= (8.25 \pm 3.41 \pm 0.72) \times 10^{-5}$ [173] (orange line).

The above limits can clearly be improved by including the contribution from the SM in the theoretical treatment. Taking this into account, the amplitude for these decay processes is written as the coherent sum of the vector, scalar and B-boson exchange contributions, $\mathcal{A} = \mathcal{A}_{\rm VMD} + \mathcal{A}_{\rm L\sigma M} + \mathcal{A}_{B\,\rm boson}$ (cf. Chapter 8, and Secs. 9.2.1 and 9.2.2). The corresponding partial decay widths depend on a total of three parameters: i) the baryonic fine-structure constant, α_B, ii) the B-boson mass, m_B, and iii) its total decay width, Γ_B. However, given that Γ_B is not an independent parameter (that is, it can be expressed in terms of α_B and m_B), we can reduce the number of free parameters from three to two. Accordingly, the denominator in Eq. (9.12), $D_B(q^2)$, is replaced by

$$\mathcal{D}_B(q^2) = m_B^2 - q^2 - i\sqrt{q^2}\,\Gamma_B(q^2)\,, \tag{9.18}$$

where $\Gamma_B(q^2) = \sum_i \Gamma_B^i(q^2)$ is the energy-dependent width of the B boson, with the sum running over the partial widths of the various decay channels the B boson can decay into. For our study, we include the partial widths of the decay channels $B \to \pi^0\gamma$, e^+e^-, $\mu^+\mu^-$, and $\pi^+\pi^-$ given, respectively, in Eqs. (9.14–9.16), whilst for the partial width of the $B \to \pi^0\pi^+\pi^-$ we make use of the amplitude in Eq. (9.17) to obtain numerical results after squaring and numerically integrating over its corresponding phase space. The energy-dependent width $\Gamma_B(q^2)$ can, therefore, be written as

$$\begin{aligned}
\Gamma_B(q^2) = {} & \theta(q^2 - M_\pi^2)\frac{\gamma_{B\to\pi^0\gamma}(q^2)}{\gamma_{B\to\pi^0\gamma}(m_B^2)}\Gamma_{B\to\pi^0\gamma} \\
& + \theta(q^2 - 4m_e^2)\frac{\gamma_{B\to e^+e^-}(q^2)}{\gamma_{B\to e^+e^-}(m_B^2)}\Gamma_{B\to e^+e^-} \\
& + \theta(q^2 - 4m_\mu^2)\frac{\gamma_{B\to \mu^+\mu^-}(q^2)}{\gamma_{B\to \mu^+\mu^-}(m_B^2)}\Gamma_{B\to \mu^+\mu^-} \\
& + \theta(q^2 - 4M_\pi^2)\frac{\gamma_{B\to \pi^+\pi^-}(q^2)}{\gamma_{B\to \pi^+\pi^-}(m_B^2)}\Gamma_{B\to \pi^+\pi^-} \\
& + \theta(q^2 - 9M_\pi^2)\frac{\gamma_{B\to \pi^+\pi^-\pi^0}(q^2)}{\gamma_{B\to \pi^+\pi^-\pi^0}(m_B^2)}\Gamma_{B\to \pi^+\pi^-\pi^0}\,,
\end{aligned} \tag{9.19}$$

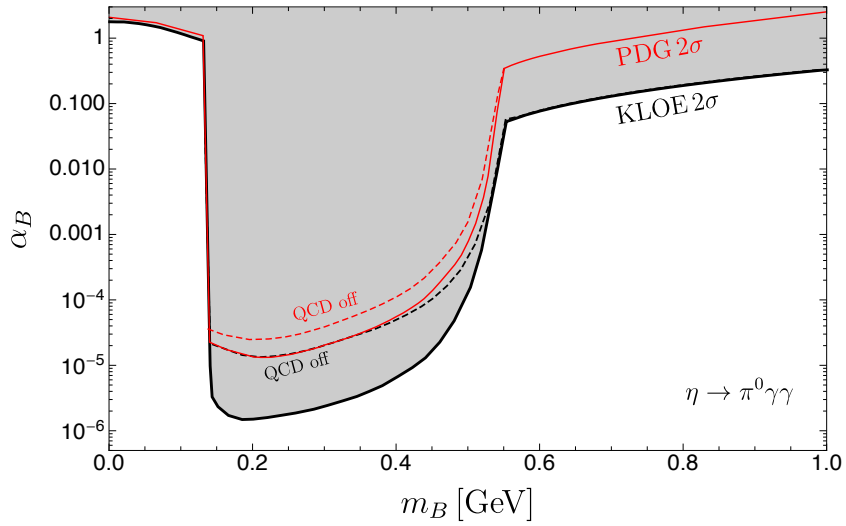

FIGURE 9.4: Limits on the leptophobic B-boson coupling α_B for different m_B masses from the $\eta \to \pi^0\gamma\gamma$ BR measurements by KLOE [182] (black line) and the PDG [1] (red line). The grey shaded region is excluded by KLOE and the dashed lines correspond to the limits with the QCD contributions turned off.

where the $\gamma_i(q^2)$ parameters are given by the following expressions

$$\begin{aligned}
\gamma_{B\to\pi^0\gamma}(q^2) &= (q^2)^{3/2}\left(1-\frac{M_\pi^2}{q^2}\right)^3 |F_\omega(q^2)|^2\,,\\
\gamma_{B\to\ell^+\ell^-}(q^2) &= \sqrt{q^2}\left(1+\frac{2m_\ell^2}{q^2}\right)\sqrt{1-\frac{4m_\ell^2}{q^2}}\,,\\
\gamma_{B\to\pi^+\pi^-}(q^2) &= \sqrt{q^2}\left(1-\frac{4M_\pi^2}{q^2}\right)^{3/2} |F_\pi(q^2)|^2\,,
\end{aligned} \tag{9.20}$$

whilst $\gamma_{B\to\pi^+\pi^-\pi^0}(q^2)$ must be evaluated numerically. In Fig. 9.3, the total normalised width $\Gamma_B(m_B^2)/\alpha_B$ is plotted as a function of m_B.

Next, we proceed to calculate the constraints on the B-boson parameters α_B and m_B set by experiment. We start with the $\eta \to \pi^0\gamma\gamma$ decay using the PDG reported value, $\text{BR} = (2.55 \pm 0.22) \times 10^{-4}$ [1], as well as the (preliminary) value from the KLOE Collaboration, $\text{BR} = (1.23 \pm 0.14) \times 10^{-4}$ [182] (see also Ref. [183]). In Fig. 9.4, we show the limits in the α_B-m_B plane, which are found by requiring our predictions to not exceed the corresponding branching ratios at 2σ. The grey area is excluded by the data from KLOE, which yield a more stringent limit than the resulting one from the PDG (solid red line). This is as expected given that the BR from KLOE is found to be in good agreement with our SM prediction from Chapter 8, $\text{BR} = (1.35 \pm 0.08) \times 10^{-4}$, and thus the KLOE constraints on the B boson turn out to be stronger. The dashed black line in the figure is found using the data from KLOE but with the SM (or, equivalently, QCD) contributions set to zero. Clearly, these contributions are not negligible as the limits on α_B become an order of magnitude weaker when their effects are turned off (labelled QCD off in the plots). The uncertainty in the exclusion limits associated to the systematic errors of our theoretical treatment is presented in Appendix D.

The shape and size of the excluded region in Fig. 9.4 contains key physical information. In this figure, three different regions can be identified. The first one corresponds to

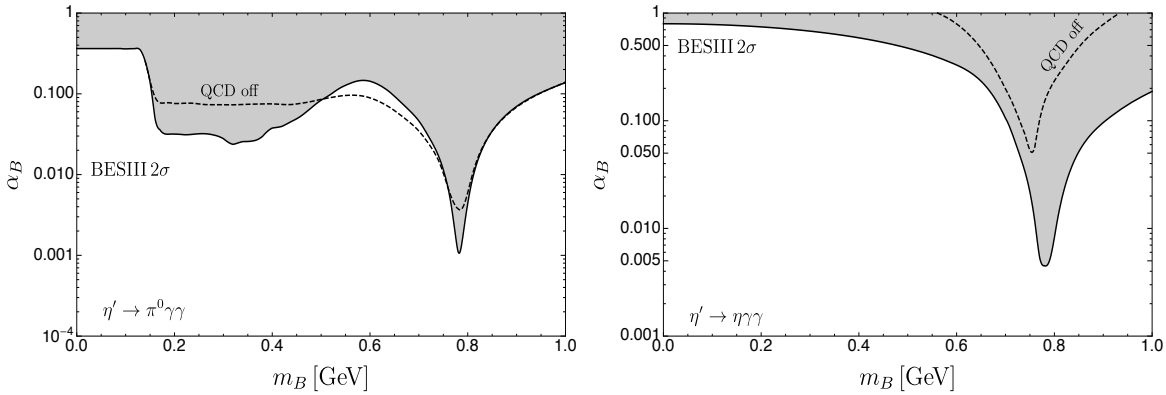

FIGURE 9.5: Limits on the leptophobic B-boson coupling α_B for different m_B masses from the BR measurements of the decays $\eta' \to \pi^0\gamma\gamma$ (left plot) [172] and $\eta' \to \eta\gamma\gamma$ (right plot) [173] by BESIII. The grey shaded region is excluded and the dashed black line corresponds to the limit with the QCD contributions set to zero.

$m_B \lesssim M_{\pi^0}$, where $\alpha_B \sim \mathcal{O}(1)$. At $m_B \sim M_{\pi^0}$, the limit placed on the coupling plummets by almost six orders of magnitude down to $\alpha_B \sim 10^{-6}$; it then moderately increases, to finally take a steep rise when m_B approaches M_η, reaching $\alpha_B \sim 10^{-2}$. Finally, for $m_B \gtrsim M_\eta$ the constraint on the coupling grows very smoothly as m_B increases. Out of the three, the $M_{\pi^0} \lesssim m_B \lesssim M_\eta$ region deserves special attention and raises the question as to why α_B is constrained so strongly there. The answer to this is related to the fact that the B-boson width is extremely small in this region of parameter space.

Let us investigate this effect in more detail. By noticing from Fig. 9.3 that within the $M_{\pi^0} \lesssim m_B \lesssim M_\eta$ mass range the NWA is valid, it allows us to write the squared modulus of the B-boson propagator as $\pi/(m_B\Gamma_B)\delta(t - m_B^2)$, under the phase-space integral. For a B boson whose squared mass falls within the kinematic space for the t variable, i.e. $t_{\min} \leq m_B^2 \leq t_{\max}$, the phase-space integral over dt places the B boson on-shell and one is allowed to write

$$\Gamma(\eta \to \pi^0\gamma\gamma) \propto \int \frac{\alpha_B^2\, dt}{|\mathcal{D}_B(t)|^2} \to \frac{\alpha_B^2\, \pi}{m_B\, \Gamma_B(m_B^2)}\,. \tag{9.21}$$

As it can be seen in Fig. 9.3, $\Gamma_B(m_B^2)/\alpha_B$ is very small within the kinematic region of interest for the present discussion (i.e. $M_{\pi^0} \lesssim m_B \lesssim M_\eta$), which, in the $\Gamma_B(t)/\alpha_B \to 0$ limit, forces $\alpha_B \to 0$ so that $\Gamma(\eta \to \pi^0\gamma\gamma)$ remains finite.

Next, we show the exclusion plots associated to the two η' decays in Fig. 9.5. On the left-hand side, we display the region of the α_B-m_B plane excluded by the BESIII Collaboration $\eta' \to \pi^0\gamma\gamma$ measurement, BR $= (3.20 \pm 0.07 \pm 0.23) \times 10^{-3}$ [172], and, on the right-hand side, the corresponding one for the $\eta' \to \eta\gamma\gamma$, BR $= (8.25 \pm 3.41 \pm 0.72) \times 10^{-5}$ [173], both at a confidence level of 2σ.

The shape of the excluded region for the $\eta' \to \pi^0\gamma\gamma$ is clearly different to that of the $\eta \to \pi^0\gamma\gamma$ decay (cf. Fig. 9.4). In particular, the limits within the $M_{\pi^0} \lesssim m_B \lesssim M_\eta$ mass range, whilst still showing the shape resembling a keel, are about 4 orders of magnitude weaker than those coming from $\eta \to \pi^0\gamma\gamma$. There are two contributing effects required to explain this. On the one hand, there are inherent dynamical differences in the B-boson production of the two decays [cf. Eq. (9.13)]. On the other hand, there are kinematic influences that also need to be accounted for. Specifically, if one applies the NWA to both the B boson[5]

[5]This approximation is reasonable for $m_B \lesssim 600$ MeV, as can be checked in Fig. 9.3. Beyond this point, the use of the NWA may be questionable. As we are only attempting to provide a qualitative explanation, this limitation does not really concern us here.

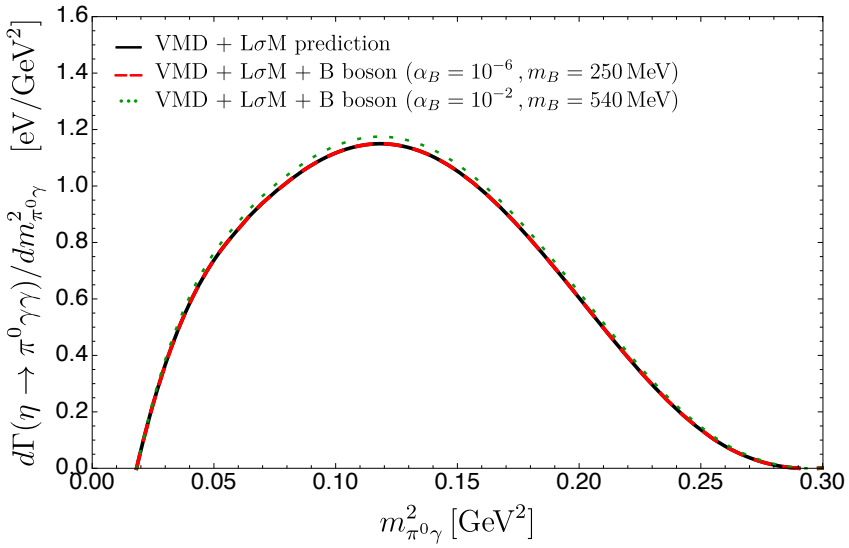

FIGURE 9.6: $m^2_{\pi^0\gamma}$ distribution for the $\eta \to \pi^0\gamma\gamma$ decay using our theoretical SM (VMD and LσM) prediction from Chapter 8 and Ref. [165] (solid black line). Also shown are the spectra including the B-boson contribution using the two sets of representative values for α_B and m_B from Eqs. (9.22) (dashed red line) and (9.23) (dotted green line).

and ω propagators, a factor like $\delta(t - m_B^2)\delta(t - M_\omega^2)$ is obtained, which under the phase-space integral results in $\delta(M_\omega^2 - m_B^2)$.[6] This Dirac delta suppresses the contribution of the B boson to the decay process when $m_B \not\approx M_\omega$ and, hence, forces the exclusion limit to be weaker in this region. In contrast, the B-boson contribution is largely amplified when $m_B \approx M_\omega$ and, therefore, the exclusion limit becomes much stronger in this area, which will make it difficult to experimentally identify a B boson with a mass around the pole of the ω resonance. The region $M_\eta \lesssim m_B \lesssim M_\omega$ is less constrained and, thus, appears to be a good place to look for an enhancement in the $\pi^0\gamma$ invariant mass spectrum.

The limits from the $\eta' \to \eta\gamma\gamma$ process (right plot in Fig. 9.5) in the $m_B \gtrsim M_\eta$ region are similar to the ones from $\eta' \to \pi^0\gamma\gamma$. Notwithstanding this, the keel shape appearing in the $M_{\pi^0} \lesssim m_B \lesssim M_\eta$ mass range of the $\eta \to \pi^0\gamma\gamma$ and $\eta' \to \pi^0\gamma\gamma$ exclusion plots is missing in the $\eta' \to \eta\gamma\gamma$ one, which is down to the fact that the phase space of the latter does not allow the B boson to resonate in this range of B-boson masses and, therefore, the constraints turn out to be weaker.

All in all, the $\eta' \to \pi^0\gamma\gamma$ and $\eta' \to \eta\gamma\gamma$ decays do not appear to be as powerful as the $\eta \to \pi^0\gamma\gamma$ at constraining the B-boson parameters.

The smoking gun signature of a B boson in the $M_{\pi^0} \lesssim m_B \lesssim M_\eta$ region would be the observation of a peak around m_B in the $\pi^0\gamma$ invariant mass distribution. In Fig. 9.6, we show the quantitative effect of a B boson on the $\eta \to \pi^0\gamma\gamma$ decay using two sets of representative values for α_B and m_B from the not-excluded region of parameter space

$$\alpha_B = 10^{-6} \quad m_B = 250\,\text{MeV}\,, \tag{9.22}$$

and

$$\alpha_B = 10^{-2} \quad m_B = 540\,\text{MeV}\,. \tag{9.23}$$

In this figure, the solid black line corresponds to our SM prediction from Chapter 8, whereas the effect of including the B boson is shown by the dashed red and dotted green lines for

[6] There is no need to consider the ϕ propagator given that the available phase space does not allow the ϕ to resonate.

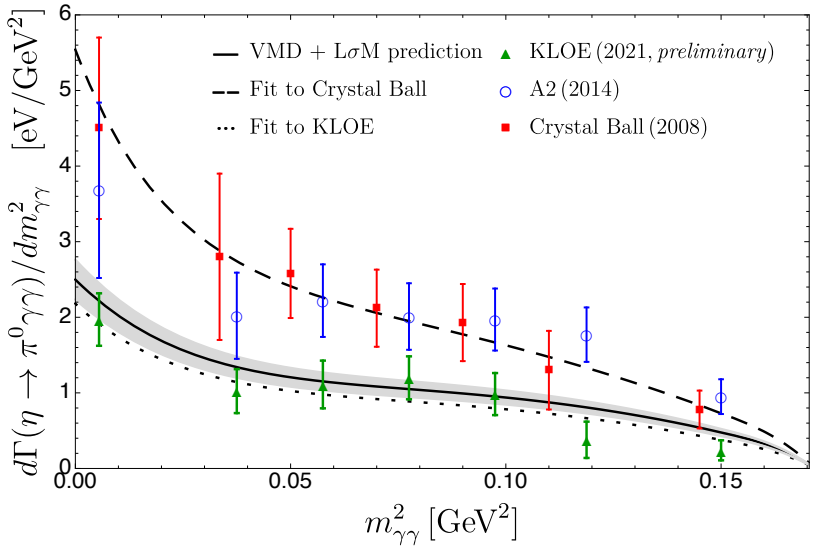

FIGURE 9.7: KLOE (green triangles) [183], A2 (blue circles) [181] and Crystal Ball (red squares) [177] measurements of the $m^2_{\gamma\gamma}$ spectrum for the $\eta \to \pi^0\gamma\gamma$ decay. Also shown is our SM (VMD and LσM) prediction from Chapter 8 and Ref. [165] (solid black line), as well as our SM with B-boson predictions using the fitted parameters from Eqs. (9.24) and (9.25).

the two sets of α_B and m_B values from Eqs. (9.22) and (9.23), respectively. As it can be seen, the differences in the distribution introduced by the B-boson contribution are very small and it is very difficult to distinguish the associated lines from the SM prediction. That is, the allowed values for α_B in the $M_{\pi^0} \lesssim m_B \lesssim M_\eta$ region are so small that it makes the B-boson signal strongly suppressed, rendering the task of experimentally identifying it nearly impossible. For this reason, a B boson in the mass range $M_{\pi^0} \lesssim m_B \lesssim M_\eta$ cannot explain the normalisation offset that appears to be affecting the experimental $\gamma\gamma$ invariant mass distribution from the A2 [181] and Crystal Ball [177] Collaborations with respect to our VMD and LσM prediction.

Let us now to perform statistical fits to the available experimental diphoton spectra to determine the region of the α_B-m_B plane (cf. Fig. 9.4) that is preferred by the data. From the Crystal Ball $\gamma\gamma$ invariant mass spectrum [177], we obtain the following best fit values

$$\alpha_B = 0.40^{+0.07}_{-0.08}\,, \quad m_B = 583^{+32}_{-20}\,\text{MeV}\,, \tag{9.24}$$

with a $\chi^2_{\text{min}}/\text{d.o.f} = 0.42/5 = 0.08$, whereas for the KLOE (preliminary) data [183][7] we find

$$\alpha_B = 0.049^{+0.040}_{-0.027}\,, \quad m_B = 135^{+1}_{-135}\,\text{MeV}\,, \tag{9.25}$$

with a $\chi^2_{\text{min}}/\text{d.o.f} = 4.46/5 = 0.89$.[8] Because of the large errors associated to the experimental points from Crystal Ball, its χ^2_{min}/d.o.f turns out to be extremely small. The χ^2_{min}/d.o.f of the fit to the KLOE data implies a good quality of the fit. The errors associated to the fitted parameters have been estimated by perturbing one of the parameters at a time such that

[7] Whilst KLOE has published a BR for the $\eta \to \pi^0\gamma\gamma$ process in a conference proceedings [182], the diphoton spectrum has not yet been published, although it was presented at The 10$^{\text{th}}$ International Workshop on Chiral Dynamics 2021 [183]. For our analysis, we have retrieved the data points from their presentation's figure. We thank KLOE for the email communications [235].

[8] We also carried out fits to the A2 data but did not find convergent solutions using two free parameters. When fits were attempted using the B-boson width as an additional free parameter, good convergence was achieved though.

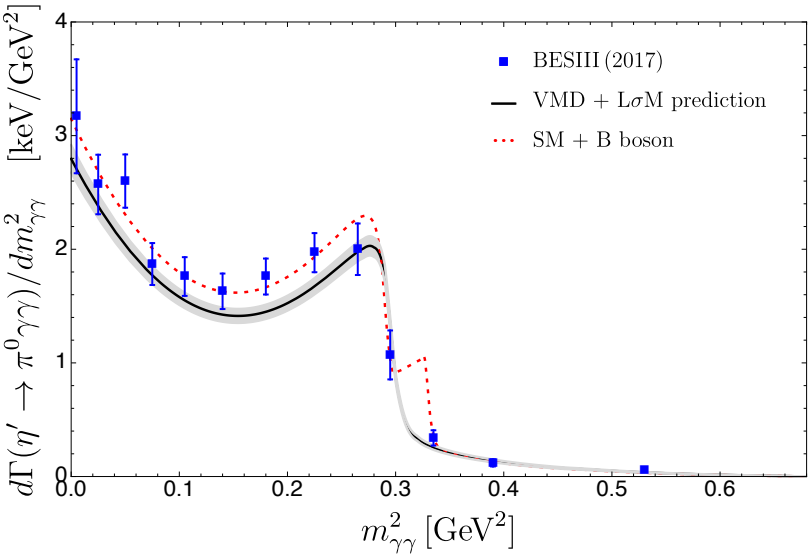

FIGURE 9.8: BESIII (blue squares) [172] measurements of the $m^2_{\gamma\gamma}$ spectrum for the $\eta' \to \pi^0\gamma\gamma$ decay. Also show is our SM (VMD and LσM) prediction from Chapter 8 and Ref. [165] (solid black line), as well as our SM with B-boson prediction using the fitted parameters from Eq. (9.26) (dotted red line).

$\chi^2 = \chi^2_{\text{min}} + 1$ [1]. The theoretical $\gamma\gamma$ invariant mass spectra using the parameters from the fits in Eqs. (9.24) and (9.25) to the Crystal Ball and KLOE data are shown in Fig. 9.7 with dashed and dotted black lines, respectively. Also plotted are the experimental data points and our SM prediction [165] (solid black line) with an estimation of the uncertainty from the error propagation of the $VP\gamma$ couplings. The different individual contributions to the invariant mass spectra are shown in Appendix E.1. It is worth noticing that the inclusion of a non-resonant B boson in the t- and u-channels, with parameters from Eq. (9.24), helps explain the tension between the Crystal Ball spectrum and our SM result [165]. Notwithstanding this, the best fit parameters from Crystal Ball in Eq. (9.24) are ruled out by the KLOE data (cf. Fig. 9.4), whose measured BR continues the decreasing trend seen over the decades associated to more precise measurements becoming available (see Ref. [196]). In turn, this trend supports the theoretical treatment without a B boson, as our VMD and LσM approach from Chapter 8 (cf. Ref. [165]) appears to be capable of successfully predicting the experimental data for the three $\eta^{(\prime)} \to \pi^0\gamma\gamma$ and $\eta' \to \eta\gamma\gamma$ decays simultaneously. Clearly, the experimental situation is far from conclusive and it may not be possible to make categorical statements about the need for a B boson until the arrival of new and more precise data, e.g. from the KLOE(-II) and JEF [225] experiments.

Next, we perform fits to the $\eta' \to \pi^0\gamma\gamma$ diphoton spectrum from the BESIII Collaboration [172], which may be used to explore larger B-boson masses. No distribution data is available for the $\eta' \to \eta\gamma\gamma$ process, so the constraints from this channel come from the branching ratio only (see Fig. 9.5). The fit to the $\eta' \to \pi^0\gamma\gamma$ data yields

$$\alpha_B = 0.005(1)\,, \quad m_B = 759(1)\ \text{MeV}\,, \tag{9.26}$$

with $\chi^2_{\text{min}}/\text{d.o.f} = 11.73/11 = 1.07$. The distribution using the fitted parameters from Eq. (9.26) is shown in Fig. 9.8 (dotted red line), together with the experimental data (blue squares) and our SM prediction [165] (solid black line) with an estimation of its uncertainty. It is worth noticing the sudden drop in the dotted red line (i.e. SM with B-boson distribution)

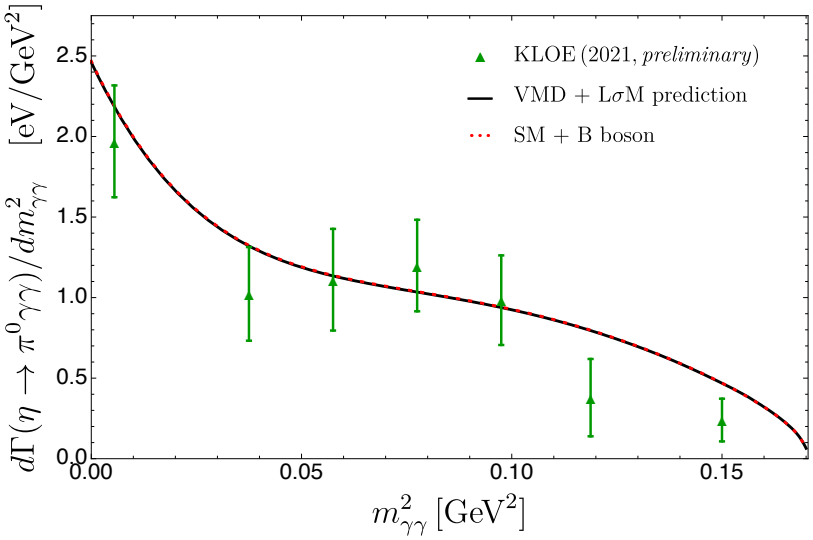

FIGURE 9.9: KLOE measurements (green triangles) [183] of the $m^2_{\gamma\gamma}$ spectrum for the $\eta \to \pi^0\gamma\gamma$ decay together with our SM (VMD and LσM) prediction from Chapter 8 and Ref. [165] (solid black line). Also shown is our SM with B-boson prediction using the fitted parameters from Eq. (9.27) (dotted red line).

at $m^2_{\gamma\gamma} \approx 0.33$ GeV^2.[9] What is interesting about this is that, even though the $\chi^2_{\rm min}/{\rm d.o.f}$ of this fit is very good, the associated integrated branching ratio deviate from the experimental counterpart due to the effect of the wiggle on the distribution. Also, the spectrum using the fit parameters would lead to larger than observed bin values for the experimental points 10 and 11. Again, the different individual contributions to the $\gamma\gamma$ invariant mass spectrum are presented in Appendix E.2.

Finally, a joint fit to the experimental invariant mass spectra from KLOE and BESIII for the $\eta \to \pi^0\gamma\gamma$ and $\eta' \to \pi^0\gamma\gamma$ decays, respectively, is carried out. The joint fit yields

$$\alpha_B = 0.005(1)\,, \quad m_B = 759(1)\,\text{MeV}\,, \tag{9.27}$$

with $\chi^2_{\rm min}/{\rm d.o.f} = 19.61/18 = 1.09$.[10] The joint fit produces the same best fit parameters as those from the fit to the $\eta' \to \pi^0\gamma\gamma$ spectrum only. The theoretical distribution for the $\eta \to \pi^0\gamma\gamma$ decay using the parameters from the joint fit is shown in Fig. 9.9 (dotted red line), which turns out to be indistinguishable from that of the SM (solid black line).

To conclude, it is worth highlighting that both our SM and SM with B-boson predictions (using the joint fit parameters for the latter) agree well with both sets of experimental data points. The largest differences between the theoretical predictions still show compatibility

[9] This sudden drop can be understood as follows: so long as $t_{\rm min}(s) \leq m_B^2 \leq t_{\rm max}(s)\ \forall\ s \in [s_{\rm min}, s_{\rm max}]$, then the available phase space allows the B boson to resonate; however, for values of s such that $t_{\rm min}(s) \geq m_B^2$ or $t_{\rm max}(s) \leq m_B^2$, then the B boson no longer resonates and its contribution to the amplitude suddenly plummets producing the sudden drop in the distribution. It must be noted that this effect also applies to the ω meson and is responsible for the sudden drop in the SM distribution around $m^2_{\gamma\gamma} \approx 0.30$ GeV^2. Given that this is a kinematic effect, it will always be present in the spectrum so long as $t_{\rm min}(s_{\rm min}) \leq m_B^2 \leq t_{\rm max}(s_{\rm min})$, although it becomes a relatively small effect and is difficult to detect beyond $m^2_{\gamma\gamma} \gtrsim 0.4$ GeV^2 for this particular decay.

[10] There is a secondary local minimum giving $\alpha_B = 5(2) \times 10^{-4}$ and $m_B = 780^{+3}_{-4}$ MeV, with $\chi^2_{\rm min}/{\rm d.o.f} = 23.71/18 = 1.32$. These values for the α_B and m_B parameters yield a B-boson width of $\Gamma_B \approx 5.1$ MeV. For this particular solution, both m_B and Γ_B are effectively the same as those of the ω vector meson. Accordingly, the end effect is to enhance the spectrum with respect to the SM prediction for $m^2_{\gamma\gamma} \lesssim 0.30$ GeV^2, where the available phase space allows both the ω and B boson to resonate, and has no effect on the spectrum beyond this point, i.e. $m^2_{\gamma\gamma} \gtrsim 0.30$ GeV^2.

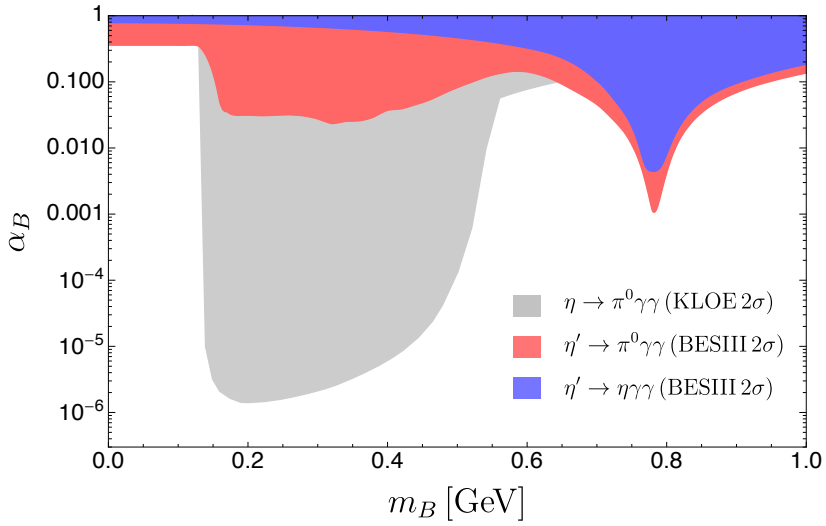

FIGURE 9.10: Limits on the leptophobic B-boson mass m_B and coupling α_B from the branching ratio measurements of the decays $\eta \to \pi^0\gamma\gamma$ (grey) by KLOE [182], and $\eta' \to \pi^0\gamma\gamma$ (red) [172] and $\eta' \to \eta\gamma\gamma$ (blue) [173] by BESIII.

at roughly the 1σ level. We, therefore, conclude that the experimental data from KLOE and BESIII for the $\eta \to \pi^0\gamma\gamma$ and $\eta' \to \pi^0\gamma\gamma$ decays, respectively, do not require a B-boson contribution, in spite of the coupling α_B being clearly non-zero.

This conclusion differs from that of the study in Ref. [236], where it is argued that the simultaneous prediction of the three processes under study may require the presence of a leptophobic B boson, which in turn was motivated by some of the conclusions from our previous work in Ref. [165] (cf. Chapter 8). It should be noted, though, that in Ref. [236] the B-boson mass and width were manually fixed to some values that the author deemed reasonable, leaving the $g_{BP\gamma}$ couplings as free constant parameters that were subsequently fitted to the experimental data. Contrary to this, in the work presented in this chapter Γ_B is not an independent variable but a function of both α_B and m_B (under the assumption that the B boson decays to SM particles only), which are then left as free parameters in our fits. It is worth noting that in our analysis the $g_{BP\gamma}$ couplings are not constant but energy dependent. More importantly, Ref. [236] did not employ the most recent experimental data for the $\eta \to \pi^0\gamma\gamma$ decay from the KLOE Collaboration [183] in his analysis.

9.4 Conclusions

We have analysed in detail the sensitivity of the rare decays $\eta^{(\prime)} \to \pi^0\gamma\gamma$ and $\eta' \to \eta\gamma\gamma$ to a leptophobic $U(1)_B$ boson in the MeV–GeV mass range. Adding the explicit B-boson exchange contribution in the t- and u-channels, in addition to our SM (VMD and LσM) amplitudes, has allowed us to place stringent limits on the B-boson parameters m_B and α_B by comparing with current experimental data. A visual summary of these limits is shown below in Fig. 9.10. From the individual analysis of the $\eta \to \pi^0\gamma\gamma$ decay, we have strengthened by one order of magnitude the current constraints in the resonant mass region $M_{\pi^0} \lesssim m_B \lesssim M_\eta$, reaching $\alpha_B \sim 10^{-6}$, as it can be seen in this figure. These constraints would make a B-boson signature strongly suppressed, rendering the task of experimentally identifying it as a peak around m_B in the $\pi^0\gamma$ invariant mass distribution practically impossible.

Our analysis of the most recent experimental $\gamma\gamma$ invariant mass distribution from the KLOE Collaboration supports the description of the processes studied in this chapter without

contribution from a potential new leptophobic B boson, as our VMD and LσM treatment is capable of simultaneously predicting the three $\eta^{(\prime)} \to \pi^0\gamma\gamma$ and $\eta' \to \eta\gamma\gamma$ decays with remarkable agreement with the experimental data. However, a B boson with a mass $m_B \gtrsim M_\eta$ and non-negligible coupling α_B may help explain the discrepancy between our SM prediction and the experimental data from the A2 and Crystal Ball Collaborations (see Fig. 9.7). The existing tension between the measurements by different experimental groups does not allow us to make an absolute statement about the need for a B boson, as the branching ratio observed by KLOE, whilst in agreement with our SM prediction, is about a factor of two smaller than those from A2 and Crystal Ball. This highlights the need for new and more precise data, e.g. from the KLOE(-II) and JEF experiments.

Finally, the $\eta' \to \pi^0\gamma\gamma$ and $\eta' \to \eta\gamma\gamma$ decays are not as powerful as the $\eta \to \pi^0\gamma\gamma$ at constraining B-boson parameters below M_η but allow exploring larger B-boson masses. As it can be observed in Fig. 9.10, the region in the α_B-m_B plane near the ω pole shows a sharp dip, which would make the task of identifying a B boson with $m_B \sim M_\omega$ very challenging. However, the mass region $M_\eta \lesssim m_B \lesssim M_\omega$ is less constrained and, thus, appears to be a good place to look for an enhancement in the $\pi^0(\eta)\gamma$ invariant mass distributions, for example, at BESIII or the JEF experiment.

Chapter 10

A theoretical analysis of the semileptonic decays $\eta^{(\prime)} \to \pi^0 l^+ l^-$ and $\eta' \to \eta l^+ l^-$[1]

A complete theoretical analysis of the C-conserving semileptonic decays $\eta^{(\prime)} \to \pi^0 l^+ l^-$ and $\eta' \to \eta l^+ l^-$ ($l = e$ or μ) is carried out within the framework of the VMD model. An existing phenomenological model is used to parameterise the VMD coupling constants and the associated numerical values are obtained from an optimisation fit to $V \to P\gamma$ and $P \to V\gamma$ radiative decays ($V = \rho^0$, ω, ϕ and $P = \pi^0$, η, η'). The decay widths and dilepton energy spectra for the two $\eta \to \pi^0 l^+ l^-$ processes obtained using this approach are compared and found to be in good agreement with other results available in the published literature. Theoretical predictions for the four $\eta' \to \pi^0 l^+ l^-$ and $\eta' \to \eta l^+ l^-$ decay widths and dilepton energy spectra are calculated and presented for the first time in this chapter.

10.1 Introduction

The electromagnetic and strong interactions conserve parity (P) and charge conjugation (C) within the well-established and well-tested Standard Model (SM) of particle physics. In this context, the η and η' pseudoscalar mesons are specially suited for the study of rare decay processes, for instance, in search of C, P and CP violations, as these mesons are C and P eigenstates of the electromagnetic and strong interactions [14].

Specifically, the semileptonic decays $\eta^{(\prime)} \to \pi^0 l^+ l^-$ and $\eta' \to \eta l^+ l^-$ ($l = e$ or μ) are of special interest given that they can be used as fine probes to assess if new physics beyond the Standard Model (BSM) is at play. This is because any contribution from BSM physics ought to be relatively small and the above decay processes only get a contribution from the SM through the C-conserving exchange of two photons that is highly suppressed, as there is no contribution at tree-level but only corrections at one-loop and higher orders. This small SM contribution would presumably be of the same order of magnitude as that of physics BSM, which in turn means that the η-η' phenomenology might play an interesting role and be an excellent arena for stress testing SM predictions [14, 174]. As an example, the $\eta^{(\prime)} \to \pi^0 l^+ l^-$ and $\eta' \to \eta l^+ l^-$ decays could be mediated by a single intermediate virtual photon, but this would entail that the electromagnetic interactions violate C-invariance (e.g. [237, 238]) and, therefore, would represent a departure from the SM.

Early theoretical studies of semileptonic decays of pseudoscalar mesons date back to the late 1960s. A significant contribution was made by Cheng in Ref. [239] where he analysed the $\eta \to \pi^0 e^+ e^-$ decay mediated by a C-conserving, two-photon intermediate state within the VMD framework. By setting the electron mass to $m_e = 0$ and neglecting in the numerator of the amplitude terms that were second or higher order in the electron or positron four-momenta, he found theoretical estimations for the decay width $\Gamma(\eta \to \pi^0 e^+ e^-) = 1.3 \times 10^{-5}$ eV, the relative BR $\Gamma(\eta \to \pi^0 e^+ e^-)/\Gamma(\eta \to \pi^0 \gamma\gamma) \approx 10^{-5}$, as well as the associated decay energy spectrum. This was an enormous endeavour given

[1] This chapter is based on Ref. [233].

the very limited access to computer algebra systems at the time. For this reason, a number of strong assumptions had to be made, as pointed out above, which may have had an undesired effect on the accuracy of Cheng's estimates. A different approach was followed by Smith [240] also in the late 1960s, whereby an S-wave $\eta\pi^0\gamma\gamma$ coupling and unitary bounds[2] were used for the calculation of the C-conserving modes associated to both $\eta \to \pi^0 l^+ l^-$ decays. By neglecting p-wave contributing terms to simplify the calculations and noting that the unknown $\eta\pi^0\gamma\gamma$ coupling constant cancels out when calculating relative branching ratios, Smith was able to find $\Gamma(\eta \to \pi^0 e^+ e^-)/\Gamma(\eta \to \pi^0\gamma\gamma) = 3.6 \times 10^{-8}$ and $\Gamma(\eta \to \pi^0 \mu^+ \mu^-)/\Gamma(\eta \to \pi^0\gamma\gamma) = 6.0 \times 10^{-5}$, after estimating the real part of the matrix element from a single dispersion relation and employing a cut-off $\Lambda = 2M_\eta$. Of course, the calculation of the latter ratio was possible because Smith did not approximate the lepton mass to zero.

Ng et al. [186] also found in the early 1990s lower limits for the decay widths of the two $\eta \to \pi^0 l^+ l^-$ processes by making use of unitary bounds and the decay chain $\eta \to \pi^0\gamma\gamma \to \pi^0 l^+ l^-$. The transition form factors associated to the $\eta \to \pi^0\gamma\gamma$ decay, which are required to perform the above calculation, were obtained using the VMD model supplemented by the exchange of an a_0 scalar meson. The lower bounds that they found are $\Gamma(\eta \to \pi^0 e^+ e^-)|_{\text{VMD}} = 1.1^{+0.6}_{-0.5}$ μeV and $\Gamma(\eta \to \pi^0 \mu^+ \mu^-)|_{\text{VMD}} = 0.5^{+0.3}_{-0.2}$ μeV, making use of VMD only. By adding the a_0 exchange[3] to the latter process, they obtained $\Gamma(\eta \to \pi^0 \mu^+ \mu^-)|_{\text{constr}} = 0.9^{+0.6}_{-0.5}$ μeV and $\Gamma(\eta \to \pi^0 \mu^+ \mu^-)|_{\text{destr}} = 0.3^{+0.4}_{-0.2}$ μeV for a constructive and destructive interference, respectively. The real parts of the amplitudes were estimated by means of a cut-off dispersive relation and the authors argued that the expected dispersive contribution should be no larger than 30% of the absorptive one. A few months later, Ng and Peters provided in Ref. [192] new estimations for the unitary bounds of the $\eta \to \pi^0 l^+ l^-$ decay widths. This new contribution was two-fold: on the one hand, they calculated the $\eta \to \pi^0\gamma\gamma$ decay width within a constituent quark model framework and, on the other hand, they recalculated the VMD transition form factors from Ref. [186] by performing a Taylor expansion and keeping terms linear in M_η^2/M_V^2, x_1 and x_2 ($x_i \equiv P_\eta \cdot q_{\gamma_i}/M_\eta^2$), which had been neglected in their previous work. Accordingly, their new findings were: (i) $\Gamma(\eta \to \pi^0 e^+ e^-)|_{\text{box}} \geq 1.2 \pm 0.2$ μeV and $\Gamma(\eta \to \pi^0 \mu^+ \mu^-)|_{\text{box}} \geq 4.3 \pm 0.7$ μeV for a constituent quark mass $m = 330$ MeV$/c^2$; and (ii) $\Gamma(\eta \to \pi^0 e^+ e^-)|_{\text{VMD}} \geq 3.5 \pm 0.8$ μeV and $\Gamma(\eta \to \pi^0 \mu^+ \mu^-)|_{\text{VMD}} \geq 2.4 \pm 0.8$ μeV. It is important to highlight that their estimations using the quark-box mechanism were strongly dependent on the specific constituent quark mass selected, especially for the electron mode.

On the experimental front, new upper limits have recently been established by the WASA-at-COSY Collaboration for the $\eta \to \pi^0 e^+ e^-$ decay width [241]. This is a useful contribution, as the previous available empirical measurements date back to the 1970s, which provided an upper limit for the relative branching ratio of the above process that was many orders of magnitude larger than the corresponding theoretical estimations at the time. In particular, Adlarson et al. [241] found from the analysis of a total of 3×10^7 events of the reaction $\text{pd} \to {}^3\text{He} + \eta$, with a recorded excess energy of $Q = 59.8$ MeV, that the results are consistent with no C-violating single-photon intermediate state event being recorded. Based on their analysis, the new upper limits $\Gamma(\eta \to \pi^0 e^+ e^-)/\Gamma(\eta \to \pi^+\pi^-\pi^0) < 3.28 \times 10^{-5}$ and $\Gamma(\eta \to \pi^0 e^+ e^-)/\Gamma(\eta \to \text{all}) < 7.5 \times 10^{-6}$ (CL $= 90\%$) have been established for the C-violating $\eta \to \pi^0\gamma^* \to \pi^0 e^+ e^-$ decay. In addition, the WASA-at-COSY Collaboration is currently analysing additional data from the $\text{pp} \to \text{pp}\eta$ reaction collected over three periods in 2008, 2010 and 2012 which should put more stringent upper limits on the $\eta \to \pi^0 e^+ e^-$

[2] As it is well known, the Cutkovsky rules [125] allow one to calculate the imaginary part of a transition amplitude by putting the intermediate virtual particles on-shell (see Chapter 5 for details).

[3] The $a_0\eta\pi^0$ and $a_0\gamma\gamma$ couplings needed to perform this calculation were roughly estimated and the authors acknowledged to be poorly known. As well as this, their signs were not unambiguously fixed.

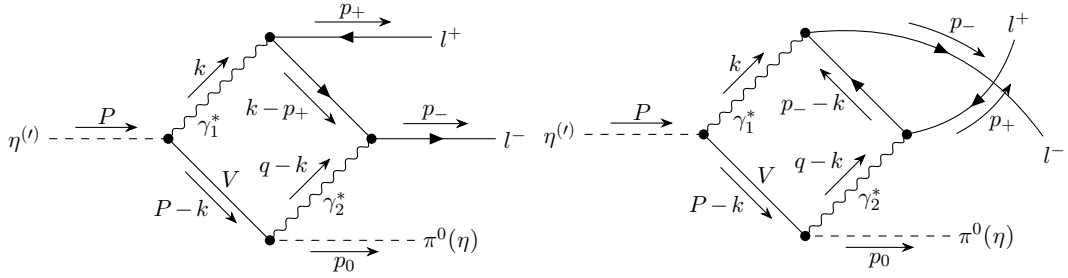

(A) t-channel Feynman diagram (B) u-channel Feynman diagram

FIGURE 10.1: Feynman diagrams contributing to the C-conserving semileptonic decays $\eta^{(\prime)} \to \pi^0 l^+ l^-$ and $\eta' \to \eta l^+ l^-$ ($l = e$ or μ). Note that $q = p_+ + p_-$ and $V = \rho^0, \omega, \phi$.

branching ratio. The experimental state of play is expected to be further improved in the near future with the advent of new experiments such as the REDTOP [15, 242], which will focus on rare decays of the η and η' mesons, providing increased sensitivity in the search for violations of SM symmetries by several orders of magnitude beyond the current experimental state of the art.

The present chapter is structured as follows. In Sec. 10.2, we present the detailed calculations for the decay widths associated to the six $\eta^{(\prime)} \to \pi^0 l^+ l^-$ and $\eta' \to \eta l^+ l^-$ processes. In Sec. 10.3, numerical results from theory for the decay widths and the corresponding dilepton energy spectra are presented and discussed for the six decays. Some final remarks and conclusions are given in Sec. 10.4.

10.2 Calculations of $\eta^{(\prime)} \to \pi^0 l^+ l^-$ and $\eta' \to \eta l^+ l^-$

The calculations in this chapter assume that the $\eta^{(\prime)} \to \pi^0 l^+ l^-$ and $\eta' \to \eta l^+ l^-$ decays processes are dominated by the exchange of vector resonances[4] [239]; that is, they proceed through the C-conserving virtual transition $\eta^{(\prime)} \to V\gamma^*$ (with $V = \rho^0$, ω or ϕ), followed by $V \to \pi^0\gamma^*$ (or $V \to \eta\gamma^*$) and $2\gamma^* \to l^+ l^-$ (see Fig. 10.1 for details).[5]

In order to perform the calculations, one first needs to select an effective vertex that has got the appropriate structure. The $VP\gamma$ interaction amplitude consistent with Lorentz, P, C and electromagnetic gauge invariance can be written as [232]

$$\mathcal{M}(V \to P\gamma) = g_{VP\gamma}\, \epsilon_{\mu\nu\alpha\beta} \epsilon^{\mu}_{(V)} p_V^{\nu} \epsilon^{*\alpha}_{(\gamma)} q^{\beta} \hat{F}_{VP\gamma}(q^2)\,, \tag{10.1}$$

where $g_{VP\gamma}$ is the coupling constant for the $VP\gamma$ transition involving on-shell photons, $\epsilon_{\mu\nu\alpha\beta}$ is the totally antisymmetric Levi-Civita tensor, $\epsilon_{(V)}$ and p_V are the polarisation and four-momentum vectors of the initial V, $\epsilon^*_{(\gamma)}$ and q are the corresponding ones for the final γ, and $\hat{F}_{VP\gamma}(q^2) \equiv F_{VP\gamma}(q^2)\,/\,F_{VP\gamma}(0)$ is a normalised form factor to account for off-shell photons mediating the transition.[6] In addition to this, the usual QED vertex is used to describe the

[4] It is worth highlighting that, based on the results presented in Chapter 8 (cf. [165]), contributions from the exchange of scalar resonances can be safely discarded as they ought to be negligible for the first four $\eta^{(\prime)} \to \pi^0 l^+ l^-$ decays and relatively small for the last two $\eta' \to \eta l^+ l^-$ processes.

[5] Note that any C-violating contributions to these processes, such as e.g. the single-photon exchange channel, would be associated to BSM physics. In this chapter, though, the focus is on the SM contribution from the C-conserving two-photon exchange channel. In Chapter 11, we investigate potential CP-violating signatures in these decays.

[6] For simplicity of the calculation, we neglect the q^2 dependence of the transition form factor in Eq. (10.1). This is not fully rigorous but, we understand, it is a tolerable approximation given that these form factors are usually determined from on-shell photon processes.

subsequent $2\gamma^* \to l^+ l^-$ transition. Accordingly, there are six diagrams (two per vector meson) contributing to each one of the six semileptonic decay processes and the corresponding Feynman diagrams are shown in Fig. 10.1.

The invariant decay amplitude in momentum space can, therefore, be written as follows

$$\begin{aligned}\mathcal{M} = ie^2 \sum_{V=\rho^0,\omega,\phi} & g_{V\eta^{(\prime)}\gamma}\, g_{V\pi^0(\eta)\gamma} \int \frac{d^4k}{(2\pi)^4} \frac{1}{k^2 + i\varepsilon} \frac{1}{(k-q)^2 + i\varepsilon} \\ & \times \epsilon_{\mu\nu\alpha\beta} \left[\frac{k^\mu (P-k)^\alpha (k-q)^\rho (P-k)^\delta}{(P-k)^2 - M_V^2 + i\varepsilon} \right] \epsilon_{\rho\sigma\delta}{}^{\beta} \\ & \times \overline{u}(p_-) \left[\gamma^\sigma \frac{\not{k} - \not{p}_+ + m_l}{(k-p_+)^2 - m_l^2 + i\varepsilon} \gamma^\nu + \gamma^\nu \frac{\not{p}_- - \not{k} + m_l}{(k-p_-)^2 - m_l^2 + i\varepsilon} \gamma^\sigma \right] v(p_+)\,,\end{aligned} \tag{10.2}$$

where $q = p_+ + p_-$ is the sum of lepton-antilepton pair four-momenta, e is the electron charge, and $g_{V\eta^{(\prime)}\gamma}$ and $g_{V\pi^0(\eta)\gamma}$ are the corresponding VMD coupling constants from Eq. (10.1). Noting that the Levi-Civita tensors are antisymmetric under the substitutions $\mu \leftrightarrow \alpha$ and $\rho \leftrightarrow \delta$, whilst the products of loop momenta $k^\mu k^\alpha$ and $k^\rho k^\delta$ are symmetric under these substitutions, one finds that the terms in Eq. (10.2) containing these combinations vanish and that the superficial degree of divergence for the loop integrals of the two diagrams in Fig. 10.1 is -1. Accordingly, both diagrams are convergent individually.

The numerator of $\mathcal{M}$ can be simplified using the usual Dirac algebra manipulations and the equations of motion. For these calculations, the mass of the leptons are not approximated to zero, as we are interested in both the electron and muon modes of the $\eta^{(\prime)} \to \pi^0 l^+ l^-$ and $\eta' \to \eta l^+ l^-$ decays. In order to manipulate and simplify the algebraic expressions, use of the Mathematica package FeynCalc 9.2.0 [243, 244] is made.

Let us now proceed to calculate the loop integral. As usual, one first introduces the Feynman parameterisation and completes the square in the new denominators Δ_i^V ($i = 1, 2$ and $V = \rho^0, \omega, \phi$) by shifting to a new loop momentum variable ℓ [3]. Therefore, the denominators become

$$\begin{aligned}\Delta_1^V =\ & 2yz(P\cdot q) + 2xy(p_+\cdot q) + (y-1)yq^2 + 2xz(P\cdot p_+) + x^2 m_l^2 \\ & + z\big[(z-1)M_{\eta^{(\prime)}}^2 + M_V(M_V - i\Gamma_V)\big]\,, \\ \Delta_2^V \equiv\ & \Delta_1^V \ \text{ with } \ p_+ \leftrightarrow p_-\ .\end{aligned} \tag{10.3}$$

Rewriting the numerators of the Feynman diagrams 1 and 2 (i.e. the t- and u-channel diagrams, respectively, from Fig. 10.1) in terms of the new momentum variable ℓ, one finds

$$\begin{aligned}\mathcal{N}_1 =\ & \big[A_1\ell^2 + B_1\big]\overline{u}(p_-)\not{P}v(p_+) + \ m_l\big[C_1\ell^2 + D_1\big]\overline{u}(p_-)v(p_+)\,, \\ \mathcal{N}_2 =\ & \big[A_2\ell^2 + B_2\big]\overline{u}(p_-)\not{P}v(p_+) + \ m_l\big[C_2\ell^2 + D_2\big]\overline{u}(p_-)v(p_+)\,,\end{aligned} \tag{10.4}$$

where the explicit expressions for the parameters A_i, B_i, C_i and D_i ($i = 1, 2$) are given in Appendix F. Finally, we perform a Wick rotation and change to four-dimensional spherical coordinates [3, 4] to carry out the momentum integral. The following expressions for the amplitudes of the Feynman diagrams are found

$$\begin{aligned}\mathcal{M}_1^V =\ & \alpha_V\big[\overline{u}(p_-)\not{P}v(p_+)\big] + \beta_V m_l\big[\overline{u}(p_-)v(p_+)\big]\,, \\ \mathcal{M}_2^V =\ & \sigma_V\big[\overline{u}(p_-)\not{P}v(p_+)\big] + \tau_V m_l\big[\overline{u}(p_-)v(p_+)\big]\,,\end{aligned} \tag{10.5}$$

where m_l is the corresponding lepton mass, and the parameters α_V, β_V, σ_V and τ_V in Eq. (10.5) are defined as

$$\begin{aligned}
\alpha_V &= e^2 \frac{g_{V\eta^{(\prime)}\gamma} g_{V\pi^0(\eta)\gamma}}{16\pi^2} \int dxdydz \left[\frac{2A_1}{\Delta_1^V - i\varepsilon} - \frac{B_1}{(\Delta_1^V - i\varepsilon)^2} \right], \\
\beta_V &= e^2 \frac{g_{V\eta^{(\prime)}\gamma} g_{V\pi^0(\eta)\gamma}}{16\pi^2} \int dxdydz \left[\frac{2C_1}{\Delta_1^V - i\varepsilon} - \frac{D_1}{(\Delta_1^V - i\varepsilon)^2} \right], \\
\sigma_V &= e^2 \frac{g_{V\eta^{(\prime)}\gamma} g_{V\pi^0(\eta)\gamma}}{16\pi^2} \int dxdydz \left[\frac{2A_2}{\Delta_2^V - i\varepsilon} - \frac{B_2}{(\Delta_2^V - i\varepsilon)^2} \right], \\
\tau_V &= e^2 \frac{g_{V\eta^{(\prime)}\gamma} g_{V\pi^0(\eta)\gamma}}{16\pi^2} \int dxdydz \left[\frac{2C_2}{\Delta_2^V - i\varepsilon} - \frac{D_2}{(\Delta_2^V - i\varepsilon)^2} \right],
\end{aligned} \tag{10.6}$$

with x, y and z being the Feynman integration parameters. Therefore, the full amplitude can now be expressed as

$$\mathcal{M} = \sum_{V=\rho^0,\omega,\phi} \mathcal{M}_1^V + \mathcal{M}_2^V = \Omega\big[\overline{u}(p_-)\not{P} v(p_+)\big] + m_l \Sigma\big[\overline{u}(p_-) v(p_+)\big], \tag{10.7}$$

where Ω and Σ are defined as follows

$$\begin{aligned}
\Omega &= \sum_{V=\rho^0,\omega,\phi} \alpha_V + \sigma_V, \\
\Sigma &= \sum_{V=\rho^0,\omega,\phi} \beta_V + \tau_V,
\end{aligned} \tag{10.8}$$

and the unpolarised squared amplitude is

$$\begin{aligned}
\overline{|\mathcal{M}|^2} = 4\Big\{ & 2(P\cdot p_+)(P\cdot p_-) - M^2_{\eta^{(\prime)}}\big[(p_+\cdot p_-) + m_l^2\big] \Big\} \times \mathrm{Abs}(\Omega)^2 \\
& + 8m_l^2\big[(P\cdot p_+) - (P\cdot p_-)\big]\mathrm{Re}(\Omega\Sigma^*) + 4m_l^2\big[(p_+\cdot p_-) - m_l^2\big]\mathrm{Abs}(\Sigma)^2 .
\end{aligned} \tag{10.9}$$

Finally, the differential decay rate for a three-body decay can be written as [1]

$$d\Gamma = \frac{1}{(2\pi)^3} \frac{1}{32 M^3_{\eta^{(\prime)}}} \overline{|\mathcal{M}|^2}\, dm^2_{l^+l^-} dm^2_{l^-\pi^0(\eta)}, \tag{10.10}$$

where $m^2_{ij} = (p_i + p_j)^2$.

10.3 Theoretical results

Making use of the theoretical expressions that have been presented in Sec. 10.2, one can find numerical predictions for the decay widths of the $\eta^{(\prime)} \to \pi^0 l^+ l^-$ and $\eta' \to \eta l^+ l^-$ processes, as well as their associated dilepton invariant mass distributions. Both, the integral over the Feynman parameters as well as the integral over phase space, must be carried out numerically, as algebraic expressions cannot be obtained. In addition to this, the numerical integrals over the Feynman parameters are to be performed using adaptive Monte Carlo methods [245], which is driven by the complexity of the expressions to be integrated and

their multidimensional nature.[7]

In the conventional VMD model, pseudoscalar mesons do not couple directly to photons but through the exchange of intermediate vectors. Thus, in this framework, a particular $VP\gamma$ coupling constant times its normalised form factor, cf. Eq. (10.1), is given by Eq. (10.11), which takes the form

$$g_{VP\gamma}\,\hat{F}_{VP\gamma}(q^2) = \sum_{V'} \frac{g_{VV'P}\,g_{V'\gamma}}{M_{V'}^2 - q^2}\,, \tag{10.11}$$

where $g_{VV'P}$ are the vector-vector-pseudoscalar couplings, $g_{V'\gamma}$ the vector-photon conversion couplings and $M_{V'}$ the intermediate vector masses. In the $SU(3)$-flavour symmetry and OZI-rule respecting limits, one could express all the $g_{VP\gamma}$ in terms of a single coupling constant and $SU(3)$-group factors [231]. However, to account for the unavoidable $SU(3)$-flavour symmetry-breaking and OZI-rule violating effects, we make use of the simple, yet powerful, phenomenological quark-based model first presented in Ref. [140], which was developed to describe $V \to P\gamma$ and $P \to V\gamma$ radiative decays (see also Chapter 7). According to this model, the relevant decay couplings can be expressed as [cf. Eq. (8.11)]

$$\begin{aligned}
g_{\rho^0\pi^0\gamma} &= \frac{1}{3}g\,, \quad g_{\omega\pi^0\gamma} = g\cos\phi_V\,, \quad g_{\phi\pi^0\gamma} = g\sin\phi_V\,,\\
g_{\rho^0\eta\gamma} &= g z_{\mathrm{NS}}\cos\phi_P\,, \qquad g_{\rho^0\eta'\gamma} = g z_{\mathrm{NS}}\sin\phi_P\,,\\
g_{\omega\eta\gamma} &= \frac{1}{3}g\Big(z_{\mathrm{NS}}\cos\phi_P\cos\phi_V - 2\frac{\overline{m}}{m_s}z_{\mathrm{S}}\sin\phi_P\sin\phi_V\Big)\,,\\
g_{\omega\eta'\gamma} &= \frac{1}{3}g\Big(z_{\mathrm{NS}}\sin\phi_P\cos\phi_V + 2\frac{\overline{m}}{m_s}z_{\mathrm{S}}\cos\phi_P\sin\phi_V\Big)\,,\\
g_{\phi\eta\gamma} &= \frac{1}{3}g\Big(z_{\mathrm{NS}}\cos\phi_P\sin\phi_V + 2\frac{\overline{m}}{m_s}z_{\mathrm{S}}\sin\phi_P\cos\phi_V\Big)\,,\\
g_{\phi\eta'\gamma} &= \frac{1}{3}g\Big(z_{\mathrm{NS}}\sin\phi_P\sin\phi_V - 2\frac{\overline{m}}{m_s}z_{\mathrm{S}}\cos\phi_P\cos\phi_V\Big)\,,
\end{aligned} \tag{10.12}$$

where g is a generic electromagnetic constant, ϕ_P is the pseudoscalar η-η' mixing angle in the quark-flavour basis, ϕ_V is the vector ω-ϕ mixing angle in the same basis, $\overline{m}/m_s$ is the quotient of constituent quark masses, and z_{NS} and z_{S} are the *non-strange* and *strange* multiplicative factors accounting for the relative meson wavefunction overlaps [137, 140]. By performing an optimisation fit to the most up-to-date $VP\gamma$ experimental data [1], we find the best fit values from Eq. (8.24) for the parameters of the model

$$\begin{aligned}
g &= 0.70 \pm 0.01\ \mathrm{GeV}^{-1}\,, \quad z_{\mathrm{S}}\overline{m}/m_s = 0.65 \pm 0.01\,,\\
\phi_P &= (41.4 \pm 0.5)^\circ\,, \qquad\qquad \phi_V = (3.3 \pm 0.1)^\circ\,,\\
&z_{\mathrm{NS}} = 0.83 \pm 0.02\,.
\end{aligned} \tag{10.13}$$

Given the very wide decay width of the ρ^0 resonance, which in turn is associated to its very short lifetime, the use of the usual Breit-Wigner description for the ρ^0 propagator is not justified. Instead, the energy-dependent width from Eq. (8.10) ought to be considered for the

[7] It is worth mentioning that comparison between the numerical results for Ω and Σ in Eq. (10.8) using the approach presented in this chapter and Passarino-Veltman reduction techniques implemented in software packages such as, for example, LoopTools [246] was carried out for different points of phase space to assess the performance of our method. It was found that our results were in agreement with those from the above package for points far from the edge of phase space, which provides a level of confidence in our approach, but in sharp disagreement for points near the edge of phase space. This is, however, a well-known drawback of the Passarino-Veltman reduction and variants due to the appearance of Gram determinants in the denominator, which spoils the numerical stability when they become small or even zero giving rise to spurious singularities (see, e.g., Refs. [247–249]). For processes with up to four external particles, this usually happens near the edge of phase space [247], which is consistent with our findings.

Decay	Γ_{th}	BR_{th}	BR_{exp}
$\eta \to \pi^0 e^+ e^-$	$2.7(1)(1)(2) \times 10^{-6}$ eV	$2.0(1)(1)(1) \times 10^{-9}$	$< 7.5 \times 10^{-6}$ (CL=90%) [241]
$\eta \to \pi^0 \mu^+ \mu^-$	$1.4(1)(1)(1) \times 10^{-6}$ eV	$1.1(1)(1)(1) \times 10^{-9}$	$< 5 \times 10^{-6}$ (CL=90%) [1]
$\eta' \to \pi^0 e^+ e^-$	$8.7(5)(6)(6) \times 10^{-4}$ eV	$4.5(3)(4)(4) \times 10^{-9}$	$< 1.4 \times 10^{-3}$ (CL=90%) [1]
$\eta' \to \pi^0 \mu^+ \mu^-$	$3.3(2)(4)(3) \times 10^{-4}$ eV	$1.7(1)(2)(2) \times 10^{-9}$	$< 6.0 \times 10^{-5}$ (CL=90%) [1]
$\eta' \to \eta e^+ e^-$	$8.3(0.5)(0.1)(3.5) \times 10^{-5}$ eV	$4.3(0.3)(0.2)(1.8) \times 10^{-10}$	$< 2.4 \times 10^{-3}$ (CL=90%) [1]
$\eta' \to \eta \mu^+ \mu^-$	$3.0(0.2)(0.1)(1.1) \times 10^{-5}$ eV	$1.5(1)(1)(5) \times 10^{-10}$	$< 1.5 \times 10^{-5}$ (CL=90%) [1]

TABLE 10.1: Decay widths and branching ratios for the six C-conserving decays $\eta^{(\prime)} \to \pi^0 l^+ l^-$ and $\eta' \to \eta l^+ l^-$ ($l = e$ or μ). First error is experimental, second is down to numerical integration and third is associated to the model dependence.

ρ^0 propagator, which for a generic $\hat{q}^2$ takes the form

$$\Gamma_{\rho^0}(\hat{q}^2) = \Gamma_{\rho^0} \times \left(\frac{\hat{q}^2 - 4M_{\pi^\pm}^2}{M_{\rho^0}^2 - 4M_{\pi^\pm}^2} \right)^{3/2} \times \theta(\hat{q}^2 - 4M_{\pi^\pm}^2)\,, \tag{10.14}$$

where $\theta(x)$ is the Heaviside step function. Strictly, one would now need to plug Eq. (10.14) into Eq. (10.2) and perform the loop integral, which represents a computation challenge in its own right and is outside of the scope of this chapter.[8] With this in mind, and for the sake of simplicity, we resolve to stick to the Breit-Wigner approximation for the ρ^0 propagator despite being a potential source of error. The energy-dependent propagator is not needed, though, for the ω and ϕ resonances, as their associated decay widths are narrow and, therefore, use of the usual Breit-Wigner approximation suffices.

Using the most recent empirical data for the meson masses and total decay widths from Ref. [1], together with all the above considerations, one arrives at the decay width results shown in Table 10.1 for the six $\eta^{(\prime)} \to \pi^0 l^+ l^-$ and $\eta' \to \eta l^+ l^-$ processes. The total decay widths associated to the electron modes turn out to be larger than the ones corresponding to the muon modes despite the second and third terms in the unpolarised squared amplitude [cf. Eq. (10.9)] being helicity suppressed for the electron modes. This suppression, though, does not overcome the phase space suppression for the muon modes, yielding $\Gamma(\eta^{(\prime)} \to \pi^0 e^+ e^-) > \Gamma(\eta^{(\prime)} \to \pi^0 \mu^+ \mu^-)$ and $\Gamma(\eta' \to \eta e^+ e^-) > \Gamma(\eta' \to \eta \mu^+ \mu^-)$.

Let us now look at the contributions from the different vector meson exchanges to the total decay widths. For the first decay, i.e. $\eta \to \pi^0 e^+ e^-$, we find that the contribution from the ρ^0 exchange is $\sim 26\%$, the contribution from the ω is $\sim 22\%$, whilst the one from the ϕ is negligible, i.e. $\sim 0\%$. The interference between the ρ^0 and the ω is constructive, accounting for the $\sim 49\%$; similarly, the interference between the ρ^0 and the ω with the ϕ is constructive and about $\sim 3\%$. The contributions to the second decay, i.e. $\eta \to \pi^0 \mu^+ \mu^-$, are $\sim 25\%$, $\sim 23\%$ and $\sim 0\%$ from the ρ^0, ω, and ϕ exchanges, respectively. As before, the interference between the ρ^0 and the ω is constructive, weighing $\sim 48\%$, and the interference between the ρ^0 and the ω with the ϕ is constructive and accounts for approximately the $\sim 4\%$. For the third decay, i.e. $\eta' \to \pi^0 e^+ e^-$, the contributions from the ρ^0, ω and ϕ turn out to be $\sim 16\%$, $\sim 39\%$ and $\sim 0\%$, respectively; the interference between the ρ^0 and the ω exchanges is constructive

[8] One could write, for example, the ρ^0 energy-dependent propagator $f(s) = \frac{M_\rho^2}{M_\rho^2 - s - iM_\rho \Gamma_\rho(s)}$ as a once-subtracted dispersion relation, $f(s) = f(s_0) + \frac{s - s_0}{\pi} \int_{s_{\text{th}}}^{\infty} \frac{\text{Im} f(s')\, ds'}{(s' - s_0)(s' - s - i\varepsilon)}$, where s_{th} is the particle production threshold, in this case $s_{\text{th}} = 4M_\pi^2$, and s_0 is the subtraction point such that $s_0 < s_{\text{th}}$, e.g. $s_0 = 0$ (see Sec. 5.3 for details). One would then perform the loop integral in the usual way, leaving the dispersion integral to the end of the computation.

and accounts for the $\sim 47\%$, whilst the interference between the ρ^0 and ω with the ϕ is destructive and weighs approximately $\sim 2\%$. The contributions to the fourth decay, i.e. $\eta' \to \pi^0\mu^+\mu^-$, from the ρ^0, ω and ϕ exchanges are $\sim 20\%$, $\sim 35\%$ and $\sim 0\%$, respectively. The interference between the ρ^0 and the ω is constructive, representing a $\sim 53\%$ contribution, whilst the interference between the ρ^0 and the ω with the ϕ is destructive and accounts for the $\sim 8\%$. The fifth decay, i.e. $\eta' \to \eta e^+ e^-$, gets contributions from the exchange of ρ^0, ω and ϕ resonances of approximately $\sim 76\%$, $\sim 1\%$ and $\sim 2\%$, respectively; the interference between the ρ^0 and the ω is constructive weighing $\sim 29\%$, and the interference between the ρ^0 and the ω with the ϕ is destructive and contributes with roughly the $\sim 8\%$. Finally, for the sixth decay, i.e. $\eta' \to \eta\mu^+\mu^-$, we find that the contribution from the ρ^0 exchange is $\sim 94\%$, the contribution from the ω is $\sim 2\%$ and the one from the ϕ is $\sim 3\%$; the interference between the ρ^0 and the ω is constructive and accounts for the $\sim 26\%$, whilst the interference between the ρ^0 and the ω with the ϕ is destructive weighing close to $\sim 25\%$. The tiny contribution from the ϕ exchange to the decay widths of the six processes is explained by the relatively small product of VMD $VP\gamma$ coupling constants. Likewise, the comparatively minute contribution from the ω exchange to the decay widths of the last two reactions is down to the significantly smaller product of coupling constants, if compared to that of the ρ^0 exchange.

In order to assess a systematic error associated to the model dependency of our predictions, we repeat all the above calculations in the context of RχT. As explained in the previous chapter, in this framework the $VP\gamma$ effective vertex is made of two contributions, a local $VP\gamma$ vertex weighted by a coupling constant, h_V, and a non-local one built from the exchange of an intermediate vector which, again, is weighted by a second coupling constant, σ_V, times the vector-photon conversion factor f_V. For a given $VP\gamma$ transition, this effective vertex can be written in the $SU(3)$-flavour symmetry limit as [232]

$$g_{VP\gamma}\,\hat{F}_{VP\gamma}(q^2) = C_{VP\gamma}\,|e|\frac{4\sqrt{2}\,h_V}{f_\pi}\left(1+\frac{\sigma_V f_V}{\sqrt{2}\,h_V}\frac{q^2}{M_{V'}^2-q^2}\right), \tag{10.15}$$

where $C_{VP\gamma}$ are $SU(3)$-group factors and, depending on the process, the exchanged vector is or is not the same as the initial vector (see Refs. [232, 250] for each particular case). To fix the $VP\gamma$ couplings in this second approach, we make use of the extended Nambu–Jona-Lasinio (ENJL) model, where h_V is found to be $h_V = 0.035$ [232]. The VVP coupling σ_V obtained using the ENJL model turns out to be $\sigma_V = 0.28$. However, σ_V can also be obtained from the analysis of the dilepton mass spectrum in $\omega \to \pi^0\mu^+\mu^-$ decays, where one finds $\sigma_V \approx 0.58$ [251]. Due to the fact that σ_V is poorly known and the dispersion of the above estimations is large, we do not consider the q^2 dependence of the form factors in the subsequent calculations. An alternative model to fix the normalisation of the form factors, $g_{VP\gamma}$, is the hidden gauge symmetry (HGS) model [78], where the vector mesons are considered as gauge bosons of a hidden symmetry (see Sec. 3.5.1 for details). Within this model, a $VP\gamma$ transition proceeds uniquely through the exchange of intermediate vector mesons. In this sense, it is equivalent to the conventional VMD model with the relevant exception of including direct γP^3 terms (P being a pseudoscalar meson), which are forbidden in the conventional VMD [252]. Due to this similarity, we will not make use of the HGS model to assess the systematic model error and refer the interested reader to Ref. [231] for a detailed calculation of the $g_{VP\gamma}$ couplings in this model.

In what follows, our results for the semileptonic decays $\eta^{(\prime)} \to \pi^0 l^+ l^-$ and $\eta' \to \eta l^+ l^-$ in the conventional VMD framework using the $VP\gamma$ couplings from the phenomenological quark-based model in Eq. (10.13) are discussed and, if available, compared with previous literature. These predictions include a first experimental error ascribed to the propagation of the parametric errors in Eq. (10.13), a second error down to the numerical integration, and a third systematic error associated to the model dependence of our approach. The latter is

calculated as the absolute difference between the predicted central values obtained from the VMD and RχT frameworks (cf. Table 10.1).

Our prediction for the decay width $\Gamma(\eta \to \pi^0 e^+ e^-) = (2.7 \pm 0.1 \pm 0.1 \pm 0.2) \times 10^{-6}$ eV is about an order of magnitude smaller than the one provided by Cheng in Ref. [239], i.e. $\Gamma(\eta \to \pi^0 e^+ e^-) = 1.3 \times 10^{-5}$ eV; however, by plugging into our expressions the couplings that Cheng used in his work, we find a decay width $\Gamma(\eta \to \pi^0 e^+ e^-) \approx 2.8 \times 10^{-5}$ eV, which is approximately a factor of two larger than Cheng's result, and the difference is thought to be down to the simplifications that he had to carry out in his calculations, as well as the propagators that have been employed in the present work.[9] In addition to this, one can also obtain from our calculations a prediction for the ratio of branching ratios[10] $\Gamma(\eta \to \pi^0 e^+ e^-)/\Gamma(\eta \to \pi^0 \gamma\gamma) = (8.0 \pm 1.6) \times 10^{-6}$, which is not far from Cheng's model independent estimation of $\Gamma(\eta \to \pi^0 e^+ e^-)/\Gamma(\eta \to \pi^0 \gamma\gamma) \approx 10^{-5}$, but more than two orders of magnitude larger than Smith's estimate[11] from Ref. [240] $\Gamma(\eta \to \pi^0 e^+ e^-)/\Gamma(\eta \to \pi^0 \gamma\gamma) = 3.6 \times 10^{-8}$; as well as this, for the muon mode we find the relative branching ratio[12] $\Gamma(\eta \to \pi^0 \mu^+ \mu^-)/\Gamma(\eta \to \pi^0 \gamma\gamma) = (4.2 \pm 0.8) \times 10^{-6}$, which is in the neighbourhood of one order of magnitude smaller than Smith's estimation $\Gamma(\eta \to \pi^0 \mu^+ \mu^-)/\Gamma(\eta \to \pi^0 \gamma\gamma) = 6.0 \times 10^{-5}$ [240].

Moreover, our results for the decay widths of the $\eta \to \pi^0 e^+ e^-$ and $\eta \to \pi^0 \mu^+ \mu^-$ processes are in good agreement with the lower bounds provided by Ng et al. in Ref. [186], i.e. $\Gamma(\eta \to \pi^0 e^+ e^-)|_{\text{VMD}} = 1.1^{+0.6}_{-0.5}$ μeV and $\Gamma(\eta \to \pi^0 \mu^+ \mu^-)|_{\text{VMD}} = 0.5^{+0.3}_{-0.2}$ μeV (where use of the VMD model was made only), and $\Gamma(\eta \to \pi^0 \mu^+ \mu^-)|_{\text{constr}} = 0.9^{+0.6}_{-0.5}$ μeV and $\Gamma(\eta \to \pi^0 \mu^+ \mu^-)|_{\text{destr}} = 0.3^{+0.4}_{-0.2}$ μeV (where the VMD model was supplemented with the exchange of an a_0 scalar meson). Using the quark-box diagram and a constituent quark mass $m = 330$ MeV$/c^2$, Ng et al. provided in Ref. [192] an estimation for the electron mode, $\Gamma(\eta \to \pi^0 e^+ e^-)|_{\text{box}} \geq 1.2 \pm 0.2$ μeV, which is in accordance with our result, and an estimate for the muon mode, $\Gamma(\eta \to \pi^0 \mu^+ \mu^-)|_{\text{box}} \geq 4.3 \pm 0.7$ μeV, which in this case is incompatible with our calculation.[13] Additionally, Ng et al. also presented in Ref. [192] a recalculation of their previous VMD results from Ref. [186], yielding $\Gamma(\eta \to \pi^0 e^+ e^-)|_{\text{VMD}} \geq 3.5 \pm 0.8$ μeV and $\Gamma(\eta \to \pi^0 \mu^+ \mu^-)|_{\text{VMD}} \geq 2.4 \pm 0.8$ μeV, which are consistent with our results if one considers the associated errors.

Our decay width calculations for the other four processes, i.e. $\eta' \to \pi^0 l^+ l^-$ and $\eta' \to \eta l^+ l^-$, cannot be compared with any previously published theoretical results, as these decays have been calculated, to the best of our knowledge, for the first time in this chapter. Likewise, comparison with the most up-to-date empirical data provides limited value given that the corresponding current experimental upper bounds, though consistent with our theoretical predictions, are many orders of magnitude larger (cf. Table 10.1).

Finally, theoretical predictions for the dilepton invariant mass distributions of the six C-conserving semileptonic decays are presented in Fig. 10.2. The energy spectra of the three

[9] Note that in Ref. [239] Cheng used vector propagators without total decay widths (i.e. Feynman propagators) for the vector exchanges whilst we use Breit-Wigner propagators.

[10] Here, we are using the experimental value for the decay width $\Gamma(\eta \to \pi^0 \gamma\gamma)$ provided in Ref. [1]. Alternatively, one could use the theoretical prediction from Ref. [165] (cf. Chapter 8), $\Gamma(\eta \to \pi^0 \gamma\gamma)|_{\text{th}} = 0.17 \pm 0.01$ eV, to obtain $\Gamma(\eta \to \pi^0 e^+ e^-)/\Gamma(\eta \to \pi^0 \gamma\gamma) = (1.6 \pm 0.3) \times 10^{-5}$.

[11] The discrepancy with Smith's relative branching ratio might be explained, though, by the effect of p-wave terms that he neglected after admitting that they are not necessarily small.

[12] Once again, if one were to use the theoretical prediction from Chapter 8 (or, alternatively, Ref. [165]), $\Gamma(\eta \to \pi^0 \gamma\gamma)|_{\text{th}} = 0.17 \pm 0.01$ eV, the result $\Gamma(\eta \to \pi^0 \mu^+ \mu^-)/\Gamma(\eta \to \pi^0 \gamma\gamma) = (8.3 \pm 1.5) \times 10^{-6}$ would be obtained.

[13] Note, however, that as part of their calculation they had to estimate the decay width of the $\eta \to \pi^0 \gamma\gamma$ process using their quark-box model and found $\Gamma(\eta \to \pi^0 \gamma\gamma) = 0.60 \pm 0.10$ eV for a constituent quark mass $m = 330$ MeV$/c^2$, which is approximately a factor of two larger than the current experimental value from Ref. [1]. Therefore, it is no surprise that their estimates for the associated $\eta \to \pi^0 l^+ l^-$ processes are at the upper end of the spectrum of estimations.

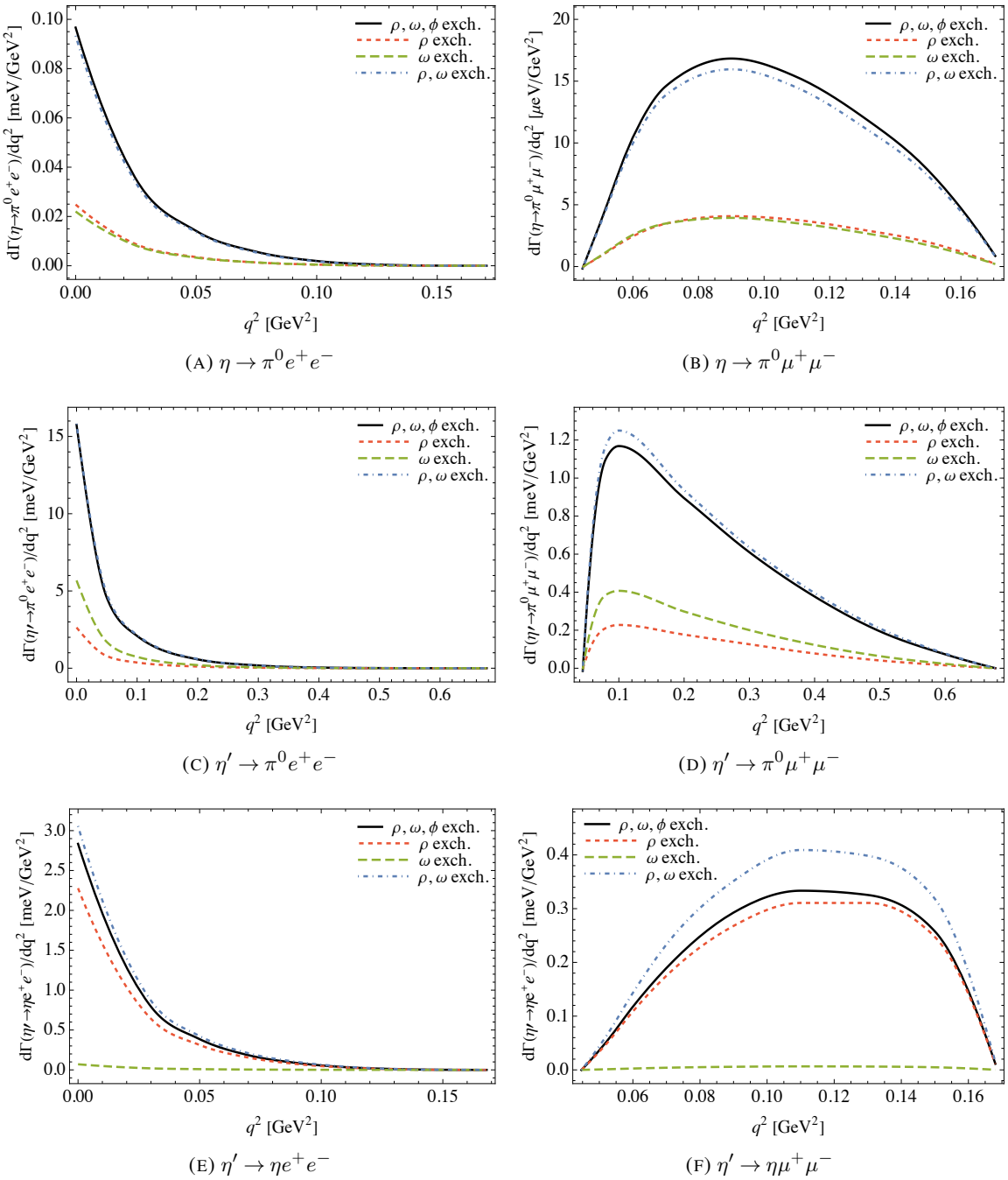

FIGURE 10.2: Dilepton energy spectra corresponding to the six C-conserving semileptonic decay processes $\eta^{(\prime)} \to \pi^0 l^+ l^-$ and $\eta' \to \eta l^+ l^-$ ($l = e$ or μ) as a function of the dilepton invariant mass q^2.

electron modes, which are displayed in Figs. 10.2a, 10.2c and 10.2e, take off as the dilepton invariant mass q^2 approaches zero. This is in line with Cheng's and Ng et al.'s energy spectra for the $\eta \to \pi^0 e^+ e^-$ (Refs. [239] and [186], respectively), which exhibit the same behaviour at low q^2. It appears as though the electron modes *prefer* to proceed through the emission of (relativistic) collinear electron-positron pairs (i.e. $\theta_{e^+e^-} \simeq 0$, where $\theta_{e^+e^-}$ is the electron-positron angle). The reason for this can easily be understood from dynamics[14] if one assumes

[14] It must be noted, though, that the kinematics of the electron modes also contribute to this particular shape of the energy spectra, producing a somewhat synergistic effect.

the electron and positron to be massless, $m_e \approx 0$; then, by inspection of Eq. (10.9), one can determine that the unpolarised squared amplitude is maximised when $q^2 \to 0$, which occurs when $\theta_{e^+e^-} \simeq 0$.[15] Physically, it may be explained to some extent by the fact that the diphoton invariant mass distributions of the three $\eta^{(\prime)} \to \pi^0\gamma\gamma$ and $\eta' \to \eta\gamma\gamma$ processes peak at low $m^2_{\gamma\gamma}$ (cf. Chapter 8). On the other hand, the dilepton energy spectra of the muon modes, shown in Figs. 10.2b, 10.2d and 10.2f, are bell-shaped, which is driven by the kinematics of the processes. This, once again, seems to be consistent with Ng et al.'s [186] mass spectrum for the $\eta \to \pi^0\mu^+\mu^-$. It is interesting to observe that the energy spectra of the $\eta \to \pi^0\mu^+\mu^-$ and $\eta' \to \pi^0\mu^+\mu^-$ are skewed to the left (i.e. small values of $\theta_{\mu^+\mu^-}$ are favoured, where $\theta_{\mu^+\mu^-}$ is the muon-antimuon angle), whilst the energy spectrum of the $\eta' \to \eta\mu^+\mu^-$ is skewed to the right (i.e. somewhat larger values for $\theta_{\mu^+\mu^-}$ are preferred). This is more difficult to explain[16] given that this effect, which is connected to the fact that $M_\eta > M_{\pi^0}$, is a consequence of the complex dynamical interplay between the different terms in Eq. (10.9). Surprisingly, the kinematics of the reactions do not seem to play a significant role in this difference in skewness.

10.4 Conclusions

In this chapter, the C-conserving decay modes $\eta^{(\prime)} \to \pi^0 l^+ l^-$ and $\eta' \to \eta l^+ l^-$ ($l = e$ or μ) have been analysed within the theoretical framework of the VMD model. The associated decay widths and dilepton invariant mass distributions have been calculated and presented for the six decay processes. To the best of our knowledge, the theoretical predictions for the four $\eta' \to \pi^0 l^+ l^-$ and $\eta' \to \eta l^+ l^-$ decays that we have presented are the first that have been published.

The decay width results that we have obtained from our calculations, which are summarised in Table 10.1, have been compared with those available in the published literature and, in general, the agreement is reasonably good considering that the previous analysis either contained important approximations or consisted of unitary lower bounds. As well as this, our predictions for the dilepton energy spectra of the six processes, which are shown in Fig. 10.2, have also been compared with those available in the literature.

Experimental measurements to date have provided upper limits to the decay processes studied in this chapter. These upper limits, though, are still many orders of magnitude larger than the theoretical results that we have presented. For this reason, we would like to encourage experimental groups, such as the WASA-at-COSY and REDTOP Collaborations, to study these semileptonic decays as we believe that they can represent a fruitful arena in the search for new physics beyond the Standard Model.

[15] Note that $q^2 \simeq 2p_{e^+}p_{e^-} \simeq 2|\mathbf{p}_{\mathbf{e}^+}||\mathbf{p}_{\mathbf{e}^-}|(1-\cos\theta_{e^+e^-})$ in the leptonic massless limit, i.e. $m_e \approx 0$.

[16] A qualitative explanation could be given from a statistical mechanics viewpoint, whereby high momentum η mesons in the final state would be Boltzmann suppressed compared to high momentum π^0 states.

Chapter 11

New-physics signatures via CP violation in $\eta^{(\prime)} \to \pi^0\mu^+\mu^-$ and $\eta' \to \eta\mu^+\mu^-$ decays[1]

In this chapter we investigate the prospect of observing new-physics signatures via CP violation in $\eta^{(\prime)} \to \pi^0\mu^+\mu^-$ and $\eta' \to \eta\mu^+\mu^-$ decays at the REDTOP experiment. We make use of the Standard Model effective field theory (SMEFT) to parameterise the new-physics CP-violating effects and find that the projected REDTOP statistics are not competitive with respect to neutron electric dipole moment (nEDM) experiments. This reasserts the leptonic $\eta \to \mu^+\mu^-$ decay process as the most promising channel to find CP-violation at this experimental facility.

11.1 Introduction

Over the past few decades, high-energy particle colliders have not succeeded in the quest for finding evidence for physics beyond the Standard Model (BSM). The purpose of large experiments such as the Large Hadron Collider (LHC), apart from settling down the question around the source of electroweak symmetry breaking, was to provide experimental evidence for either supersymmetric particles or extra dimensions or both, as they enjoy from good theoretical motivation based on naturalness arguments, but this has not happened.

The current lack of experimental evidence for new physics in direct searches, that would help guide theoretical effort, is forcing the community to increase their focus on low-energy, high-luminosity precision measurements that attempt to find effects from BSM physics by looking for small discrepancies between SM predictions and measurements. To this end, one focuses on processes whose SM contribution is very precisely known or that have a very small SM background, hence, any positive experimental finding would be a confirmation for new physics. Accordingly, interest in BSM searches in meson factories has significantly increased in recent years,[2] as they can very precisely measure branching ratios of rare decays and test for violations of the basic symmetries. As an example, the observation of CP violation in processes mediated by the strong or electromagnetic interactions would be an unambiguous sign of new physics, and the study of the η and η' decays represents the perfect laboratory for this endeavour. This is because both mesons are eigenstates of the C, P, CP and G operators (i.e. $I^G J^{PC} = 0^+0^{-+}$) and their additive quantum numbers are zero, which amounts to all their decays being flavour-conserving. As a consequence, and unlike flavoured meson decays, they can be used to test C and CP symmetries, provided a large sample of η and η' mesons is available. Furthermore, their strong and electromagnetic decays are forbidden at lowest order, increasing their sensitivity to rare decays.

[1] This chapter is based on Ref. [253].

[2] Another example of a low-energy experiment that has recently attracted much interest is the Muon g-2 at Fermilab [254].

In this context, the REDTOP experiment has been proposed [15, 242, 255], which aims at producing the largest sample of η and η' mesons envisaged thus far, and is considering implementing dedicated detectors to perform muon polarimetry. In order to set their priorities, it is crucial to assess the most promising channels and the physics within reach. In Ref. [256], the possibility of observing new-physics signatures via CP-violating effects at REDTOP was assessed using muon polarisation observables in η leptonic decays. In particular, the purely leptonic channels $\mu^+\mu^-$, $\mu^+\mu^-\gamma$ and $\mu^+\mu^-\ell^+\ell^-$ were studied, finding that CP violation in the $\mu^+\mu^-$ final state could be observed at REDTOP, while evading nEDM constraints.

In this chapter, we investigate the suitability of some η and η' semileptonic decays, which were not covered in Ref. [256] as they require a dedicated analysis of hadronic matrix elements. In particular, we investigate the $\eta^{(\prime)} \to \pi^0\mu^+\mu^-$ and $\eta' \to \eta\mu^+\mu^-$ decays using the SMEFT as the general theoretical framework to capture new physics. Using muon polarisation observables, we quantify the sensitivity that could be achieved at REDTOP for the relevant CP-violating Wilson coefficients. Our results show that these decays are not competitive when confronted against the stringent bounds derived from nEDM and $D_s^- \to \mu\bar{\nu}_\mu$ decays. This contrasts with the $\eta \to \mu^+\mu^-$ decay that evades these bounds and ought to receive the highest priority.

This chapter is structured as follows. In Sec. 11.2, we discuss the general properties of the decay amplitudes and narrow down the range of SMEFT operators that are relevant to our study. In Sec. 11.3, we present the theoretical expressions for the required hadronic matrix elements obtained using large-N_C chiral perturbation theory (large-N_C χPT). The polarised decay widths and the asymmetries that quantify the CP-violating effects in $\eta^{(\prime)} \to \pi^0\mu^+\mu^-$ and $\eta' \to \eta\mu^+\mu^-$ decays are analysed in Sec. 11.4. The results from our investigation are presented in Sec. 11.5 and we briefly discuss their implications. Finally, in Sec. 11.6 we provide a summary of the work carried out in this chapter and some final conclusions.

11.2 Decay amplitudes

We begin by defining the following momenta $q = p_{\mu^+} + p_{\mu^-} = p_{\eta^{(\prime)}} + p_{\pi(\eta)}$, $\bar{q} = p_{\mu^+} - p_{\mu^-}$, and $k = p_{\eta^{(\prime)}} - p_{\pi(\eta)}$. With these definitions, the most general form factor decomposition for the matrix element $\langle \mu^+\mu^-|iT|\eta^{(\prime)}\pi^0(\eta)\rangle = i\mathcal{M}(2\pi)^4\delta(p_{\mu^+} + p_{\mu^-} - p_{\eta^{(\prime)}} - p_{\pi(\eta)})$ takes the form

$$\mathcal{M} = m_\mu(\bar{u}v)F_1 + (\bar{u}i\gamma^5 v)F_2 + (\bar{u}\not{k}v)F_3 + i(\bar{u}\not{k}\gamma^5 v)F_4\,, \tag{11.1}$$

where the $F_i \equiv F_i(q^2, \bar{q}\cdot k)$ form factors have been introduced. Note that the connection to the $\eta^{(\prime)} \to \pi^0\mu^+\mu^-$ and $\eta' \to \eta\mu^+\mu^-$ decays is obtained via crossing symmetry with $k \to p_{\eta^{(\prime)}} + p_{\pi(\eta)}$.

General considerations on discrete symmetries can be used to show that electromagnetic interactions can only contribute to the $F_1(q^2, [\bar{q}\cdot k]^{2n})$ and $F_3(q^2, [\bar{q}\cdot k]^{2n+1})$ form factors, with $n = 0, 1, 2\ldots$, and that they can in turn be expressed in terms of the Σ and Ω parameters from Chapter 10 [cf. Eq. (10.8)] as $F_1 = \Sigma$ and $F_3 = \frac{1}{2}\Omega$ (see also Ref. [233]). Furthermore, tree-level electroweak contributions appear via intermediate Higgs-boson exchange only, which contribute to the C- and P-conserving F_1 form factor, providing an unimportant correction to the present study. At higher orders, electroweak contributions to $F_{2,4}(q^2, [\bar{q}\cdot k]^{2n+1})$ of C- and P-odd nature can appear via γZ boxes, but these are CP-even and are, once again, irrelevant to the observables in this study.

Turning to the BSM CP-violating contribution, which requires a careful study of the underlying hadron dynamics, one starts by assuming that the SMEFT provides a correct description of Nature. Accordingly, the new physics degrees of freedom are expected to lie above the electroweak scale and, therefore, only the SM particle spectra are considered (see

Sec. 3.7 for details). In addition, the new-physics effects come from higher dimension operators, that are suppressed by increasing powers of a large energy scale, starting with $D = 6$ so long as B-L number conservation is assumed. In particular, the contribution from the different operators were outlined in Ref. [256] and we briefly recapitulate here. Quark and lepton EDM operators are highly constrained by nEDM bounds; likewise, CP violation in the hadronic sector requires CP-violating form factors with an additional electromagnetic α suppression, required in order to couple hadrons to leptons, which renders any such contribution not competitive. In addition, vector, axial and tensor operators have a vanishing coupling to the $\eta^{(\prime)}\pi^0$ and $\eta'\eta$ systems based on discrete symmetries. Finally, Fermi operators involving quarks and leptons (cf. Sec. 3.7.1) provide the most significant contribution and, thus, the operators that are considered in this study are[3]

$$\mathcal{O}^{prst}_{\ell edq} = (\bar{\ell}^i_p e_r)(\bar{d}_s q^i_t)\,, \qquad \mathcal{O}^{(1)prst}_{\ell equ} = (\bar{\ell}^i_p e_r)(\bar{q}^j_s u_t)\epsilon_{ij}\,, \tag{11.2}$$

where $prst$ are family indices (i.e. $p, r, s, t = 1$ or 2) [109]. These operators produce a non-vanishing CP-odd F_2 form factor[4]

$$\begin{aligned} F_2 = \Big[&\operatorname{Im} c^{2211}_{\ell edq} \langle 0|\,\bar{d}d\,|\eta^{(\prime)}\pi^0(\eta)\rangle + \operatorname{Im} c^{2222}_{\ell edq} \langle 0|\,\bar{s}s\,|\eta^{(\prime)}\pi^0(\eta)\rangle \\ &- \operatorname{Im} c^{(1)2211}_{\ell equ} \langle 0|\,\bar{u}u\,|\eta^{(\prime)}\pi^0(\eta)\rangle\Big]/v^2\,, \end{aligned} \tag{11.3}$$

where $v^2 = 1/(\sqrt{2}G_F)$ and the corresponding hadronic matrix elements need a careful treatment that we discuss in the following section within the framework of large-N_C χPT. To conclude this section, it is worth highlighting that at this order in the SMEFT there is no contribution to F_4.

11.3 Hadronic matrix elements

The scalar-current matrix elements appearing in Eq. (11.3), which are required for the calculation of the longitudinal and transverse asymmetries [see Eqs. (11.21) and (11.22) below], can be calculated within the framework of large-N_C χPT, see Refs. [57, 116, 118, 257, 258]. In the following, we evaluate them at NLO, after renormalising the fields and diagonalising the mass matrix (see, e.g., Appendix B from Ref. [58] for a detailed account of the procedure). To simplify the expressions, we adopt the approach followed in Ref. [161], assuming that the q^2 dependence of the associated form factors is saturated by the corresponding scalar resonances, and make use of the RχT prediction $4L_5/F_0^2 = 8L_8/F_0^2 = 1/M_S^2$ from Refs. [60, 63, 259]. Furthermore, to obtain non-vanishing $\langle 0|\,\bar{s}s\,|\pi^0\eta^{(\prime)}\rangle$ matrix elements, one needs to take into account isospin-breaking effects.[5] To this end, we follow the procedure from Chapter 7 (cf. Ref. [137]) keeping only the leading isospin-breaking terms. Our results for the $\eta\pi^0$ matrix elements are

$$\begin{aligned} \langle 0|\,\bar{u}u/\bar{d}d\,|\eta\pi^0\rangle = \pm B_0 \Bigg[&\left(1 - \frac{M_\eta^2 - M_\pi^2}{M_S^2}\right)(\cos\phi_{23} \pm \epsilon_{13}\sin\phi_{23}) \\ &- \left(\cos\phi_{23} - \frac{\sin\phi_{23}}{\sqrt{2}}\right)\frac{\widetilde{\Lambda}}{3}\Bigg]\left(\frac{M_S^2}{M_S^2 - s}\right), \end{aligned} \tag{11.4}$$

[3] Interestingly, these operators generate the desired CP-odd contribution to our processes at tree level whilst, for the nEDM, contributions appear at the two-loops order weakening the nEDM bounds.

[4] Since our focus is on CP-violating effects, we are only concerned with the corresponding imaginary parts, as in Ref. [256].

[5] This is particularly important in this study since the Wilson coefficients associated to the strange quark are comparatively far less constrained by the nEDM bounds than the light-quark ones, see Ref. [256].

and

$$\langle 0|\,\bar{s}s\,|\eta\pi^0\rangle = -2B_0\epsilon_{13}\left[\left(1-\frac{M_\eta^2+3M_\pi^2-4M_K^2}{M_S^2}\right)\sin\phi_{23} + \frac{\widetilde{\Lambda}}{3}\left(\frac{\cos\phi_{23}}{\sqrt{2}}-\sin\phi_{23}-\frac{\epsilon_{12}\sin\phi_{23}}{\sqrt{2}\epsilon_{13}}\right)\right]\left(\frac{M_S^2}{M_S^2-s}\right), \tag{11.5}$$

where we have introduced the scale invariant parameter $\widetilde{\Lambda} = \Lambda_1 - 2\Lambda_2$, ϕ_{23} is the η-η' mixing angle in the quark-flavour basis, ϵ_{12} and ϵ_{13} are first order approximations to the corresponding ϕ_{12} and ϕ_{13} isospin-breaking mixing angles in the π^0-η and π^0-η' sectors, respectively (see Chapter 7 or Ref. [137] for further details), and M_S is the mass of a generic octet scalar resonance. The corresponding expressions for $\eta \to \eta'$ can be obtained by substituting $\cos\phi_{23} \to \sin\phi_{23}$, $\sin\phi_{23} \to -\cos\phi_{23}$ and $M_\eta \to M_{\eta'}$. For the $\eta' \to \eta\mu^+\mu^-$ decay, the matrix elements read

$$\langle 0|\,\bar{u}u/\bar{d}d\,|\eta'\eta\rangle = B_0\left[\left(1-\frac{M_{\eta'}^2+M_\eta^2-2M_\pi^2}{M_S^2}\right)\left(\frac{\sin 2\phi_{23}}{2}\mp\epsilon_{13}\cos 2\phi_{23}\right) - \left(\frac{\cos 2\phi_{23}}{\sqrt{2}}+\sin 2\phi_{23}\right)\frac{\widetilde{\Lambda}}{3}\right]\left(\frac{M_S^2}{M_S^2-s}\right), \tag{11.6}$$

$$\langle 0|\,\bar{s}s\,|\eta'\eta\rangle = -B_0\left[\left(1-\frac{M_{\eta'}^2+M_\eta^2+2M_\pi^2-4M_K^2}{M_S^2}\right)\sin 2\phi_{23} + \left(\sqrt{2}\cos 2\phi_{23}-\sin 2\phi_{23}\right)\frac{\widetilde{\Lambda}}{3}\right]\left(\frac{M_S^2}{M_S^2-s}\right). \tag{11.7}$$

The numerical inputs to our computations are $B_0 = m_{\pi^0}^2/2\overline{m} = 2.64^{+0.11}_{-0.42}$ GeV at a renormalisation scale of $\mu = 2$ GeV, $M_S = 980$ MeV [1], $\widetilde{\Lambda} = -0.46 \pm 0.19$ from lattice QCD [260] which is in agreement with other phenomenological results [116, 118, 119, 261], and the mixing parameters $\phi_{23} = (41.5 \pm 0.5)^\circ$, $\epsilon_{12} = (2.4 \pm 1.0)\%$ and $\epsilon_{13} = (2.5 \pm 0.9)\%$ from Chapter 7 (cf. Ref. [137]). For the other masses we also take the PDG values.

Before concluding this section, two remarks are in order: first, the matrix elements of the strange quark scalar current with $\eta^{(\prime)}\pi^0$ are suppressed by the isospin symmetry-breaking parameter ϵ_{13} and, second, the contribution of the $\widetilde{\Lambda}$ parameter is in general significant for the matrix elements involving the η'.

11.4 Polarised decays and asymmetries

Let us now compute the squared amplitude from Eq. (11.1), $|\mathcal{M}(\lambda\boldsymbol{n}, \bar{\lambda}\bar{\boldsymbol{n}})|^2$, for the polarised decays that we are investigating. Using the conventions for the kinematics and the phase space given in Appendix G, and neglecting any contribution from the F_4 form factor as already mentioned at the end of Sec. 11.2, we find

$$|\mathcal{M}(\lambda\boldsymbol{n}, \bar{\lambda}\bar{\boldsymbol{n}})|^2 = \frac{1}{4}\Big[c_1|F_1|^2 + c_2|F_2|^2 + c_3|F_3|^2 + c_{13}^R\,\mathrm{Re}\,F_1F_3^* + c_{13}^I\,\mathrm{Im}\,F_1F_3^* + c_{12}^R\,\mathrm{Re}\,F_1F_2^* + c_{12}^I\,\mathrm{Im}\,F_1F_2^* + c_{23}^R\,\mathrm{Re}\,F_2F_3^* + c_{23}^I\,\mathrm{Im}\,F_2F_3^*\Big], \tag{11.8}$$

where $\boldsymbol{n}(\bar{\boldsymbol{n}})$ is the $\mu^+(\mu^-)$ spin-polarisation axis defined in the $\mu^\pm$ rest frames and $\lambda = \pm$ denotes the two spin states. Note that terms in the first and second lines are CP conserving and violating, respectively, provided that $F_{1,2} \equiv F_{1,2}(s, [\bar{q}\cdot k]^{2n})$ and $F_3 \equiv F_3(s, [\bar{q}\cdot k]^{2n+1})$. The coefficients in Eq. (11.8) are given in Appendix H and are the necessary input for implementation in the GEANT4 software [262]. The polarisation of the muons, however, cannot be directly measured and must be inferred from the velocities of the $e^\pm$ associated to the corresponding $\mu^\pm$ decays. Using the expressions provided in Appendix H and making use of the spin-density formalism [263], one finds

$$\begin{aligned} d\Gamma = \frac{ds dc\theta}{64(2\pi)^3}\frac{\lambda_K^{1/2}\beta_\mu}{M^3_{\eta^{(\prime)}}}\left[\frac{d\Omega}{4\pi}dx\; n(x)\right]\left[\frac{d\overline{\Omega}}{4\pi}d\bar{x}\; n(\bar{x})\right]\Big[\tilde{c}_1|F_1|^2 + \tilde{c}_3|F_3|^2 \\ + \tilde{c}^R_{13}\,\mathrm{Re}\,F_1F_3^* + \tilde{c}^I_{13}\,\mathrm{Im}\,F_1F_3^* + \tilde{c}_2|F_2|^2 + \tilde{c}^R_{12}\,\mathrm{Re}\,F_1F_2^* + \tilde{c}^I_{12}\,\mathrm{Im}\,F_1F_2^* \\ + \tilde{c}^R_{23}\,\mathrm{Re}\,F_2F_3^* + \tilde{c}^I_{23}\,\mathrm{Im}\,F_2F_3^*\Big], \end{aligned} \tag{11.9}$$

where the 3-body phase-space description from Appendix G has been employed for the initial $\eta^{(\prime)} \to \pi^0\mu^+\mu^-$ and $\eta' \to \eta\mu^+\mu^-$ decays, and the first two brackets account for the phase space of the subsequent $\mu^\pm$ decays, cf. Appendix I. The coefficients in Eq. (11.9) are calculated from those in Appendix H and read

$$\tilde{c}_1 = 2\beta_\mu^2 m_\mu^2 s(1 + b\bar{b}[\beta_L\bar{\beta}_L - \boldsymbol{\beta}_T\cdot\bar{\boldsymbol{\beta}}_T]), \tag{11.10}$$

$$\tilde{c}_2 = 2s(1 + b\bar{b}[\boldsymbol{\beta}\cdot\bar{\boldsymbol{\beta}}]), \tag{11.11}$$

$$\tilde{c}_3 = 2\lambda_K\Big\{(1-\beta_\mu^2c^2\theta)(1 + b\bar{b}[\beta_L\bar{\beta}_L - \boldsymbol{\beta}_T\cdot\bar{\boldsymbol{\beta}}_T]) \tag{11.12}$$

$$+ 2s^2\theta b\bar{b}\,[(\boldsymbol{\beta}_T\cdot\boldsymbol{n}_{kT})(\bar{\boldsymbol{\beta}}_T\cdot\boldsymbol{n}_{kT}) - \beta_L\bar{\beta}_L] - 4s\theta c\theta m_\mu s^{-1/2} b\bar{b}\,[(\boldsymbol{\beta}_T\cdot\boldsymbol{n}_{kT})\bar{\beta}_L + (\bar{\boldsymbol{\beta}}_T\cdot\boldsymbol{n}_{kT})\beta_L]\Big\}, \tag{11.13}$$

$$\tilde{c}^R_{13} = 4\beta_\mu\lambda_K^{1/2}m_\mu\Big\{2m_\mu c\theta(1 + b\bar{b}[\beta_L\bar{\beta}_L - \boldsymbol{\beta}_T\cdot\bar{\boldsymbol{\beta}}_T]) - \sqrt{s}s\theta b\bar{b}\,[(\boldsymbol{\beta}_T\cdot\boldsymbol{n}_{kT})\bar{\beta}_L + (\bar{\boldsymbol{\beta}}_T\cdot\boldsymbol{n}_{kT})\beta_L]\Big\}, \tag{11.14}$$

$$\tilde{c}^I_{13} = 4\beta_\mu\lambda_K^{1/2}m_\mu\sqrt{s}s\theta\,[b(\boldsymbol{\beta}_T\times\boldsymbol{n}_{kT}) - \bar{b}(\bar{\boldsymbol{\beta}}_T\times\boldsymbol{n}_{kT})], \tag{11.15}$$

$$\tilde{c}^R_{12} = 4\beta_\mu m_\mu s b\bar{b}(\boldsymbol{\beta}_T\times\bar{\boldsymbol{\beta}}_T), \tag{11.16}$$

$$\tilde{c}^I_{12} = 4\beta_\mu m_\mu s(b\beta_L + \bar{b}\bar{\beta}_L), \tag{11.17}$$

$$\tilde{c}^R_{23} = 4\lambda_K^{1/2}b\bar{b}\left\{\sqrt{s}s\theta\,[(\boldsymbol{\beta}_T\times\boldsymbol{n}_{kT})\cdot\bar{\beta}_L - (\bar{\boldsymbol{\beta}}_T\times\boldsymbol{n}_{kT})\cdot\beta_L] + 2m_\mu c\theta(\boldsymbol{\beta}_T\times\bar{\boldsymbol{\beta}}_T)\right\}, \tag{11.18}$$

$$\tilde{c}^I_{23} = 4\lambda_K^{1/2}\left\{\sqrt{s}s\theta\,[b(\boldsymbol{\beta}_T\cdot\boldsymbol{n}_{kT}) + \bar{b}(\bar{\boldsymbol{\beta}}_T\cdot\boldsymbol{n}_{kT})] - 2m_\mu c\theta(b\beta_L + \bar{b}\bar{\beta}_L)\right\}, \tag{11.19}$$

where we have used the shorthand notation $b(x) \equiv b$ and $b(\bar{x}) \equiv \bar{b}$. As expected, integration over $d\Omega d\overline{\Omega}$ results in the vanishing of all the terms involving spin correlations. Next, we make use of the identity $\int d\Omega/(4\pi)n(x)dx = 1$, which allows one to write the total decay width as

$$\begin{aligned} d\Gamma = \frac{ds dc\theta}{64(2\pi)^3 M_{\eta^{(\prime)}}}\frac{\lambda_K^{1/2}\beta_\mu}{M^2_{\eta^{(\prime)}}}2\Big[\beta_\mu^2m_\mu^2 s|F_1|^2 + s|F_2|^2 + \lambda_K(1-\beta_\mu^2c\theta^2)|F_3|^2 \\ + 4\beta_\mu\lambda_K^{1/2}m_\mu^2c\theta\,\mathrm{Re}(F_1F_3^*)\Big]. \end{aligned} \tag{11.20}$$

In order to quantify the CP-violating effects, one needs to construct the appropriate asymmetries that arise as a result of the interference of the SM CP-even and the SMEFT CP-odd amplitudes. Accordingly, we define the longitudinal and transverse asymmetries as follows[6]

$$\begin{aligned} A_L &= \frac{N(c\theta_{e^+}>0)-N(c\theta_{e^+}<0)}{N(c\theta_{e^+}>0)+N(c\theta_{e^+}<0)} \\ &= -\frac{2}{3}\frac{\int ds dc\theta \lambda_K^{1/2}\beta_\mu m_\mu \left[\beta_\mu s \,\mathrm{Im}\, F_1 F_2^* + 2\lambda_K^{1/2} c\theta \,\mathrm{Im}\, F_3 F_2^*\right]}{64(2\pi)^3 M^3_{\eta^{(\prime)}} \int d\Gamma}, \end{aligned} \tag{11.21}$$

$$\begin{aligned} A_T &= \frac{N[s(\bar\phi-\phi)>0]-N[s(\bar\phi-\phi)<0]}{N[s(\bar\phi-\phi)>0]+N[s(\bar\phi-\phi)<0]} \\ &= \frac{\pi}{18}\frac{\int ds dc\theta \lambda_K^{1/2}\beta_\mu m_\mu \left[\beta_\mu s \,\mathrm{Re}\, F_1 F_2^* + 2\lambda_K^{1/2} c\theta \,\mathrm{Re}\, F_3 F_2^*\right]}{64(2\pi)^3 M^3_{\eta^{(\prime)}} \int d\Gamma}, \end{aligned} \tag{11.22}$$

where the polar angles $\theta_{e^\pm}$ refer to those of the $e^\pm$ in the $\mu^\pm$ rest frames, $\phi(\bar\phi)$ correspond to the azimuthal $e^\pm$ angles in the $\mu^\pm$ rest frames, and N refers to the number of $\eta^{(\prime)}$ decays. It is important to highlight that only the terms associated to $\tilde c_{12}^{R,I}$ and $\tilde c_{23}^{R,I}$ contribute to the above asymmetries.

11.5 Results and discussion

In this section, we present quantitative results for the longitudinal and transverse asymmetries by plugging into Eqs. (11.21) and (11.22) the theoretical expressions for F_1 and F_3 from Chapter 10 (or Ref. [233]), and the hadronic matrix elements from Sec. 11.3, which in turn are required to compute F_2. The asymmetries for the three semileptonic processes read

$$A_L^{\eta\to\pi^0\mu^+\mu^-} = -0.19(6)\,\mathrm{Im}\, c_{\ell equ}^{(1)2211} - 0.19(6)\,\mathrm{Im}\, c_{\ell edq}^{2211} - 0.020(9)\,\mathrm{Im}\, c_{\ell edq}^{2222}, \tag{11.23}$$

$$A_T^{\eta\to\pi^0\mu^+\mu^-} = 0.07(2)\,\mathrm{Im}\, c_{\ell equ}^{(1)2211} + 0.07(2)\,\mathrm{Im}\, c_{\ell edq}^{2211} + 7(3)\times10^{-3}\,\mathrm{Im}\, c_{\ell edq}^{2222}, \tag{11.24}$$

$$A_L^{\eta'\to\pi^0\mu^+\mu^-} = -0.04(8)\,\mathrm{Im}\, c_{\ell equ}^{(1)2211} - 0.04(8)\,\mathrm{Im}\, c_{\ell edq}^{2211} + 10(3)\times10^{-3}\,\mathrm{Im}\, c_{\ell edq}^{2222}, \tag{11.25}$$

$$\begin{aligned} A_T^{\eta'\to\pi^0\mu^+\mu^-} &= 3(6)\times10^{-3}\,\mathrm{Im}\, c_{\ell equ}^{(1)2211} + 3(6)\times10^{-3}\,\mathrm{Im}\, c_{\ell edq}^{2211} \\ &\quad - 7(2)\times10^{-4}\,\mathrm{Im}\, c_{\ell edq}^{2222}, \end{aligned} \tag{11.26}$$

$$\begin{aligned} A_L^{\eta'\to\eta\mu^+\mu^-} &= -5(39)\times10^{-3}\,\mathrm{Im}\, c_{\ell equ}^{(1)2211} + 5(46)\times10^{-3}\,\mathrm{Im}\, c_{\ell edq}^{2211} \\ &\quad - 0.08(1)\,\mathrm{Im}\, c_{\ell edq}^{2222}, \end{aligned} \tag{11.27}$$

$$\begin{aligned} A_T^{\eta'\to\eta\mu^+\mu^-} &= 7(50)\times10^{-5}\,\mathrm{Im}\, c_{\ell equ}^{(1)2211} - 6(65)\times10^{-5}\,\mathrm{Im}\, c_{\ell edq}^{2211} \\ &\quad + 1(19)\times10^{-3}\,\mathrm{Im}\, c_{\ell edq}^{2222}, \end{aligned} \tag{11.28}$$

where the error quoted accounts for both the numerical integration and the model-dependence[7] uncertainties, with the latter strongly dominating over the former.

[6] Note that the C- and P-odd SM contributions that may appear in the F_2 form factor are odd in $(\bar q\cdot k)$ and, therefore, in $\cos\theta$, which vanishes for the defined asymmetries. The same would apply to F_4.

[7] In particular, we use the difference between the large-N_C χPT LO and NLO results as an estimation for the residual error associated to truncating the perturbative series. This in turn is used to, rather conservatively, quantify the error corresponding to the model.

TABLE 11.1: Summary of REDTOP sensitivities to (the imaginary parts of) the Wilson coefficients associated to the SMEFT CP-violating operators in Eq. (11.2) for the processes studied in this chapter, as well as the $\eta \to \mu^+\mu^-$ decay analysed in Ref. [256]. In addition, the upper bounds from nEDM experiments are given in the last row for comparison purposes.

Process	Asymmetry	$\mathrm{Im}\, c_{\ell equ}^{(1)2211}$	$\mathrm{Im}\, c_{\ell edq}^{2211}$	$\mathrm{Im}\, c_{\ell edq}^{2222}$
$\eta \to \pi^0\mu^+\mu^-$	A_L	0.0695	0.0720	0.686
	A_T	0.194	0.203	1.93
$\eta' \to \pi^0\mu^+\mu^-$	A_L	2.36	2.56	10.96
	A_T	33.1	35.8	154
$\eta' \to \eta\mu^+\mu^-$	A_L	67.5	78.5	4.46
	A_T	5264	5549	328
$\eta \to \mu^+\mu^-$	A_L	0.007	0.007	0.005
nEDM	-	≤ 0.001	≤ 0.002	≤ 0.02

Next, in order to assess the sensitivity to new physics, one starts by estimating the expected number of events at REDTOP, which can be obtained from the projected statistics[8] of 5×10^{12} η/yr and 5×10^{10} η'/yr, and the SM branching ratios for the three muonic semileptonic processes from Table 10.1. Accordingly, the estimated (statistical) SM backgrounds at the 1σ level, which can be assessed using $\sigma = 1/\sqrt{N}$, are found to be $\sigma_{\eta\to\pi^0\mu^+\mu^-} = 1.35 \times 10^{-2}$, $\sigma_{\eta'\to\pi^0\mu^+\mu^-} = 0.105$ and $\sigma_{\eta'\to\eta\mu^+\mu^-} = 0.354$. It is now straightforward to estimate the REDTOP sensitivity to each of the SMEFT CP-violating Wilson coefficients from Eq. (11.2) by setting to zero two out of the three coefficients in Eqs. (11.23–11.28). The corresponding results for the three decays studied in this chapter are summarised in Table 11.1. We also show in this table the REDTOP sensitivity to the same coefficients from $\eta \to \mu^+\mu^-$ [256], as well as the bounds set by nEDM experiments using the most recent measurement from Ref. [266] (the bounds derived from $D_s^- \to \mu\bar{\nu}_\mu$ decays are weaker and, thus, we do not quote them [265]). It must be highlighted that, strictly speaking, the nEDM experiments set bounds on a particular linear combination of the three Wilson coefficients, which raises the question about possible cancellations that may weaken the nEDM bounds. From Eqs. (4.17) and (4.20) in Ref. [256], one can clearly see that partial cancellations are possible for $c_{\ell equ}^{(1)2211} \sim c_{\ell edq}^{2211}$, which would weaken the nEDM bounds by an order of magnitude.[9] Even in such scenario, REDTOP would still not be competitive.

Clearly, the most competitive observable amongst those studied in this chapter is the longitudinal asymmetry of the $\eta \to \pi^0\mu^+\mu^-$ decay. As well as this, it can be seen that the constraints imposed by the η' semileptonic decays are comparatively much weaker, which is down to the η' REDTOP projected statistics being two orders of magnitude smaller than that of the η. If one compares the sensitivities obtained from the $\eta^{(\prime)} \to \pi^0\mu^+\mu^-$ and $\eta' \to \eta\mu^+\mu^-$ decays to the CP-violating Wilson coefficients with the bounds extracted from nEDM experiments, one must conclude that the projected REDTOP statistics are not competitive enough for the above semileptonic processes, which can be attributed to the isospin-breaking suppression in the hadronic matrix elements, subject to the assumption that new physics can be parameterised by the SMEFT. Consequently, the leptonic $\eta \to \mu^+\mu^-$ decay studied in Ref. [256] remains the most promising channel to be studied at REDTOP.

[8] A total production of 2.5×10^{13} η/yr and 2.5×10^{11} η'/yr is expected [264], with assumed reconstruction efficiencies of approximately 20% [265].

[9] More drastic cancellations would require what it seems to us a large degree of fine-tuning. Furthermore, it seems unlikely that these cancellations would remain stable at higher-order corrections.

11.6 Conclusions

In this chapter, we have analysed in detail possible effects of physics BSM via CP violation in $\eta^{(\prime)} \to \pi^0\mu^+\mu^-$ and $\eta' \to \eta\mu^+\mu^-$ decays. This is particularly timely at present as the REDTOP experiment is studying the possibility of using polarisation techniques to study CP-violating new-physics effects. Assuming that BSM CP-violation appears in Nature via new heavy degrees of freedom, the use of the SMEFT is justified, which in turn provides a convenient connection to different observables, such as those from nEDM experiments and $D_s^- \to \mu\bar{\nu}_\mu$ decays. The outcome of the present work is that the predicted statistics at REDTOP will fall short to detect any CP-violating effects in the semileptonic $\eta^{(\prime)} \to \pi^0\mu^+\mu^-$ and $\eta' \to \eta\mu^+\mu^-$ decays, should one take into account the constraints set by nEDM and $D_s^- \to \mu\bar{\nu}_\mu$. This stands in contrast with the $\eta \to \mu^+\mu^-$ decay studied in Ref. [256] and can be understood by the fact that the less constrained strange-quark contribution (cf. Table 11.1) is of isospin-breaking origin, which is very small in Nature. Accordingly, the purely leptonic $\eta \to \mu^+\mu^-$ decay is still the most promising channel to be investigated at REDTOP in search of new-physics signatures via CP-violating effects using muon polarimetry.

Chapter 12

Conclusions

The phenomenology of the neutral η and η' pseudoscalar mesons represents a perfect playground for testing the low-energy domain of QCD, including phenomena such as the spontaneous and explicit chiral-symmetry breaking, as well as the axial $U(1)_A$ anomaly. In addition to that, since these two mesons are eigenstates of the C, P, CP and G-parity operators, their additive quantum numbers are zero, and their decays do not receive SM contributions at tree level, the phenomenology of the η and η' turns out to be a great probe to search for discrepancies with SM predictions and, therefore, new physics BSM.

In this thesis, we have studied several phenomenological aspects of the η and η' mesons. We began in Chapter 7 by showing that the quality of the most up-to-date experimental data on $VP\gamma$ radiative transitions is sufficiently good to reveal discrepancies between the predictions from the phenomenological model based on the conventional quark model with two sources of flavour $SU(3)$-symmetry breaking from Ref. [140] and experiment. As a result of this, we have enhanced the model by allowing for isospin symmetry-breaking effects and have performed new statistical fits to the empirical data. The quality of the new fits is good, with e.g. $\chi^2_{\text{min}}/\text{d.o.f.} \simeq 1.9$, and the estimations for the parameters of the model appear to be very robust across fits. Moreover, the fitted values for $g = 0.69 \pm 0.01$ GeV^{-1}, $\phi_{23} = (41.5 \pm 0.5)^\circ$, $\phi_V = (4.0 \pm 0.2)^\circ$ and $m_s/\overline{m} = 1.17 \pm 0.06$ are in good agreement with those from other analyses in the published literature. In contrast to this, our estimates for the parameters controlling the mixing in the π^0-η and π^0-η' sectors, i.e. $\epsilon_{12} = (2.4 \pm 1.0)$ % and $\epsilon_{13} = (2.5 \pm 0.9)$ %, disagree with those provided in Refs. [156] and [161]. All in all, the results from this chapter indicate that the above phenomenological model, based on simple quark model ideas with an enhancement to allow for violations of the isospin symmetry, suffices to describe the $VP\gamma$ radiative decays, and the rich and complex mixing phenomenology in the pseudoscalar meson sector.

A thorough theoretical analysis of the doubly radiative decays $\eta^{(\prime)} \to \pi^0\gamma\gamma$ and $\eta' \to \eta\gamma\gamma$ has been presented in Chapter 8, where the scalar and vector meson exchange contributions have been assessed within the LσM and VMD frameworks, respectively. A summary of the predicted decay widths, theoretical branching ratios and contributions to the total signals for the three processes is given in Table 8.2, and a discussion of how they compare to available experimental data is provided in Sec. 8.5. Furthermore, the predicted $m^2_{\gamma\gamma}$ invariant mass distributions of the three processes can be found in Figs. 8.2, 8.3 and 8.4, where we have made use of the model-based VMD couplings. It is worth noting that the theoretical predictions for the $\eta' \to \pi^0\gamma\gamma$ and $\eta' \to \eta\gamma\gamma$ decays that we have presented in this chapter are the first that have been published in the peer-reviewed literature. We have found that, whilst vector meson exchanges vastly dominate over the scalar contributions for the two $\eta^{(\prime)} \to \pi^0\gamma\gamma$ decays, the scalar meson effects turn out to be sizeable for the $\eta' \to \eta\gamma\gamma$, specially that of the σ meson, which represents an opportunity for learning about this poorly understood scalar state. Our predictions from theory for the $\eta' \to \pi^0\gamma\gamma$ and $\eta' \to \eta\gamma\gamma$ decays are in good agreement with recent measurements carried out by BESIII [172, 173]. However, the situation is not as clear for the $\eta \to \pi^0\gamma\gamma$: whilst our prediction is in very good agreement with the very recent measurement by KLOE [183], it appears to be approximately a factor of two smaller than

the measurements from A2 [181] and Crystal Ball [177]. Clearly, the experimental situation needs to be resolved before it is deemed necessary to improve the theoretical treatment.

The sensitivity of the radiative decays studied in Chapter 8, i.e. $\eta^{(\prime)} \to \pi^0\gamma\gamma$ and $\eta' \to \eta\gamma\gamma$, to a hypothetical leptophobic $U(1)_B$ boson in the MeV–GeV mass range has been investigated in detail in Chapter 9. In this analysis, we explicitly added a B-boson exchange contribution to the t- and u-channels of our SM (VMD and LσM) amplitudes. From the analysis of the $\eta \to \pi^0\gamma\gamma$ decay, the current constraints in the resonant mass region $M_{\pi^0} \lesssim m_B \lesssim M_\eta$ have been strengthened by one order of magnitude, reaching $\alpha_B \sim 10^{-6}$ (cf. Fig. 9.4), which renders the task of experimentally identifying the B-boson as a peak around m_B in the $\pi^0\gamma$ invariant mass distribution effectively impossible. The $\eta' \to \pi^0\gamma\gamma$ and $\eta' \to \eta\gamma\gamma$ decays, on the other hand, are not as powerful as the $\eta \to \pi^0\gamma\gamma$ at constraining B-boson parameters below M_η but allow, instead, exploring larger B-boson masses. That being said, the region in the α_B-m_B plane near the ω pole shows a sharp dip (see Fig. 9.5), which, once again, makes the process of identification of a B boson with $m_B \sim M_\omega$ very challenging. It is important to note that the most recent experimental diphoton invariant mass distribution from the KLOE Collaboration supports the description of the three decays without contribution from a leptophobic B boson, although, a B boson with a mass $m_B \gtrsim M_\eta$ and non-negligible coupling α_B may help explain the discrepancy between our SM prediction for $\eta \to \pi^0\gamma\gamma$ and the experimental data from the A2 and Crystal Ball Collaborations (see Fig. 9.7). The existing tension between the measurements by different experimental groups highlights the need for new and more precise data, e.g. from the KLOE(-II) and JEF experiments.

The SM contribution through the C-conserving exchange of two photons to the semileptonic decays $\eta^{(\prime)} \to \pi^0 l^+ l^-$ and $\eta' \to \eta l^+ l^-$, with $l = e$ or μ, have been investigated in detail in Chapter 10 using the VMD model. We have presented a set of theoretical expressions for the decay widths (cf. Sec. 10.2) and the corresponding numerical results, which are summarised in Table 10.1. To the best of our knowledge, our theoretical predictions for the four $\eta' \to \pi^0 l^+ l^-$ and $\eta' \to \eta l^+ l^-$ processes are the first ones that have been published. A thorough discussion of our results, including a comparison with estimations from other analyses available in the literature and the contribution to the total signals from the different exchanged vectors, can be found in Sec. 10.3. In addition to this, predictions for the dilepton invariant mass distributions associated to the six decay processes have been presented in Fig. 10.2. The experimental measurements to date have only provided upper limits to these decays and these limits are still many orders of magnitude larger than the corresponding theoretical counterparts. On this account, we hope that the results from this chapter are relevant for future measurements by experimental groups such as the WASA-at-COSY and REDTOP Collaborations.

Potential new-physics via CP-violating signatures in the three semileptonic decays $\eta^{(\prime)} \to \pi^0\mu^+\mu^-$ and $\eta' \to \eta\mu^+\mu^-$ have been analysed in Chapter 11, which turns out to be particularly relevant to the REDTOP experiment as they are at present contemplating the possibility of implementing muon polarimetry to study BSM effects through CP-violation. For the analysis, we have assumed that CP-violating BSM physics appears in Nature through new heavy degrees of freedom, thus, justifying the use of the SMEFT as the theoretical framework to capture new physics. This in turn provides a convenient connection to different observables, such as those arising from nEDM experiments and $D_s^- \to \mu\bar{\nu}_\mu$ decays. The outcome of this investigation is that the predicted REDTOP statistics is insufficient to allow for the detection of any CP-violating effects in the semileptonic processes $\eta^{(\prime)} \to \pi^0\mu^+\mu^-$ and $\eta' \to \eta\mu^+\mu^-$, if one takes into account the constraints already set by nEDM and $D_s^- \to \mu\bar{\nu}_\mu$ on the associated Wilson coefficients. This result contrasts with the conclusions obtained in Ref. [256] for the purely leptonic $\eta \to \mu^+\mu^-$ decay, which is down to the fact that the less constrained strange-quark contribution (cf. Table 11.1) is of isospin-breaking origin and this

is, of course, very small in Nature. Consequently, the $\eta \to \mu^+\mu^-$ process remains the most promising channel to be investigated at REDTOP in search of new-physics signatures via CP-violating effects.

Appendix A

Mathematical bases for the mixing in the meson sector

Mixing phenomena of neutral states in the meson sector is directly associated to the explicit flavour-$SU(3)$ symmetry breaking, which in turn is a consequence of the strange quark being much heavier than the up and down quarks, i.e. $m_s \gg m_u \approx m_d$, as well as electromagnetic effects. As a result of this, the physical neutral mesons become linear combinations of the mathematical $SU(3)$ states and one can parameterise the admixtures by means of rotations with one or several mixing angles.

In particular, in the pseudoscalar meson sector two different mathematical bases are widely used in the literature:

- on the one hand, one has what is known as the octet-singlet basis, which becomes exact in the $m_u = m_d = m_s$ limit. In this basis, one uses $|\eta_8\rangle = \frac{1}{\sqrt{6}}|u\bar{u} + d\bar{d} - 2s\bar{s}\rangle$ and $|\eta_1\rangle = \frac{1}{\sqrt{3}}|u\bar{u} + d\bar{d} + s\bar{s}\rangle$ as the basis states, such that[1]

$$\begin{pmatrix} \eta \\ \eta' \end{pmatrix} = \begin{pmatrix} \cos\theta_P & -\sin\theta_P \\ \sin\theta_P & \cos\theta_P \end{pmatrix} \begin{pmatrix} \eta_8 \\ \eta_1 \end{pmatrix}, \tag{A.1}$$

  where θ_P is the mixing angle in the octet-singlet basis, and η and η' are the physical pseudoscalar states;

- on the other hand, we have the so-called quark-flavour basis, which becomes exact in the $m_s \to \infty$ limit. This basis employs $|\eta_{\mathrm{NS}}\rangle = \frac{1}{\sqrt{2}}|u\bar{u} + d\bar{d}\rangle$ and $|\eta_{\mathrm{S}}\rangle = |s\bar{s}\rangle$ as the basis states, so that

$$\begin{pmatrix} \eta \\ \eta' \end{pmatrix} = \begin{pmatrix} \cos\phi_P & -\sin\phi_P \\ \sin\phi_P & \cos\phi_P \end{pmatrix} \begin{pmatrix} \eta_{\mathrm{NS}} \\ \eta_{\mathrm{S}} \end{pmatrix}, \tag{A.2}$$

  with ϕ_P being the mixing angle in the quark-flavour basis.

The two mathematical bases are related by the following linear transformation

$$\begin{pmatrix} \eta_8 \\ \eta_1 \end{pmatrix} = \frac{1}{\sqrt{3}} \begin{pmatrix} 1 & -\sqrt{2} \\ \sqrt{2} & 1 \end{pmatrix} \begin{pmatrix} \eta_{\mathrm{NS}} \\ \eta_{\mathrm{S}} \end{pmatrix}. \tag{A.3}$$

Furthermore, the relationship between the two mixing angles in the pseudoscalar sector is $\theta_P = \phi_P - \arctan\sqrt{2} \approx \phi_P - 54.7^\circ$. Of course, we have assumed the isospin limit in this discussion.

In the vector meson sector, where the spins of the quark-antiquark bound states are parallel, the mixing in the ω-ϕ system is usually described in the quark-flavour basis by means of

$$\begin{pmatrix} \omega \\ \phi \end{pmatrix} = \begin{pmatrix} \cos\phi_V & -\sin\phi_V \\ \sin\phi_V & \cos\phi_V \end{pmatrix} \begin{pmatrix} \omega_{\mathrm{NS}} \\ \omega_{\mathrm{S}} \end{pmatrix}, \tag{A.4}$$

[1] Note that the correct description of the mixing in the pseudoscalar sector using the singlet-octet basis generally requires two mixing angles, whilst a single mixing angle suffices in the quark-flavour basis [119–122].

where $|\omega_{\rm NS}\rangle = \frac{1}{\sqrt{2}}|u\bar{u} + d\bar{d}\rangle$ and $|\omega_{\rm S}\rangle = |s\bar{s}\rangle$ are the basis states, and ϕ_V is the associated mixing angle in this basis.

In complete analogy with the above, one can parameterise the mixing of neutral states in the scalar meson sector using the quark-flavour basis

$$\begin{pmatrix} \sigma \\ f_0 \end{pmatrix} = \begin{pmatrix} \cos\phi_S & -\sin\phi_S \\ \sin\phi_S & \cos\phi_S \end{pmatrix} \begin{pmatrix} \sigma_{\rm NS} \\ \sigma_{\rm S} \end{pmatrix}, \tag{A.5}$$

where the basis states are $|\sigma_{\rm NS}\rangle = \frac{1}{\sqrt{2}}|u\bar{u} + d\bar{d}\rangle$ and $|\sigma_{\rm S}\rangle = |s\bar{s}\rangle$, and ϕ_S is the mixing angle of the σ-f_0 system in this basis.

Appendix B

Mapping of states for the π^0-η-η' mixing

The theoretical expressions for the mathematical states π_3, $\eta_{\rm NS}$ and $\eta_{\rm S}$ in Sec. 4.4, Chapter 4, as functions of the physical states π^0, η and η' at NLO in large-N_C χPT are

$$
\begin{aligned}
\pi_3 = & \left[1-\frac{4L_5}{F^2}(\overset{\circ}{M}{}^2_3-\epsilon_{12}\overset{\circ}{M}{}^2_{\rm NS3})\right]\pi^0 \\
& + \left[\left(1-\frac{4L_5}{F^2}\overset{\circ}{M}{}^2_3\right)\epsilon_{13}\sin\phi_{23}-\left(\epsilon_{12}-\frac{4L_5}{F^2}(\overset{\circ}{M}{}^2_{\rm NS3}+\epsilon_{12}\overset{\circ}{M}{}^2_3)\right)\cos\phi_{23}\right]\eta \\
& - \left[\left(1-\frac{4L_5}{F^2}\overset{\circ}{M}{}^2_3\right)\epsilon_{13}\cos\phi_{23}+\left(\epsilon_{12}-\frac{4L_5}{F^2}(\overset{\circ}{M}{}^2_{\rm NS3}+\epsilon_{12}\overset{\circ}{M}{}^2_3)\right)\sin\phi_{23}\right]\eta\,, \\
\eta_{\rm NS} = & \left[\epsilon_{12}-\frac{\Lambda_1}{3\sqrt{2}}(\sqrt{2}\epsilon_{12}+\epsilon_{13})+\frac{4L_5}{F^2}(\overset{\circ}{M}{}^2_{\rm NS3}-\epsilon_{12}\overset{\circ}{M}{}^2_{\rm NS})\right]\pi^0 \\
& + \left[\left(\frac{\Lambda_1}{3\sqrt{2}}+\frac{4L_5}{F^2}\epsilon_{13}\overset{\circ}{M}{}^2_{\rm NS3}\right)\sin\phi_{23}+\left(1-\frac{\Lambda_1}{3}-\frac{4L_5}{F^2}(\overset{\circ}{M}{}^2_{\rm NS}+\epsilon_{12}\overset{\circ}{M}{}^2_{\rm NS3})\right)\cos\phi_{23}\right]\eta \\
& - \left[\left(\frac{\Lambda_1}{3\sqrt{2}}+\frac{4L_5}{F^2}\epsilon_{13}\overset{\circ}{M}{}^2_{\rm NS3}\right)\cos\phi_{23}-\left(1-\frac{\Lambda_1}{3}-\frac{4L_5}{F^2}(\overset{\circ}{M}{}^2_{\rm NS}+\epsilon_{12}\overset{\circ}{M}{}^2_{\rm NS3})\right)\sin\phi_{23}\right]\eta'\,, \\
\eta_{\rm S} = & \left[\epsilon_{13}-\frac{\Lambda_1}{6}(\sqrt{2}\epsilon_{12}+\epsilon_{13})-\frac{4L_5}{F^2}\epsilon_{13}\overset{\circ}{M}{}^2_{\rm S}\right]\pi^0 \\
& - \left[\frac{\Lambda_1}{3\sqrt{2}}\cos\phi_{23}+\left(1-\frac{\Lambda_1}{6}-\frac{4L_5}{F^2}\overset{\circ}{M}{}^2_{\rm S}\right)\sin\phi_{23}\right]\eta \\
& - \left[\frac{\Lambda_1}{3\sqrt{2}}\sin\phi_{23}-\left(1-\frac{\Lambda_1}{6}-\frac{4L_5}{F^2}\overset{\circ}{M}{}^2_{\rm S}\right)\cos\phi_{23}\right]\eta'\,.
\end{aligned}
\tag{B.1}
$$

These relations are also relevant for Sec. 11.3.

Appendix C

Complete one-loop propagators

The complete one-loop propagators for the σ, f_0 and a_0 scalar resonances in Chapters 8 and 9 are defined as follows

$$D(s) = s - M_R^2 + \mathrm{Re}\Pi(s) - \mathrm{Re}\Pi(M_R^2) + i\mathrm{Im}\Pi(s)\,, \tag{C.1}$$

where M_R is the renormalised mass of the scalar meson and $\Pi(s)$ is the one-particle irreducible two-point function. Note that the $\mathrm{Re}\Pi(M_R^2)$ term is introduced to regularise the divergent behaviour of $\Pi(s)$. This propagator is well behaved when a threshold is approached from below, thus, improving the usual Breit-Wigner prescription, which is not particularly suited for spinless resonances (see Ref. [126] for details).

The real and imaginary parts of $\Pi(s)$ for the σ resonance in the first Riemann sheet[1] can be written as

$$\begin{aligned} R(s) = {} & \frac{g_{\sigma\pi\pi}^2}{16\pi^2}\left[2 - \beta_\pi \log\left(\frac{1+\beta_\pi}{1-\beta_\pi}\right)\theta_\pi - 2\bar{\beta}_\pi \arctan\left(\frac{1}{\bar{\beta}_\pi}\right)\bar{\theta}_\pi\right] \\ & + \frac{g_{\sigma K\overline{K}}^2}{16\pi^2}\left[2 - \beta_K \log\left(\frac{1+\beta_K}{1-\beta_K}\right)\theta_K - 2\bar{\beta}_K \arctan\left(\frac{1}{\bar{\beta}_K}\right)\bar{\theta}_K\right], \\ I(s) = {} & -\frac{g_{\sigma\pi\pi}^2}{16\pi}\beta_\pi\theta_\pi - \frac{g_{\sigma K\overline{K}}^2}{16\pi}\beta_K\theta_K\,, \end{aligned} \tag{C.2}$$

where $R(s) \equiv \mathrm{Re}\Pi(s)$ and $I(s) \equiv \mathrm{Im}\Pi(s)$. In addition, $\beta_i = \sqrt{1 - 4M_i^2/s}$ for $i = (\pi, K)$, $\bar{\beta}_i = \sqrt{4M_i^2/s - 1}$, $\theta_i = \theta(s - 4M_i^2)$, and $\bar{\theta}_i = \theta(4M_i^2 - s)$. The couplings of the σ to pions and kaons in the isospin limit[2] take the form

$$\begin{aligned} g_{\sigma\pi\pi}^2 &= \frac{3}{2} g_{\sigma\pi^+\pi^-}^2 = \frac{3}{2}\left(\frac{M_\pi^2 - M_\sigma^2}{f_\pi}\cos\phi_S\right)^2, \\ g_{\sigma K\overline{K}}^2 &= 2 g_{\sigma K^+K^-}^2 = \frac{1}{2}\left[\frac{M_K^2 - M_\sigma^2}{f_K}(\cos\phi_S - \sqrt{2}\sin\phi_S)\right]^2. \end{aligned} \tag{C.3}$$

The renormalised mass of the σ meson for our calculations is fixed to $M_\sigma = 498$ MeV.[3]

[1] We follow the convention from Ref. [130] for the definition of the first Riemann sheet of the complex square root and complex logarithm functions.

[2] In our analysis, the isospin limit is observed and, thus, the mass difference between K^0 and K^+ is not taken into account for the $K\overline{K}$ threshold.

[3] This value is obtained by solving the corresponding pole equation $D(s_P) = 0$ in the second Riemann sheet, with $s_P = M_P^2 - iM_P\Gamma_P$. In addition, one needs to ensure that the pole mass and width are consistent with experimental data.

For the f_0 exchange, the real and imaginary parts of the two-point function in the first Riemann sheet are

$$\begin{aligned} R(s) &= \frac{g^2_{f_0\pi\pi}}{16\pi^2}\left[2-\beta_\pi \log\left(\frac{1+\beta_\pi}{1-\beta_\pi}\right)\theta_\pi - 2\bar{\beta}_\pi \arctan\left(\frac{1}{\bar{\beta}_\pi}\right)\bar{\theta}_\pi\right] \\ &\quad + \frac{g^2_{f_0K\overline{K}}}{16\pi^2}\left[2-\beta_K \log\left(\frac{1+\beta_K}{1-\beta_K}\right)\theta_K - 2\bar{\beta}_K \arctan\left(\frac{1}{\bar{\beta}_K}\right)\bar{\theta}_K\right], \\ I(s) &= -\frac{g^2_{f_0\pi\pi}}{16\pi}\beta_\pi\theta_\pi - \frac{g^2_{f_0K\overline{K}}}{16\pi}\beta_K\theta_K\,, \end{aligned} \tag{C.4}$$

where β_i, $\bar{\beta}_i$, θ_i and $\bar{\theta}_i$ are defined as before. Once again, the couplings of the f_0 to pions and kaons in the isospin limit are

$$\begin{aligned} g^2_{f_0\pi\pi} &= \frac{3}{2}g^2_{f_0\pi^+\pi^-} = \frac{3}{2}\left(\frac{M_\pi^2 - M_{f_0}^2}{f_\pi}\sin\phi_S\right)^2, \\ g^2_{f_0K\overline{K}} &= 2g^2_{f_0K^+K^-} = \frac{1}{2}\left[\frac{M_K^2 - M_{f_0}^2}{f_K}(\sin\phi_S + \sqrt{2}\cos\phi_S)\right]^2. \end{aligned} \tag{C.5}$$

The renormalised mass of the f_0 meson for our calculations is fixed to $M_{f_0} = 990$ MeV.

Finally, the real and imaginary parts of $\Pi(s)$ for the a_0 resonance in the first Riemann sheet are given by

$$\begin{aligned} R(s) &= \frac{g^2_{a_0K\overline{K}}}{16\pi^2}\left[2-\beta_K \log\left(\frac{1+\beta_K}{1-\beta_K}\right)\theta_K - 2\bar{\beta}_K \arctan\left(\frac{1}{\bar{\beta}_K}\right)\bar{\theta}_K\right] \\ &\quad + \frac{g^2_{a_0\pi\eta}}{16\pi^2}\left[2 - \frac{m_\eta^2 - m_\pi^2}{s}\log\left(\frac{m_\eta}{M_\pi}\right) - \beta^+_{\pi\eta}\beta^-_{\pi\eta}\log\left(\frac{\beta^-_{\pi\eta}+\beta^+_{\pi\eta}}{\beta^-_{\pi\eta}-\beta^+_{\pi\eta}}\right)\theta_{\pi\eta}\right. \\ &\quad \left. - 2\bar{\beta}^+_{\pi\eta}\beta^-_{\pi\eta}\arctan\left(\frac{\beta^-_{\pi\eta}}{\bar{\beta}^+_{\pi\eta}}\right)\bar{\theta}_{\pi\eta} + \bar{\beta}^+_{\pi\eta}\bar{\beta}^-_{\pi\eta}\log\left(\frac{\bar{\beta}^+_{\pi\eta}+\bar{\beta}^-_{\pi\eta}}{\bar{\beta}^+_{\pi\eta}-\bar{\beta}^-_{\pi\eta}}\right)\bar{\bar{\theta}}_{\pi\eta}\right], \\ I(s) &= -\frac{g^2_{a_0K\overline{K}}}{16\pi}\beta_K\theta_K - \frac{g^2_{a_0\pi\eta}}{16\pi}\beta^+_{\pi\eta}\beta^-_{\pi\eta}\theta_{\pi\eta}\,, \end{aligned} \tag{C.6}$$

where $\beta^\pm_{\pi\eta} = \sqrt{1-(M_\pi \pm M_\eta)^2/s}$, $\bar{\beta}^\pm_{\pi\eta} = \sqrt{(M_\pi \pm M_\eta)^2/s - 1}$, $\theta_{\pi\eta} = \theta[s-(M_\pi+M_\eta)^2]$, $\bar{\theta}_{\pi\eta} = \theta[s-(M_\pi-M_\eta)^2] \times \theta[(M_\pi+M_\eta)^2 - s]$ and $\bar{\bar{\theta}}_{\pi\eta} = \theta[(M_\pi-M_\eta)^2 - s]$. The couplings of the a_0 to kaons are also written in the isospin limit

$$\begin{aligned} g^2_{a_0K\overline{K}} &= 2g^2_{a_0K^+K^-} = \frac{1}{2}\left(\frac{M_K^2 - M_{a_0}^2}{f_K}\right)^2 \\ g^2_{a_0\pi\eta} &= \left(\frac{M_\eta^2 - M_{a_0}^2}{f_\pi}\cos\phi_P\right)^2. \end{aligned} \tag{C.7}$$

For our calculations, the renormalised mass of the a_0 meson is fixed to $M_{a_0} = 980$ MeV.

Appendix D

Models uncertainty analysis

In this appendix, we provide an estimation of the uncertainty associated to the effective models that we employ in our theoretical treatment, and corresponding results, of Chapter 9.

In particular, and based on the arguments laid out in the last two paragraphs of Sec. 9.2.1, one can assess the uncertainty of our predictions by propagating the errors of the $VP\gamma$ couplings in Table 8.1 to the final results. In Fig. D.1, we show the limits on the leptophobic B-boson coupling α_B for different m_B masses corresponding to the $\eta \to \pi^0\gamma\gamma$ branching ratio measurement from KLOE (black line), along with an error band associated to the uncertainties of the $VP\gamma$ couplings (grey band). Despite the error band being rather large, the corresponding limits are clearly different from those with the QCD contributions turned off (dashed line).

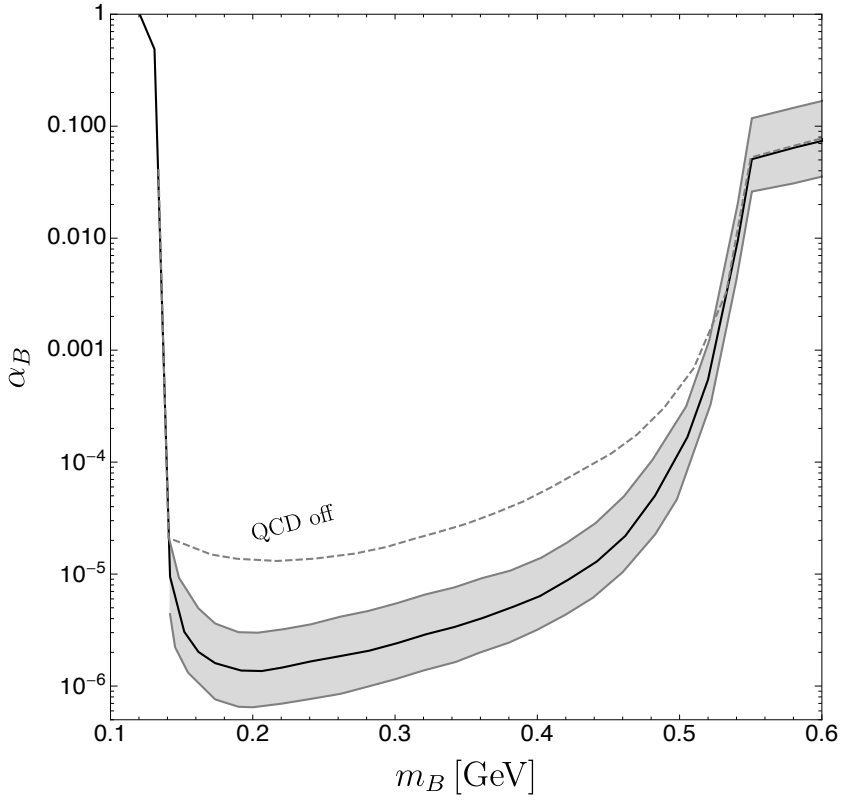

FIGURE D.1: Limits on the leptophobic B-boson coupling α_B for different m_B masses from the $\eta \to \pi^0\gamma\gamma$ BR measurement by KLOE [182] (black line), along with an error band due to the uncertainties of the $VP\gamma$ couplings in Table 8.1.

Appendix E

Individual contributions to the invariant mass distribution

In this appendix, we summarise the different contributions from vector, scalar and B-boson exchanges, as well as their interference, to the invariant mass distributions of the two $\eta^{(\prime)} \to \pi^0\gamma\gamma$ processes of Chapter 9.

E.1 $\eta \to \pi^0\gamma\gamma$ decay

In Fig. E.1 below, the different individual contributions to the $\gamma\gamma$ and $\pi^0\gamma$ invariant mass distributions of the $\eta \to \pi^0\gamma\gamma$ decay are presented, where we have employed the B-boson parameters from Eqs. (9.24) and (9.25), which in turn are obtained from the fits to the Crystal Ball and KLOE experimental datasets, respectively. The entire contribution to the spectra (solid black), together with the separate VMD (dashed black), LσM (dotted black) and B-boson (dot-dashed black) contributions, as well as their interferences, are displayed.

The exchange of vector mesons contribute with 49% to the entire signal of the Crystal Ball spectra. The interference between vector and B-boson exchanges is constructive and almost as large as the VMD contribution, with 38% of the signal. The remaining 13% comes from the individual effect of the B boson, which accounts for 8%, the interference between vector and scalar exchanges, accounting for 4%, and the interference between scalar and B-boson exchanges, which is constructive and around 1%. The contribution of scalar meson exchanges is very small.

The contributions to the KLOE spectra are rather different. Vector meson exchanges completely dominate the entire signal, accounting for 114%. The contribution of scalar exchanges accounts for less than 1%, whilst the contribution from the B boson is only 1.9%, making their separate effects very challenging to isolate even with the arrival of new and more precise data. The interference between vector and scalar exchanges is constructive and accounts for about 8%, whereas the interference between vector and B-boson exchanges is destructive, -23%, with a visible effect in the distributions at low $\gamma\gamma$ and $\pi^0\gamma$ invariant masses. The interference between scalar and B-boson exchanges is tiny, with less than -1%, and destructive.

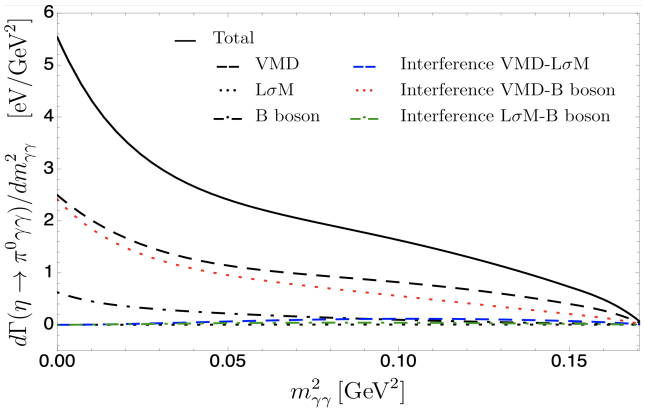

(A) $m^2_{\gamma\gamma}$ invariant mass distribution using B-boson parameters from Eq. (9.24) (fit to Crystal Ball data)

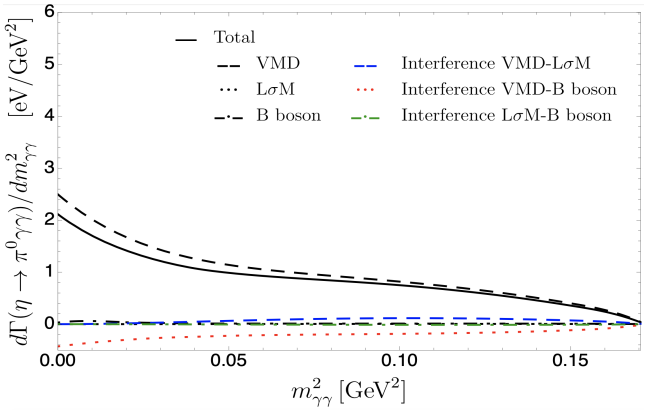

(B) $m^2_{\gamma\gamma}$ invariant mass distribution using B-boson parameters from Eq. (9.25) (fit to KLOE data)

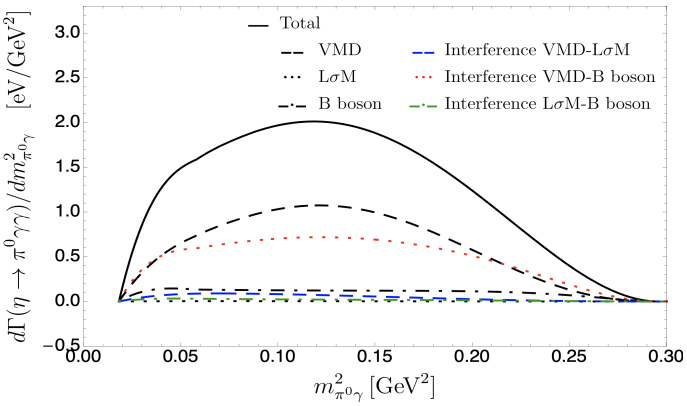

(C) $m^2_{\pi^0\gamma}$ invariant mass distribution using B-boson parameters from Eq. (9.24) (fit to Crystal Ball data)

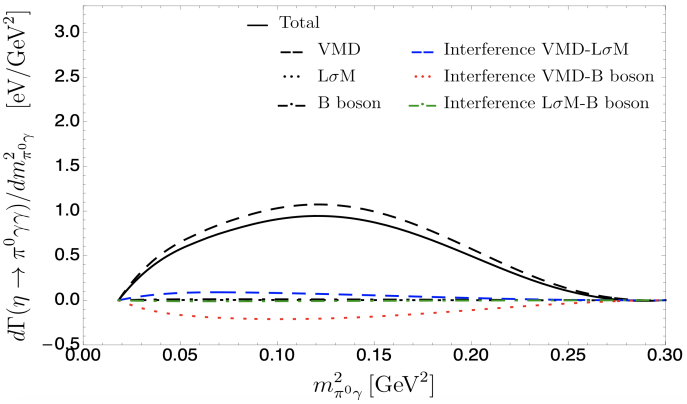

(D) $m^2_{\pi^0\gamma}$ invariant mass distribution using B-boson parameters from Eq. (9.25) (fit to KLOE data)

FIGURE E.1: Individual contributions to the $m^2_{\gamma\gamma}$ and $m^2_{\pi^0\gamma}$ invariant mass distributions of the $\eta \to \pi^0\gamma\gamma$ decay corresponding to the fit results presented in Eqs. (9.24) and (9.25).

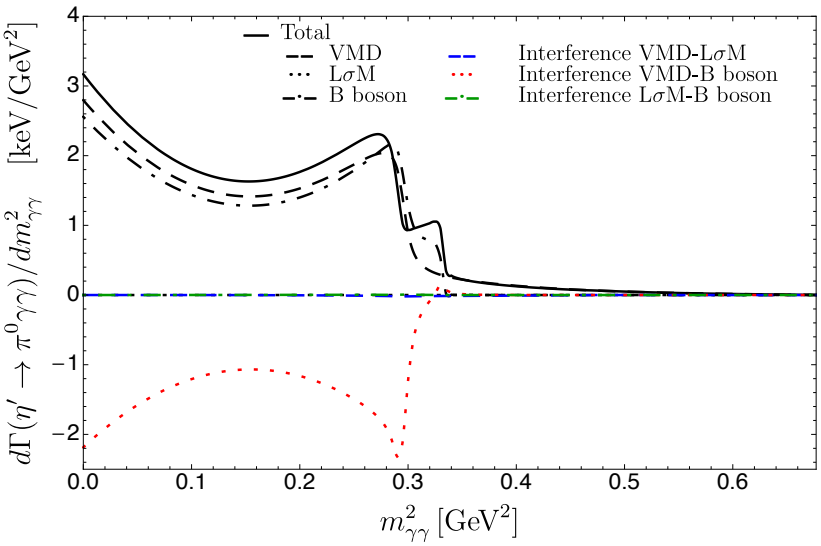

FIGURE E.2: Individual contributions to the $m^2_{\gamma\gamma}$ invariant mass distribution of the $\eta' \to \pi^0\gamma\gamma$ decay using the fit result in Eq. (9.26) obtained from the BESIII experimental data.

E.2 $\eta' \to \pi^0\gamma\gamma$ decay

In Fig. E.2, the different individual contributions to the $\gamma\gamma$ invariant mass distribution of the $\eta' \to \pi^0\gamma\gamma$ decay using the fit result in Eq. (9.26) are presented. The entire contribution to the spectrum (solid black), together with the separate VMD (dashed black), LσM (dotted black) and B boson (dot-dashed black) contributions, as well as their interferences, are shown. The exchange of vector mesons dominate, accounting for 76% of the entire signal. The individual contribution of the B boson is about the same as VMD and the rest comes from the interference terms, out of which the destructive interference between vector and B-boson exchanges dominates with -66%. The contribution of scalar mesons is insignificant.

Appendix F

Definition of parameters A_i, B_i, C_i and D_i

The parameters A_i, B_i, C_i and D_i $(i = 1, 2)$ from Eq. (10.4), Chapter 10, are defined as follows

$$\begin{aligned} A_1 = & -(x+y+2z)(P\cdot p_+) - (y+2z-1)(P\cdot p_-) + (-x+y+1)(p_-\cdot p_+) \\ & + m_l^2(2x+y+1) + \frac{3zM_{\eta^{(\prime)}}^2}{2}, \end{aligned} \tag{F.1}$$

$$A_2 \equiv -A_1 \ \text{ with } \ p_+ \leftrightarrow p_-\,, \tag{F.2}$$

$$\begin{aligned} B_1 = & -2z(x+y)(x+y+z-1)(P\cdot p_+)^2 - 2yz(y+z-1)(P\cdot p_-)^2 \\ & - 2xy(x+y-1)(p_-\cdot p_+)^2 + (P\cdot p_-)\Big\{-2z\big[x(2y+z-1)+2y(y+z-1)\big](P\cdot p_+) \\ & + 2y(p_-\cdot p_+)(-2xz+x+y+z-1) + m_l^2\big[x^2(1-2z)+2xy+2y(y+z-1)\big]\Big\} \\ & + (P\cdot p_+)\Big\{m_l^2\big[x^2(2z-1)+2xy(2z-1)-2y(y+z-1)\big] \\ & - 2y(p_-\cdot p_+)(x+y+z-1)\Big\} - x^3m_l^2(p_-\cdot p_+) \\ & + zM_{\eta^{(\prime)}}^2\Big\{(p_-\cdot p_+)\big[x(4y+z-1)+4y(y+z-1)\big] \\ & + m_l^2\big[2x^2+x(4y+3z-3)+4y(y+z-1)\big]\Big\} + xm_l^4\big[x^2+2xy+2(y-1)y\big], \end{aligned} \tag{F.3}$$

$$B_2 \equiv -B_1 \ \text{ with } \ p_+ \leftrightarrow p_-\,, \tag{F.4}$$

$$C_1 = (x+1)(P\cdot p_-) + (4x+1)(P\cdot p_+) - \Big(\frac{5}{2}x+1\Big)M_{\eta^{(\prime)}}^2\,, \tag{F.5}$$

$$C_2 \equiv C_1 \ \text{ with } \ p_+ \leftrightarrow p_-\,, \tag{F.6}$$

$$\begin{aligned} D_1 = & \,2\big[x^3+x^2(2y+2z-1)+xy(y+2z)+y(y+z-1)\big](P\cdot p_+)^2 \\ & + 2y(xy+y+z-1)(P\cdot p_-)^2 + x(P\cdot p_+)\Big\{-2(x^2-y^2+y)(p_-\cdot p_+) \\ & + m_l^2\big[x^2+2(y-1)y\big] + (z-1)zM_{\eta^{(\prime)}}^2\Big\} + (P\cdot p_-)\Big\{x\big[-2(y-1)y(p_-\cdot p_+ + m_l^2) \\ & + x^2m_l^2 - (z-1)zM_{\eta^{(\prime)}}^2\big] + 4(x+1)y(x+y+z-1)(P\cdot p_+)\Big\} \\ & - M_{\eta^{(\prime)}}^2\Big\{(p_-\cdot p_+ + m_l^2)\big[x^2(4y+2z-1)+4xy(y+z)+4y(y+z-1)\big] + 2x^3m_l^2\Big\}, \end{aligned} \tag{F.7}$$

and

$$D_2 \equiv D_1 \;\text{ with }\; p_+ \leftrightarrow p_- \,, \tag{F.8}$$

where x, y and z are Feynman integration parameters, $M_{\eta^{(\prime)}}$ is the mass of the decaying $\eta^{(\prime)}$ particle, m_l is the mass of the final leptons, and the four-momenta P, p_+ and p_- are as defined in Fig. 10.1.

Appendix G

Kinematics and phase space conventions

In Chapter 11, the phase space is described in terms of invariant masses and the μ^+ angle in the dilepton rest-frame, as shown in Fig. G.1 below. This choice is convenient for the computation of the scalar products involving spin directions. The independent momenta for the $\eta \to \pi^0\mu^+\mu^-$ decay can be written as

$$q = p_{\mu^+} + p_{\mu^-} = p_\eta - p_\pi\,, \qquad \bar{q} = p_{\mu^+} - p_{\mu^-}\,, \qquad k = p_\eta + p_\pi\,. \tag{G.1}$$

The relevant scalar products can in turn be expressed as

$$q^2 = s\,, \quad \bar{q}^2 = 4m_\mu^2 - s\,, \quad k^2 = 2(M_\eta^2 + M_\pi^2) - s\,, \quad q\cdot\bar{q} = 0\,, \tag{G.2}$$

$$q\cdot k = M_\eta^2 - M_\pi^2\,, \qquad \bar{q}\cdot k = \beta_\mu \lambda_K^{1/2} c\theta\,, \tag{G.3}$$

with $\beta_\mu^2 = 1 - 4m_\mu^2/s$, $\lambda_K \equiv \lambda(M_\eta^2, M_\pi^2, s)$ and $\lambda(a,b,c) = a^2+b^2+c^2-2ab-2ac-2bc$. Like in many other places in this thesis, we employ the shorthand notation $c\theta \equiv \cos\theta$ and $s\theta \equiv \sin\theta$. With these conventions, the differential decay width is

$$d\Gamma = \frac{1}{64(2\pi)^3 M_\eta} \frac{\lambda_K^{1/2}\beta_\mu}{M_\eta^2} |\mathcal{M}|^2 \, ds dc\theta\,. \tag{G.4}$$

It is also useful to quote all four-momenta in the dilepton rest frame

$$q^* = (\sqrt{s},0,0,0)\,, \quad \bar{q}^* = (0,0,0,\sqrt{s}\beta_\mu)\,, \quad p_\pm^* = \sqrt{s}/2(1,0,0,\pm\beta_\mu)\,, \tag{G.5}$$

$$n^* = (+\gamma\beta_\mu n_L, \boldsymbol{n}_T, \gamma n_L)\,, \qquad \bar{n}^* = (-\gamma\beta_\mu \bar{n}_L, \bar{\boldsymbol{n}}_T, \gamma\bar{n}_L)\,, \tag{G.6}$$

$$k^* = \frac{1}{\sqrt{s}}(M_\eta^2 - M_\pi^2, \lambda_K^{1/2} s\theta \boldsymbol{n}_{kT}, -\lambda_K^{1/2} c\theta)\,, \tag{G.7}$$

$$p^*_{\eta(\pi)} = \frac{1}{2\sqrt{s}}(M_\eta^2 \pm s - M_\pi^2, \lambda_K^{1/2} s\theta \boldsymbol{n}_{kT}\,, -\lambda_K^{1/2} c\theta)\,, \tag{G.8}$$

where $\boldsymbol{n}_T(\bar{\boldsymbol{n}}_T)$ and $n_L(\bar{n}_L)$ are, respectively, the transverse and longitudinal $\mu^\pm$ spin components with respect to the μ^+ direction, and $\boldsymbol{n}_{kT}$ is a unit vector representing the k momentum transverse to the μ^+ direction. Note that $\boldsymbol{n}_T$, $\bar{\boldsymbol{n}}_T$ and $\boldsymbol{n}_{kT}$ are 2-dimensional objects. The corresponding expressions for the other two processes are found by substituting $\eta \to \eta'$ for $\eta' \to \pi^0\mu^+\mu^-$, and $\eta \to \eta'$ and $\pi^0 \to \eta$ for $\eta' \to \eta\mu^+\mu^-$.

The spin projectors, required when one does not sum over spins, are given here for completeness

$$u(p,\bar{\lambda}\bar{\boldsymbol{n}})\bar{u}(p,\bar{\lambda}\bar{\boldsymbol{n}}) = \frac{1}{2}(\not{p}+m)(1+\bar{\lambda}\gamma^5\not{\bar{n}})\,, \tag{G.9}$$

$$v(p,\lambda\boldsymbol{n})\bar{v}(p,\lambda\boldsymbol{n}) = \frac{1}{2}(\not{p}-m)(1+\lambda\gamma^5\not{n})\,. \tag{G.10}$$

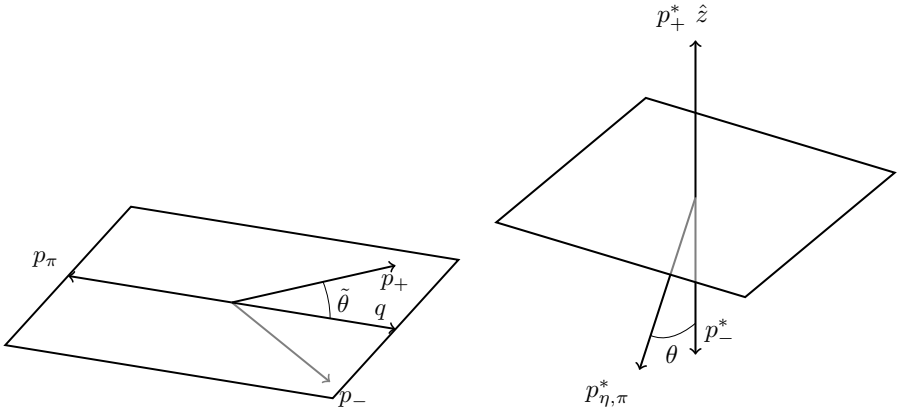

FIGURE G.1: Left: the coordinates in the η rest frame. Right: the coordinates in the dilepton frame. Note that the longitudinal ($\hat{z}$) axis is chosen along the μ^+ direction and that $\theta \neq \tilde{\theta}$. Only $\vec{p}_\pm \sin\tilde{\theta} = \vec{p}_\pm^{\,*} \sin\theta$ is preserved in the boost.

Note that the results obtained from the above equations are easily adapted to the Bouchiat-Michel formulae, Refs. [267, 268], required in the spin-density formalism (see Ref. [263], Sec. 1.6).

Appendix H

Polarised amplitudes

The c_i coefficients in Eq. (11.8), Chapter 11, are used as an intermediate step in our calculation but are relevant for implementing the decay processes in a Monte Carlo program, where the subsequent polarised $\mu^{\pm}$ decays are taken care of by GEANT4. On these grounds, we provide them here for completeness

$$c_1 = 2\beta_\mu^2 m_\mu^2 s(1+\boldsymbol{n}_T\cdot\bar{\boldsymbol{n}}_T - n_L\bar{n}_L)\,, \tag{H.1}$$

$$c_2 = 2s(1-\boldsymbol{n}\cdot\bar{\boldsymbol{n}})\,, \tag{H.2}$$

$$\begin{aligned} c_3 = 2\lambda_K\Big\{&(1-\beta_\mu^2 c^2\theta)(1+\boldsymbol{n}_T\cdot\bar{\boldsymbol{n}}_T - n_L n_L) + 2s^2\theta\,[n_L\bar{n}_L - (\boldsymbol{n}_T\cdot\boldsymbol{n}_{kT})(\bar{\boldsymbol{n}}_T\cdot\boldsymbol{n}_{kT})] \\ &+ 4s\theta c\theta m_\mu s^{-1/2}\,[(\boldsymbol{n}_T\cdot\boldsymbol{n}_{kT})\bar{n}_L + (\bar{\boldsymbol{n}}_T\cdot\boldsymbol{n}_{kT})n_L]\Big\}\,, \end{aligned} \tag{H.3}$$

$$\begin{aligned} c_{13}^R = 4\beta_\mu\lambda_K^{1/2} m_\mu\Big\{&2m_\mu c\theta(1+\boldsymbol{n}_T\cdot\bar{\boldsymbol{n}}_T - n_L\bar{n}_L) \\ &+ \sqrt{s}s\theta\,[(\boldsymbol{n}_T\cdot\boldsymbol{n}_{kT})\bar{n}_L + (\bar{\boldsymbol{n}}_T\cdot\boldsymbol{n}_{kT})n_L]\Big\}\,, \end{aligned} \tag{H.4}$$

$$c_{13}^I = -4\beta_\mu\lambda_K^{1/2} m_\mu\sqrt{s}s\theta\,[(\boldsymbol{n}_T\times\boldsymbol{n}_{kT}) + (\bar{\boldsymbol{n}}_T\times\boldsymbol{n}_{kT})]\,, \tag{H.5}$$

$$c_{12}^R = -4\beta_\mu m_\mu s(\boldsymbol{n}_T\times\bar{\boldsymbol{n}}_T)\,, \tag{H.6}$$

$$c_{12}^I = 4\beta_\mu m_\mu s(\bar{n}_L - n_L)\,, \tag{H.7}$$

$$c_{23}^R = -4\lambda_K^{1/2}\left\{\sqrt{s}s\theta\,[(\boldsymbol{n}_T\times\boldsymbol{n}_{kT})\cdot\bar{n}_L - (\bar{\boldsymbol{n}}_T\times\boldsymbol{n}_{kT})\cdot n_L] + 2m_\mu c\theta(\boldsymbol{n}_T\times\bar{\boldsymbol{n}}_T)\right\}\,, \tag{H.8}$$

$$c_{23}^I = -4\lambda_K^{1/2}\left\{2m_\mu c\theta(\bar{n}_L - n_L) + \sqrt{s}s\theta\,[(\boldsymbol{n}_T\cdot\boldsymbol{n}_{kT}) - (\bar{\boldsymbol{n}}_T\cdot\boldsymbol{n}_{kT})]\right\}\,, \tag{H.9}$$

where the shorthand notation $\lambda\boldsymbol{n}\to\boldsymbol{n}$ and $\bar{\lambda}\bar{\boldsymbol{n}}\to\bar{\boldsymbol{n}}$ has been employed.

Appendix I

Polarised muon decay

In order to study the relevant asymmetries of Chapter 11, it is necessary to supplement the $\eta^{(\prime)} \to \pi^0\mu^+\mu^-$ and $\eta' \to \eta\mu^+\mu^-$ processes with the subsequent $\mu^\pm$ decays. The corresponding result reads [256]

$$\left|\mathcal{M}\left(\mu^+, \lambda\boldsymbol{n}\right)\right|^2 = 64 G_F^2 k_\alpha (p_\beta + \lambda m_\mu n_\beta) q_1^\alpha q_2^\beta \,. \tag{I.1}$$

Including the phase space and integrating over the neutrino spectra (note that the muon rest frame is employed), the above result becomes[1,2]

$$\frac{d\Gamma(\mu^+, \lambda\boldsymbol{n})}{dx d\Omega} = \frac{m_\mu}{24\pi^4} W_{e\mu}^4 G_F^2 \beta x^2 n(x, x_0) \left[1 - \lambda b(x, x_0) \boldsymbol{\beta}\cdot\boldsymbol{n}\right], \tag{I.2}$$

$$d\mathrm{BR}(\mu^+, \lambda\boldsymbol{n}) = \frac{d\Omega}{4\pi} \frac{2x^2\beta}{1-2\epsilon} n(x, x_0) \left[1 - \lambda b(x, x_0) \boldsymbol{\beta}\cdot\boldsymbol{n}\right] dx \,, \tag{I.3}$$

where $n(x, x_0) = (3 - 2x - x_0^2/x)$ and $n(x, x_0) b(x, x_0) = 2 - 2x - \sqrt{1 - x_0^2}$. Furthermore, $W_{e\mu} = (m_\mu^2 + m_e^2)/2m_\mu$ is the maximum positron energy, $x = E_e/W_{e\mu}$ is the reduced positron energy, $x_0 = m_e/W_{e\mu}$ is the minimum reduced positron energy and $\beta = \sqrt{1 - x_0^2/x^2}$. Typically, the approximation $m_e/m_\mu \to 0$ is employed, which results in the simpler expression

$$d\mathrm{BR}(\mu^+, \lambda\boldsymbol{n}) = \frac{d\Omega}{4\pi} n(x) \left[1 - \lambda b(x) \boldsymbol{\beta}\cdot\boldsymbol{n}\right] dx \,, \tag{I.4}$$

with $x = 2E_e/m_\mu$, $n(x) = 2x^2(3-2x)$ and $b(x) = (1-2x)/(3-2x)$. The corresponding expressions for the μ^- are found by replacing $n \to -\bar{n}$ or $\boldsymbol{n} \to -\bar{\boldsymbol{n}}$ on the right hand side of Eqs. (I.1–I.4).

[1] In the second line, the result of integrating over $d\Omega dx$ has been employed, which in turn introduces $\epsilon = m_e^2\{m_e^2(m_\mu^2 - m_e^2)^2 + 6m_\mu^6 + 2m_e^2 m_\mu^4[1 + 6\ln(m_e/m_\mu)]\}/(m_e^2 + m_\mu^2)^4$.

[2] Note that Eq. (I.3) is the SM result from Ref. [1], as well as the expression implemented in GEANT4, though this simulation package includes, in addition, radiative corrections.

Bibliography

[1] R. L. Workman et al. *PTEP* 2022 (2022), p. 083C01.

[2] P. Langacker. Taylor & Francis, 2017.

[3] M. E. Peskin and D. V. Schroeder. Addison-Wesley, 1995.

[4] M. D. Schwartz. Cambridge University Press, 2014.

[5] J. F. Donoghue, E. Golowich, and Barry R. Holstein. Vol. 2. Cambridge University Press, 2014.

[6] S. Weinberg. Cambridge University Press, 2005.

[7] D. J. Gross and F. Wilczek. *Phys. Rev. Lett.* 30 (1973), pp. 1343–1346.

[8] H. D. Politzer. *Phys. Rev. Lett.* 30 (1973), pp. 1346–1349.

[9] R. K. Ellis, W. J. Stirling, and B. R. Webber. Vol. 8. Cambridge University Press, 2011.

[10] X. Fan et al. *Phys. Rev. Lett.* 130.7 (2023), p. 071801. arXiv: 2209.13084 [physics.atom-ph].

[11] S. Weinberg. *Eur. Phys. J. C* 34 (2004), pp. 5–13. arXiv: hep-ph/0401010.

[12] S. Weinberg. Pantheon Books, 1992.

[13] M. Shaposhnikov. *Astroparticle Physics: Current Issues, 2007 (APCI07)*. 2007. arXiv: 0708.3550 [hep-th].

[14] L. Gan et al. *Phys. Rept.* 945 (2022), pp. 1–105. arXiv: 2007.00664 [hep-ph].

[15] J. Elam et al. (2022). arXiv: 2203.07651 [hep-ex].

[16] C. Quigg. Princeton University Press, 2013.

[17] R. D. Peccei and H. R. Quinn. *Phys. Rev. Lett.* 38 (1977), pp. 1440–1443.

[18] R. D. Peccei and H. R. Quinn. *Phys. Rev. D* 16 (1977), pp. 1791–1797.

[19] S. Davidson et al. Vol. 108. Oxford University Press, 2020.

[20] F. Halzen and Alan D. Martin. New Publisher, 1984.

[21] S. Weinberg. *Conference on Historical Examination and Philosophical Reflections on the Foundations of Quantum Field Theory*. 1996, pp. 241–251. arXiv: hep-th/9702027.

[22] G. 't Hooft. *Nuclear Physics B* 33.1 (1971), pp. 173–199.

[23] G. 't Hooft. *Phys. Rev. Lett.* 37 (1976), pp. 8–11.

[24] G. 't Hooft. *Phys. Rev. D* 14 (1976). [Erratum: Phys.Rev.D 18, 2199 (1978)], pp. 3432–3450.

[25] M. Kuster et al. Vol. 741. Springer-Verlag Berlin Heidelberg, 2008.

[26] S. Weinberg. Cambridge University Press, 2013.

[27] B. Borasoy. *Springer Proc. Phys.* 118 (2008), pp. 1–26. arXiv: hep-ph/0703297.

[28] S. Scherer and M. R. Schindler. Vol. 830. Springer-Verlag Berlin Heidelberg, 2012.

[29] M. Gell-Mann. *https://www.osti.gov/biblio/4008239* (1961).

[30] Y. Ne'eman. *Nucl. Phys.* 26 (1961), pp. 222–229.

[31] C. P. Burgess. Cambridge University Press, 2020.

[32] S. Weinberg. *Phys. Rev. D* 11 (1975), pp. 3583–3593.

[33] S. L. Adler. *Phys. Rev.* 177 (1969), pp. 2426–2438.

[34] J. S. Bell and R. Jackiw. *Nuovo Cim. A* 60 (1969), pp. 47–61.

[35] K. Fujikawa. *Phys. Rev. Lett.* 42 (1979), pp. 1195–1198.

[36] A. Zee. Princeton University Press, 2003.

[37] W. A. Bardeen. *Nucl. Phys. B* 75 (1974), pp. 246–258.

[38] R. Jackiw (2005). arXiv: hep-th/0501178.

[39] S. Weinberg. *Physica A* 96.1-2 (1979), pp. 327–340.

[40] K. G. Wilson. *Phys. Rev. B* 4 (1971), pp. 3174–3183.

[41] K. G. Wilson. *Rev. Mod. Phys.* 47 (4 1975), pp. 773–840.

[42] J. Gasser and H. Leutwyler. *Nucl. Phys. B* 250 (1985), pp. 465–516.

[43] M. Gell-Mann, R. J. Oakes, and B. Renner. *Phys. Rev.* 175 (1968), pp. 2195–2199.

[44] S. Weinberg. *Trans. New York Acad. Sci.* 38 (1977), pp. 185–201.

[45] M. Gell-Mann. *Phys. Rev.* 125 (1962), pp. 1067–1084.

[46] S. Okubo. *Prog. Theor. Phys.* 27 (1962), pp. 949–966.

[47] J. Bijnens and G. Ecker. *Ann. Rev. Nucl. Part. Sci.* 64 (2014), pp. 149–174. arXiv: 1405.6488 [hep-ph].

[48] R. J. Dowdall et al. *Phys. Rev. D* 88 (2013), p. 074504. arXiv: 1303.1670 [hep-lat].

[49] W. A. Bardeen. *Phys. Rev.* 184 (1969), pp. 1848–1857.

[50] J. Wess and B. Zumino. *Phys. Lett. B* 37 (1971), pp. 95–97.

[51] E. Witten. *Nucl. Phys. B* 223 (1983), pp. 422–432.

[52] G. 't Hooft. *Nucl. Phys. B* 72 (1974), p. 461.

[53] G. 't Hooft. *Nucl. Phys. B* 75 (1974), pp. 461–470.

[54] E. Witten. *Nucl. Phys. B* 160 (1979), pp. 57–115.

[55] S. Peris and E. de Rafael. *Phys. Lett. B* 348 (1995), pp. 539–542. arXiv: hep-ph/9412343.

[56] A. Pich. *The Phenomenology of Large N(c) QCD*. 2002, pp. 239–258. arXiv: hep-ph/0205030.

[57] R. Kaiser and H. Leutwyler. *Eur. Phys. J. C* 17 (2000), pp. 623–649. arXiv: hep-ph/0007101.

[58] R. Escribano, P. Masjuan, and J. J. Sanz-Cillero. *JHEP* 05 (2011), p. 094. arXiv: 1011.5884 [hep-ph].

[59] H. Leutwyler. *Phys. Lett. B* 374 (1996), pp. 163–168. arXiv: hep-ph/9601234.

[60] G. Ecker et al. *Nucl. Phys. B* 321 (1989), pp. 311–342.

[61] J. Gasser and H. Leutwyler. *Annals Phys.* 158 (1984), p. 142.

[62] S. Weinberg. *Phys. Rev. Lett.* 18 (1967), pp. 507–509.

[63] G. Ecker et al. *Phys. Lett. B* 223 (1989), pp. 425–432.

[64] G. P. Lepage and S. J. Brodsky. *Phys. Rev. D* 22 (1980), p. 2157.

[65] M. Jamin, J. A. Oller, and A. Pich. *Nucl. Phys. B* 587 (2000), pp. 331–362. arXiv: hep-ph/0006045.

[66] M. Jamin, J. A. Oller, and A. Pich. *Nucl. Phys. B* 622 (2002), pp. 279–308. arXiv: hep-ph/0110193.

[67] M. F. L. Golterman and S. Peris. *Phys. Rev. D* 61 (2000), p. 034018. arXiv: hep-ph/9908252.

[68] M. Jamin and M. Munz. *Z. Phys. C* 66 (1995), pp. 633–646. arXiv: hep - ph / 9409335.

[69] M. A. Shifman, A. I. Vainshtein, and V. I. Zakharov. *Nucl. Phys. B* 147 (1979), pp. 385–447.

[70] M. A. Shifman, A. I. Vainshtein, and V. I. Zakharov. *Nucl. Phys. B* 147 (1979), pp. 448–518.

[71] H. B. O'Connell et al. *Prog. Part. Nucl. Phys.* 39 (1997), pp. 201–252. arXiv: hep-ph/9501251.

[72] J. J. Sakurai. *Annals Phys.* 11 (1960), pp. 1–48.

[73] C.-N. Yang and R. L. Mills. *Phys. Rev.* 96 (1954), pp. 191–195.

[74] N. M. Kroll, T. D. Lee, and B. Zumino. *Phys. Rev.* 157 (1967), pp. 1376–1399.

[75] A. Bramon, A. Grau, and G. Pancheri (1997), pp. 477–514.

[76] D. Lurie. John Wiley and Sons, 1968.

[77] M Bando, T. Kugo, and K. Yamawaki. *Nucl. Phys. B* 259 (1985), p. 493.

[78] M. Bando, T. Kugo, and K. Yamawaki. *Phys. Rept.* 164 (1988), pp. 217–314.

[79] U. G. Meissner. *Phys. Rept.* 161 (1988), p. 213.

[80] P. Jain et al. *Phys. Rev. D* 37 (1988), p. 3252.

[81] O. Kaymakcalan and J. Schechter. *Phys. Rev. D* 31 (1985), p. 1109.

[82] J. Schechter. *Phys. Rev. D* 34 (1986), p. 868.

[83] F. Klingl, N. Kaiser, and W. Weise. *Z. Phys. A* 356 (1996), pp. 193–206. arXiv: hep-ph/9607431.

[84] J. Bijnens, A. Bramon, and F. Cornet. *Z. Phys. C* 46 (1990), pp. 599–608.

[85] A. Bramon, A. Grau, and G. Pancheri. *Phys. Lett. B* 283 (1992), pp. 416–420.

[86] M. Napsuciale (1998). arXiv: hep-ph/9803396.

[87] N. A. Tornqvist. *Eur. Phys. J. C* 11 (1999), pp. 359–363. arXiv: hep-ph/9905282.

[88] M. Napsuciale and S. Rodriguez. *Int. J. Mod. Phys. A* 16 (2001), pp. 3011–3024. arXiv: hep-ph/0204149.

[89] J. D. Weinstein and N. Isgur. *Phys. Rev. D* 27 (1983), p. 588.

[90] T. Barnes. *Phys. Lett. B* 165 (1985), pp. 434–440.

[91] R. L. Jaffe. *Phys. Rev. D* 15 (1977), p. 267.

[92] N. N. Achasov and V. N. Ivanchenko. *Nucl. Phys. B* 315 (1989), pp. 465–476.

[93] M. Gell-Mann and M Levy. *Nuovo Cim.* 16 (1960), p. 705.

[94] S. Gasiorowicz and D. A. Geffen. *Rev. Mod. Phys.* 41 (1969), pp. 531–573.

[95] J. Schechter and Y. Ueda. *Phys. Rev. D* 3 (1971). [Erratum: Phys.Rev.D 8, 987 (1973)], pp. 2874–2893.

[96] R. Escribano. *Phys. Rev. D* 74 (2006), p. 114020. arXiv: hep-ph/0606314.

[97] E. Oset, J. R. Pelaez, and L. Roca. *Phys. Rev. D* 67 (2003), p. 073013. arXiv: hep-ph/0210282.

[98] E. Oset, J. R. Pelaez, and L. Roca. *Phys. Rev. D* 77 (2008), p. 073001. arXiv: 0801.2633 [hep-ph].

[99] T. Appelquist and J. Carazzone. *Phys. Rev. D* 11 (1975), p. 2856.

[100] A. A. Petrov and A. E. Blechman. World Scientific Publishing, 2016.

[101] S. L. Glashow. *Nucl. Phys.* 22 (1961), pp. 579–588.

[102] S. Weinberg. *Phys. Rev. Lett.* 19 (1967), pp. 1264–1266.

[103] A. Salam. *Conf. Proc. C* 680519 (1968), pp. 367–377.

[104] C. Arzt. *Phys. Lett. B* 342 (1995), pp. 189–195. arXiv: hep-ph/9304230.

[105] I. Brivio and M. Trott. *Phys. Rept.* 793 (2019), pp. 1–98. arXiv: 1706.08945 [hep-ph].

[106] S. Weinberg. *Phys. Rev. D* 22 (1980), p. 1694.

[107] C. N. Leung, S. T. Love, and S. Rao. *Z. Phys. C* 31 (1986), p. 433.

[108] W. Buchmuller and D. Wyler. *Nucl. Phys. B* 268 (1986), pp. 621–653.

[109] B. Grzadkowski et al. *JHEP* 10 (2010), p. 085. arXiv: 1008.4884 [hep-ph].

[110] G. F. Giudice et al. *JHEP* 06 (2007), p. 045. arXiv: hep-ph/0703164.

[111] E. Masso and V. Sanz. *Phys. Rev. D* 87.3 (2013), p. 033001. arXiv: 1211.1320 [hep-ph].

[112] R. Contino et al. *Comput. Phys. Commun.* 185 (2014), pp. 3412–3423. arXiv: 1403.3381 [hep-ph].

[113] J. Elias-Miro et al. *JHEP* 08 (2013), p. 033. arXiv: 1302.5661 [hep-ph].

[114] J. Elias-Miro et al. *JHEP* 11 (2013), p. 066. arXiv: 1308.1879 [hep-ph].

[115] A. Pomarol and F. Riva. *JHEP* 01 (2014), p. 151. arXiv: 1308.2803 [hep-ph].

[116] P. Bickert, P. Masjuan, and S. Scherer. *Phys. Rev. D* 95.5 (2017), p. 054023. arXiv: 1612.05473 [hep-ph].

[117] Z.-H. Guo and J. A. Oller. *Phys. Rev. D* 84 (2011), p. 034005. arXiv: 1104.2849 [hep-ph].

[118] X-K. Guo et al. *JHEP* 06 (2015), p. 175. arXiv: 1503.02248 [hep-ph].

[119] H. Leutwyler. *Nucl. Phys. B Proc. Suppl.* 64 (1998), pp. 223–231. arXiv: hep-ph/9709408.

[120] R. Escribano and J. M. Frere. *JHEP* 06 (2005), p. 029. arXiv: hep-ph/0501072.

[121] T. Feldmann, P. Kroll, and B. Stech. *Phys. Rev. D* 58 (1998), p. 114006. arXiv: hep-ph/9802409.

[122] T. Feldmann. *Int. J. Mod. Phys. A* 15 (2000), pp. 159–207. arXiv: hep-ph/9907491.

[123] R. J. Eden et al. Cambridge University Press, 1966.

[124] M. Gell-Mann, M. L. Goldberger, and W. E. Thirring. *Phys. Rev.* 95 (1954), pp. 1612–1627.

[125] R. E. Cutkosky. *J. Math. Phys.* 1 (1960), pp. 429–433.

[126] R. Escribano et al. *Eur. Phys. J. C* 28 (2003), pp. 107–114. arXiv: hep-ph/0204338.

[127] A. Bernicha, G. Lopez Castro, and J. Pestieau. *Nucl. Phys. A* 597 (1996), pp. 623–635. arXiv: hep-ph/9508388.

[128] R. Escribano et al. *JHEP* 05 (2021), p. 121. arXiv: 2102.11241 [hep-ph].

[129] D. Morgan and M. R. Pennington. *Phys. Rev. D* 48 (1993), pp. 1185–1204.

[130] T. Bhattacharya and S. Willenbrock. *Phys. Rev. D* 47 (1993), pp. 4022–4027.

[131] A. M. Badalian et al. *Phys. Rept.* 82 (1982), pp. 31–177.

[132] F. Guerrero and A. Pich. *Phys. Lett. B* 412 (1997), pp. 382–388. arXiv: hep-ph/9707347.

[133] R. Omnes. *Nuovo Cim.* 8 (1958), pp. 316–326.

[134] M. Thomson. Cambridge University Press, 2013.

[135] H. Georgi. Dover Publications, 1984.

[136] A. D. Sakharov. *Pisma Zh. Eksp. Teor. Fiz.* 5 (1967), pp. 32–35.

[137] R. Escribano and E. Royo. *Phys. Lett. B* 807 (2020), p. 135534. arXiv: 2003.08379 [hep-ph].

[138] A. Bramon, R. Escribano, and M. D. Scadron. *Eur. Phys. J. C* 7 (1999), pp. 271–278. arXiv: hep-ph/9711229.

[139] T. Feldmann. *Nucl. Phys. B Proc. Suppl.* 74 (1999), pp. 151–154. arXiv: hep-ph/9807367.

[140] A. Bramon, R. Escribano, and M. D. Scadron. *Phys. Lett. B* 503 (2001), pp. 271–276. arXiv: hep-ph/0012049.

[141] F. J. Gilman and R. Kauffman. *Phys. Rev. D* 36 (1987). [Erratum: Phys.Rev.D 37, 3348 (1988)], p. 2761.

[142] A. Bramon, R. Escribano, and M. D. Scadron. *Phys. Lett. B* 403 (1997), pp. 339–343. arXiv: hep-ph/9703313.

[143] M. Benayoun et al. *Phys. Rev. D* 59 (1999), p. 114027. arXiv: hep-ph/9902326.

[144] P. Ball, J. M. Frere, and M. Tytgat. *Phys. Lett. B* 365 (1996), pp. 367–376. arXiv: hep-ph/9508359.

[145] A. V. Kiselev and V. A. Petrov. *Z. Phys. C* 58 (1993), pp. 595–600.

[146] R. Escribano. *Nucl. Phys. B Proc. Suppl.* 164 (2007), pp. 109–112. arXiv: hep-ph/0510206.

[147] R. Escribano and J. M. Frere. *Phys. Lett. B* 459 (1999), pp. 288–294. arXiv: hep-ph/9901405.

[148] T. Feldmann and P. Kroll. *Phys. Scripta T* 99 (2002), pp. 13–22. arXiv: hep-ph/0201044.

[149] J. Schechter, A. Subbaraman, and H. Weigel. *Phys. Rev. D* 48 (1993), pp. 339–355. arXiv: hep-ph/9211239.

[150] R. Escribano, P. Masjuan, and P. Sanchez-Puertas. *Eur. Phys. J. C* 75.9 (2015), p. 414. arXiv: 1504.07742 [hep-ph].

[151] R. Escribano et al. *Phys. Rev. D* 94.5 (2016), p. 054033. arXiv: 1512.07520 [hep-ph].

[152] T. Feldmann and P. Kroll. *Eur. Phys. J. C* 5 (1998), pp. 327–335. arXiv: hep-ph/9711231.

[153] T. Feldmann, P. Kroll, and B. Stech. *Phys. Lett. B* 449 (1999), pp. 339–346. arXiv: hep-ph/9812269.

[154] R. Escribano, P. Masjuan, and P. Sanchez-Puertas. *Phys. Rev. D* 89.3 (2014), p. 034014. arXiv: 1307.2061 [hep-ph].

[155] T. Feldmann and P. Kroll. *Phys. Rev. D* 58 (1998), p. 057501. arXiv: hep-ph/9805294.

[156] P. Kroll. *Mod. Phys. Lett. A* 20 (2005), pp. 2667–2684. arXiv: hep-ph/0509031.

[157] R. Escribano and J. Nadal. *JHEP* 05 (2007), p. 006. arXiv: hep-ph/0703187.

[158] C. E. Thomas. *JHEP* 10 (2007), p. 026. arXiv: 0705.1500 [hep-ph].

[159] H. Leutwyler. *Phys. Lett. B* 374 (1996), pp. 181–185. arXiv: hep-ph/9601236.

[160] D. J. Gross, S. B. Treiman, and F. Wilczek. *Phys. Rev. D* 19 (1979), p. 2188.

[161] R. Escribano, S. Gonzalez-Solis, and P. Roig. *Phys. Rev. D* 94.3 (2016), p. 034008. arXiv: 1601.03989 [hep-ph].

[162] R. Escribano. *Eur. Phys. J. C* 65 (2010), pp. 467–473. arXiv: 0807.4201 [hep-ph].

[163] F. Ambrosino et al. *JHEP* 07 (2009), p. 105. arXiv: 0906.3819 [hep-ph].

[164] C. Di Donato, G. Ricciardi, and I. Bigi. *Phys. Rev. D* 85 (2012), p. 013016. arXiv: 1105.3557 [hep-ph].

[165] R. Escribano et al. *Phys. Rev. D* 102.3 (2020), p. 034026. arXiv: 1812.08454 [hep-ph].

[166] G. Oppo and S. Oneda. *Phys. Rev.* 160 (1967), pp. 1397–1406.

[167] A. Baracca and A. Bramon. *Nuovo Cim. A* 69 (1970), pp. 613–631.

[168] L. Ametller et al. *Phys. Lett. B* 276 (1992), pp. 185–190.

[169] I. Danilkin, O. Deineka, and M. Vanderhaeghen. *Phys. Rev. D* 96.11 (2017), p. 114018. arXiv: 1709.08595 [hep-ph].

[170] Y. Balytskyi (2018). arXiv: 1804.02607 [hep-ph].

[171] Y. Balytskyi (2018). arXiv: 1811.01402 [hep-ph].

[172] M. Ablikim et al. *Phys. Rev. D* 96.1 (2017), p. 012005. arXiv: 1612.05721 [hep-ex].

[173] M. Ablikim et al. *Phys. Rev. D* 100.5 (2019), p. 052015. arXiv: 1906.10346 [hep-ex].

[174] S-S. Fang, A. Kupsc, and D-H. Wei. *Chin. Phys. C* 42.4 (2018), p. 042002. arXiv: 1710.05173 [hep-ex].

[175] D. Alde et al. *Z. Phys. C* 25 (1984), pp. 225–229.

[176] S. Prakhov et al. *Phys. Rev. C* 72 (2005), p. 025201.

[177] S. Prakhov et al. *Phys. Rev. C* 78 (2008), p. 015206.

[178] N. Knecht et al. *Phys. Lett. B* 589 (2004), pp. 14–20.

[179] L. G. Landsberg. *Phys. Rept.* 128 (1985), pp. 301–376.

[180] B. Di Micco et al. *Acta Phys. Slov.* 56.3 (2006), pp. 403–409.

[181] B. M. K. Nefkens et al. *Phys. Rev. C* 90.2 (2014), p. 025206. arXiv: 1405.4904 [hep-ex].

[182] B. Cao. *PoS* EPS-HEP2021 (2022), p. 409.

[183] E. Perez del Rio. Hadron physics results at KLOE-2 experiment at *The 10^{th} International Workshop on Chiral Dynamics 2021, Beijing, 2021*.

[184] D. Alde et al. *Z. Phys. C* 36 (1987), p. 603.

[185] C. Picciotto. *Nuovo Cim. A* 105 (1992), pp. 27–32.

[186] J. N. Ng and D. J. Peters. *Phys. Rev. D* 46 (1992), pp. 5034–5039.

[187] P. Ko. *Phys. Rev. D* 47 (1993), pp. 3933–3937.

[188] P. Ko. *Phys. Lett. B* 349 (1995), pp. 555–560. arXiv: hep-ph/9503253.

[189] A. A. Bel'kov, A. V. Lanyov, and S. Scherer. *J. Phys. G* 22 (1996), pp. 1383–1394. arXiv: hep-ph/9506406.

[190] S. Bellucci and C. Bruno. *Nucl. Phys. B* 452 (1995), pp. 626–648. arXiv: hep-ph/9502243.

[191] J. Bijnens, A. Fayyazuddin, and J. Prades. *Phys. Lett. B* 379 (1996), pp. 209–218. arXiv: hep-ph/9512374.

[192] J. N. Ng and D. J. Peters. *Phys. Rev. D* 47 (1993), pp. 4939–4948.

[193] Y. Nemoto, M. Oka, and M. Takizawa. *Phys. Rev. D* 54 (1996), pp. 6777–6781. arXiv: hep-ph/9602253.

[194] S. Gonzàlez-Solís and E. Passemar. *Eur. Phys. J. C* 78.9 (2018), p. 758. arXiv: 1807.04313 [hep-ph].

[195] R. Escribano, S. Gonzàlez-Solís, and E. Royo. *Phys. Rev. D* 106.11 (2022), p. 114007. arXiv: 2207.14263 [hep-ph].

[196] M. N. Achasov et al. *Nucl. Phys. B* 600 (2001), pp. 3–20. arXiv: hep-ex/0101043.

[197] S. Tulin. *Phys. Rev. D* 89.11 (2014), p. 114008. arXiv: 1404.4370 [hep-ph].

[198] T. D. Lee and Chen-Ning Yang. *Phys. Rev.* 98 (1955), p. 1501.

[199] A. E. Nelson and N. Tetradis. *Phys. Lett. B* 221 (1989), pp. 80–84.

[200] S. Rajpoot. *Phys. Rev. D* 40 (1989), p. 2421.

[201] R. Foot, G. C. Joshi, and H. Lew. *Phys. Rev. D* 40 (1989), pp. 2487–2489.

[202] X-G. He and S. Rajpoot. *Phys. Rev. D* 41 (1990), p. 1636.

[203] E. G. Adelberger, Blayne R. Heckel, and A. E. Nelson. *Ann. Rev. Nucl. Part. Sci.* 53 (2003), pp. 77–121. arXiv: hep-ph/0307284.

[204] R. Barbieri and T. E. O. Ericson. *Phys. Lett. B* 57 (1975), pp. 270–272.

[205] H. Leeb and J. Schmiedmayer. *Phys. Rev. Lett.* 68 (1992), pp. 1472–1475.

[206] V. V. Nesvizhevsky, G. Pignol, and K. V. Protasov. *Phys. Rev. D* 77 (2008), p. 034020. arXiv: 0711.2298 [hep-ph].

[207] C. D. Carone and H. Murayama. *Phys. Rev. Lett.* 74 (1995), pp. 3122–3125. arXiv: hep-ph/9411256.

[208] D. C. Bailey and S. Davidson. *Phys. Lett. B* 348 (1995), pp. 185–189. arXiv: hep-ph/9411355.

[209] C. D. Carone and H. Murayama. *Phys. Rev. D* 52 (1995), pp. 484–493. arXiv: hep-ph/9501220.

[210] A. Aranda and C. D. Carone. *Phys. Lett. B* 443 (1998), pp. 352–358. arXiv: hep-ph/9809522.

[211] B. A. Dobrescu and F. Yu. *Phys. Rev. D* 88.3 (2013). [Erratum: Phys.Rev.D 90, 079901 (2014)], p. 035021. arXiv: 1306.2629 [hep-ph].

[212] B. A. Dobrescu and C. Frugiuele. *Phys. Rev. Lett.* 113 (2014), p. 061801. arXiv: 1404.3947 [hep-ph].

[213] S. Abrahamyan et al. *Phys. Rev. Lett.* 107 (2011), p. 191804. arXiv: 1108.2750 [hep-ex].

[214] R. Essig et al. *Community Summer Study 2013: Snowmass on the Mississippi*. 2013. arXiv: 1311.0029 [hep-ph].

[215] J. R. Batley et al. *Physics Letters B* 746 (2015), pp. 178–185.

[216] J. Alexander et al. 2016. arXiv: 1608.08632 [hep-ph].

[217] D. Babusci et al. *Physics Letters B* 720.1 (2013), pp. 111–115.

[218] A. Anastasi et al. *Phys. Lett. B* 750 (2015), pp. 633–637. arXiv: 1509.00740 [hep-ex].

[219] A. Anastasi et al. *Physics Letters B* 784 (2018), pp. 336–341.

[220] J. P. Lees et al. *Phys. Rev. Lett.* 113.20 (2014), p. 201801. arXiv: 1406.2980 [hep-ex].

[221] H. Merkel et al. *Phys. Rev. Lett.* 112.22 (2014), p. 221802. arXiv: 1404.5502 [hep-ex].

[222] P. H. Adrian et al. *Phys. Rev. D* 98.9 (2018), p. 091101. arXiv: 1807.11530 [hep-ex].

[223] R. Aaij et al. *Phys. Rev. Lett.* 124.4 (2020), p. 041801. arXiv: 1910.06926 [hep-ex].

[224] E. Perez del Rio (2021). arXiv: 2112.10110 [hep-ex].

[225] L. Gan et al. Update to the JEF proposal (PR12-14-004).

[226] E. Won et al. *Phys. Rev. D* 94.9 (2016), p. 092006. arXiv: 1609.05599 [hep-ex].

[227] C. Fanelli and M. Williams. *J. Phys. G* 44.1 (2017), p. 014002. arXiv: 1605.07161 [hep-ph].

[228] B. Batell et al. *Phys. Rev. D* 90.11 (2014), p. 115014. arXiv: 1405.7049 [hep-ph].

[229] T. Cohen, M. Lisanti, and H. K. Lou. *Phys. Rev. Lett.* 115.17 (2015), p. 171804. arXiv: 1503.00009 [hep-ph].

[230] J. Lu and B. Moussallam. *Eur. Phys. J. C* 80.5 (2020), p. 436. arXiv: 2002.04441 [hep-ph].

[231] A. Bramon, A. Grau, and G. Pancheri. *Phys. Lett. B* 344 (1995), pp. 240–244.

[232] J. Prades. *Z. Phys. C* 63 (1994). [Erratum: Z.Phys.C 11, 571 (1999)], pp. 491–506. arXiv: hep-ph/9302246.

[233] R. Escribano and E. Royo. *Eur. Phys. J. C* 80.12 (2020). [Erratum: Eur.Phys.J.C 81, 140 (2021)], p. 1190. arXiv: 2007.12467 [hep-ph].

[234] B. Moussallam. *Eur. Phys. J. C* 81.11 (2021), p. 993. arXiv: 2107.14147 [hep-ph].

[235] M. Berlowski. Private communication.

[236] Y. Balytskyi (2021). arXiv: 2112.02769 [hep-ph].

[237] J. Bernstein, G. Feinberg, and T. D. Lee. *Phys. Rev.* 139 (1965), B1650–B1659.

[238] T. D. Lee. *Phys. Rev.* 140 (1965), B959–B966.

[239] T. P. Cheng. *Phys. Rev.* 162 (1967), pp. 1734–1738.

[240] J. Smith. *Phys. Rev.* 166 (5 1968), pp. 1629–1632.

[241] P. Adlarson et al. *Phys. Lett. B* 784 (2018), pp. 378–384. arXiv: 1802.08642 [hep-ex].

[242] C. Gatto (2019). arXiv: 1910.08505 [physics.ins-det].

[243] V. Shtabovenko, R. Mertig, and F. Orellana. *Comput. Phys. Commun.* 207 (2016), pp. 432–444. arXiv: 1601.01167 [hep-ph].

[244] R. Mertig, M. Bohm, and A. Denner. *Comput. Phys. Commun.* 64 (1991), pp. 345–359.

[245] W. H. Press et al. 3rd ed. Cambridge University Press, 2007.

[246] T. Hahn and M. Perez-Victoria. *Comput. Phys. Commun.* 118 (1999), pp. 153–165. arXiv: hep-ph/9807565.

[247] A. Denner and S. Dittmaier. *Nucl. Phys. B* 734 (2006), pp. 62–115. arXiv: hep-ph/0509141.

[248] J. M. Campbell, E. W. N. Glover, and D. J. Miller. *Nucl. Phys. B* 498 (1997), pp. 397–442. arXiv: hep-ph/9612413.

[249] G. Heinrich et al. *JHEP* 10 (2010), p. 105. arXiv: 1008.2441 [hep-ph].

[250] S. Eidelman et al. *Eur. Phys. J. C* 69 (2010), pp. 103–118. arXiv: 1003.2141 [hep-ph].

[251] S. Ivashyn. *Prob. Atomic Sci. Technol.* 2012N1 (2012), pp. 179–182. arXiv: 1111.1291 [hep-ph].

[252] T. Fujiwara et al. *Prog. Theor. Phys.* 73 (1985), p. 926.

[253] R. Escribano, E. Royo, and P. Sanchez-Puertas. *JHEP* 05 (2022), p. 147. arXiv: 2202.04886 [hep-ph].

[254] B. Abi et al. *Phys. Rev. Lett.* 126.14 (2021), p. 141801. arXiv: 2104.03281 [hep-ex].

[255] C. Gatto, B. Fabela Enriquez, and M. I. Pedraza Morales. *PoS* ICHEP2016 (2016), p. 812.

[256] P. Sanchez-Puertas. *JHEP* 01 (2019), p. 031. arXiv: 1810.13228 [hep-ph].

[257] P. Herrera-Siklody et al. *Nucl. Phys. B* 497 (1997), pp. 345–386. arXiv: hep-ph/9610549.

[258] P. Herrera-Siklody et al. *Phys. Lett. B* 419 (1998), pp. 326–332. arXiv: hep-ph/9710268.

[259] V. Cirigliano et al. *Nucl. Phys. B* 753 (2006), pp. 139–177. arXiv: hep-ph/0603205.

[260] G. S. Bali et al. *JHEP* 08 (2021), p. 137. arXiv: 2106.05398 [hep-lat].

[261] M. Benayoun, L. DelBuono, and Heath Bland O'Connell. *Eur. Phys. J. C* 17 (2000), pp. 593–610. arXiv: hep-ph/9905350.

[262] S. Agostinelli et al. *Nucl. Instrum. Meth.* A506 (2003), pp. 250–303.

[263] H. E. Haber. *21st Annual SLAC Summer Institute on Particle Physics: Spin Structure in High-energy Processes (School: 26 Jul - 3 Aug, Topical Conference: 4-6 Aug) (SSI 93)*. 1994, pp. 231–272. arXiv: hep-ph/9405376.

[264] https://redtop.fnal.gov.

[265] P. Sanchez-Puertas. *Nucl. Part. Phys. Proc.* 312-317 (2021), pp. 201–206. arXiv: 1909.07491 [hep-ph].

[266] C. Abel et al. *Phys. Rev. Lett.* 124.8 (2020), p. 081803. arXiv: 2001.11966 [hep-ex].

[267] C. Bouchiat and L. Michel. *Nucl. Phys.* 5 (1958), pp. 416–434.

[268] L. Michel. *Nuovo Cim.* 14.Suppl 1 (1959), pp. 95–104.